Diogo André Costa Messias Dias

Licenciado em Engenharia do Ambiente
Mestre em Energia e Bioenergia

Recuperação de metais com elevado valor comercial através da adsorção por carbonizados provenientes de resíduos da cultura do arroz (Rice2Metal)

Recovery of metals with high commercial value through adsorption by chars from rice wastes (Rice2Metal)

Dissertação para obtenção do Grau de Doutor
em Química Sustentável

Orientador: Professor Doutor Nuno Carlos Lapa dos Santos Nunes, Professor Auxiliar, Faculdade de Ciências e Tecnologia – Universidade Nova de Lisboa

Co-orientadora: Doutora Maria Manuel Serrano Bernardo, Investigadora, Faculdade de Ciências e Tecnologia – Universidade Nova de Lisboa

Co-orientadora: Doutora Maria Filomena Jesus Pinto, Investigadora Principal, Unidade de Bioenergia e Biorrefinarias – Laboratório Nacional de Energia e Geologia

Júri:

Presidente: Prof. Doutor José Paulo Barbosa Mota

Arguentes: Prof. Doutor Luís António da Cruz Tarelho
Prof.ª Doutora Margarida Maria João de Quina

Vogais: Prof.ª Doutora Isabel Maria de Figueiredo Ligeiro da Fonseca
Doutora Maria Manuel Serrano Bernardo

FACULDADE DE CIÊNCIAS E TECNOLOGIA
UNIVERSIDADE NOVA DE LISBOA

Abril 2020

Recuperação de metais com elevado valor comercial através da adsorção por carbonizados provenientes de resíduos da cultura do arroz (Rice2Metal)

Direitos de cópia

Recovery of metals with high commercial value through adsorption by chars from rice wastes (Rice2Metal)

Copyright

Dedicated to my two guardian angels in the sky

AGRADECIMENTOS

A entrega deste documento significa muito mais do que apenas o término de um programa de doutoramento. Na verdade, encerra, por agora, uma jornada que se iniciou em 2011, quando me foi dada a oportunidade de iniciar o meu percurso como investigador através de uma bolsa de investigação. Durante todos estes anos foram várias as pessoas que me ajudaram e apoiaram. Gostaria agora de agradecer a todo/as o/as que de alguma forma contribuíram para o meu sucesso ao longo desse percurso.

À Fundação para a Ciência e Tecnologia por financiar a minha Bolsa de Doutoramento (SFRH/BD/101751/2014) e à Unidade de Investigação LAQV/REQUIMTE, financiada através de Fundos Nacionais da FCT/MEC (UID/QUI/50006/2013) e cofinanciada pelo FEDER, no âmbito do Acordo de Parceria PT2020 (POCI-01-0145-FEDER-007265). Este trabalho foi ainda financiado pelo FEDER, através do Programa Operacional Fatores de Competitividade COMPETE, e por Fundos Nacionais, através da Fundação para a Ciência e a Tecnologia, que apoiaram o projeto PTDC/AAG - REC/3477/2012 - "RICEVALOR – Aproveitamento energético de resíduos obtidos durante a produção de arroz em Portugal" (FCOMP-01-0124-FEDER-027827), um projeto apoiado por FCT/MTCES, QREN, COMPETE e FEDER.

À pessoa com a qual trabalho desde o dia 1, ao meu mentor, à pessoa que sempre me acompanhou, guiou, ajudou, aconselhou, (...), ao Professor Doutor Nuno Lapa. Várias são as vezes que, em conversas com colegas, refiro a sorte que tive em ter o Professor Nuno Lapa como orientador. Mais que um orientador, o Professor Nuno Lapa tornou-se um amigo. Muito obrigado por tudo Professor! Do coração!

À Doutora Maria Bernardo por também ela ter sido bem mais que uma coorientadora, mas uma amiga. Devido ao muito trabalho que o Professor Nuno Lapa sempre foi tendo, várias foram as vezes em que teve de ser a Doutora Maria Bernardo a tomar as rédeas da orientação, dando-me sempre todo o apoio que fui necessitando ao longo destes anos. Da mesma forma, não poderia escolher uma melhor coorientadora, sempre presente, sempre pronta para ajudar. Também para ti Maria, o meu muito, muito obrigado por tudo, do fundo do coração!!!

Ao Doutor Rui Barbosa que, apesar de já estar ausente do trabalho académico, há alguns anos, foi o coorientador na minha dissertação de mestrado e uma pessoa muito importante na minha iniciação e crescimento como investigador.

À Doutora Filomena Pinto, pela coorientação, pela produção dos carvões, por sempre se mostrar disponível e pelo apoio constante.

Ao Professor Doutor Manuel Nunes da Ponte, por me ter dado a possibilidade de realizar o Plano Doutoral em Química Sustentável (PDQS) e por sempre mostrar disponibilidade para ajudar no que fosse necessário.

À Professora Doutora Isabel Fonseca, por me deixar utilizar todas as infraestruturas existentes nos seus laboratórios, pelo apoio constante, e por se ter tornado quase numa coorientadora emprestada.

À Doutora Inês Matos pelos vários conselhos durante as diversas reuniões que tivemos e pelo igual apoio sempre demonstrado.

À Professora Doutora Benilde Mendes por me ter permitido realizar a maior parte do meu trabalho laboratorial no Departamento de Ciências e Tecnologia da Biomassa (DCTB) apesar do meu doutoramento estar inserido no Departamento de Química (DQ).

À técnica de laboratório Rita Braga e à Dona Rosa Pinto do DCTB, por todo o apoio que me deram ao longo de todos estes anos. Da mesma forma, um agradecimento à Dona Palminha pelo apoio dado nos laboratórios do DQ.

A todos os Professores do DCTB que de alguma forma contribuíram para a minha formação, por todos os ensinamentos, por toda a ajuda e disponibilidade, pelos diversos conselhos e pela amizade.

A todos os alunos de mestrado que trabalharam comigo no laboratório. Delfina Godinho, Wendy Ribeiro, Marta Miguel e Davide Don, foi um prazer acompanhar-vos neste vosso percurso e uma aprendizagem muito grande também para mim. Este trabalho também é vosso. O meu muito obrigado a todos vocês! Um agradecimento especial ao Davide pela sua imensurável ajuda, pela paciência em lidar com as minhas manias e perfecionismos, mas em especial pela amizade.

A todos os colegas de laboratório e departamento pelo apoio constante, mas principalmente pelas amizades que se foram cimentando. Um agradecimento muito especial à recém Doutora Elena Surra, que foi a minha companheira de laboratório durante toda esta jornada. Por se ter tornado numa verdadeira amiga e numa inspiração constante, e por me demonstrar que de facto existem super-heróis disfarçados de mães, esposas, alunas de doutoramento, maratonistas, triatletas, *iron-man* e sei lá eu mais o quê. És verdadeiramente uma inspiração!!!

A todos os meus colegas de doutoramento, pelo apoio durante as aulas de doutoramento e pelos bons momentos de amizade que passamos juntos.

Ao meu pai, mãe e irmão que estão lá sempre, nos bons e maus momentos e que acreditam em mim mais do que ninguém.

À Margarida, por ter sido a pessoa que sempre esteve lá, no bom e no mau. Pelo amor, pelo companheirismo, pela crença, pela força, pela motivação e por ter passado umas férias inteiras fechada em casa a tratar de tudo para que eu pudesse ter mais tempo para me dedicar à escrita da dissertação. Tenho de facto muita sorte em ter-te a meu lado.

Aos meus avós, por terem sido a maior inspiração na minha vida, por me terem demonstrado o que é o amor no seu estado mais imensurável e inquestionável, por não haver palavras suficientes para conseguir expressar a gratidão que terei eternamente com vocês. Tenho tantas saudades vossas…

RESUMO

O arroz é o segundo cereal mais produzido no mundo e Portugal é o maior consumidor e quinto maior produtor da Europa. A produção de arroz gera quantidades significativas de resíduos como a casca de arroz (CA), a palha de arroz (PA) e o polietileno (PE), o qual é resultante de plásticos agrícolas. Atualmente, os destinos destes resíduos não são os mais adequados do ponto de vista ambiental, sendo necessário encontrar-se novas vias de valorização para estes resíduos. Uma vez que estes materiais têm poderes caloríficos inferiores (P.C.I.) interessantes, é possível valorizá-los através de processos termoquímicos, como a pirólise e a gasificação. Estes processos geram diferentes produtos com valor energético (na gasificação gera-se maioritariamente um gás de síntese e na pirólise um biocombustível líquido, embora alguns gases também sejam gerados). No entanto, uma fração sólida (carbonizados - *chars*) também é produzida em ambos os processos termoquímicos, a qual pode ser valorizada como material adsorvente.

Diversas indústrias contribuíram para o aumento da contaminação de águas residuais com metais, que são, direta ou indiretamente, enviados para o ambiente, especialmente em países subdesenvolvidos e em desenvolvimento. Assim, é necessário tratar estas águas residuais contaminadas antes da sua libertação para o ambiente. O crómio (Cr) e o tungsténio (W) são dois elementos metálicos que podem ser encontrados em várias águas residuais industriais. Simultaneamente, a União Europeia (UE) publicou, em 2014, uma lista de 20 substâncias cuja recuperação é uma prioridade para a Europa; ambos os elementos estavam nessa lista, devido à sua importância económica para o setor industrial.

Neste contexto, o principal objetivo deste trabalho foi o de se avaliar a viabilidade de se utilizar carbonizados de pirólise e gasificação de CA, PA e PE, na remoção de Cr (na forma de Cr(III)) e W (na forma de WO_4^{2-}) de meios líquidos. Em alguns casos, foi necessário otimizar-se os carbonizados, com o intuito de se melhorar as suas propriedades e eficiência em processos de adsorção/remoção. Para fins de comparação, foi também utilizado um carvão ativado comercial (CAC).

Dos diversos carbonizados estudados, apenas dois de gasificação (G4C e G5C) e um de pirólise (P1C) foram selecionados para serem utilizados nos ensaios de remoção de Cr(III), em fluxo descontínuo (*batch*). Apesar da área superficial dos carbonizados ser muito baixa, não foi necessária nenhuma ativação dos carbonizados de gasificação, pois o seu elevado conteúdo mineral permitiu remover Cr(III) através de trocas iónicas. No entanto, o carbonizado de pirólise necessitou de ser otimizado para melhorar a sua capacidade de adsorção. Assim, diferentes ativações (físicas e químicas) foram realizadas ao carbonizado P1C.

De entre os carbonizados de gasificação utilizados, o G4C foi o que apresentou os melhores resultados, apresentando capacidades de adsorção de 8.19 mg g^{-1} na solução sintética (o CAC obteve 3.93 mg g^{-1}) e de 14,9 mg g^{-1} na água residual industrial de curtumes (o CAC obteve 16,1 mg g^{-1}).

O carbonizado P1C ativado fisicamente (P1C+PA) apresentou as maiores capacidades de adsorção de entre os carvões ativados provenientes de pirólise, obtendo valores de 9.23 mg g^{-1} na solução sintética (o CAC obteve 9,80 mg g^{-1}) e 12,4 mg g^{-1} na água residual industrial (o CAC obteve 16,1 mg g^{-1}).

O carbonizado G4C foi selecionado para ser utilizado nos ensaios de coluna, em condições dinâmicas, mas o desempenho dos carvões G4C e CAC foi inferior aos obtidos nos ensaios em *batch*, registando capacidades de adsorção de 1,60 e 2,14 mg g^{-1}, na solução sintética, e 3,25 e 7,83 mg g^{-1}, na água residual industrial.

Estes resultados sugerem que, em condições *batch*, o carbonizado G4C e o carvão ativado P1C+PA mostram ter propriedades para serem adsorventes alternativos na remoção de Cr(III) de efluentes líquidos, uma vez que o seu desempenho pode ser considerado comparável ao carvão comercial.

Para os ensaios de adsorção de WO_4^{2-}, foram produzidos seis carvões ativados provenientes de pirólise. A ativação química com KOH originou o carvão ativado de pirólise (P4C+KOH) com os melhores resultados na adsorção de WO_4^{2-}. As maiores capacidades de adsorção encontradas para o carvão ativado P4C+KOH foram de 854 mg g^{-1}, na solução sintética, e de 1561 mg g^{-1}, na água residual de uma indústria de mineração, enquanto que os valores do CAC foram significativamente mais baixos (113 e 572 mg g^{-1}, respetivamente). O carvão ativado P4C+KOH mostrou claramente melhores propriedades do que o CAC na adsorção de WO_4^{2-}, obtendo capacidades de adsorção quase 8 vezes superiores na solução sintética e quase 3 vezes superiores na água residual de mineração.

Estes resultados sugerem que o carvão ativado P4C+KOH parece ser uma alternativa muito mais eficiente que o CAC na adsorção de WO_4^{2-} a partir de efluentes líquidos de mineração.

O principal objetivo do trabalho foi alcançado, pois tanto para a remoção de Cr como de W foi possível produzir-se adsorventes alternativos ao carvão ativado comercial comum. Nos ensaios de Cr, os adsorventes produzidos obtiveram resultados semelhantes ao CAC, enquanto que nos ensaios de W as expectativas foram amplamente superadas, uma vez que os adsorventes produzidos superaram largamente os resultados do CAC.

ABSTRACT

Rice is the second most produced cereal in the world and Portugal is the major consumer and fifth larger producer in Europe. Its production generates significant amounts of wastes, namely rice husk (RH), rice straw (RS) and polyethylene (PE) from agricultural plastics. Currently, the destinations of these wastes are not the most environmental adequate, so different routes of valorisation are required. Having these materials interesting lower heating values (LHV), their valorisation in thermochemical processes, such as pyrolysis and gasification, became a possibility. These processes generate different products with energetic value (gasification generates mainly synthesis gas and pyrolysis mainly products are liquids, though some gases are also obtained). However, a solid fraction (char) is also produced in both thermochemical processes, which can be valorised as adsorbent materials.

Several industries have led to an increase in metal-contaminated wastewaters, which are directly or indirectly discharged into the environment, especially in underdevelopment and developing countries. Therefore, it is necessary to treat metal-contaminated wastewaters prior to their discharge into the environment. Chromium (Cr) and Tungsten (W) are two metallic elements that can be found in several industrial wastewaters. Additionally, the European Union (EU) published, in 2014, a list of 20 substances whose recovery is a priority for Europe. Chromium (Cr) and tungsten (W) were in this list due to their economic importance to the industry sector.

In this context, the main objective of this work was to evaluate the feasibility of using chars from the pyrolysis and gasification of RH, RS and PE, in the removal of Cr (as Cr(III)) and W (as WO_4^{2-}) from aqueous solutions. In some situations, optimisation processes were necessary in order to improve the chars' properties and efficiency in the adsorption/removal processes. For comparison purposes, a commercial activated carbon (CAC) was also used.

Regarding the several chars used on Cr(III) removal only two gasification chars (G4C and G5C) and one pyrolysis char (P1C) were selected to be used in the removal assays under batch conditions. Despite of the very low surface area of the chars, the gasification chars were used without any activation, due to their high mineral content, allowing removal by ion exchange. However, the pyrolysis char required further optimization to improve its adsorptive capacity. Different activations (physical and chemical) were applied to P1C char.

G4C char presented the best result among the gasification chars, achieving uptake capacities of 8.19 mg g^{-1} in the synthetic solution (3.93 mg g^{-1} for CAC) and 14.9 mg g^{-1} in the tannery industry wastewater (16.1 mg g^{-1} for CAC).

P1C physically activated (P1C+PA) presented the highest uptake capacities of all pyrolysis-derived activated carbons obtaining values of 9.23 mg g^{-1} in the synthetic solution (9.80 mg g^{-1} for CAC) and 12.4 mg g^{-1} in the industrial wastewater (16.1 mg g^{-1} for CAC).

G4C char was selected to be used in the column assays under dynamic conditions, but the performance of both G4C and CAC was lower than in the batch assays, obtaining uptake

capacities of 1.60 and 2.14 mg g^{-1} in the synthetic solution and 3.25 and 7.83 mg g^{-1} in the industrial wastewater, respectively.

These results suggest that under batch conditions G4C and P1C+PA showed good properties to be alternative adsorbents in the removal of Cr(III) from liquid effluents, since their performance can be considered comparable to the commercial sample.

For the WO_4^2 adsorption assays, six pyrolysis-derived activated carbons were produced.

The chemical activation with KOH originated the pyrolysis-derived activated carbon (P4C+KOH) with the best results on WO_4^2 adsorption. The highest uptake capacities found for P4C+KOH were 854 mg g^{-1} in the synthetic solution, and 1561 mg g^{-1} in the industrial wastewater from a mining industry, while CAC's values were significantly lower (113 and 572 mg g^{-1}, respectively). P4C+KOH activated carbon clearly showed better properties than CAC on WO_4^{2-} adsorption, obtaining uptake capacities almost 8 times higher in the synthetic solution and almost 3 times higher in the mining wastewater.

These results suggest that P4C+KOH seems to be a much more efficient alternative to CAC in the adsorption of WO_4^{2-} from liquid effluents.

The main objective of the work was achieved as for both Cr and W removal it was possible to produce alternative adsorbents to the typical commercial activated carbon. Concerning Cr, the adsorbents produced obtained similar results to CAC, while for W the expectations were widely exceeded, as the produced adsorbents largely overcame CAC's results.

LIST OF CONTENTS

LIST OF FIGURES

LIST OF TABLES

LIST OF ACRONYMS AND ABBREVIATIONS

AAEMs: Alkaline and alkaline-earth metals

AAS: Atomic absorption spectrometry

AC: Activated carbon

ACs: Activated carbons

ar: As-received basis

a_R: Redlich-Peterson's isotherm constant

ASAP: Accelerated Surface Area and Porosimetry System

b: Langmuir's constant or critical concentration limit

BET: Brunauer, Emmett and Teller

C: Concentration of Cr(III) in the equilibrium

CAC: Commercial activated carbon

CAC-2.5: Assay with CAC at a S/L of 2.5 g L^{-1}

CAC-5: Assay with CAC at a S/L of 5 g L^{-1}

CAC-10: Assay with CAC at a S/L of 10 g L^{-1}

CAC+CT: Commercial activated carbon chemically treated

CAC+CT-5: Assay with the adsorbent CAC+CT at a S/L of 5 g L^{-1}

CAC+CT-10: Assay with the adsorbent CAC+CT at a S/L of 10 g L^{-1}

C_0: Concentration of the ion before the removal assays (batch assays) or on the column inflow (column assays)

C_e: Concentration of the ion in the equilibrium

C_f: Concentration of the ion after the removal assays

Cond.: Conductivity

CRM: Critical raw materials

C_t: Cr(III) concentration on the column outflow on time t

CV: Concentration variation

daf: Dry ash-free basis

db: Dry basis

EC: European Commission

EC_{50}–30 min: Effective concentration (% v/v) of the eluate that promotes 50% decrease in the bioluminescence of *Vibrio fischeri*, after 30 minutes of exposure.

ER: Equivalence ratio

EU: European Union

exp: Experimental data

FC: Fixed carbon

FS: fixed solids

G1: Gasification assay #1

G2: Gasification assay #2

G3: Gasification assay #3

G4: Gasification assay #4

G5: Gasification assay #5

GC: Gasification char(s)

G1C: Char resulting from the gasification assay #1

G2C: Char resulting from the gasification assay #2

G3C: Char resulting from the gasification assay #3

G4C: Char resulting from the gasification assay #4

G4C-2.5: Assay with the adsorbent G4C at a S/L of 2.5 g L^{-1}

G4C-5: Assay with the adsorbent G4C at a S/L of 5 g L^{-1}

G4C-10: Assay with the adsorbent G4C at a S/L of 10 g L^{-1}

G5C: Char resulting from the gasification assay #5

G5C-2.5: Assay with the adsorbent G5C at a S/L of 2.5 g L^{-1}

G5C-5: Assay with the adsorbent G5C at a S/L of 5 g L^{-1}

G5C-10: Assay with the adsorbent G5C at a S/L of 10 g L^{-1}

ICP-AES: Inductively coupled plasma-atomic emission spectrometry

ITER: International Thermonuclear Experimental Reactor project

IUPAC: International Union of Pure and Applied Chemistry

K: Equilibrium constant

k_f: Pseudo-first order kinetic constant

K_F: Freundlich's constant

K_R: Redlich-Peterson's model constant

k_s: Pseudo-second order kinetic constant

k_{th}: Thomas model constant

LHV: Lower heating value

L/S: Liquid/solid ratio

M: Moisture content

m_{ads}: Mass of adsorbent in the column

$m_{Cr(III)\_ads}$: Mass of C(III) adsorbed

$m_{\mathrm{Cr(III)\_total}}$: Total mass of Cr(III) that crossed the column

n: Number of replicates

n: Freundlich intensity parameter

n.a.: Not applicable

n.d.: Not determined

n_i: solute's average degree of association in Multi-step isotherm model

n.q.: Not quantifiable

p: Pressure

p_0: Initial pressure

p/p_0: Relative pressure

P1: Pyrolysis assay #1

P2: Pyrolysis assay #2

P3: Pyrolysis assay #3

PC: Pyrolysis char(s)

P1C: Char resulting from the pyrolysis assay #1

P1C-5: Assay with the adsorbent P1C at a S/L of 5 g L^{-1}

P1C-10: Assay with the adsorbent P1C at a S/L of 10 g L^{-1}

P1C+CA: Activated carbon resulting from the chemical activation of P1C with H_3PO_4 (1:1)

P1C+CA-5: Assay with the adsorbent P1C+CA at a S/L of 5 g L^{-1}

P1C+CA-10: Assay with the adsorbent P1C+CA at a S/L of 10 g L^{-1}

P1C+KOH: Activated carbon resulting from the chemical activation of P1C with KOH (1:3)

P1C+K_2CO_3: Activated carbon resulting from the chemical activation of P1C with K_2CO_3 (1:4)

P1C+H_3PO_4: Activated carbon resulting from the chemical activation of P1C with H_3PO_4 (1:3)

P1C+PA: Activated carbon resulting from the physical activation of P1C without washing

P1C+PA-5: Assay with the adsorbent P1C+PA at a S/L of 5 g L^{-1}

P1C+PA-10: Assay with the adsorbent P1C+PA at a S/L of 10 g L^{-1}

P1C+PA+CT: Activated carbon resulting from the physical activation followed by chemical treatment of P1C

P1C+PA+CT-5: Assay with the adsorbent P1C+PA+CT at a S/L of 5 g L^{-1}

P1C+PA+CT-10: Assay with the adsorbent P1C+PA+CT at a S/L of 10 g L^{-1}

P1C+PA+W: Activated carbon resulting from the physical activation of P1C followed by washing

P1C+PA+W1: Activated carbon resulting from the physical activation of P1C at 800 °C for 2h followed by washing

P1C+PA+W2: Activated carbon resulting from the physical activation of P1C at 850 °C for 2h followed by washing

P1C+PA+W3: Activated carbon resulting from the physical activation of P1C at 800 °C for 4h followed by washing

P1C+PA+W4: Activated carbon resulting from the physical activation of P1C at 850 °C for 4h followed by washing

P1C+PA+W-5: Assay with the adsorbent P1C+PA+W at a S/L of 5 g L^{-1}

P1C+PA+W-10: Assay with the adsorbent P1C+PA+W at a S/L of 10 g L^{-1}

P2C: Char resulting from the pyrolysis assay #2

P3C: Char resulting from the pyrolysis assay #3

P4C: Char resulting from the pyrolysis assay #4

P4C+KOH: Activated carbon resulting from the chemical activation of P4C with KOH (1:4)

P4C+K_2CO_3: Activated carbon resulting from the chemical activation of P4C with K_2CO_3 (1:4)

PE: Polyethylene

PFM: Plasma-facing materials

pH_{pzc}: pH at the point of zero charge

pH t_b: pH value at breakthrough time

pH t_s: pH value at saturation time

PID: Proportional-integral-derivative

POMs: Poly-oxometallates

PV: Percentage variation

Q: Flow rate

q_0: Maximum adsorption capacity of the column

q_e: Uptake capacity in the equilibrium

q_{exp}: Experimental uptake capacity

q_{max}: Maximum uptake capacity

q_t: Uptake capacity at time t

q_T: Adsorption capacity of the layer n_i

q_{th}: Thomas model uptake capacity

q_{total}: Total uptake capacity of the column

RH: Rice husk

RHA: Rice husk ashes

RHC: Rice husk gasification chars

RH+H_3PO_4: Activated carbon resulting from the chemical activation of rice husk with H_3PO_4 (1:2)

rpm: Rotation per minute

RS: Rice straw

s: Total number of steps

S_{BET}: BET surface area

sCOD: Soluble Chemical Oxygen Demand

S/L: Solid/liquid ratio

STP: Standard temperature and pressure

t: Reaction time or contact time

T: Temperature

t_b: Breakthrough time

tCOD: Total Chemical Oxygen Demand

TGA: Thermogravimetric analysis

th: Theoretical data

t_s: Saturation time

TS: Total solids

TSS: Total suspended solids

V. fischeri: *Vibrio fischeri* bacterium

VM: Volatile matter

V_{meso}: Mesopore volume

V_{micro}: Micropore volume

VS: Volatile solids

V_{total}: Total pore volume

v/v: Volume/volume ratio

w/v: Weight/volume ratio

w/w: Weight/weight ratio

$\overline{X}$: Average

σ: Standard deviation

β: Redlich-Peterson's model constant

η: Removal efficiency

Ŷ: Solid yield

1. INTRODUCTION

1.1 Background and motivation

Over the last few decades, the fast development of certain industrial sectors such as metal plating, mining, fertilizer industries, tanneries, production of batteries, pulp and paper, pesticide industries, among others, has led to an increase in the generation of metal-contaminated wastewaters, being directly or indirectly discharged into the environment, especially in developing countries[1,2]. Because of the high lipo-solubility of some of these metals, they can be absorbed by aquatic organisms and bioaccumulate in their tissues. Once they enter the food chain, large concentrations of these metals may accumulate in the human body through contaminated food consumption. If the metals are ingested beyond the permitted concentrations, they can cause serious health disorders[3]. Therefore, it is mandatory to treat metal-contaminated wastewaters prior to their discharge into the environment.

Chromium (Cr) and Tungsten (W) are two metallic elements that can be found in several industrial wastewaters. Cr is used in metal finishing, wood preservation, textile production, leather tanning, among other applications, while W is applied for lighting and electronic uses, catalysts, mining and construction tools, hard jewellery, etc. Additionally, Cr and W are two of the most economically important raw materials for the European Union (EU), which makes their recovery a priority from liquid and solid wastes[4].

Metal removal from liquid effluents can be achieved by conventional treatment processes such as chemical precipitation, solvent extraction, ion exchange, electrochemical removal, among others. Some of these processes have significant disadvantages, namely incomplete removal, high-energy requirements and production of toxic sludge[2].

Recently, numerous approaches have been studied for the development of cheaper and more effective technologies to improve the quality of treated effluents. Adsorption has become a relevant alternative process, which has led to an increase in the demand for low-cost adsorbents that have metal-binding capacities. Over the last years, chars resulting from pyrolysis and gasification have been studied as possible adsorbent materials[5–8]. The textural properties of these chars may be poorer than the ones of activated carbons, which are the conventional adsorbent materials used in the adsorption of pollutants from wastewater[9]. However, the surface of chars may be enriched with functional groups and mineral components that improve their adsorptive capacity. Lastly, if necessary, these chars may even be activated in order to increase their adsorptive capacities[10].

Gasification and pyrolysis are thermochemical processes that convert the feedstocks into energy and materials. Many feedstocks have been tested in gasification and pyrolysis assays, but lately, biomass and solid wastes of high calorific value are being the most used feedstocks as they bring environmental and economic benefits to these thermal technologies[11–14].

Rice is an important staple food for approximately half of the world population[15]. Its production generates several wastes (mainly rice straw, rice husk and plastic bags from fertilizer and seed transportation) with interesting lower heating values (LHV), which has given way to the

appearance of several studies regarding the valorisation of these wastes into energy through gasification and pyrolysis[16–19]. Despite the increasing level of interest and research on this issue, there are still limited studies on the adsorption of metals from aqueous media by chars produced from the pyrolysis of rice wastes[20–23] and no studies regarding pyrolysis or gasification chars from rice waste blends, aside from the studies performed by the team in which the PhD candidate developed his work[24]. This presents a clear opportunity to indulge in this investigation gap.

In order to attempt all these issues, a National Project named "Ricevalor" was assembled. The aim of the project was to study thermal valorisation routes for RH, RS and PE through co-gasification and co-pyrolysis thermal processes. The main objective of the project was to test several wastes' blends and thermal conversion conditions (such as temperature, pressure, and reaction time) in order to maximize the energetic fraction of the process. Secondary objectives were also established, namely the valorisation of the resulting chars from the co-pyrolysis and co-gasification processes into the removal of valuable pollutants from aqueous solutions. This PhD was developed in the framework of this secondary objectives.

The global aim of this work is to characterize the chars resulting from the co-gasification and co-pyrolysis of rice waste streams and use them in the removal of Cr(III) and WO_4^{2-} from aqueous solutions. The results obtained are compared with a commercial activated carbon, in order to access the feasibility of chars into metal removal.

1.2 Research objectives

The main objective of this doctoral thesis is to access the feasibility of using chars from the pyrolysis and gasification of rice waste (rice straw, rice husk and polyethylene) blends in the removal/adsorption of trivalent chromium and tungstate from aqueous solutions.

To achieve this main objective, the following specific tasks were defined:

1. Characterisation of different rice waste streams;
2. Gasification and pyrolysis assays;
3. Characterisation of chars;
4. Optimization of chars selected for the adsorption assays;
5. Adsorption assays under batch conditions;
6. Adsorption assays in fixed columns under dynamic conditions using the chars that performed better in the batch tests.

1.3 Literature review

In order to access the scientific relevance and innovation of the present work, a literature review was previously performed. This review focused on the following topics:

1. Rice wastes;

2. Pyrolysis and gasification;
3. Chars as removal agents of metal ions from aqueous solutions;
4. Activated carbons: activation processes and adsorption mechanisms;
5. Significance of chromium and tungsten recovery;
6. Adsorption in fixed-bed column systems.

1.3.1 Rice wastes

Rice (*Oryza sativa* L.) is the second most produced cereal worldwide[25]. The most recent statistics refer that, in 2017, the rice world production was between 759.6 Mt[25] and 769.7 Mt[26]. In Europe, 4.1 Mt of paddy rice were produced, and Portugal was the fifth European producer with 0.180 Mt, after Italy (1.59 Mt), Russia (0.987 Mt), Spain (0.835 Mt) and Greece (0.185 Mt)[26].

During cultivation, collection, and processing of rice, different wastes are produced. Due to high amounts generated, the most significant wastes are rice straw (RS), rice husk (RH), and plastic bags, mainly composed of polyethylene (PE), being used in the transportation of seeds and fertilizers.

About 23% of the total paddy rice mass is composed by RH[27] and each kilogram of the harvested grain produces 1.0-1.5 kg of RS[28], which means that a very high amount of these wastes is generated during rice production. In Portugal, RS is either burnt in open-air at the rice fields or directly incorporated in soils; RH is either used as bed material in poultry farms or as feedstock for animal feeding; plastics are mechanically treated to be exported and recycled in Asian countries.

As some of these destinations are not environmentally sound, several studies have been performed intending to recover/recycle some of these wastes. The valorisation of rice bio-wastes (RH and RS) can be done by biochemical processes, such as co-composting[29], anaerobic digestion and co-digestion[30,31], bio-fermentation for bioethanol production[32,33], or dark-fermentation for bio-hydrogen production[34,35]. However, these processes need a previous pre-treatment step to make the sugars contained in the polymeric fraction of cellulose and hemicelluloses bioavailable, increasing the cost of final products.

Rice crop wastes also have interesting lower heating values (LHV) allowing to be used in thermal processes: 12.4 MJ kg^{-1} for RS[36], 12.9 MJ kg^{-1} for RH[18], and 44.0 MJ kg^{-1} for PE[37]. Thermal processes seem to be interesting technologies to valorise these wastes, whether by direct combustion[38–40], liquefaction[41,42], gasification[16,18,43], or pyrolysis[44–46].

According to the European Waste Directive 2008/98/EC[47], pyrolysis and gasification are also considered recovery operations. Incineration is only considered as such whenever both energy recovery and electricity production are performed. Gasification and pyrolysis can also be included in the category of recycling technologies, as organic wastes can be reprocessed into new products for several applications.

1.3.2 Pyrolysis and gasification

Through gasification and pyrolysis, the wastes are thermally treated with the primary goal of obtaining high added-value products, such as syngas (in the case of gasification), bio-oils (in the case of pyrolysis), and chars (in both thermal processes). From these final products, energy can be generated. In addition, these products can be used in chemical industry for the production of new materials[48], based on the Circular Economy concept.

Gasification occurs in a partial oxidation environment. Different oxidation agents may be use, such as air, steam, carbon dioxide, oxygen or a combination of these[49]. Syngas is the main energy product, being composed of CO, H_2, CH_4, and a mixture of other minor gases[50]. Also, a carbonaceous solid by-product with a relatively high ash content is produced[51]. Temperature is one of the most important parameters in gasification. Lower gasification temperatures increase the char yield and reduce CO_2 and H_2 concentrations in syngas. Higher gasification temperatures (over 1000 °C) can lead to ash fusion and secondary char reactions, decreasing the char yield. Also, a special design gasification reactor is needed for higher temperatures. The optimal temperature range is between 750 °C to 900 °C[52]. Different chemical reactions are involved in the gasification process. Equation 1.1 shows the overall reaction in an air and/or steam gasifier[49]. However, there are other reactions that can occur during gasification, being the major represented by equations 1.2-1.8[49].

$C_xH_yO_z$ (biomass components) + O_2 (air) + H_2O (steam)		→	CH_4 + CO + CO_2 + H_2 + H_2O + C (char) + tar	(1.1)
Partial oxidation reaction	$2C + O_2$	→	$2CO$	(1.2)
Complete oxidation reaction	$C + O_2$	→	CO_2	(1.3)
Hydrogasification reaction	$C + 2H_2$	→	CH_4	(1.4)
Water gas shift reaction	$CO + H_2O$	→	$CO_2 + H_2$	(1.5)
Steam reforming reaction	$CH_4 + H_2O$	→	$CO + 3H_2$	(1.6)
Water gas reaction	$C + H_2O$	→	$CO + H_2$	(1.7)
Boudouard reaction	$C + CO_2$	→	$2CO$	(1.8)

Pyrolysis is the thermal decomposition process performed under moderate pressure, at relatively high temperatures (400-800 °C), in the absence of oxygen supply. The final products are in the form of gases, bio-oils, and chars[15,53]. The proportion of products depends on the operating conditions[15]: temperatures up to 600 °C maximize the production of bio-oil, and temperatures above 700 °C maximize the production of gas, minimizing the formation of char[54]; lower pressures promote the production of char, while higher pressures favour the production of gases[55]. Among the thermal conversion processes of biomass, pyrolysis process is recognized as the most versatile, since it can be used either as an independent process for the production of liquid fuels and other valuable chemical, or as an initial step in the gasification or combustion[56]. Several reactions of dehydration, decarboxylation, decarbonylation, aromatization, ketonization, hydrodeoxygenation, repolymerization, etc., occur in biomass pyrolysis associated to very complex mechanisms[57,58]. Also, much of the reaction present in the gasification process are common to pyrolysis. The simplified chemical reaction that occurs in pyrolysis can be seen in equation 1.9[57,59].

$$C_xH_yO_z \text{ (biomass components)} \rightarrow \text{condensable volatile tar + light gases + char} \quad (1.9)$$

Although there are already some studies on the gasification and pyrolysis of RH[15,60], RS[15,60], and PE[61,62] as raw materials, pyrolysis and gasification using blends of these wastes are poorly studied and can be an important topic to be explored.

1.3.3 Chars as removal agents of metal ions from aqueous solutions

Among the products of pyrolysis and gasification, char can be seen as an interesting by-product material, since it has numerous applications[48], such as (i) combustion for energy recovery[63], (ii) reducing agent in metallurgical applications[64,65], (iii) catalyst[66], (iv) soil amendment material[67], and (v) precursor of activated carbons[68,69].

Furthermore, there has been increasing interest in using chars in water treatment[70–72]. The specific properties of chars that make possible their use as adsorbent of pollutants from aqueous solutions include relatively porous structure, enriched surface with functional groups and/or mineral clusters. As adsorbents, chars resemble some properties to activated carbons which are the most commonly employed and efficient adsorbents for the removal of diverse pollutants from water[9]. According to the width size, pores may be divided in micropores (< 2 nm), mesopores (2 > 50 nm) and macropores (> 50 nm)[73]. Different pollutants have different molecular sizes, so the size of the pores is a significant factor to take into consideration when selecting a char or activated char for removing pollutants.

Compared to the commercial activated carbons, chars appear to be new potential low-cost and effective adsorbents, as their production is cheaper with lower energy requirements[74]. The

feedstocks for char production are abundant and of low-cost, being mainly obtained from agro-forestry biomass and solid bio-wastes[75]. In some cases, these carbonaceous materials show even higher adsorption affinity and capacity for removing pollutants than the commercial activated carbons[76–78]. Being a renewable resource and due to its economic and environmental benefits (**Figure 1**), chars are therefore promising resources for environmental technology used for wastewater treatments.

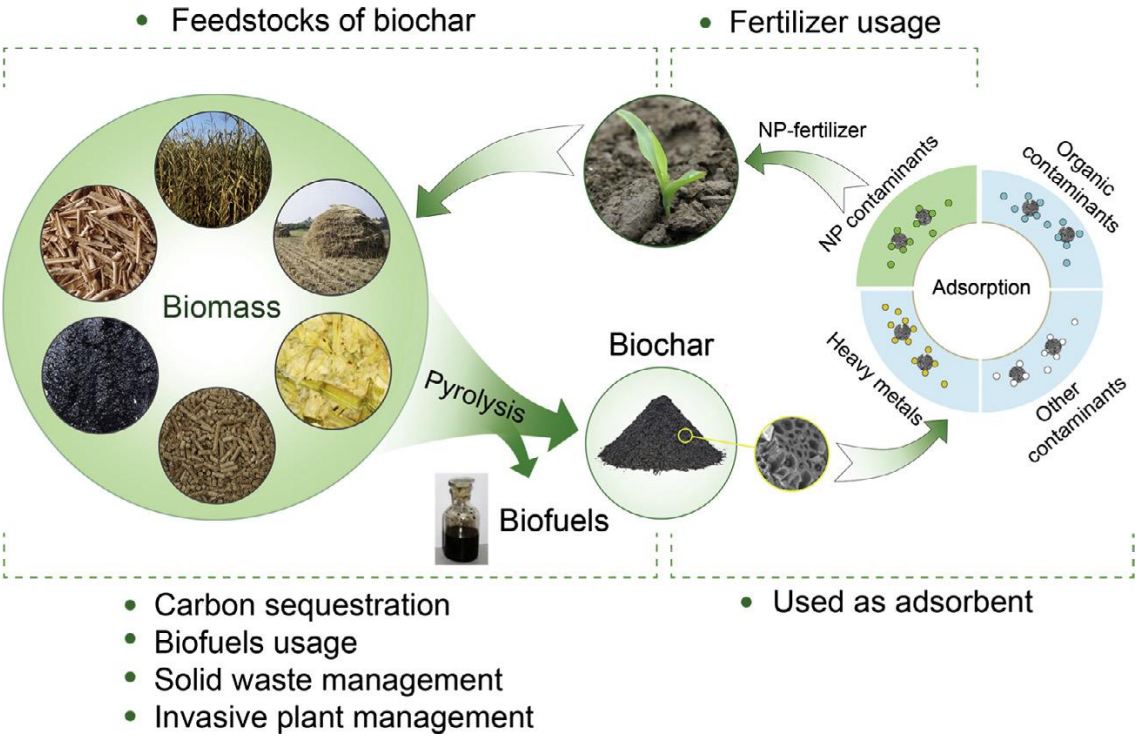

Figure 1. Possibilities of using chars as effective adsorbents of different pollutants in wastewater treatment[70] (reproduction under the kind written permission of Elsevier).

Water pollutants can be divided into two types: organic and inorganic compounds. Organic compounds include dyes, phenolics, pesticides, polynuclear aromatic compounds, anti-inflammatory compounds, hormones, antibiotics, among others. Although inorganic compounds can be of different types, in wastewaters they can be divided mainly in two groups: cations and anions[71]. Regarding inorganic pollutants which are the focus of the present work, there are 3 main mechanisms to remove metals from aqueous media by using chars:

(1) Pore filling – Ions are retained in the chars' pores through physical (electrostatic) sorption between the positively charged ions and the delocalised cloud of electrons associated with aromatic groups on the surface of the carbonaceous chars, creating cation-π interactions with the CC aromatic bonds. This merely affects the pollutant concentration in the aqueous solution;

(2) Precipitation – If the pH of the char is too alkaline or too acidic, the pH of the medium may change. By altering the pH of the medium, the metal speciation can be changed into insoluble forms and precipitation occurs;

(3) Adsorption – The chars' surface interacts with ions in aqueous solutions. According to Li et al.[79], ion adsorption can occur by five different ways (**Figure 2**):

(i) Surface precipitation – The chars' surface may contain some ions, such as phosphate and carbonate, which will interact with the ion in the aqueous solution and form insoluble compounds that will precipitate in the chars' surface;

(ii) Cation exchange – Gasification and pyrolysis chars may have high ash content, depending on the feedstock used[6]. These ashes are typically composed by Ca, Na, K, and Mg minerals if biomass is used as feedstock[79,80]. These cations can be replaced by the cation pollutants.

(iii) Complexation – If the chars' surface contains atoms with empty electron orbitals (for instance, oxygen-containing functional groups), the metal ions will be attracted to the chars' surface forming metallic complexes with functional groups.

(iv) Electrostatic attraction – If the chars' surface and metal ion are charged with opposing charges the metal will be attracted to the chars' surface by electrostatic forces. When the pH of the medium is lower than the pH_{pzc} of the char, char's surface will have positive charges, so anions will be attracted to char's surface. When the opposite occurs, i.e., the pH of the medium is higher than the pH_{pzc} of the char, char's surface will have negative charges, so cations will be attracted to char's surface.

(v) Reduction – Metal species are reduced by gaining electrons from oxygen surface functional groups or π-π electrons from the carbon aromatic structure of the char. The reduced metal species is then adsorbed.

Adsorption is an effective and economic method for wastewater treatment contaminated with metals. The adsorption process offers flexibility in design and operation, and in many cases will produce high-quality treated effluents. In addition, because adsorption is sometimes reversible, adsorbents may be regenerated by suitable desorption process.

Pyrolysis chars/activated chars from several feedstocks (**Table 1**) and specifically from rice wastes (**Table 2**), have been studied in the adsorption of several metal ions from aqueous solutions. However, no studies were found concerning the adsorption of metal ions by chars produced from the pyrolysis of rice waste blends.

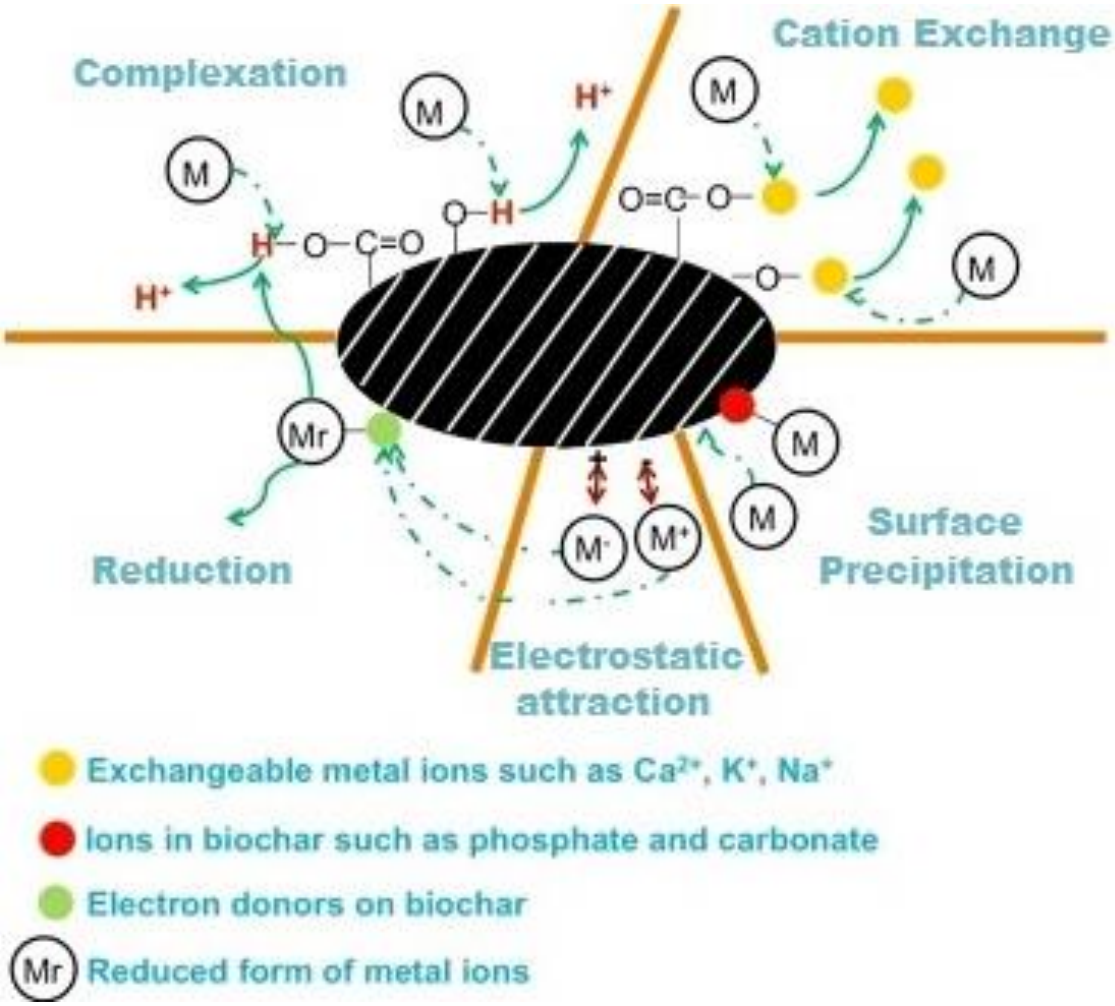

Figure 2. Adsorption mechanisms of metal ions by chars (adapted from Li et al.[79]).

Table 1. Bibliographic references on adsorption capacity of chars/activated chars from different feedstocks for the removal of metal ions from aqueous solutions.

Metal ion	Thermal process	Temperature (°C)	Feedstock	Activation/ Treatment	Adsorption capacity (mg g^{-1})	Reference
As(III)	Pyrolysis	400 + 450	Pine wood	No	1.20	Mohan et al.[81]
			Oak wood		5.85	
			Pine bark		12.15	
			Oak bark		7.40	
Cd(II)			Oak wood		0.37	
			Pine bark		0.34	
			Oak bark		5.40	

Table 1. (continuation)

Metal ion	Thermal process	Temperature (°C)	Feedstock	Activation/ Treatment	Adsorption capacity (mg g^{-1})	Reference
Cu(II)	Pyrolysis	700	Pinewood	No	4.46	Liu et al.[82]
Cu(II)	Pyrolysis	450	Hard wood	No	6.79	Chen et al.[83]
		600	Corn straw		12.52	
Zn(II)		450	Hard wood	No	4.54	
		600	Corn straw		11.00	
Cu(II)	Pyrolysis	400	Peanut straw	No	0.05 – 0.09	Tong et al.[84]
			Soybean straw		0.03 – 0.05	
			Canola straw		0.03 – 0.04	
Cu(II)	Pyrolysis	300 and 600	Orange waste	Chemically treated with HCl	4.921 and 0.422	Pellera et al.[23]
			Compost		7.937 and 3.384	
			Dried olive pomace		5.118 and 0.660	
Pb(II)	Pyrolysis	420	Pine, plastics and used tires	No	1.18 – 1.87	Bernardo et al.[85]
Co(II)	Pyrolysis	650	Almond shells	No	26.95 – 28.09	Kılıç et al.[86]
Ni(II)					20.00 – 22.22	
Cu(II)	Gasification	1000	Pine and spruce chips	No	10.3	Runtti et al.[68]
				Chemically activated with $ZnCl_2$	23.1	
Fe(II)				No	24.1	
				Chemically activated with $ZnCl_2$	20.5	
Ni(II)				No	5.6	
				Chemically activated with $ZnCl_2$	18.2	

Table 2. Bibliographic references on adsorption capacity of chars/activated chars from pyrolysis of rice wastes for the removal of metal ions from aqueous solutions.

Metal ion	Temperature (°C)	Feedstock	Activation/ Treatment	Adsorption capacity (mg g^{-1})	Reference
Al(III)	350, 500 and 700	Rice straw	No	9.58, 8.77 and 9.31	Qian and Chen[87]
			Oxidation with HNO_3 and H_2SO_4	5.94 – 12.8, 2.70 – 3.10 and 2.02 – 3.37	
Cd(II)	700	Rice bran	No	16.18	Jing and Yangsheng[88]
		Rice straw		60.61	
Pb(II)		Rice bran		33.00	
		Rice straw		126.58	
Cd(II)	350	Rice husk	No	7.81	Xu et al.[89]
Cu(II)				4.16	
Pb(II)				29.0	
Zn(II)				6.60	
Na^+	400, 600 and 800	Rice husk	No	35.2, 60.8 and 53.9	Rostamian et al.[90]
	400 and 600		Physical activation with steam	63.4 and 73.5	
	600		Chemical activation with KOH	104.8 – 158.0	
	600		Chemical activation with KOH followed by physical activation with steam	96.3 – 102.1	
Ni	550 and 700	Rice husk	No	6.87 and 10.2	Shen et al.[91]
Sr(II)	550	Rice straw	Washed with distilled water	198	Yakout and Elsherif[92]
Zn(II)	300 and 700	Rice straw	No	21.1 and 44.7	Dai et al.[93]

Regarding gasification chars/activated chars from different feedstocks, other than rice wastes, for metal removal, the number of studies available decreases significantly (**Table 1**). Author found no studies concerning the adsorption of metal ions by chars produced from the gasification of rice wastes or rice waste blends.

1.3.4 Activated carbons: activation processes and adsorption mechanisms

In order to improve its adsorption properties, activation processes can be performed over the gasification and pyrolysis chars. Two types of activations can be done: physical and/or chemical activations[94]. Physical activation involves the reaction between the char and an oxidizing gas at high temperatures. Chemical activation involves the impregnation of the char with chemical agents (dehydrating agents and/or oxidants) followed by heating under inert atmosphere. Also, physical and chemical activations can be used simultaneously (**Figure 3**).

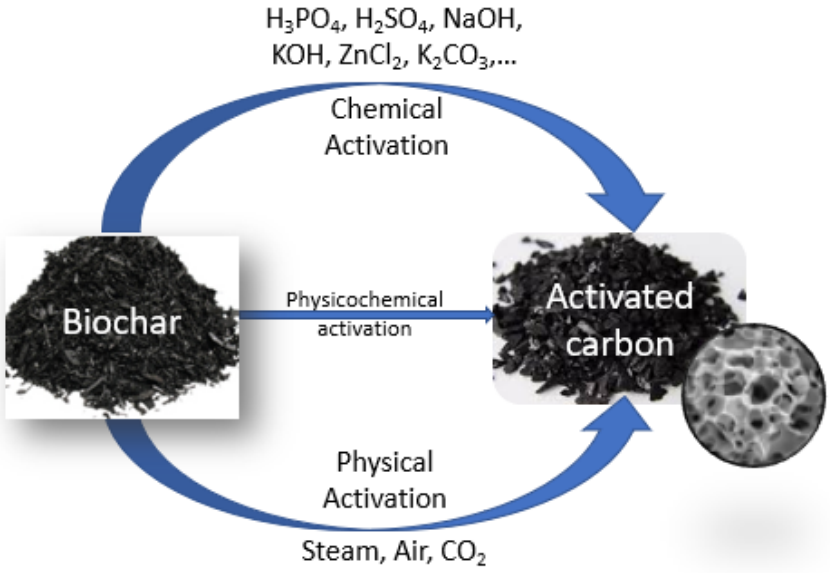

Figure 3. Schematic illustration of chars' activation processes.

1.3.4.1 Physical activation

The physical activation is used to increase the porosity of the char by removing some compounds that can be blocking the pores, for instance, some volatile matter that remained after the pyrolysis processes or tarry products (**Figure 4**), and at the same time the width of pores created during the pyrolysis process is enlarged. It involves a reaction between the char and an oxidizing gas, such as CO_2, steam, air or mixtures of both these gases[95].

Physical activation is a partial gasification of the char with the oxidizing agent, being carried out at temperatures usually above 800 °C. CO_2 has been used in many research works, because it is a clean gas, relatively easy to handle and the activation process is easily controlled at temperatures around 800 °C due to the low oxidation rate. In addition, when compared to other oxidizing agents, CO_2 activation provides greater uniformity of surface pores[76,96,97].

In order to add oxygenated groups (e.g. carboxyl groups, lactones, phenols, ketones, quinones, alcohols and esters) to the activated carbon's surface, chemical treatments by oxidation can be applied to the physically activated carbon. This type of treatments makes the material more

hydrophilic and acidic, lowering its pH_{pzc} and increasing its density of negative charges on the surface. Several reagents have been used as oxidants: HNO_3, HSO_4, NaClO, $KMnO_4$, $Cr_2O_7^{2-}$, H_2O_2, transition metals and oxidizing gas mixtures. Oxidation with HNO_3 allows the introduction of a small amount of functional groups with nitrogen, although most studies focus on the introduction of oxygen-containing functional groups, mainly carboxyl groups, lactones and phenols[97–100].

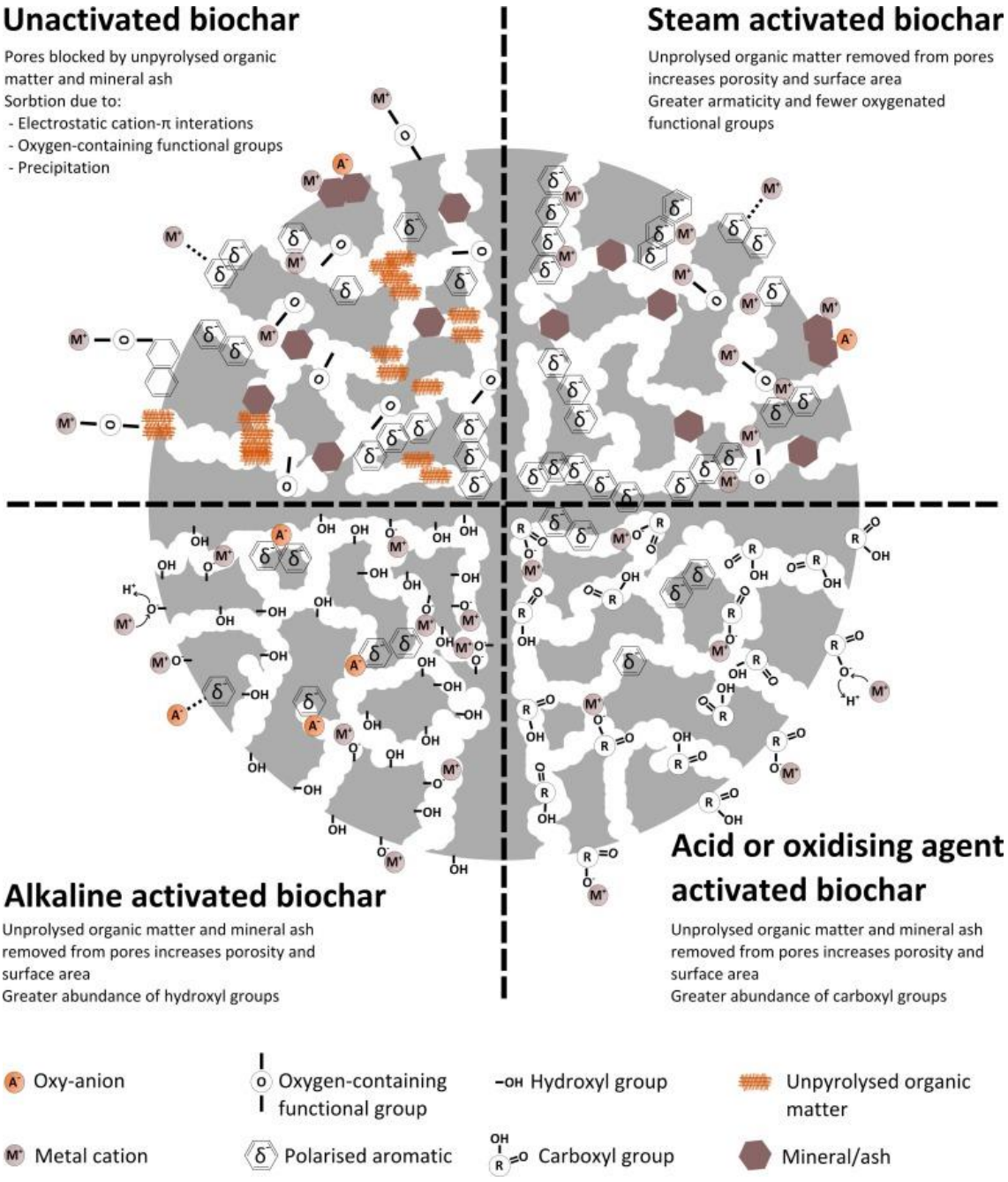

Figure 4. Adsorption mechanisms of metal cations on raw biochar and on physically and chemically activated biochar[101] (reproduction under the kind written permission of Elsevier).

1.3.4.2 Chemical activation

The chemical activation is used to increase the porosity and surface area of the char, and to increase the functional groups present on the char's surface (**Figure 4**). Several functional groups (e.g. carboxyl, hydroxyl, phenol, etc.) can bind chemically with the metal ions present on the solution and remove them[101]. Chemical activation has the advantage of producing activated carbons with high surface area, at lower temperatures than physical activation (400-800 °C)[95], but the washing step to remove the residual reactants and inorganic matter (ash) is a disadvantage[102].

Impregnation of chars with metallic chlorides, such as $ZnCl_2$, allow obtaining activated carbons with a well-developed meso and microstructures. Alkaline treatments are commonly performed by metal hydroxides, such as KOH or NaOH, which increase the hydroxyl functional groups present on the char's surface and provide activated carbons with a narrow pore size distribution and well-developed porosity. On the other hand, acidic treatments provide more carboxylic groups. Among the acidic activators currently used (H_3PO_4, H_2SO_4, HNO_3), H_3PO_4 is one of the most widely tested, because in addition to introducing a relatively high amount of stable phosphoric complexes, which contribute to a higher oxidation resistance and high acidity added to the char's surface, it also provides very high surface areas at relatively low temperatures (400-500 °C)[76,96,97]. The main problem is that H_3PO_4 is produced from phosphoric rocks which are critical raw materials for agriculture sector due to the world limited resources.

1.3.5 Significance of chromium and tungsten recovery

In 2013, the European Commission (EC) analysed 44 non-energetic and non-agricultural raw materials, in order to select the most critical raw materials (CRM) regarding their economic importance and supply risk to Europe. In 2014, the EC published a list of 20 CRM for Europe according to those two factors (**Figure 5**)[103].

According to this list, chromium (Cr) and tungsten (W) were two of the raw materials in the first four initial positions with the highest economic importance (**Figure 5**). In addition, the global supply of Cr and W coming from the EU was less than 3%[103]. Although Cr was removed from the revised CRM list in 2017[4], since its supply risk decreased slightly below the threshold, it is still one of the raw materials with the highest economic importance. In this context, the recovery of Cr from secondary raw materials and wastewaters is extremely important.

From all the listed raw materials, chromium is the most problematic in what concerns environmental issues[104]. Chromium occurs in aqueous environments mainly in the trivalent, Cr(III), and hexavalent, Cr(VI), oxidation states. Cr(III) is widely used in metal finishing, wood preservation, textile production and leather tanning, and therefore is present in industrial effluents produced in developed and developing countries[105].

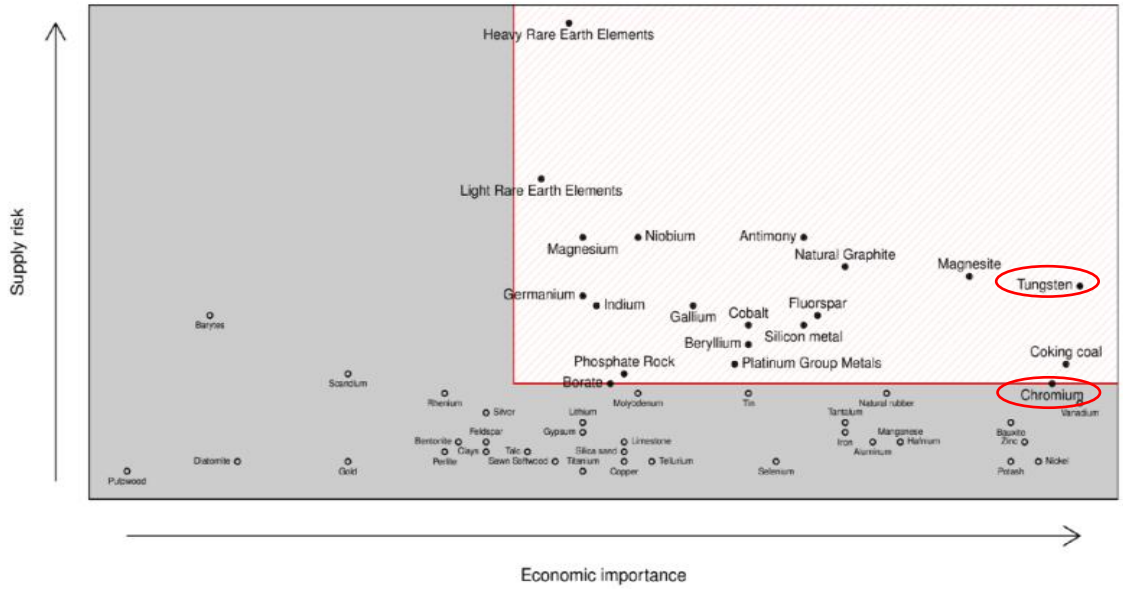

Figure 5. Overall results of the 2013 assessment for the critical raw materials to Europe[103].

On the other hand, it is known that tungsten is a metal widely used in various applications (halogen lamps, armaments, hard materials, jewellery, etc.). Lately, due to its favourable properties, tungsten has been a first choice for several high-tech structural applications[106]. However, the EU supplying-dependence from third countries, namely China, is enormous (91%)[103]. Therefore, tungsten recovery from secondary raw materials and wastewaters is also mandatory.

Based on this list of CRM, EC has reinforced the need to find new alternative methods and technologies to recover CRM from secondary raw materials and wastewaters in which they can be found in high concentrations. These alternative methods and technologies must be economically and environmentally sustainable.

In this framework, the use of chars from co-pyrolysis and co-gasification of rice waste streams to adsorb and recover Cr and W from wastewaters is an important research area to be explored. This strategy adds an economic high value to by-products (chars) of thermal processes, contributing for their valorisation. Simultaneously, it contributes to the EC objective of recovering critical raw materials to Europe.

Concerning the scientific data on Cr(III) removal, there are already some studies on the adsorption of this metal onto chars/activated chars from pyrolysis of biomass (**Table 3**); however, the number of papers decreases dramatically when rice wastes are used as feedstocks to produce the chars/activated chars (**Table 4**). Regarding the adsorption of Cr(III) by chars from biomass gasification, or from pyrolysis and gasification of rice waste blends, the only study available was performed by the team in which this PhD thesis was performed[24].

Table 3. Bibliographic references on the adsorption capacities of chars/activated chars from pyrolysis of different feedstocks for Cr(III) removal from aqueous solutions.

Temperature (°C)	Feedstock	Activation/Treatment	Adsorption capacity (mg g^{-1})	Reference
800	*Eucalyptus grandis* wood sawdust	Physically activated with direct CO_2 and oxidized with HNO_3	17.5	Milich et al.[107]
		Physically activated with partial CO_2 and oxidized with HNO_3	25.5	
		Physically activated with partial air and oxidized with HNO_3	29.0	
400	Peanut straw	No	25.0	Pan et al.[22]
	Soybean straw		17.2	
	Canola straw		14.6	
500	Sugarcane pulp	No	15.9	Yang et al.[108]
300	Organic fraction of municipal solid wastes	No	42.4	Agrafioti et al.[109]
	Sewage sludge		30.1	
900	Municipal sewage sludge	No	20 – 30	Chen et al.[110]

Table 4. Bibliographic references on the adsorption capacities of chars/activated chars from pyrolysis of rice wastes for Cr(III) removal from aqueous solutions.

Temperature (°C)	Feedstock	Activation/Treatment	Adsorption capacity (mg g^{-1})	Reference
400	Rice straw	No	14.0	Pan et al.[22]
250 – 700	Rice husk	No	4.61 – 10.6	Vassileva et al.[111]
300	Rice husk	No	15.1	Agrafioti et al.[109]
100 – 700	Rice straw	Washed with distilled water and sonicated	2.4 – 6.5	Qian et al.[112]

Regarding tungsten (W), some adsorption studies of W(VI) (usually in the form of tungstate – WO_4^{2-}) from aqueous solutions have been performed, mainly by using mineral adsorbents (**Table 5**). Concerning carbon-based materials there is only one work dealing with carbon cloth[113]. This C-cloth was obtained by pyrolyzing a phenolic C-film polymer between 800 and 900 °C in N_2. Two

different treatments were made to the adsorbent: i) a distilled water washing to avoid leaching from the adsorbent, and ii) an acidic treatment with H_2SO_4 for the modification of surface functional groups and porous structures. The water treated C-cloth and the acid treated C-cloth obtained adsorption capacities of 154 and 208 mg g^{-1}, respectively.

Table 5. Bibliographic references on the adsorption capacities of different adsorbents for tungstate from aqueous solutions.

Adsorbent	Activation/Treatment	Adsorption capacity (mg g^{-1})	Reference
Fly ash	No	4.72 – 7.62	Ogata et al.[114]
	Hydrothermal treatment	21.72 – 74.12	
Fly ash	No	11.25	Ogata et al.[115]
	Hydrothermal treatment	43.45 – 62.34	
Fly ash	No	6.76	Ogata et al.[116]
	Hydrothermal treatment	36.54	
Fe-Mg type hydrotalcite	No	14.4 – 86.2	Ogata et al.[117]
Al-Mg type hydrotalcite		22.0 – 35.7	
Kaolinite	No	6.53	Ruiping et al.[118]
Sepiolite	Treated with H_2SO_4 followed by heat treatment	5.3 – 48.3	Wang et al.[119]
Montmorillonite clay	No	2.11 – 5.54	Gecol et al.[120]
	Coated with chitosan	11.4 – 23.9	
Montmorillonite clay	Coated with chitosan	62.11	Gecol et al.[121]
Pyrite	Washed with deoxygenated water and deoxygenated HCl	4.65 – 13.20	Cui and Johannesson[122]
Goethite	No	9.16 – 18.55	
Montmorillonite clay	Organically modified with quaternary ammonium salts	29.4 – 68.0	Muir et al.[123]
Ferrihydride	No	0.607 – 37.0	Sun and Bostick[124]
Silica gel	Coated with 1,8-diaminonaphthalene formaldehyde resin and treated with HCl	55.32 – 63.27	Dinker et al.[125]
Silica polyamine composites	Functionalized with phosphorus acid and Zr(IV) immobilization	67 – 89	Kailasam and Rosenberg[126]
Polymer based adsorbents	No	82 – 95	

1.3.6. Adsorption in fixed-bed column systems

Most studies regarding adsorption of different elements are processed using batch assays, as this type of system is cheap and easy to operate[127,128]. However, since in industrial processes, continuous systems are preferred in purification processes including adsorption[129,130], the data obtained under batch conditions are hardly applied to continuous treatment processes operating through column systems[131]. Fixed-bed column systems allow continuous flow processes by means of adsorption/regeneration cycles. After column saturation, the adsorbent may be regenerated using suitable solutions[132], which in the case of metallic contaminants acids such as HCl, HNO_3, H_2SO_4, chelating agents, among other, are usually used[133–136]. This allows cyclic sorption/desorption processes, as it makes the best use of concentration, osmotic pressure and pH as the driving forces for sorption/desorption and allows more efficient utilization of the sorbent capacity[137].

Another advantage of the fixed-bed column systems is the relatively easy scaling up from a laboratory scale system. The stages in sorption/desorption protocol can also be automated, and high degrees of purification can often be achieved in a single step process. A large volume of wastewater can be continuously treated, using a defined mass of adsorbent in the column[137].

Still, there are some disadvantages in column systems, namely adsorbent attrition, feed channelling, and mass transfer limitations[128].

The performance of a fixed-bed column is studied by the effluent concentration along time. This relation is represented by breakthrough curves [128,138], as represented in **Figure 6**.

The surface of a fixed-bed column, where the adsorption occurs is the so called “mass transfer zone”. When the effluent reaches the column, the mass transfer zone goes from 0 to 100% of the initial adsorbate concentration, i.e., from total removal to total saturation. The breakthrough curves are usually expressed as the ratio between the adsorbate concentrations in the outflow and inflow (C_i/C_0) of the column, as a function of time or volume of the effluent, for a fixed bed height [128,138].

The breakthrough time, t_r, is obtained when the adsorbate concentration in the effluent reaches a certain value, generally related to the permitted limit value for the studied adsorbate in a wastewater. t_r makes possible to determine the volume of the effluent that can be treated up to the permitted limit value. On the other hand, when the concentration in the effluent is higher than 95% of the initial adsorbate concentration the saturation time, t_s, is reached[128,138].

Studies conducted in fixed-bed columns under continuous flow indicated that the adsorption process is influenced by several parameters, such as the initial adsorbate concentration, flow of the effluent, and mass of adsorbent in the column, temperature and pH [129,138].

As seen in **Table 6** some biomasses have already been used by different authors into Cr(III) removal in column assays. However, very few studies have been performed using biochars and no studies were found on chars produced from rice wastes into Cr(III) removal in column assays.

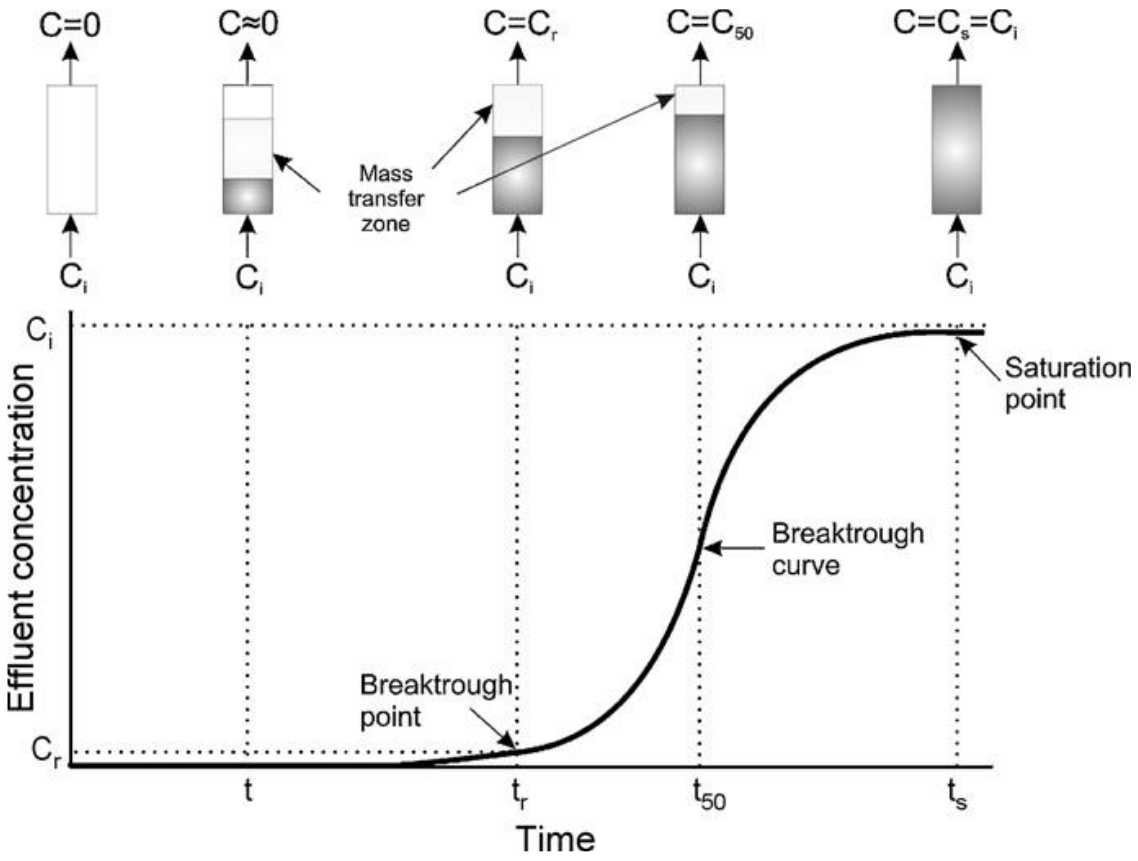

Figure 6. Representation of a typical breakthrough curve[8] (reproduction under the kind written permission of Elsevier).

Table 6. Bibliographic references on the adsorption capacities of different adsorbents for Cr(III) removal

Material	Temperature (°C)	Adsorption capacity (mg g^{-1})	Reference
Wood biochar	800 - 900	45.5 – 67.7	Zhang et al.[139]
Caltrop shell biochar		62.3 – 78.5	
Brown seaweed *Sargassum sp.*	n.a.	60.3 - 68.1	Cossich et al.[132]
Modified pin bark	n.a.	30.96	Arim et al.[135]
Brewer's spent grain	n.a.	11.14 - 15.58	Ferraz et al.[140]
Orange waste	n.a.	12.5	Pérez Marín et al.[130]
Improved hemp fibres	n.a.	6.894 - 10.781	Tofan et al.[141]
Wheat straw	n.a.	5.58 – 9.98	Farooq et al.[131]
Palm flower	n.a.	5.878	Elangovan et al.[142]
Olive stone	n.a.	0.331 - 0.806	Calero et al.[138]

n.a.: not applicable.

2. ORIGIN AND PROPERTIES OF CHARS USED IN THE Cr(III) REMOVAL ASSAYS

The results presented in this chapter were published, partially or completely, in the following scientific publications:

Papers:

D. Dias, N. Lapa, M. Bernardo, D. Godinho, I. Fonseca, M. Miranda, F. Pinto, F. Lemos, Properties of chars from the gasification and pyrolysis of rice waste streams towards their valorisation as adsorbent materials, *Waste Management*, 65 (2017) 186–194.
(doi: 10.1016/j.wasman.2017.04.011)

D. Dias, N. Lapa, M. Bernardo, W. Ribeiro, I. Matos, I. Fonseca, F. Pinto, Cr(III) removal from synthetic and industrial wastewaters by using co-gasification chars of rice waste streams, *Bioresource Technology*, 266 (2018) 139-150.
(doi: 10.1016/j.biortech.2018.06.054)

Oral Presentations:

D. Dias, N. Lapa, M. Bernardo, D. Godinho, I. Fonseca, H. Lopes, M. Miranda, F. Pinto, F. Lemos, Bed chars from the co-gasification of rice wastes: chemical and ecotoxic properties, *The Energy & Materials Research Conference (EMR2015)*, 25-27 February 2015, Madrid, Spain.

D. Dias, W. Ribeiro, N. Lapa, M. Bernardo, I. Matos, I. Fonseca, F. Pinto, Chars from co-gasification of rice wastes as Cr(III) removal agents, *4th International Conference "WASTES: Solutions, Treatments and Opportunities"*, 25-26 September 2017, Porto, Portugal.

Poster:

D. Dias, M. Bernardo, F. Pinto, N. Lapa, Recovery of high-value metals through adsorption onto chars produced from waste streams of rice production: the case-study of Cr^{3+}, *1st Scientific Meeting of the Doctoral Programme in Sustainable Chemistry (PDQS)*, 26 September 2016, Aveiro, Portugal.

2.1 Introduction

In this chapter, the chars used in the Cr(III) removal assays resulting from the gasification and pyrolysis of rice wastes were characterised. The rice waste streams (RS, RH and PE) that were used as feedstocks in the gasification and pyrolysis assays were also fully characterised.

2.2 Materials and methods

2.2.1 Origin and characterisation of feedstocks

RS samples were collected from the rice fields of Orivárzea Company, located in Ribatejo region, after the field drainage and rice harvesting by cutting straw of an area of about 10 000 m^2. RH samples were collected from the silos of dried rice husk in Orivárzea rice processing mill. PE bags were supplied by farmers after rice sowing.

These feedstocks were submitted to the following characterisation assays:

a) Proximate analysis – It comprised the quantification of moisture content (M) (105 °C, for 2 h, in open vessels - EN 14774-1), volatile matter (VM) (900 °C, for 7 min, in closed vessels - EN 15148), and ashes (Ash) (550 °C, for 120 min, in open vessels - EN 14775) that were determined by gravimetric method in a CEM microwave furnace MAS 7000; fixed carbon (FC) was determined as follows: Fixed-C = 100% – (M + VM + Ash).

b) Elemental analysis – It comprised the quantification of CHNS (ASTM D 5373 for C, H, N, and ASTM D4239 for S) in a LECO CHN 2000 analyser and in an Elemental Thermo Finnigan analyser.

c) Thermogravimetric analysis (TGA) – It was determined as the sample mass loss in argon atmosphere (20 cm^3 min^{-1}), from 30 °C to 850 °C, with a heating rate of 10 °C min^{-1} in a Setaram Labsys EVO thermogravimetric analyser.

d) Mineral content – An acidic digestion based on the EN 15290 standard was performed in a Milestone ETHOS 1600 microwave heating system by digesting 0.5 g of sample with 3 mL H_2O_2 (30% v/v), 8 mL HNO_3 (65% v/v) and 2 mL HF (40% v/v) at 190 °C for 20 min. Then, HF was neutralised by adding 20 mL H_3BO_3 (4% w/v) to the solution and digested it again at 150 °C for 15 min. The solution was then filtered through Whatman® 41 ashless filter papers (20-25 µm) and 20 metals and metalloids were quantified in the acidic eluates by atomic absorption spectrometry (AAS) in a Solaar S series AA spectrometer (Thermo Scientific) or a Zeenit 700 spectrometer, or by Inductively Coupled Plasma-Atomic Emission Spectrometry (ICP-AES) in a Horiba Jobin-Yvon Ultima, equipped with a 40.68 MHz RF generator, Czerny-Turner monochromator with 1.00 m (sequential), and an autosampler AS500. The metals and metalloids quantified were the following: aluminium (Al), arsenic (As), barium (Ba), calcium (Ca), cadmium (Cd), chromium (Cr), copper (Cu), iron (Fe), mercury (Hg), potassium (K), magnesium (Mg), molybdenum (Mo), sodium (Na), nickel (Ni), lead (Pb), antimony (Sb), selenium (Se), silicon (Si), titanium (Ti) and zinc (Zn).

e) Mobility of chemical species – These assays were performed by submitting the samples to a leaching test for 24 h with deionized water under a liquid/solid ratio (L/S) of 10 L kg^{-1} (EN 12457-2). The aqueous eluates were filtered through Whatman® ME 25/21 ST membrane filters (0.45 µm) and characterised for pH (Hanna Instruments edge® HI 2002 pH meter), conductivity (Thermo Scientific Orion Star A215 conductivity meter) and the same 20 metals and metalloids referred in d). Before the quantification of metals and metalloids by AAS or by ICP-AES (same equipment referred in d)), the eluates were acidified with HNO_3 (65%) down to pH < 2.00. The relative mobility (%) of chemical elements was determined by equation 2.1:

$$\text{Relative mobility} = \frac{\text{Concentration in aqueous eluates}}{\text{Concentration in acidic eluates}} \times 100 \quad (2.1)$$

d) Ecotoxic level – The aqueous eluates produced in e) were also characterised for the bioluminescence inhibition of the bacterium *Vibrio fischeri* (Microtox assay) (ISO 11348-3). The ecotoxic results were expressed as the effective concentration (% v/v) of the eluate that promotes 50% decrease in the bioluminescence of *V. fischeri*, after 30 minutes of exposure (EC_{50}–30 min).

2.2.2 Gasification and pyrolysis assays

Before the gasification and pyrolysis assays, different blends of RH, RS and PE were chosen. These blends were defined according to the criteria of maximizing the production of the liquid (pyrolysis assays) and gas (gasification assays) fractions, as the main objective of Ricevalor project was to maximize the most energetically interesting fractions. Afterwards, some chars were selected, considering the gasification and pyrolysis assays that were carried out under experimental conditions that allow obtaining high char production yield. The conditions of the gasification and pyrolysis assays of the selected chars are shown in **Table 7** and **Table 8**, respectively.

Table 7. Conditions of the gasification assays.

Gasification assay code	Fuel blends (% w/w)			Fuel flow (g daf min^{-1})	T (°C)	Gasification agent	ER	Steam flow (g min^{-1})
	RH	RS	PE					
G1	100	0	0			Air		
G2	80	0	20			Air		
G3	100	0	0	5	850	O_2	0.2	5
G4	80	0	20			O_2		
G5	50	50	0			O_2		

RH: rice husk; RS: rice straw; PE: polyethylene; daf: dry ash-free basis; ER: equivalence ratio

Table 8. Conditions of the pyrolysis assays.

Pyrolysis assay code	Fuel blends (% w/w)			Reaction conditions		
	RH	RS	PE	P (MPa)	T (°C)	t (min)
P1	50	0	50	0.6	390	35
P2	20	0	80	0.6	390	35
P3	0	20	80	0.2	430	10

RH: rice husk; RS: rice straw; PE: polyethylene; P: pressure; T: temperature; t: reaction time at temperature T

A bubbling fluidized bed gasifier (**Figure 7a**) with 0.08 m internal diameter and 1.5 m height was used in the gasification assays[143]. Previously washed fine sand was used as bed material. The syngas produced was passed through a cyclone, a gas condensation system and filters before being collected for further characterisation. Each gasification experiment lasted between 90 and 120 min. The study of syngas composition was the main objective of other works from LNEG[16,144]. The mixed bed material – a mixture of sand and chars – was collected at the bottom of the gasifier and sieved to separate the chars from sand. The chars were then stored in air-tight reservoirs.

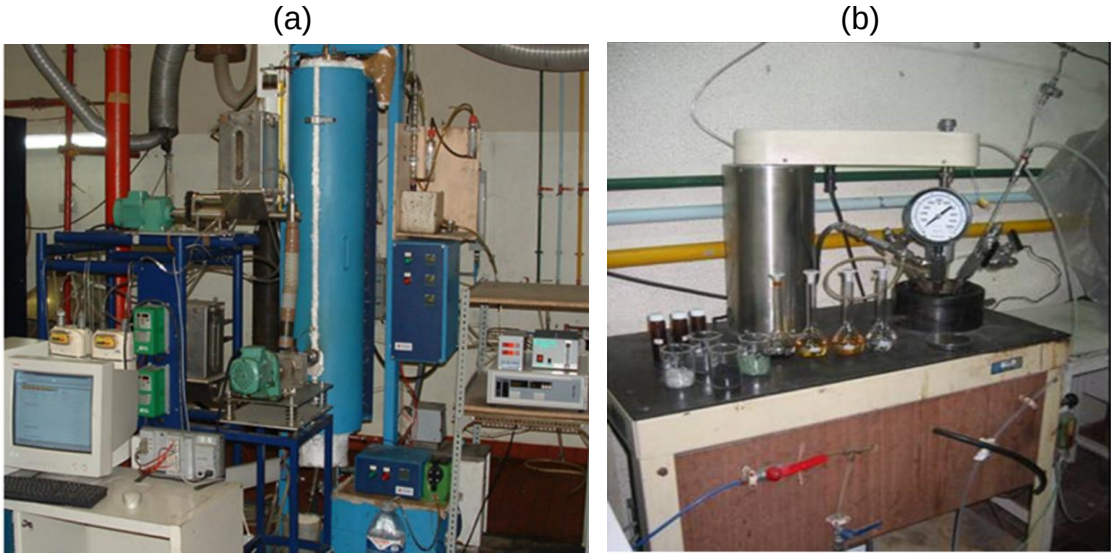

Figure 7. (a) Bench-scale gasifier and (b) bench-scale pyrolysis reactor.

The pyrolysis assays were performed in a 1 L batch reactor (**Figure 7b**) made of Hastelloy C276 (Parr Instruments)[44]. At the end of the pyrolysis experiments, the chars were separated from the liquid fraction through settling and extraction with hexane (hexane/char ratio: 17 mL g^{-1}) in a Soxhlet extractor, during 3 h. The chars were also stored in air-tight vessels up to their characterisation.

After the gasification and pyrolysis assays, all chars were milled and sieved to <100 μm.

2.2.3 Characterisation of chars

After the gasification and pyrolysis assays, all chars were characterised for the following assays:

a) Proximate analysis – The parameters were the same as described in section 2.2.1, but the temperatures were as defined in ASTM D1762 for moisture content (105 °C), volatile matter (950 °C), and ashes (750 °C). Fixed-C was calculated as described above for feedstocks;

b) Elemental analysis – The same as described in section 2.2.1;

c) Mineral content – The same as described in section 2.2.1;

d) Textural analysis – Surface area and pore volume were determined through the adsorption-desorption isotherms of N_2, at 77 K, after sample degasification overnight under vacuum conditions, at 150 °C. An Accelerated Surface Area and Porosimetry system (ASAP) 2010 Micromeritics apparatus was used for this characterisation. The following parameters were calculated: (i) apparent surface area (S_{BET}) through the Brunauer, Emmett and Tellers' (BET) equation; (ii) total pore volume (V_{total}) by the amount of nitrogen adsorbed at the relative pressure $p/p_0 = 0.99$; (iii) micropore volume (V_{micro}) by the t-plot method; (iv) mesopore volume (V_{meso}) by the difference between V_{total} and V_{micro}.

The experimental data obtained in these characterisations were used for the selection of a char from gasification and a char from pyrolysis that presented the best potential properties to be used as an adsorbent material in Cr(III) removal assays.

2.2.4 Additional characterisation of chars selected for the Cr(III) removal assays

The chars selected to be used in the Cr(III) removal assays were further tested for the following characterisations:

a) Mobility assessment of chemical species and ecotoxic level – The same as described in section 2.2.1;

b) pH at the point of zero charge, pH_{pzc} – 0.1 M NaCl solutions with pH values between 2 and 12 were prepared. The pH was adjusted with 0.1 M NaOH and 0.1 M HCl solutions. The pH values were measured in a Hanna Instruments edge® HI 2002 pH meter. 0.1 g of char was added to 20 mL of each 0.1 M NaCl solution. The assays were performed in an Infors AG AK 82 roller-table agitator, under constant mixing of 150 rpm, for 24 h. The pH_{pzc} value corresponds to the plateau of the curve pH_{final} *vs* $pH_{initial}$.

2.3 Results and discussion

2.3.1 Properties of feedstocks

2.3.1.1 Proximate and elemental analyses

Volatile matter was the main fraction in all feedstocks (**Table 9**), being significantly higher for the synthetic polymer (PE), which is directly linked to the higher heating value of this feedstock. RH and RS also showed significant contents of both moisture and ashes, which are typical values for these types of biomasses[15,19,145].

Table 9. Proximate and elemental analyses of feedstocks.

Parameter	Feedstocks		
	RH	RS	PE
Proximate analysis (% w/w ar)			
Moisture content	12.28	22.88	0.66
Volatile matter	64.88	50.53	98.65
Ashes	14.34	21.98	0.60
Fixed carbon	8.50	4.61	0.04
Elemental analysis (% w/w ar)			
C	49.20	53.30	85.10
H	2.20	7.30	14.30
N	0.40	1.30	< 0.20
S	0.06	0.10	< 0.03

ar: as-received basis

2.3.1.2 TGA

The thermal degradation of RH and RS (**Figure 8**) can be divided into three steps: 1) the weight loss between 50 °C and 100 °C (10-15% w/w), which was mainly due to water evaporation, 2) the significant weight loss (about 40% w/w) from 250 °C to 380 °C, which was due to thermal degradation of hemicellulose and cellulose, and 3) the weight loss (approximately 30% w/w) between 400 °C and 850 °C, which was related to the degradation of cellulose and lignin[146]. At 850 °C, the carbonaceous residue – char – at the end of TGA was approximately 19% w/w for RH and 12% w/w for RS.

The highest carbonaceous residue yield obtained with RH must be related to the highest lignin fraction present in this material[147]. Lignin is the main source of carbonaceous residue, as its individual decomposition is responsible for approximately 40-50% w/w of this residue yield. Hemicellulose decomposition contributes to approximately 20-30% w/w of the carbonaceous residue yield, while cellulose decomposition only yields for about 10% w/w[146,148].

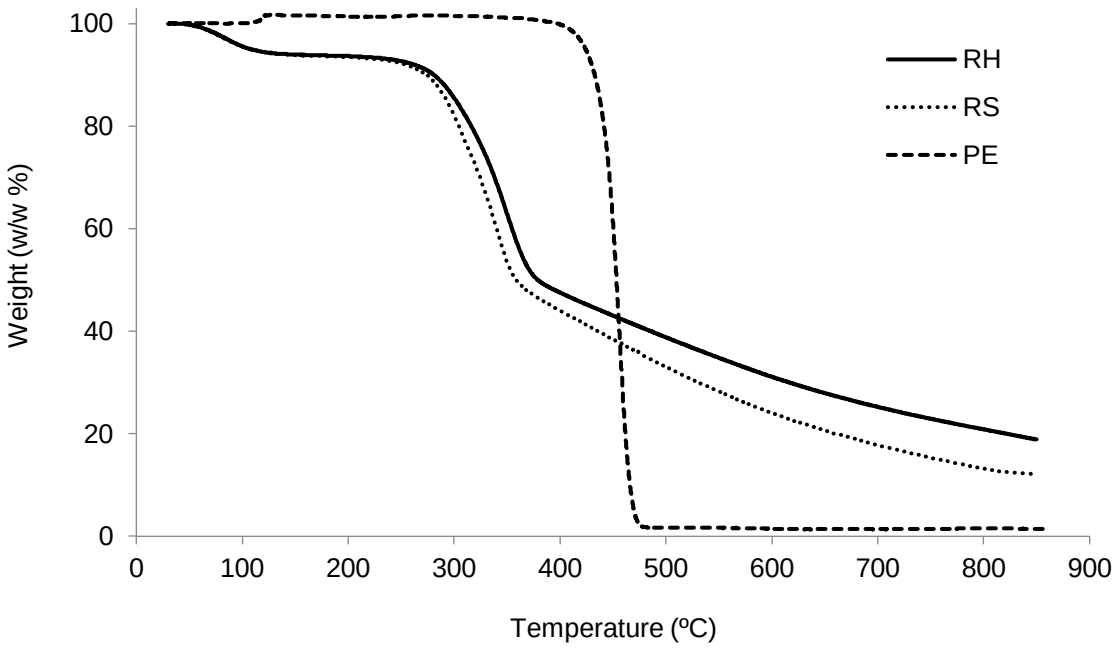

Figure 8. TGA of rice husk (RH), rice straw (RS) and polyethylene (PE).

TGA of PE indicated that its thermal degradation begins at approximately 400 °C and is almost completed (> 98% w/w) at approximately 480 °C. The carbonaceous residue at 480 °C is less than 2% w/w of the initial mass, which is in agreement with the percentages of ash and fixed-C determined for this material (**Table 9**).

2.3.1.3 Mineral content

The mineral content of the three feedstocks is showed in **Table 10**.

Si was the common major element present in the rice-derived materials. It is commonly known the high content of this element in RH and RS[15,145].

Although with significantly lower concentrations than Si, alkaline and alkaline-earth metals (AAEMs), as well as aluminium were also present with significant amounts in the feedstocks, particularly in RH and RS. In general, the mineral content of RS was higher than for RH, which agrees with the higher ash content of RS (**Table 9**). PE presented the lowest mineral content, although a remark must be done to the high concentration of Ti, due to the current use of titanium dioxide in this polymer as a pigment[149].

These results are in line with those reported in the literature. For RH, Tavlieva et al.[150] reported similar concentrations for Si (103778 mg kg^{-1} db) and Tarley and Arruda[151] reported similar concentrations of K (2572 ± 67 mg kg^{-1} db) and Ca (1434 ± 286 mg kg^{-1} db), but a lower concentration of Na (961 ± 106 mg kg^{-1} db). For RS, Liu et al.[152] found similar concentrations of K (8200 mg kg^{-1}), Ca (2128 mg kg^{-1}) and Mg (2072 mg kg^{-1}), but also a lower concentration of Na (2072 mg kg^{-1}).

Table 10. Mineral content of feedstocks (mg kg^{-1} db; $\overline{X}$ ± σ).

Chemical element	RH	RS	PE
Si	129 137 ± 9637	232 459 ± 22 331	1 349 ± 114
Na	7 898 ± 762	10 352 ± 896	3 962 ± 340
K	3 345 ± 308	9 991 ± 102	497 ± 43
Al	5 588 ± 515	9 148 ± 877	3 963 ± 33
Ca	875 ± 2	3 943 ± 377	538 ± 14
Mg	889 ± 88	1 614 ± 147	69.4 ± 1.5
Ti	< 336	492 ± 44	8 405 ± 505
Fe	257 ± 19	1 778 ± 122	75.2 ± 6.7
Ba	113 ± 11	154 ± 15	< 94.3
Zn	52.6 ± 5.1	53.8 ± 5.0	< 11.2
Pb	< 50.3	< 50.3	< 50.3
Mo	< 49.3	< 49.3	< 49.3
Cr	< 29.5	37.4 ± 1.4	< 29.5
Ni	< 20.9	< 20.9	< 20.9
Cd	< 16.1	< 16.1	< 16.1
Cu	< 13.6	< 13.6	< 13.6
Sb	13.6 ± 1.3	11.8 ± 1.0	0.373 ± 0.047
Hg	2.53 ± 0.20	1.53 ± 0.15	< 0.707
Se	< 0.458	< 0.458	< 0.458
As	< 0.276	< 0.276	0.863 ± 0.084

db: dry basis; $\overline{X}$ ± σ: average ± standard deviation.

2.3.1.4 Mobility test

Many of the elements present in the feedstocks, especially AAEMs, are involved in reactions leading to ash slagging and fouling in thermal systems, which negatively affect their performance[152]. Moreover, they can be retained in the chars produced during gasification and pyrolysis, affecting their chemical properties and conditioning the valorisation routes; for example, the retention of some elements (Ca, Mg, Na, K, etc) can play an important role in ion exchange capacity of a char used in adsorption processes.

To assess the mobility of these elements from the feedstocks, a water leaching test was performed, and the eluates were analysed for several chemical parameters. **Table 11** shows the chemical characterisation of the feedstock eluates. The mobility of chemical species was calculated relatively to the mineral content obtained in microwave-assisted digestion.

In general, the mobility of minerals was low. K was the exception, with concentrations of 1580 mg kg^{-1} db for RH and 3907 mg kg^{-1} db for RS, which corresponds to a solubility of 47.2% and 39.1%, respectively. Ca, Si, Na and Mg were also found in the eluates of RH and RS, but in much lower concentrations.

Table 11. Chemical characterisation of aqueous eluates of feedstocks and mobility of chemical elements relatively to the mineral content (relative mobility) (all eluate concentrations are expressed as $\overline{X}$ ± σ in mg kg^{-1} db, except for conductivity that is expressed in µS cm^{-1} and for pH that is expressed in Sørensen scale).

Element/ Parameter	RH		RS		PE	
	Eluate	Relative mobility (%)	Eluate	Relative mobility (%)	Eluate	Relative mobility (%)
K	1 580 ± 69	47.2	3 907 ± 210	39.1	< 0.604	< 0.121
Ca	172 ±17	19.7	676 ± 49	17.1	3.37 ± 0.26	0.625
Si	352 ± 35	0.273	379 ± 30	0.163	< 50.3	< 3.73
Na	231 ± 10	2.93	313 ± 28	3.03	< 0.654	< 0.017
Mg	213 ± 20	23.9	196 ± 1	12.1	4.23 ± 0.37	6.09
Ti	< 37.1	n.a.	< 37.1	< 7.54	< 37.1	< 0.442
Fe	8.78 ± 0.85	3.41	41.3 ± 0.5	2.32	< 3.02	< 4.02
Al	< 19.4	< 0.347	27.2 ± 0.6	0.297	< 19.4	< 0.490
Ba	< 10.4	< 9.26	< 10.4	< 6.78	< 10.4	n.a.
Pb	< 6.51	n.a.	< 6.51	n.a.	< 6.51	n.a.
Mo	< 6.38	n.a.	< 6.38	n.a.	< 6.38	n.a.
Zn	4.65 ± 0.40	8.83	5.73 ± 0.57	10.6	< 0.654	n.a.
Ni	< 4.10	n.a.	< 4.10	n.a.	< 4.10	n.a.
Cr	< 3.26	n.a.	< 3.26	< 8.70	< 3.26	n.a.
Cu	< 2.67	n.a.	< 2.67	n.a.	< 2.67	n.a.
Cd	< 2.08	n.a.	< 2.08	n.a.	< 2.08	n.a.
As	$(4.59 \pm 0.37)\times10^{-2}$	> 16.6	0.105 ± 0.010	> 37.9	$< 1.6\times10^{-2}$	< 1.87
Hg	$< 6.85\times10^{-2}$	< 2.70	0.227 ± 0.019	14.8	$< 6.85\times10^{-2}$	n.a.
Se	$< 5.93\times10^{-2}$	n.a.	$< 5.93\times10^{-2}$	n.a.	$< 5.93\times10^{-2}$	n.a.
Sb	$< 1.71\times10^{-2}$	< 0.126	$(2.57 \pm 0.24)\times10^{-2}$	0.218	$< 1.71\times10^{-2}$	< 4.59
pH	7.01 ± 0.06	n.a.	7.74 ± 0.03	n.a.	7.01 ± 0.48	n.a.
Cond.	290 ± 14	n.a.	810 ± 1	n.a.	10 ± 1	n.a.

$\overline{X}$ ± σ: average ± standard deviation; db: dry basis; n.a.: not applicable; Cond.: Conductivity.

Overall, RS eluate presented higher concentrations of the quantified elements than RH, but not necessarily higher mobilities, meaning that the higher concentrations in RS eluate were due to the higher mineral content in this material (**Table 10**).

Being a stable polymer, PE did not mobilise chemical species in the water leaching test.

Liu et al.[152] performed a leaching test on RS using deionised water with a L/S of 50 L kg^{-1}, during 2 h. Although the experimental conditions employed by these authors were different from those used in the present work, similar results were found (Na: 346 mg kg^{-1} db; K: 2094 mg kg^{-1} db; Ca: 962 mg kg^{-1} db; Mg: 193 mg kg^{-1} db). Karnowo et al.[153] have studied the mobility of alkali and alkali-earth metals from RH through leaching with deionized water at a L/S of 20 L kg^{-1}, during 24 h. The mobility percentages obtained (K: 70.9%; Mg: 45.5%; Ca: 36.5%; Na: 69.0%) were higher than those obtained in the present work.

2.3.1.5 Ecotoxicity level

The ecotoxicity levels of the eluates for *Vibrio fischeri* bacterium intended to give insight into their variation from the feedstocks to the chars. The EC_{50}-30 min values for all the feedstock eluates were above 99.0% v/v, indicating that the feedstocks have not mobilised ecotoxic substances to the bacterium.

2.3.2 Properties of chars

2.3.2.1 Proximate and elemental analyses

The proximate and elemental analyses of the gasification and pyrolysis chars are presented in **Table 12**.

The proximate analysis indicated that GCs were mainly composed of ashes due to the high conversion of organic matter into syngas during the gasification assays and to the high oxidation rate. However, G4C presented a lower ash content (68.29% w/w ar) than all the other GCs. The volatile matter was low for all GC samples (5.02-8.52% w/w ar), and the fixed-C was even lower for almost all of them. The exception occurred again in GC4, which had a fixed-C of 20.41% w/w ar, due to the lower ash content.

These gasification solid by-products are closer to carbonized ashes than to carbonaceous chars, because they are mainly composed of ashes with low C-content, being more correctly designated as black ashes[51,154]. Shen et al.[155] studied rice husk gasification chars (RHC) and ashes (RHA); the ash contents of GCs shown in **Table 12** are very similar to those obtained by these authors for RHA.

The proximate analysis of PC showed that they were mainly composed of fixed-C, followed by ashes and volatile matter. The high fixed-C content was due to the relatively low pyrolysis

temperatures used (390-430 °C). These data are comparable to the results previously reported for pyrolysis chars of RH and RS obtained at around 400-500 °C[156–158].

Table 12. Proximate and elemental analyses of the gasification and pyrolysis chars.

Parameter	Gasification Chars (GC)					Pyrolysis Chars (PC)		
	G1C	G2C	G3C	G4C	G5C	P1C	P2C	P3C
Proximate analysis (% w/w ar)								
Moisture content	2.04	1.79	2.08	2.76	0.80	1.38	1.02	3.55
Volatile matter	7.07	5.02	7.16	8.54	6.45	22.67	17.05	16.22
Ashes	86.91	89.78	86.75	68.29	92.63	29.98	34.65	35.42
Fixed-C	3.98	3.41	4.01	20.41	0.12	45.97	47.28	44.81
Elemental analysis (% w/w ar)								
C	9.00	5.80	10.10	25.90	5.19	59.65	57.60	53.00
H	0.50	0.30	0.60	2.88	< 0.01	4.46	2.60	2.70
N	< 0.20	< 0.20	< 0.20	< 0.20	< 0.20	0.51	0.50	0.60
S	0.09	< 0.03	< 0.03	< 0.03	< 0.03	< 0.03	0.04	0.06

ar: as-received

2.3.2.2 Mineral content

The mineral content of both gasification and pyrolysis chars is shown in **Table 13**.

Si was the major element in almost all GCs due to the mineral composition of RS and RH. The exception occurred for G1C, where Fe concentration was even higher than Si. Cr, Ca and Ni were also quantified with high concentrations in G1C, but still in much lower concentrations than Si and Fe. In the other GC samples, Fe, Cr and Ca were also present, but in much lower concentrations than for G1C. Given the fact that these elements were in low amounts in RH, their high concentrations in G1C may be due to a concentration factor to which the feedstocks are submitted during the gasification assays, and eventually to an elutriation from the metallic alloy of the gasification reactor.

Like in the feedstocks (**Table 10**), most of the other elements found in GC samples were AAEMs, but also Al (especially in G5C, related to the use of RS in this assay) and Ti (especially in G2C and G4C, related to the use of PE in these assays).

G2C had a lowest mineral content than G1C, except for Ti, due to the presence of PE in its fuel blend, which promoted the dilution of the metallic content of the co-fuel. Comparing G1C-G3C and G2C-G4C, the use of O_2 as a gasification agent decreased the concentration of minerals in the chars, probably due to a higher oxidation rate and volatilization to the syngas. G4C had the lowest mineral content of all GC samples once it had the lowest ash content of all GC (**Table 12)**.

Table 13. Mineral content (mg kg^{-1} db; $\overline{X}$ ± σ) of gasification and pyrolysis chars.

Chemical element	Gasification Chars (GC)					Pyrolysis Chars (PC)		
	G1C	G2C	G3C	G4C	G5C	P1C	P2C	P3C
Si	162 455 ± 2 651	155 839 ± 12 828	134 040 ± 12 908	129 707 ± 8 110	124 466 ± 7 306	160 916 ± 2 950	159 525 ± 1 777	138 723 ± 3 064
Fe	187 810 ± 17 011	9 349 ± 365	6 108 ± 588	1 486 ± 60	5 573 ± 408	388 ± 2	88.2 ± 8.4	1 541 ± 140
K	3 636 ± 149	5 805 ± 580	10 023 ± 469	7 757 ± 25	20 217 ± 459	4 339 ± 208	4 139 ± 31	21 300 ± 324
Ca	19 500 ± 1 914	4 685 ± 466	4 817 ± 67	5 763 ± 56	7 010 ± 289	2 434 ± 42	2 043 ± 23	6 684 ± 131
Cr	48 581 ± 4 794	2 129 ± 207	1 263 ± 91	185 ± 10	213 ± 11	33.7 ± 0.5	< 25.6	< 25.6
Ni	7 382 ± 704	825 ± 57	196 ± 17	124 ± 6	175 ± 0	21.9 ± 2.1	< 32.2	< 32.2
Mg	2 038 ± 138	2 570 ± 254	2 787 ± 7	3 365 ± 196	4 287 ± 318	1 093 ± 4	1 195 ± 115	5 374 ± 93
Al	2 525 ± 248	2 230 ± 143	2 648 ± 260	1 390 ± 7	12 086 ± 344	557 ± 5	658 ± 12	4 029 ± 394
Ti	1 366 ± 136	4 277 ± 400	3 025 ± 290	5 028 ± 126	1 246 ± 4	12 211 ± 21	44 405 ± 1 198	63 447 ± 292
Na	2 492 ± 249	721 ± 69	247 ± 25	553 ± 20	2 521 ± 57	366 ± 5	269 ± 24	572 ± 52
Zn	2 770 ± 132	80.4 ± 7.8	86.1 ± 8.5	44.8 ± 0.3	86.9 ± 5.4	80.9 ± 0.7	27.2 ± 1.5	58.8 ± 4.9
Cu	1 006 ± 97	28.1 ± 2.4	< 16.6	17.6 ±1.6	20.2 ± 1.8	27.1 ± 1.3	29.4 ± 2.9	36.4 ± 3.5
Mo	389 ± 36	< 80.3	< 80.3	< 80.3	< 80.3	< 50.2	< 50.2	< 50.2
Pb	< 66.1	< 66.1	< 66.1	< 66.1	< 66.1	4.72 ± 0.41	111 ± 2	148 ± 15
Ba	185 ± 18	< 131	< 131	< 131	< 131	< 81.9	< 81.9	< 81.9
Cd	< 26.2	< 26.2	< 26.2	< 26.2	< 26.2	< 16.4	< 16.4	< 16.4
As	5.52 ± 0.47	< 0.212	0.763 ± 0.074	10.5 ± 0.5	13.0 ± 1.3	< 0.101	0.205 ± 0.007	2.33 ± 0.21
Sb	3.67 ± 0.34	< 0.246	< 0.246	14.6 ± 0.0	20.7 ± 1.8	< 0.154	< 0.154	< 0.154
W	< 2.03	< 2.03	< 2.03	< 2.03	< 2.03	< 2.03	< 2.03	< 2.03
Hg	< 0.983	< 0.983	< 0.983	2.35 ± 0.21	4.61 ± 0.41	< 0.614	< 0.614	< 0.614
Se	< 0.746	< 0.746	< 0.746	7.04 ± 0.69	15.6 ± 1.4	< 0.466	< 0.466	< 0.466

db: dry basis; $\overline{X}$ ± σ: average ± standard deviation.

Concerning PC samples, Si was also the predominant major element, with concentrations similar to GC samples. Ti was present in all chars with high concentrations, particularly in the P2C and P3C samples, as they resulted from a fuel blend containing 80% w/w PE, which was the main source of Ti (**Table 10**). P3C had also a high concentration of K since this char resulted from a fuel mixture with RS, which is the feedstock with a higher concentration of this metal (**Table 10**). Ca and Mg were also present in a high concentration in P3C, although in a lower level. P3C showed the highest mineral content of all PC samples (except for Si), because RH was used in P3 assay and this was the feedstock with the highest mineral content (**Table 10**).

Globally, the mineral content in GC samples was higher than in PC samples, which agrees with their higher ash content (**Table 12**).

Experimental data on the mineral content of chars resulting from gasification and pyrolysis of rice waste blends was not found in literature. However, Jeong et al.[159] studied the mineral content of biochars produced from the pyrolysis of RH and RS used as separate fuels. These authors reported similar results to those presented in **Table 13**, except for Si (720 mg kg^{-1} db for RH and 1230 mg kg^{-1} db for RS) and Al (1.4 mg kg^{-1} db for RH and 2.4 mg kg^{-1} db for RS), which were much lower. This can be attributed to the digestion method used by these authors, which did not include the use of HF. Prakongkep et al.[157] reported a comparable Si content for RH pyrolysis chars produced at around 400 °C, even though no HF was used in acidic digestion of chars (10% HCl). These authors also found higher Na and K contents for the RH char.

2.3.2.3 Textural characterisation

The N_2 adsorption-desorption isotherms of GC samples (**Figure 9**) can be considered as a mix of types I and IV isotherms of the International Union of Pure and Applied Chemistry (IUPAC) classification[73], which corresponds to particles with both micro- and meso-porosity. The presence of hysteresis in the multilayer range of isotherms is usually associated with capillary condensation in mesopore structures. The hysteresis is of H3 type[73,160] for G1C, G2C and G5C samples, which is commonly observed in non-rigid aggregates of plate-like particles giving rise to slit-shaped pores. Similarly, the H4 type loop observed for G3C and G4C samples is often associated with narrow slit-like pores. These N_2 isotherms are similar to those obtained by Hu et al.[161] and Fu et al.[162,163] for chars obtained from rice straw and rice husk.

For PCs, the amount of N_2 adsorbed (**Figure 10**) was very small in the entire relative pressure (p/p_0) range, which indicates that these chars are almost non-porous materials. Their isotherms are typical of non-porous or macroporous materials. However, again, the presence of hysteresis in the isotherms indicates the existence of some mesopores in their structures.

The textural parameters obtained from the N_2 adsorption-desorption isotherms are shown in **Table 14**.

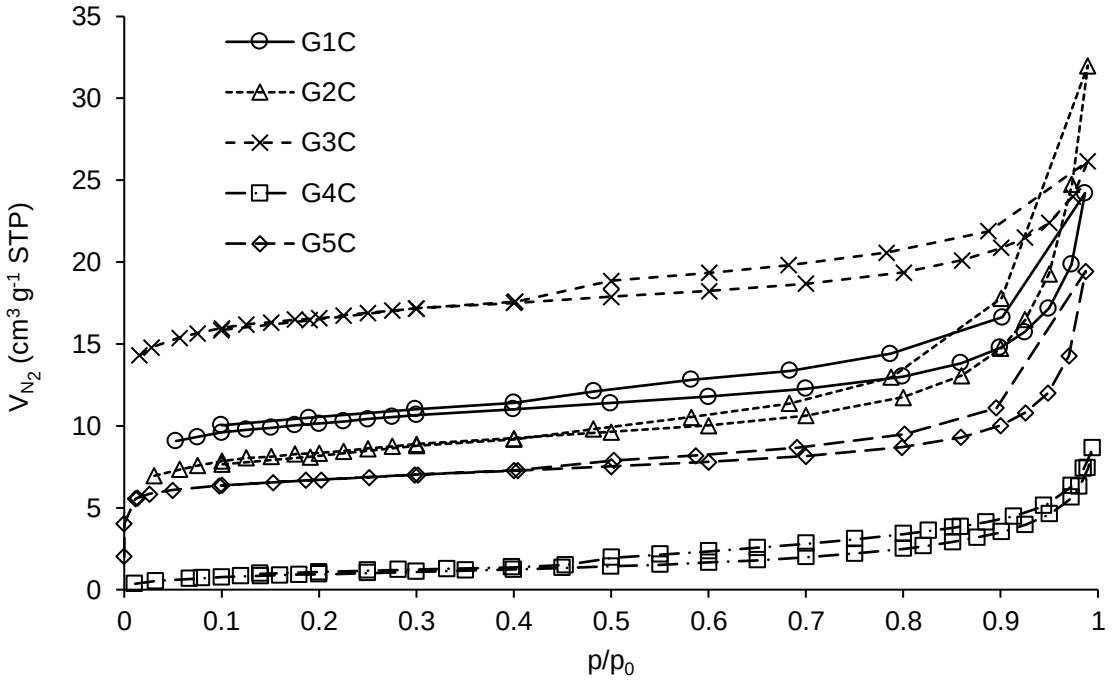

Figure 9. N_2 adsorption-desorption isotherms of the gasification chars (STP: standard temperature and pressure; p: pressure at moment *t*; p_0: initial pressure).

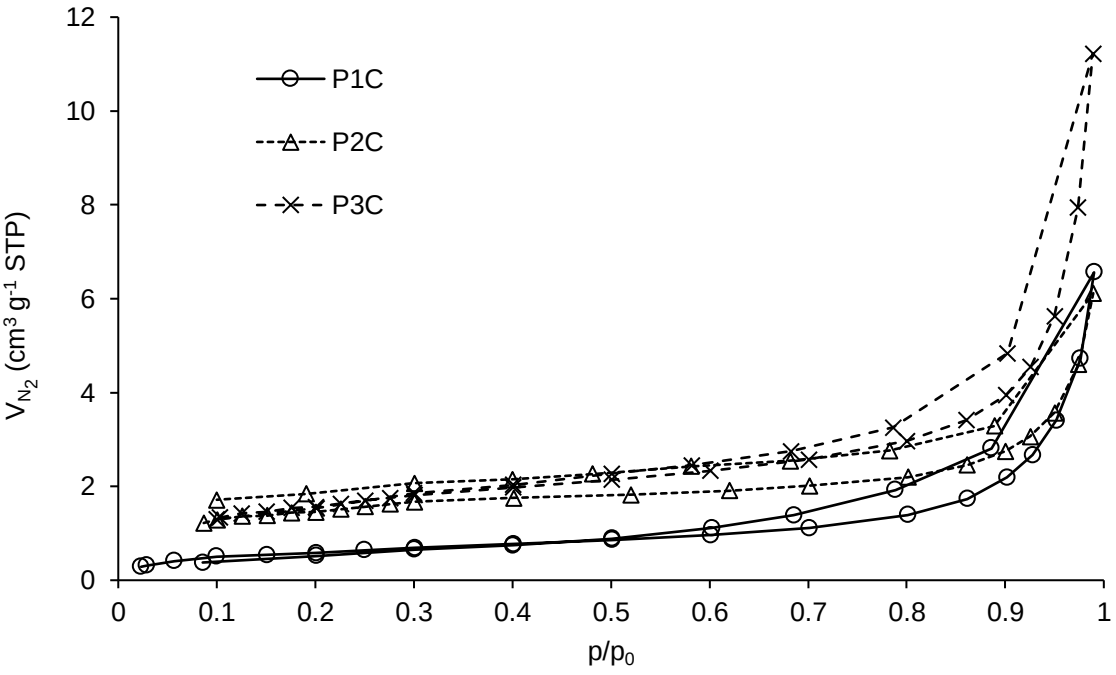

Figure 10. N_2 adsorption-desorption isotherms of the pyrolysis chars (STP: standard temperature and pressure; p: pressure at moment t; p_0: initial pressure).

Table 14. Textural properties of chars produced in the gasification and pyrolysis assays.

Parameter	Gasification chars (GC)					Pyrolysis chars (PC)		
	G1C	G2C	G3C	G4C	G5C	P1C	P2C	P3C
S_{BET} (m^2 g^{-1})	32.3	26.9	62.9	<5.0	25.0	<5.0	5.14	5.63
V_{total} (cm^3 g^{-1})	0.04	0.05	0.04	0.01	0.02	n.q.	0.01	0.02
V_{micro} (cm^3 g^{-1})	0.01	0.01	0.02	n.q.	0.01	n.q.	n.q.	n.q.
V_{meso} (cm^3 g^{-1})	0.03	0.04	0.02	0.01	0.01	n.q.	0.01	0.02

n.q.: not quantifiable

GC presented highest surface areas than PC, except for G4C which was characterised as a non-porous material. G3C presented the highest surface area and pore volume of all GCs. The higher surface areas of gasification chars might be related with a higher content of porous silica, while pyrolysis chars are richer in a non-porous carbonaceous matrix.

Globally, all GCs presented low surface areas, which agrees with the fact that they have resulted from thermochemical processes with no further activation step. In the case of PC, the high volatile matter content of these samples was blocking the incipient porosity of the chars. To improve their porosity and surface area, physical and chemical activations/treatments were performed (Chapter 3). Regarding gasification chars, given their high ash content and low volatile matter, it can be difficult to increase their surface area.

Shen et al.[155] have studied the gasification chars (RHC) and ashes (RHA) of rice husk produced at 800 °C. RHA showed a surface area (65.4 m^2 g^{-1}) very similar to G3C, even if a higher temperature (850 °C) has been used in the gasification assay that originated G3C.

The pyrolysis temperature seems to control the surface area of PC, as higher temperatures promote the release of volatile matter and consequently increase the surface area. Ye et al.[164] produced a char by submitting RH to pyrolytic conditions at 300 °C. This char has shown a lower surface area (<5 m^2 g^{-1}) than those obtained in the present work (**Table 14**), namely for P2C and P3C, which were produced at 390 °C and 430 °C, respectively. At 450 °C, Jeong et al.[159] obtained a pyrolysis char from RS with a surface area of 22.9 m^2 g^{-1} and an ash content of 34.3%, while at 750 °C the surface area was 164.1 m^2 g^{-1}, but the ash content was much higher (43.0% w/w).

2.3.2.4 Additional characterisation of chars selected for the Cr(III) removal assays

Considering the results obtained in the previous sections, two gasification chars (G4C and G5C) and one pyrolysis char (P1C) were selected to be further characterised and used in the Cr(III) removal assays. Once all chars presented poor textural properties, different factors were taken into consideration for this selection.

G5C was selected because it was the GC with the highest concentration of metal cations with exchangeable capacity (AAEMs) (which can play an important role in adsorption processes,

through ion exchange mechanism), while G4C was selected because it had 20% PE in its origin and as mentioned above, Ricevalor's main objective was to valorise the energetic fraction of the assays, and the presence of 20% PE in the gasification assays significantly improves the quality of the syngas. Between G2C (the other GC with PE in its origin) and G4C, G4C was selected because it also had higher concentration of AAEMs.

P1C was selected because it was the PC with the highest quantity of biomass in its origin.

In this regard, additional characterisations were performed to these selected chars, as described hereafter.

Mobility assessment of chemical species and ecotoxic level

The chemical characterisation of the selected chars' aqueous eluates and the mobility of the chemical elements are presented in **Table 15**.

Overall, the mobility of minerals from the adsorbents was low. K was the exception, with concentrations of 1399 mg kg^{-1} db for G4C, 3356 mg kg^{-1} db for G5C and 1985 mg kg^{-1} db for P1C, which corresponded to mobility percentages of 18.0%, 16.6% and 45.7%, respectively. Other minerals, such as Si, Mg, Ca and Na were also present in the aqueous eluates, but in lower concentrations than K. The same elements were present in the aqueous eluates of the feedstocks (**Table 11**). The mobility of these metals plays an important role in ion exchange with Cr(III), as it will be discussed later in this thesis.

Regarding the ecotoxicity of the eluates, as the bacterium *V. fischeri* is very sensitive to acidic and extremely alkaline pH conditions of the medium (optimal pH range is of 6.00-8.50[165]), the eluates of G4C and G5C appeared to be toxic to this bacterium, due to the alkaline conditions generated by chars (pH of the eluates of G4C and G5C was 10.4 and 9.74, respectively - **Table 15**). For that reason, G4C eluate had an EC50-30 min of 20.5 ± 1.8% and G5C eluate showed a value of 58.5 ± 4.9%. The highest ecotoxic level of G2C eluate was due to its higher pH. For both chars' eluates, no ecotoxicity was found after the pH correction for 8.00 with HCl 0.1 M, emphasising that the ecotoxicity was due to the pH of the medium. P1C eluate did not present ecotoxicity (EC50-30 min > 99%), as its pH (7.05 - **Table 15**) was in the optimal range for *V. fischeri*.

pH_{pzc}

G4C and G5C were characterised as alkaline materials as they presented a pH_{pzc} of 9.58 ± 0.02 and 9.34 ± 0.03, respectively, while P1C presented a neutral to slightly acidic pH_{pzc} (6.35 ± 0.02). The highest pH_{pzc} of the gasification chars may be related with their higher ash and mineral contents.

Table 15. Chemical characterisation of aqueous eluates of selected chars and mobility of chemical elements relatively to the mineral content (relative mobility) (all eluate concentrations expressed as $\overline{X}$ ± σ in mg kg^{-1} db, except for conductivity that is expressed in µS cm^{-1} and for pH that is expressed in Sørensen scale).

Element/ Parameter	G4C		G5C		P1C	
	Eluate	Mobility (%)	Eluate	Mobility (%)	Eluate	Mobility (%)
K	1 399 ± 20	18.0	3 356 ± 48	16.6	1 985 ± 25	45.7
Si	678 ± 6	0.523	361 ± 4	0.290	81.3 ± 0.8	5.05×10^{-2}
Ca	46.9 ± 3.4	0.762	87.9 ± 2.8	1.25	592 ± 2	24.3
Mg	52.7 ± 0.4	1.57	140 ± 7	3.27	142 ± 11	13.0
Na	65.7 ± 1.7	11.9	40.2 ± 0.7	1.60	140 ± 13	38.3
Mo	0.402 ± 0.015	7.24	3.05 ± 0.16	21.5	0.140 ± 0.014	5.05
Ni	2.49 ± 0.13	2.01	$< 4.85\times10^{-2}$	$< 2.76\times10^{-2}$	2.17 ± 0.10	9.91
Cr	< 0.792	< 0.428	1.50 ± 0.01	0.706	$< 6.69\times10^{-2}$	< 0.199
Al	0.850 ± 0.080	6.11×10^{-2}	0.382 ± 0.023	3.16×10^{-3}	0.290 ± 0.023	5.21×10^{-2}
Se	0.381 ± 0.029	5.41	$< 6.06\times10^{-3}$	$< 3.89\times10^{-2}$	< 0.145	n.a.
As	0.340 ± 0.015	3.24	0.376 ± 0.012	2.89	< 0.213	n.a.
Cu	0.294 ± 0.022	1.67	$< 4.60\times10^{-2}$	< 0.228	< 0.116	< 0.428
Pb	0.247 ± 0.015	0.893	$< 5.04\times10^{-3}$	$< 2.32\times10^{-2}$	< 0.193	< 4.09
Sb	0.242 ± 0.022	1.66	$< 6.06\times10^{-3}$	$< 2.93\times10^{-2}$	$< 5.15\times10^{-3}$	n.a.
Fe	$< 8.24\times10^{-3}$	$< 5.55\times10^{-4}$	0.237 ± 0.003	4.26×10^{-3}	$< 8.12\times10^{-3}$	$< 2.09\times10^{-3}$
Ti	0.103 ± 0.000	2.05×10^{-3}	$< 6.06\times10^{-2}$	$< 4.86\times10^{-3}$	$< 5.07\times10^{-2}$	4.15×10^{-4}
W	< 0.101	n.a.	< 0.101	n.a.	< 0.101	n.a.
Ba	$(3.61 \pm 0.29)\times10^{-2}$	0.153	$< 1.01\times10^{-3}$	$< 8.24\times10^{-2}$	0.194 ± 0.019	3.96
Zn	$< 4.85\times10^{-3}$	$< 1.08\times10^{-2}$	$< 4.85\times10^{-3}$	$< 5.58\times10^{-3}$	2.67 ± 0.24	3.30
Hg	$(5.15 \pm 0.44)\times10^{-2}$	2.19	$< 3.63\times10^{-4}$	$< 7.88\times10^{-3}$	$< 3.59\times10^{-2}$	n.a.
Cd	$< 4.85\times10^{-3}$	n.a.	$< 4.85\times10^{-3}$	n.a.	$< 4.06\times10^{-3}$	n.a.
pH	10.4 ± 0.0	n.a.	9.74 ± 0.01	n.a.	7.05 ± 0.09	n.a.
Cond.	552 ± 5	n.a.	1854 ± 59	n.a.	1092 ± 51	n.a.

$\overline{X}$ ± σ: average ± standard deviation; db: dry basis; n.a.: not applicable; Cond.: Conductivity.

2.4 Conclusions

The properties of the chars were greatly influenced by the composition of the rice waste streams used as feedstocks and the conditions used in the gasification and pyrolysis assays. Due to the high conversion of organic matter into syngas, the characteristics of gasification solid residues were mainly of carbonized ashes rather than carbonaceous chars. On the contrary, pyrolysis chars were mainly composed by carbon, due to the relatively low pyrolysis temperatures used.

Due to the high concentrations of Si in the feedstocks, the gasification and pyrolysis chars were mainly composed by this chemical element followed by AAEMs. In the pyrolysis chars, Ti was also a major element, as the feedstock blends contained high fractions of PE which was the main source of Ti.

Globally, all chars presented low surface areas (up to 62.9 $m^2 g^{-1}$ in the gasification chars and up to 5.63 $m^2 g^{-1}$ in the pyrolysis chars). However, due to the presence of several minerals in the gasification chars (that may be used for ion exchange in the adsorption assays), these materials may present adequate properties to be valorised as adsorption agents. On the other hand, the pyrolysis chars require further physical and/or chemical activations before such valorisation to remove the volatile matter that is blocking the char's pores (increasing the porosity of the char,) and concentrate the ash content (allowing adsorption by ion exchange).

Considering the results obtained, two gasification chars (G4C and G5C) and one pyrolysis char (P1C) were selected to be used in the Cr(III) removal assays. Prior to that, P1C was optimized through physical and chemical activations/treatments as presented in Chapter 3.

3. ORIGIN AND PROPERTIES OF ACTIVATED CARBONS USED IN THE CR(III) REMOVAL ASSAYS

The results presented in this chapter were published, partially or completely, in the following scientific publications:

Papers:

D. Dias, M. Bernardo, N. Lapa, F. Pinto, I. Matos and I. Fonseca, Activated Carbons from the Co-pyrolysis of Rice Wastes for Cr(III) Removal, *Chemical Engineering Transactions*, 65 (2018) 601-606.
(doi: 10.3303/CET1865101)

D. Dias, N. Lapa, M. Bernardo, W. Ribeiro, I. Matos, I. Fonseca, F. Pinto, Cr(III) removal from synthetic and industrial wastewaters by using co-gasification chars of rice waste streams, *Bioresource Technology*, 266 (2018) 139-150.
(doi: 10.1016/j.biortech.2018.06.054)

D. Dias, M. Bernardo, I. Matos, I. Fonseca, F. Pinto, N. Lapa, Activation of co-pyrolysis chars from rice wastes to improve the removal of Cr^{3+} from simulated and real industrial wastewaters, *Journal of Cleaner Production*, 267 (2020) 121993.

Oral Presentations:

D. Dias, W. Ribeiro, N. Lapa, M. Bernardo, I. Matos, I. Fonseca, F. Pinto, Chars from co-gasification of rice wastes as Cr(III) removal agents, *4th International Conference "WASTES: Solutions, Treatments and Opportunities"*, 25-26 September 2017, Porto, Portugal.

D. Dias, M. Miguel, M. Bernardo, N. Lapa, I. Matos, I. Fonseca, F. Pinto. Removal of Cr(III) by using activated carbons produced from rice waste chars, *DCE17 - 2nd Doctoral Congress of Engineering, 8-9 June 2017*, Porto, Portugal

D. Dias, M. Miguel, N. Lapa, M. Bernardo, I. Matos, I. Fonseca and F. Pinto, Efficient activated carbons from chars of the co-pyrolysis of rice wastes, *4th International Conference "WASTES: Solutions, Treatments and Opportunities"*, 25-26 September 2017, Porto, Portugal.

D. Dias, M. Bernardo, N. Lapa, F. Pinto, I. Matos and I. Fonseca, Activated Carbons from the Co-pyrolysis of Rice Wastes for Cr(III) Removal, *International Conference on Biomass (IconBM)*, 17-20 June 2018, Bologna, Italy.

D. Dias, M. Bernardo, N. Lapa, F. Pinto, I. Matos, I. Fonseca, Cr(III) Removal from Aqueous Solution by Activated Carbons obtained through the Co-pyrolysis of Wastes from Rice Production, *13th International Chemical and Biological Engineering Conference (CHEMPOR 2018)*, 2-4 October 2018, Aveiro, Portugal.

3.1 Introduction

In order to improve the adsorptive properties of chars selected for Cr(III) removal assays, different optimizations were tested. These optimizations were defined considering the results obtained in section 2.3.2. The high ash content of the gasification chars precluded any possible activation. On the other hand, the higher volatile matter of the pyrolysis chars created an opportunity for different optimizations. These optimizations could (i) remove the volatile matter that was blocking the char's pores and consequently increase the porosity of the char, (ii) add functional groups to the char's surface and (ii) concentrate the ash content of the char, increasing the ions available (Ca, K, Na, etc) for ion exchange.

3.2 Materials and methods

3.2.1 Optimization of chars selected for the Cr(III) removal assays

The pyrolysis char selected (P1C) was submitted to 4 different activations: (i) physical activation followed by washing, (ii) physical activation without washing, (iii) physical activation followed by chemical acidic treatment and (iv) chemical activation.

All activations were performed in a quartz reactor placed in a custom-made electric vertical tube furnace with a PID (Proportional-integral-derivative) programmable temperature controller (RKC, REX-P96) (**Figure 11**). The temperature inside the furnace was measured by a thermocouple connected to the PID controller. In the end of the activations, all activated carbons were milled, sieved to <100 µm.

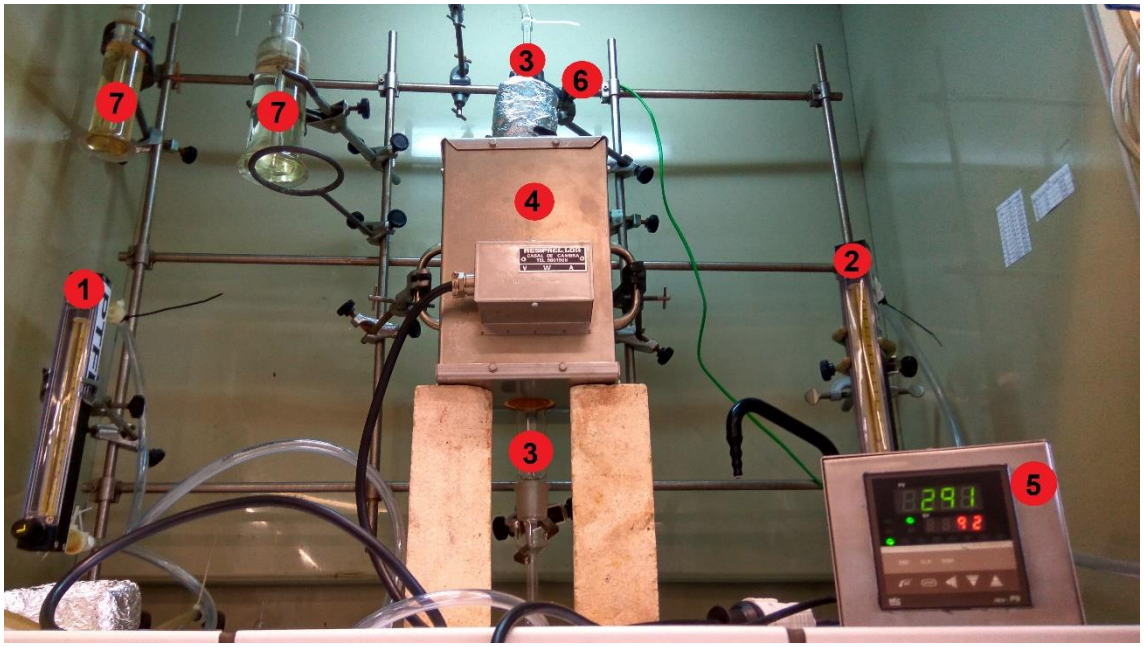

Figure 11. P1C activation setup: 1 - N_2 flowmeter; 2 - CO_2 flowmeter; 3 - Vertical quartz reactor; 4 - Electric vertical furnace; 5 - PID controller; 6 - Thermocouple; 7 - Gas washing flasks.

3.2.1.1 Physical activation followed by washing

The aim of the physical activation followed by washing was to remove the high volatile matter and mineral content that could be blocking the char's pores. CO_2 was used as activation agent once this gas increases the microporosity of the adsorbent. Four experimental conditions were tested (**Table 16**). The activations were performed with a heating rate of 5 °C min^{-1}, under a CO_2 flow of 150 cm^3 min^{-1}. Heating and cooling processes were carried out under a N_2 flow of 150 cm^3 min^{-1}. In the end, the samples were washed in a Soxhlet extractor with deionized water, until stable pH, and dried at 100 °C overnight. The code P1C+PA+W was attributed to the activated carbons (ACs) resulting from the physical activation (PA) of P1C followed by washing (W).

Table 16. Experimental conditions of the physical activations of P1C followed by washing.

Activation assay	Code	Time (h)	Temperature (°C)
1	P1C+PA+W1	2	800
2	P1C+PA+W2	2	850
3	P1C+PA+W3	4	800
4	P1C+PA+W4	4	850

In order to select the experimental conditions (temperature and time) to be used in all the other physical activations (physical activation without washing and physical activation followed by chemical acidic treatment), a preliminary characterisation was performed to all P1C+PA+W samples. The preliminary characterisation consisted on analysing the textural properties and solid yields of P1C+PA+W samples. The experimental conditions (temperature and time) that generated the P1C+PA+W with the best textural properties were selected for the other physical activations.

The textural characterisation was performed as described in section 2.2.3 and solid yields, $\hat{Y}$ (%), were calculated through equation 3.1.

$$\hat{Y} = \frac{m_f}{m_0} \times 100 \quad (3.1)$$

where m_0 is the initial P1C mass (g) and m_f is the P1C+PA+W mass (g) (mass of activated carbon obtained after the physical activation of P1C).

3.2.1.2 Physical activation without washing

The aim of the physical activation was to remove the volatile matter and increase the microporosity but keeping the mineral components that could improve the ionic exchanges. The procedure was the same as described in section 3.2.1.1, but without the washing step. The code P1C+PA was attributed to the AC resulting from the physical activation (PA) of P1C.

3.2.1.3 Physical activation followed by chemical acidic treatment

The aim of the physical activation followed by chemical acidic treatment was to unblock the char's pores, increase the microporosity and add functional groups to the char's surface. The physical activation was the same as described in item 3.2.1.1. The chemical treatment was performed with HNO_3 solution (13 M) under L/S of 20 mL g^{-1}, and placed in a silicone bath, at 90 °C, for 6 h. The char was then washed in a Soxhlet extractor with deionized water, until stable pH, and dried at 100 °C overnight. The code P1C+PA+CT was attributed to the activated carbon (AC) resulting from the physical activation (PA) of P1C followed by chemical acidic (CT) treatment.

3.2.1.4 Chemical activation

The chemical activation also had the objective of unblock the char's pores, increase both micro and mesoporosity, and add functional groups to the char's surface. Unlike the physical activations, in this case, an earlier chemical impregnation was performed to the char, and only then the activation was performed. The char was impregnated with H_3PO_4 under a mass ratio of 1:1. The mixture was placed in a 100 mL volumetric flask and filled with deionized water. The solution was heated-up to 50 °C, kept for 5 h under constant agitation, and dried at 130 °C. Finally, the char was activated at 500 °C (heating rate of 5 °C min^{-1}), for 2 h, under a N_2 flow of 150 cm^3 min^{-1}. The heating and cooling processes were carried out under N_2 flow. The samples were then washed in a Soxhlet extractor with deionized water, until stable pH, and dried at 100 °C overnight. The code P1C+CA was attributed to the AC resulting from the chemical activation (CA) of P1C.

3.2.1.5 Commercial activated carbon (CAC)

For comparison purposes a commercial activated carbon (CAC) (Norit GAC 1240) was used in this study. Being an AC, the only optimization done to this adsorbent was the chemical treatment as described in section 3.2.1.3. The code CAC+CT was attributed to the AC resulting from the chemical treatment with HNO_3 of CAC.

3.2.2 Characterisation of activated carbons used in Cr(III) removal assays

All activated carbons were characterised for the following assays:

a) Proximate analysis – The same as described in section 2.2.3;

b) Elemental analysis – The same as described in section 2.2.1;

c) Textural analysis – The same as described in section 2.2.3;

d) pH_{pzc} – The same as described in section 2.2.4.

Aside from these parameters, some additional characterisations were performed on CAC, namely:

a) Mineral content – The same as described in section 2.2.1;

b) Mobility assessment of chemical species and ecotoxic level – The same as described in section 2.2.1.

3.3. Results and discussion

3.3.1 Preliminary characterisation of activated carbons from physical activation of P1C followed by washing

The solid yields of the physical activations of P1C followed by washing and textural properties of the resulting activated carbons (P1C+PA+W_x) are presented in **Table 17**.

Table 17. Solid yields of the physical activations of P1C followed by washing and textural properties of the resulting activated carbons.

Activated carbons	Ŷ (%)	Textural properties			
		S_{BET} ($m^2\ g^{-1}$)	V_{total} ($cm^3\ g^{-1}$)	V_{micro} ($cm^3\ g^{-1}$)	V_{meso} ($cm^3\ g^{-1}$)
P1C+PA+W1	79.1	190	0.11	0.06	0.05
P1C+PA+W2	70.0	223	0.12	0.07	0.05
P1C+PA+W3	66.1	341	0.20	0.12	0.08
P1C+PA+W4	32.6	n.q.	n.q.	n.q.	n.q.

n.q.: not quantifiable

P1C+PA+W4 presented the lowest solid yield of all activated carbons and its textural analysis indicated that the activation conditions were very aggressive, promoting the collapse of porous structure. For the other samples, all surface areas and pore volumes increased when compared to P1C (**Table 14**), indicating successful activations. P1C+PA+W3 had the second lowest solid yield (66.1%), meaning that more volatile matter was removed during this activation, providing

more available pores, and consequently originating the AC with the highest surface area (341 m^2 g^{-1}) and total pore volume (0.20 cm^3 g^{-1}).

Considering these results, P1C+PA+W3 was the AC obtained from the physical activation followed by washing of P1C selected to be further characterised and used in Cr(III) removal assays. On the other hand, the experimental conditions that originated P1C+PA+W3 (800 °C and 4h) were selected to be used on the other physical activations.

In order to simplify the reading of the results, from this point on, P1C+PA+W3 will be referred only as P1C+PA+W.

3.3.2 Properties of activated carbons used in the Cr(III) removal assays

3.3.2.1 Proximate and elemental analyses

The proximate and elemental analyses of the activated carbons which was used in Cr(III) removal assays are presented in **Table 18**.

Table 18. Proximate and elemental analyses of the activated carbons used in the Cr(III) removal assays and P1C (for comparison purposes).

Parameter	P1C	Activated carbons					
		P1C+PA	P1C+PA+W	P1C+PA+CT	P1C+CA	CAC	CAC+CT
Proximate analysis (% w/w ar)							
Moisture content	1.38	4.36	4.49	9.58	11.22	13.09	21.60
Volatile matter	22.67	4.25	8.15	13.75	10.26	7.04	15.66
Ashes	29.98	40.39	30.55	36.94	22.68	5.70	4.10
Fixed carbon	45.97	51.00	56.81	39.73	55.84	74.17	58.64
Elemental analysis (% w/w ar)							
C	59.65	50.22	58.65	43.72	58.19	86.28	61.21
H	4.46	0.26	0.49	0.94	2.12	0.47	1.82
N	0.51	0.47	0.44	0.68	0.54	< 0.20	0.65
S	< 0.03	< 0.03	< 0.03	< 0.03	< 0.03	0.57	0.27

ar: as-received basis; P1C+PA: P1C physically activated; P1C+PA+W: P1C physically activated and washed; P1C+PA+CT: P1C physically activated and chemically treated; P1C+CA: P1C chemically activated; CAC+CT: CAC chemically treated.

Comparing these results with P1C, after the physical activation (P1C+PA), most of the volatile matter was removed, concentrating the other elements on the adsorbent. Washing the AC (P1C+PA+W) decreased the percentage of ashes. The chemical treatment on the AC (P1C+PA+CT) increased the amount of volatile matter, decreasing the percentage of other

elements. The chemical activation on the initial char (P1C+CA) also decreased the volatile matter similarly to the physical activation, although in this case, the ash-content also decreased, concentrating the fixed-C. CAC was mainly composed by fixed-C, as expected, but after being chemically treated (CAC+CT), the volatile matter increased, decreasing the fixed-C content.

3.3.2.2 Textural analysis and pH_{pzc}

According to the IUPAC classification[73], the adsorption-desorption isotherms of P1C-derived ACs (**Figure 12**a) and commercial ACs (**Figure 12b**) were a mix of type I (in the beginning of the isotherm) and type IV (at the end of the isotherm) with H4 hysteresis, indicating narrow slit-shaped micropores and mesopores.

Table 19 presents the textural properties and pH_{pzc} of the produced activated carbons.

Table 19. Textural properties and pH_{pzc} of the activated carbons used in the Cr(III) removal assays and P1C (for comparison purposes).

Parameter	P1C	Activated carbons					
		P1C+PA	P1C+PA+W	P1C+PA+CT	P1C+CA	CAC	CAC+CT
S_{BET} (m^2 g^{-1})	<5.0	325	341	164	415	1030	893
V_{total} (cm^3 g^{-1})	n.q.	0.18	0.20	0.10	0.22	0.56	0.49
V_{micro} (cm^3 g^{-1})	n.q.	0.10	0.12	0.05	0.15	0.30	0.25
V_{meso} (cm^3 g^{-1})	n.q.	0.08	0.08	0.05	0.07	0.26	0.24
pH_{pzc}	6.35	9.89	6.87	2.04	2.01	9.13	2.27

P1C+PA: P1C physically activated; P1C+PA+W: P1C physically activated and washed; P1C+PA+CT: P1C physically activated and chemically treated; P1C+CA: P1C chemically activated; CAC+CT: CAC chemically treated.

The physical activation increased significantly the surface area and pore volume of the AC (P1C+PA) when compared to the P1C results, since the volatile matter that was blocking the pores was removed (**Table 18**) and the partial gasification of the char induced by CO_2 occurred. After washing (P1C+PA+W), the surface area and pore volume also increased slightly, due to ash removal (**Table 18**). The chemical treatment of AC P1C+PA+CT decreased significantly the surface area and pore volume, probably because (i) the acidic treatment was too aggressive and some pores were broken, and/or (ii) some functional groups are positioned in the entrance of the pores. Also, this probably occurred for CAC+CT. The chemical activation on the initial char (P1C+CA) originated the material with the highest surface area and pore volume of all P1C-derived ACs. Still, the values were significantly lower than for CAC and CAC+CT.

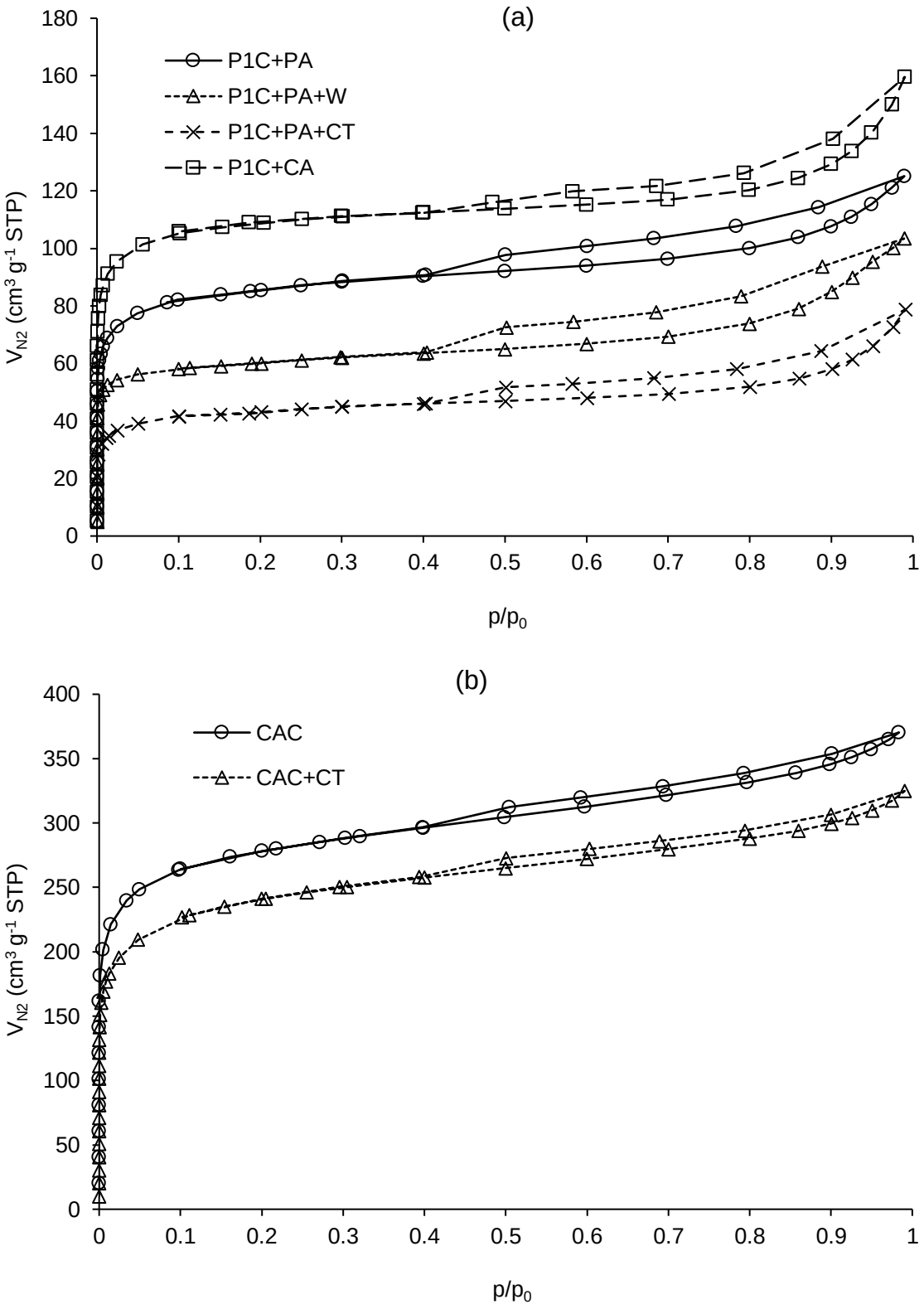

Figure 12. N_2 adsorption-desorption isotherms and textural properties of the (a) P1C-derived activated carbons and (b) CAC.

Similar results were found in literature for ACs from pyrolysis of rice husk (**Table 20**).

Table 20. Textural properties of ACs from pyrolysis of rice husk available in literature.

Type of activation	Activation agent	Activation conditions		Textural properties		Reference
		Temperature (°C)	Time (h)	S_{BET} ($m^2\ g^{-1}$)	V_{total} ($cm^3\ g^{-1}$)	
Physical activation without washing	CO_2	850	1	334	207	Kumagai et al.[166]
		875	1	324	212	
Physical activation with washing	CO_2	750	n.a.	240.9	n.d.	Li et al.[167]
		850	n.a.	350.1	n.d.	
Chemical activation	H_3PO_4	500	1	508	0.278	Liou et al.[168]

n.a.: not available; n.d.: not determined

As mentioned before in section 2.3.2.4, P1C presented a neutral to slightly acidic pH_{pzc}, but after the physical activation, the removal of volatile matter and subsequent concentration of ashes (**Table 18**) increased the pH_{pzc} of P1C+PA to an alkaline value, very similar to CAC (**Table 19**). The washing removed some of the ash content, decreasing the pH_{pzc} of P1C+PA+W. Finally, P1C+PA+CT, P1C+CA and CAC+CT, being materials activated/treated with acids, presented very acidic pH_{pzc} values.

3.3.2.3 Additional characterisations of CAC

Table 21 shows the mineral content, the chemical characterization of eluates and the mineral mobility of CAC.

Si was also the major element in CAC, followed by Al, Fe, Ca and K, although in lower concentrations. Considering that the ash content of CAC was much lower than the ash content of the gasification and pyrolysis chars (**Table 12**), the mineral content of CAC was also much lower than the mineral content of those chars (**Table 13**).

The mineral mobility of CAC was very low, only Ca (51.7 ± 48 mg kg^{-1} db) and Si (24.7 ± 0.5 mg kg^{-1} db) were slightly mobilized by water, with mobility percentages of 3.15% and 0.169%, respectively. These results suggested that Cr(III) removal by CAC would not be governed by ion exchange, but instead by other removal mechanisms.

CAC eluate did not present ecotoxicity (EC_{50}-30 min > 99%), as its pH was in the optimal range for *V. fischeri* (optimal pH range is of 6.00 to 8.50[165]).

Table 21. Mineral content, chemical characterization of eluates and mineral mobility of CAC ($\overline{X}$ ± σ; n = 2; all parameters in mg kg^{-1} db, except the mobility which is expressed in %, pH in Sørensen scale and conductivity in µS cm^{-1}).

Element / Parameter	CAC		
	Acidic eluate	Aqueous eluate	Mobility
Si	14 629 ± 681	24.7 ± 0.5	0.169
Al	8 780 ± 23	5.10 ± 0.38	0.0581
Fe	3 182 ± 228	0.170 ± 0.004	5.34×10^{-3}
Ca	1 642 ± 41	51.7 ± 4.6	3.15
K	1 032 ± 3	5.67 ± 0.12	0.549
Ti	626 ± 14	$< 6.06\text{x}10^{-2}$	$< 9.68\times10^{-3}$
Mg	444 ± 20	4.76 ± 0.15	1.07
Cr	265 ± 16	< 0.792	$< 7.77\times10^{-3}$
Ba	112 ± 6	$(7.27\pm 0.34)\times10^{-2}$	6.49×10^{-2}
Na	53.4 ± 0.7	0.848 ± 0.031	1.59
Cu	26.7 ± 2.1	$< 4.60\times10^{-2}$	< 0.172
Ni	22.6 ± 1.0	$< 4.85\text{x}10^{-2}$	< 0.215
Sb	9.21 ± 0.38	$< 6.06\times10^{-3}$	$< 6.58\times10^{-2}$
As	6.68 ± 0.54	$< 6.06\times10^{-3}$	$< 9.07\times10^{-2}$
Zn	3.91 ± 0.06	$< 4.85\text{x}10^{-3}$	< 0.124
Se	< 1.51	$< 6.06\times10^{-3}$	n.a.
Mo	< 0.138	$< 7.27\times10^{-3}$	n.a.
Pb	< 0.115	$(6.06 \pm 0.23)\times10^{-3}$	> 5.27
Cd	$<9.21\times10^{-2}$	$< 4.85\times10^{-3}$	n.a.
Hg	$< 6.91\times10^{-3}$	$< 3.63\times10^{-4}$	n.a.
pH	n.d.	7.50 ± 0.18	n.a.
Cond.	n.d.	281 ± 25	n.a.

db: dry basis; X ± σ: average ± standard deviation; n.d.: not determined; n.a.: not applicable; Cond.: Conductivity

3.4 Conclusions

The most favourable conditions for physical activation of P1C were 800 ºC for 4h.

All activations removed most volatile matter that was present in the original char (P1C), leading to higher surface areas and pore volumes than P1C. The chemical activation generated the pyrolysis-derived AC (P1C+CA) with the highest surface area (415 $m^2\ g^{-1}$) and pore volume (0.22 $cm^3\ g^{-1}$) because some ashes were also removed besides the volatile matter. Still, these results were significantly lower than the ones obtained for CAC and CAC+CT.

P1C+PA and CAC presented alkaline pH_{pzc} values, while the ACs activated/treated with acids, presented very acidic pH_{pzc} values.

4. Cr(III) REMOVAL ASSAYS BY GASIFICATION CHARS UNDER BATCH CONDITIONS

The results presented in this chapter were published, partially or completely, in the following scientific publications:

Paper:

D. Dias, N. Lapa, M. Bernardo, W. Ribeiro, I. Matos, I. Fonseca, F. Pinto, Cr(III) removal from synthetic and industrial wastewaters by using co-gasification chars of rice waste streams, *Bioresource Technology*, 266 (2018) 139-150.
(doi: 10.1016/j.biortech.2018.06.054)

Oral Presentation:

D. Dias, W. Ribeiro, N. Lapa, M. Bernardo, I. Matos, I. Fonseca, F. Pinto, Chars from co-gasification of rice wastes as Cr(III) removal agents, *4th International Conference "WASTES: Solutions, Treatments and Opportunities"*, 25-26 September 2017, Porto, Portugal.

Poster:

D. Dias, M. Bernardo, F. Pinto, N. Lapa, Recovery of high-value metals through adsorption onto chars produced from waste streams of rice production: the case-study of Cr3+, *1st Scientific Meeting of the Doctoral Programme in Sustainable Chemistry (PDQS)*, 26 September 2016, Aveiro, Portugal.

4.1 Introduction

In this chapter, the gasification chars that were selected in Chapter 2 (G4C and G5C) were used in removal assays of Cr(III) from a synthetic solution and from an industrial wastewater.

For comparison purposes, CAC (section 3.2.1.5) was also used in the Cr(III) removal assays.

4.2 Materials and methods

4.2.1 Cr(III) synthetic solution

The Cr(III) synthetic solution was prepared with $CrN_3O_9.9H_2O$ (99%). The solution had an initial concentration of 80 ± 5 mg Cr(III) L^{-1}.

4.2.2 Industrial wastewater – origin and characterisation

The industrial wastewater was collected in SIRECRO-AUSTRA – a chromium recovery plant from leather tanning wastewaters (Alcanena, Portugal). The sample was collected at the plant inflow, after the screening operation unit, where the concentration of Cr(III) in solution is around 2000 mg L^{-1}. This high concentration remains dissolved, as the pH is very low (< 4.00); this assumption is supported by the Cr(III) speciation diagram (**Figure 13**).

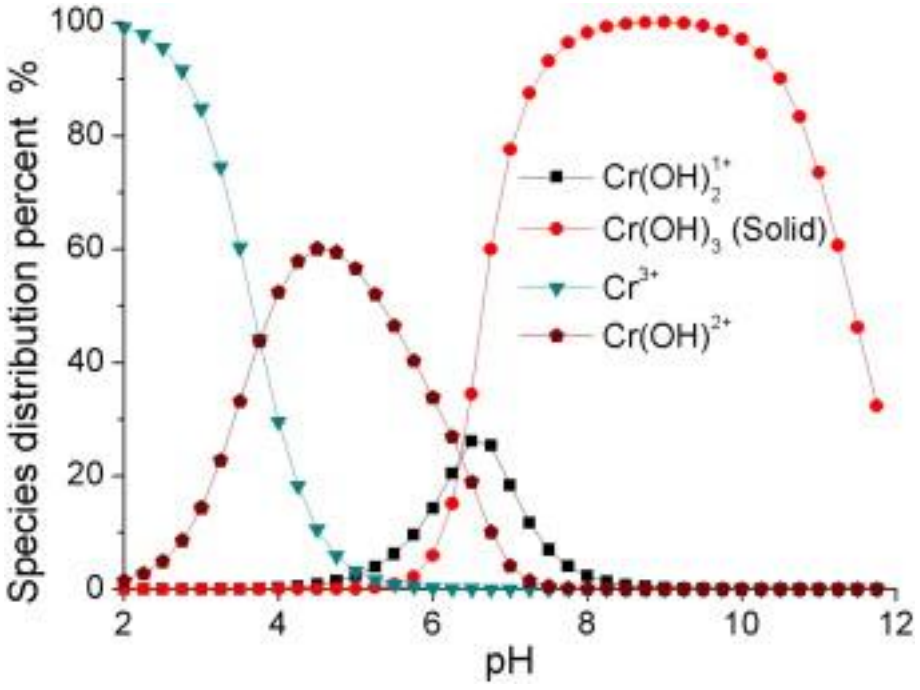

Figure 13. Cr(III) speciation diagram[169] (reproduction under the kind written permission of Elsevier).

The industrial wastewater was characterised for:

(a) pH (Hanna Instruments edge® HI 2002 pH meter) and conductivity (Thermo Scientific Orion Star A215 conductivity meter), by electrometric methods 4500 and 2510 A, respectively, of APHA/AWWA/WEF[170];

(b) Total solids (TS) (method 2540 B[170]), fixed solids (FS) (method 2540 E[170]), total suspended solids (TSS) (method 2540 D[170]) and volatile solids (VS) (method 2540 E[170]);

(c) Total Chemical Oxygen Demand (tCOD) and soluble Chemical Oxygen Demand (sCOD) in an open-reflux system (method 5220 B [170]);

(d) Mineral content of the filtered wastewater after being filtered thought Whatman® ME 25/21 ST membrane filters (0.45 µm) and acidified with HNO_3 to pH < 2.00. 11 metals and metalloids (Al, Ca, Cd, Cr, Cu, Fe, K, Mg, Na, Si, and Zn) were quantified in the filtered and acidified wastewater by ICP-AES, as described in section 2.2.1;

(e) Mineral content after acidic digestion (US EPA 3015 A) performed in a Milestone ETHOS 1600 microwave heating system by digesting an aliquot of 45 mL with 4 mL HNO_3 (65% v/v) and 1 mL HCl (37% v/v), at 170 °C, for 10 min after a 10 min ramp. The solution was then filtered through Whatman® 41 ashless filter papers (20-25 µm) and the same 11 metals and metalloids mentioned in item (d) were quantified in the acidic eluates by ICP-AES (described in section 2.2.1).

(f) Solubility of the species in the wastewater by equation 4.1.

$$\text{Solubility (\%)} = \frac{\text{Concentration in filtered eluates}}{\text{Concentration in acidic eluates}} \times 100 \quad (4.1)$$

4.2.3 Cr(III) removal assays from synthetic solution

Cr(III) removal assays were performed under batch conditions, in an Infors AG AK 82 roller-table agitator, at a constant mixing of 150 rpm, and room temperature of 25 ± 1 ºC. The samples were then filtered through 0.45 µm cellulose nitrate membranes (Whatman® ME 25/21 ST) and the pH of filtrates was measured (Hanna Instruments edge® HI 2002 pH meter). The filtrates were then acidified with HNO_3 for a pH < 2, before Cr quantification by ICP-AES (described in section 2.2.1).

4.2.3.1 Effects of adsorbent loading (solid/liquid ratio, S/L) and initial pH value

All adsorbents were submitted to a preliminary study, in which the effects of adsorbent loading (solid/liquid ratio, S/L) and initial pH were tested. Two initial pH values were used (3.50 and 4.50) and three S/L values were tested (2.5, 5.0 and 10 g L^{-1}). To simplify the data reading, codes were attributed to each assay: the name of the adsorbent was followed by the S/L used; for instance, the assay with the adsorbent G5C at a S/L of 5 g L^{-1} was named as G5C-5. The contact time for

all these removal assays was of 24 h, which was verified to be more than enough to reach the equilibrium phase.

Cr(III) removal efficiency, η (%), and experimental adsorbent removal capacity, q_{exp} (mg g^{-1}), were calculated by equations 4.2 and 4.3, respectively:

$$\eta = \frac{C_0 - C_f}{C_0} \times 100 \quad (4.2)$$

$$q_{exp} = \frac{C_0 - C_f}{m} \times V \quad (4.3)$$

where C_0 and C_f are Cr(III) concentrations (mg L^{-1}) before and after the removal assays, respectively, m is the adsorbent mass (g), and V is the solution volume (L).

The conditions (adsorbent, pH and S/L) under which Cr(III) removal performed better were selected for kinetic and isotherm adsorption studies.

4.2.3.2 Kinetic study

Contact times between 0.25 and 72 h were tested. The results were adjusted to pseudo-first order and pseudo-second order kinetic models, through the equations 4.4 and 4.5[171], respectively:

$$q_t = q_e \times \left[1 - e^{k_f \times t}\right] \quad (4.4)$$

$$q_t = \frac{k_s \times {q_e}^2 \times t}{1 + q_e \times k_s \times t} \quad (4.5)$$

where q_t is the Cr(III) uptake capacity in time t (mg g^{-1}), q_e is the Cr(III) uptake capacity in equilibrium (mg g^{-1}), k_f is the pseudo-first order kinetic constant (h^{-1}), k_s is the pseudo-second order kinetic constant (g mg^{-1} h^{-1}), and t is the contact time (h). These empirical kinetic models assume that the uptake rate is first- or second-order with respect to the available surface coverage and, although they not allow to determine the specific rate-controlling mechanism of adsorption, their widespread acceptance allow to compare the obtained modelling results with kinetic data already published in the literature. These lumped kinetic models assume that the process is controlled by the irreversible adsorption reaction at the liquid/solid interface in the adsorbent, neglecting the effects of film and pore diffusion[94,172].

Through the kinetic study it was possible to perceive at which contact time the adsorbent reached its maximum removal capacity; this contact time was used for the adsorption isotherm study.

4.2.3.3 Adsorption isotherm study

Cr(III) concentrations between 10 and 80 ± 5 mg L^{-1} were tested. The results were adjusted to Langmuir's non-linear model (equation 4.6) and Freundlich's non-linear model (equation 4.7)[173]:

$$q_e = \frac{q_{max} \times b \times C_e}{1 + b \times C_e} \tag{4.6}$$

$$q_e = K_F \times C_e^{\frac{1}{n}} \tag{4.7}$$

where q_e is the Cr(III) uptake capacity in the equilibrium (mg g^{-1}), q_{max} is the maximum uptake capacity (mg g^{-1}), b is the Langmuir's constant (L mg^{-1}), C_e is the concentration of Cr(III) in the equilibrium (mg L^{-1}), K_F is the Freundlich's constant (mg g^{-1} mg^{-n} L^{n}) and n is the Freundlich intensity parameter (dimensionless), which indicates the magnitude of the adsorption driving force or the surface heterogeneity.

The Langmuir model assumes that the active sites on the adsorbent's surface are energetically homogeneous and only one atom/molecule can be positioned in each site until a monolayer is formed. Moreover, the adsorption is localized and the energy needed for the process does not depend on the coverage degree[173,174].

Freundlich isotherm was the first empiric equation developed for equilibrium data modelling describing the non-ideal and reversible adsorption, not restricted to the formation of monolayer[173,174]. This model can be applied to multilayer adsorption, with non-uniform distribution of adsorption heat and affinities over the heterogeneous surface. The adsorption process occurs first in the sites with stronger binding forces, then as the adsorption energy exponentially decreases all other sites with weakest binding forces are also filled[173].

4.2.3.4. Model adjustment

SOLVER function of MS EXCEL 2016 was used to adjust the kinetic and isotherm adsorption models through the minimum of the least-square method (equation 4.8):

$$Min\left[\sum Least\ squares\right] = Min\left[\sum \left(q_{exp} - q_{th}\right)^2\right] \tag{4.8}$$

where q_{exp} is the experimental Cr(III) uptake capacity ($mg_{Cr(III)}\ g^{-1}_{adsorbent}$) and q_{th} is the modelled Cr(III) uptake capacity ($mg_{Cr(III)}\ g^{-1}_{adsorbent}$). The models with the highest determination coefficient (R^2) were considered as the best-fitting models.

4.2.4. Cr(III) removal assays from industrial wastewater

Cr(III) removal assays from the industrial wastewater were done with the adsorbent and conditions (S/L and contact time) that performed better for synthetic solution. Three initial concentrations were tested (50, 100 and 200 mg Cr(III) L^{-1}), which were obtained through the dilution of industrial wastewater with ultrapure water (Milli-Q Academic); the initial pH was not corrected.

The procedure for the Cr(III) removal assays was the same as described in section 4.2.3.

4.2.5. Cr(III) removal mechanisms

The adsorbents may remove Cr(III) from aqueous solutions through different mechanisms: physical adsorption which will be here defined as pore filling (electrostatic sorption between positively charged ions in water and the delocalised cloud of electrons associated with aromatic groups on the surface of the carbonaceous adsorbents, creating cation-π interactions with the CC aromatic bonds), chemical adsorption (ion exchange, electrostatic interactions, among others) and precipitation. To evaluate the Cr(III) removal mechanisms, a study was performed on the removal assay that provided the highest Cr(III) removal from the industrial wastewater, in which no precipitation had occurred and adsorption mechanisms ruled Cr(III) removal.

To evaluate if ion exchange mechanism had an important role in Cr(III) removal, the elements Al, Ca, Fe, K, Mg, Na and Si were quantified in the industrial wastewater before and after the removal assays. These elements were selected because they were present in both the industrial wastewater and adsorbent, and they may play a role in Cr(III) removal. Concentration variation, CV (mg L^{-1}), and percentage variation, PV (%), were calculated by equations 4.9 and 4.10, respectively:

$$CV = C_f - C_0 \tag{4.9}$$

$$PV = \left(\frac{C_f}{C_0} \times 100\right) - 100 \tag{4.10}$$

where C_0 and C_f are Cr(III) concentrations before and after the removal assay, respectively.

The procedure for the removal assays was the same as described in section 4.2.3, but instead of just Cr, all elements mentioned above were quantified by ICP-AES.

4.3 Results and discussion

4.3.1 Industrial wastewater characterisation

The industrial wastewater showed acidic properties (pH = 3.91), due to the use of inorganic acids and Cr(III) in the leather tanning processes. The relatively high conductivity (68.2 mS cm^{-1}) indicates a high content of ionic salts (**Table 22**). As expected, Cr was quantified in the acidic eluate in a high concentration (1810 mg L^{-1}). Similarly, Mg (1923 mg L^{-1}) and Na (1387 mg L^{-1}) were also detected in very high concentrations. In the wastewater filtrate, the results were very similar, with almost all these chemical elements presenting a solubility percentage close to 100%. Only Mg (41.1%) showed a lower concentration in the filtrate. The data obtained for solids and COD (**Table 22**) indicate that only 0.1% of the total solids were constituted by suspended solids and consequently 99.9% were dissolved solids; 77.7% tCOD (6327 mg O_2 L^{-1}) were in soluble form. These data mean that almost all salts, solids and COD were in soluble form.

Table 22. Industrial wastewater characterisation ($\overline{X}$ ± σ; n=2; pH in Sørensen scale; conductivity in mS cm^{-1}; TS, FS, VS, TSS, and metals or metalloids in mg L^{-1}; tCOD and sCOD in mg O_2 L^{-1}; Solubility in %).

Parameters	Industrial wastewater	Metal or metalloid	Industrial wastewater		
			Acidic eluate	Filtrate	Solubility
pH	3.91 ± 0.06	Mg	1 923 ± 26	790 ± 0	41.1
Cond.	68.2 ± 0.0	Cr	1 810 ± 172	1 799 ± 33	99.4
TS	76 837 ± 1 166	Na	1 387 ± 134	1 330 ± 120	95.9
FS	62 622 ± 1 960	Ca	564 ± 53	534 ± 52	94.5
VS	14 215 ± 794	K	126 ± 3	123 ± 2	97.4
TSS	102 ± 7	Si	28.2 ± 0.2	24.3 ± 0.0	86.0
tCOD	6 327 ± 228	Fe	10.7 ± 0.3	8.34 ± 0.21	78.0
sCOD	4 914 ± 78	Al	2.79 ± 0.25	2.50 ± 0.19	89.4
		Zn	1.18 ± 0.09	0.556 ± 0.040	47.2
		Ti	< 0.404	< 0.404	n.a.
		Cu	< 4.10×10^{-2}	< 4.10×10^{-2}	n.a.
		Cd	< 3.20×10^{-2}	< 3.20×10^{-2}	n.a.

n.a.: not applicable; Cond.: Conductivity; TS: Total Solids; FS: Fixed Solids; VS: Volatile Solids; TSS: Total Suspended Solids; tCOD: total Chemical Oxygen Demand; sCOD: soluble Chemical Oxygen Demand.

The studies identified in literature (**Table 23**) point out for the same acidic nature of leather tanning effluents with pH values between 3.63 and 4.07. Mella et al.[175] reported values of conductivity similar to the average value found in the industrial wastewater analysed in the present study, while Ramírez-Estrada et al.[176] showed TS and VS concentrations similar to those reported in the present work. Concerning COD, the values of tCOD and sCOD referred in literature are also similar to those determined in the industrial wastewater[177,178]. Finally, Mella et al.[175] and Ramírez-Estrada et al.[176] presented very similar concentrations of Cr and Ca to those quantified in the leather tanning wastewater.

Table 23. Comparison of the industrial wastewater composition with literature (pH in Sørensen scale; conductivity in mS cm^{-1}; TS, VS, TSS, Cr, Ca and Na in mg L^{-1}; tCOD and sCOD in mg O_2 L^{-1}).

Parameters										Reference
pH	Cond.	TS	VS	TSS	tCOD	sCOD	Cr	Ca	Na	
4.07	71.9	n.d.	n.d.	456	387	n.d.	2 000	n.d.	n.d.	Mella et al.[175]
4.0	n.d.	97 704	20 460	1 067	5 843	n.d.	2 775	803	22 320	Ramírez-Estrada et al.[176]
3.65	n.d.	n.d.	n.d.	8 430	19 400	n.d.	552	n.d.	n.d.	George et al.[177]
3.63	n.d.	n.d.	n.d.	4 863	8 058	5 600	5 363	n.d.	n.d.	Guo et al.[178]
3.91	68.2	76 837	14 215	102	6 327	4 914	1 810	564	1 387	Present work

n.d.: not determined

4.3.2 Cr(III) removal assays from synthetic solution

4.3.2.1 Influence of S/L and initial pH

For an initial pH of 3.50, the preliminary studies (**Figure 14**) showed that almost all Cr(III) present in the synthetic solution (98.4%) was removed in G5C-10 assay (**Figure 14a**). Consequently, G5C-10 showed the highest Cr(III) uptake capacity (q_{exp}) (6.91 mg g^{-1}) of all the assays (**Figure 14b**). The final pH of this assay was 6.66, indicating that Cr(III) might be removed through precipitation, as at a pH higher than 5.00 Cr(III) changes for insoluble chemical species[169]. The same mechanism occurred in G4C-10 assay; in this case, the final pH (5.51) was lower than for G5C-10, which may promote a slightly lower Cr(III) precipitation and consequently a lower removal level (74.7%). Therefore, q_{exp} of G4C-10 (5.25 mg g^{-1}) was lower than for G5C-10 (6.91 mg g^{-1}). In CAC-10 assay, less Cr(III) was removed (30.6%) than for chars submitted to the same S/L; however, the final pH of this assay was 4.63, which is much lower than for both assays with chars and critical pH value for precipitation (5.00); consequently, no significant precipitation might have occurred with CAC.

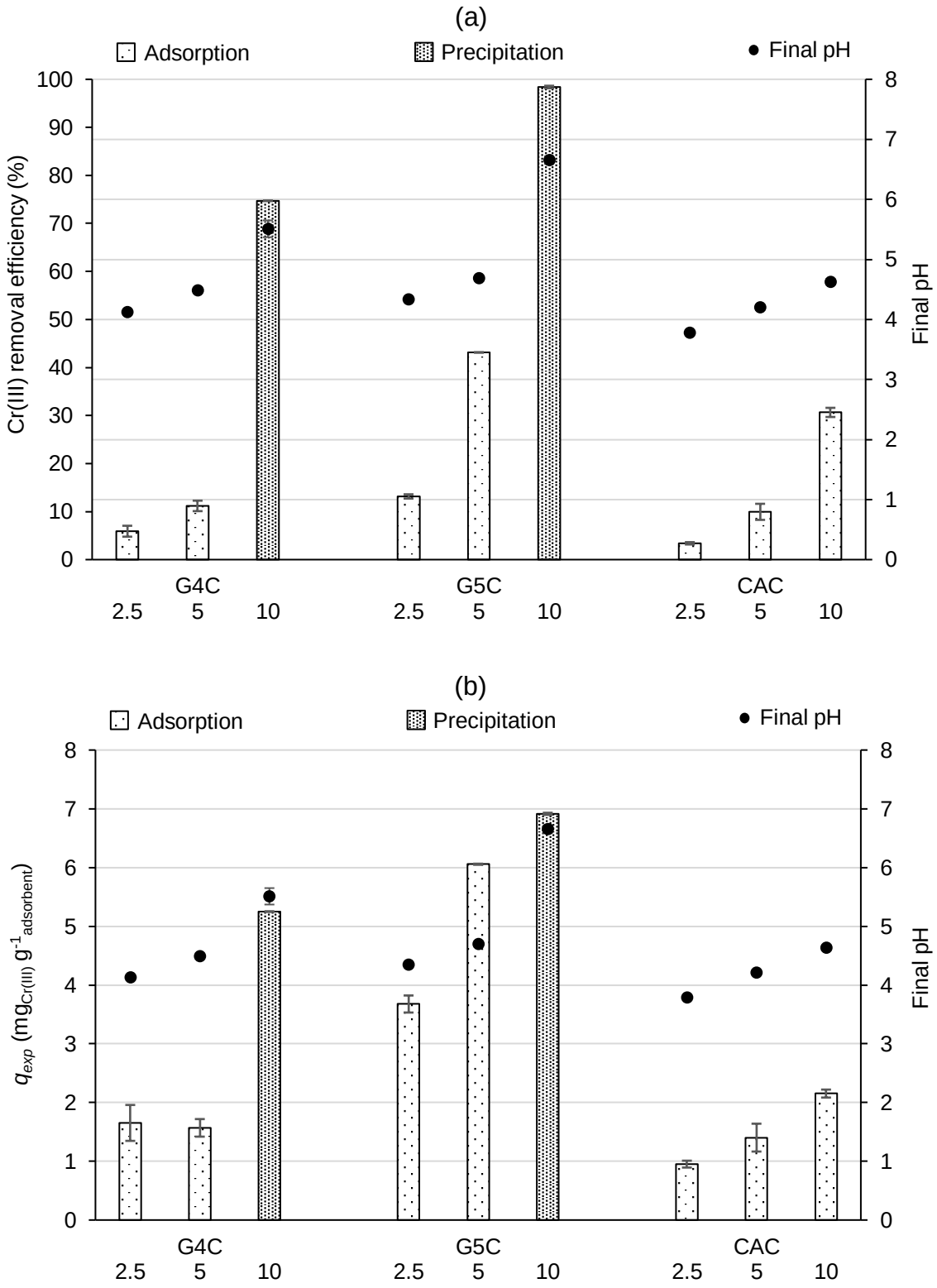

Figure 14. Effect of S/L on the Cr(III) (a) removal efficiency and (b) uptake capacity in the synthetic solution, for an initial pH 3.50. Final pH represented by dark dots; values of 2.5, 5 and 10 in x-axis represent the S/L in g L^{-1}.

The final pH values of all the assays at S/L 2.5 and 5.0 g L^{-1} were below 5.00. Since Cr could not precipitate out under these low pH conditions, adsorption should be the main removal mechanism. In these assays, Cr(III) removal was very low (bellow 13.2%). The exception occurred for G5C-5, in which a removal percentage of 43.1% was achieved; its q_{exp} of 6.06 mg g^{-1} was the second highest one, surpassing G4C-10 in which precipitation had occurred.

Globally, both chars removed more Cr(III) from the synthetic solution than CAC for an initial pH of 3.50. G5C presented the best Cr(III) removal properties, whether the removal process was by precipitation (G5C-10) or by adsorption (G5C-5).

For an initial pH of 4.50 (**Figure 15**), all adsorbents at a S/L of 10 g L^{-1} and G5C at a S/L of 5 g L^{-1} (G5C-5) removed almost all Cr(III) present in the synthetic solution (71.7 – 98.4%) (**Figure 15a**), again because the final pH of these assays were above 5.00 (5.39 – 7.52), leading to Cr precipitation. G5C-5 obtained the highest q_{exp} (11.2 mg g^{-1}) (**Figure 15b**).

All the other assays had a final pH bellow 5.00; hence, no precipitation occurred, or, at least, this removal mechanism was not very significant. Cr(III) removal was low for G4C-2.5 and CAC-2.5 (3.28% and 6.84%, respectively), but G5C-2.5 achieved a removal of 28.1%, obtaining the second highest q_{exp} (8.51 mg g^{-1}) of all the assays. Finally, G4C-5 showed a Cr(III) removal percentage of 42.3%, more than the double of CAC-5 (19.7%); this was the highest Cr(III) removal percentage by adsorption of all the assays, with a q_{exp} of 6.20 mg g^{-1}.

In all assays, as the adsorbent loading increased, the final pH of the assays also increased, due to the alkaline properties of the adsorbents, as pointed out by pH_{pzc} (section 2.3.2.4 for gasification-derived chars and section 3.3.2.2 for CAC).

Pan et al.[22] studied the pH effect on Cr(III) adsorption by using pyrolytic chars of RS (produced at 400 ºC). These authors also found that by increasing the pH, higher Cr(III) uptake capacities were registered. With similar experimental conditions (S/L of 4 g L^{-1} and initial Cr(III) concentration of 78 mg L^{-1}), for initial pH values of 4, 4.5 and 5, those authors obtained uptake capacities of 9.88, 11.4 and 12.5 mg g^{-1}, respectively. However, the authors kept the pH correction procedure during the adsorption assays until stable pH was reached, which may explain the slightly higher uptake capacities.

To select the adsorbent and experimental conditions to be used on the kinetic and adsorption isotherm studies, several factors were considered. The assays in which precipitation occurred were discarded, because this mechanism was not the core of the work. The assays in which adsorption prevailed and highest Cr(III) uptake capacities were registered comprised G5C-2.5 and G4C-5, both for an initial pH of 4.50. From these two assays, G4C-5 was selected because although G5C-2.5 assay showed a higher q_{exp}, G4C-5 assay presented a significantly higher Cr(III) removal, which is the main objective of this work. Also, G4C had 20% PE in its origin and as mentioned above, Ricevalor's main objective was to valorise the energetic fraction of the assays, and the presence of 20% PE in the gasification assays significantly improves the quality of the syngas.

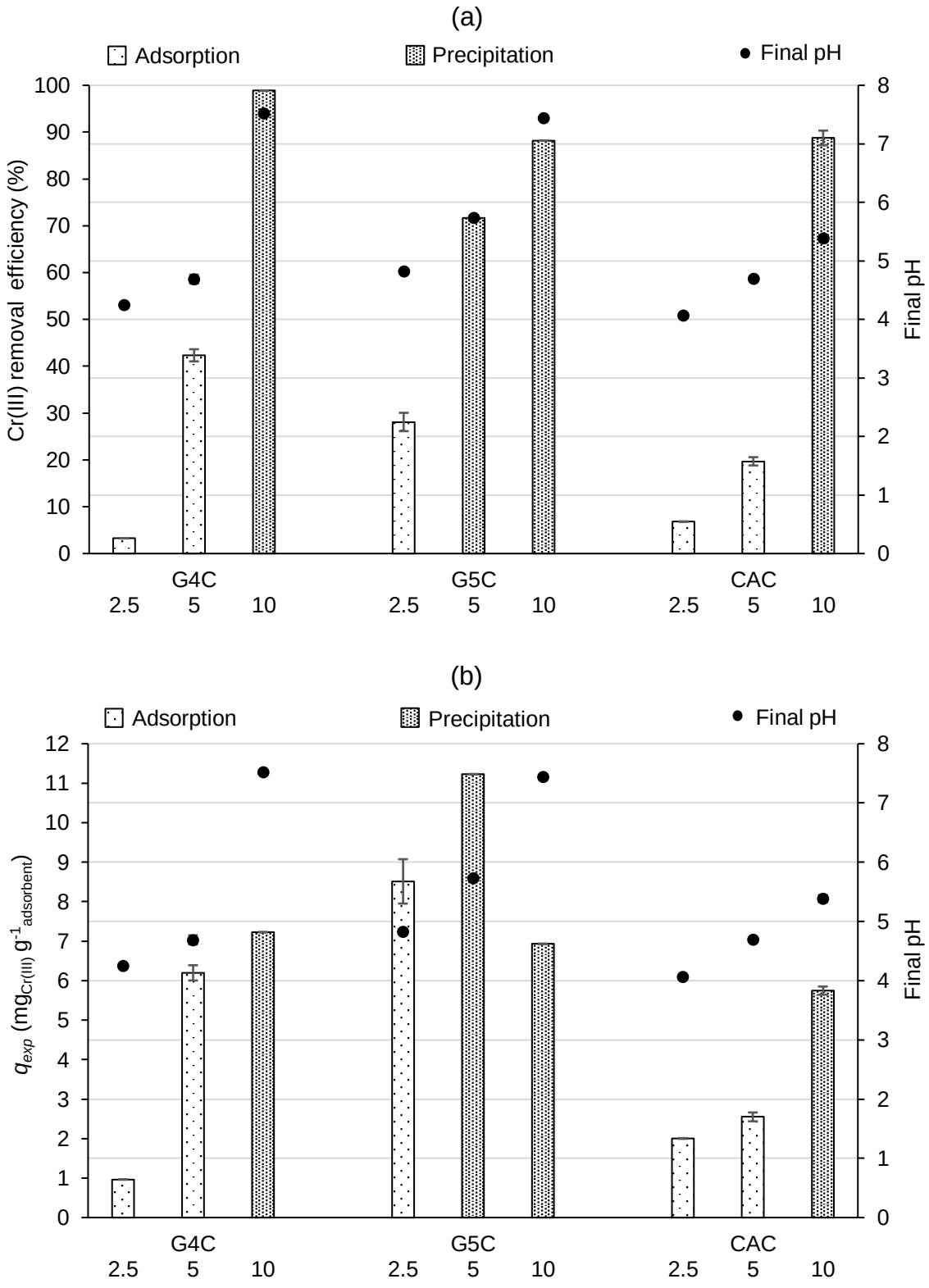

Figure 15. Effect of S/L on the (a) Cr(III) removal efficiency and (b) Cr(III) uptake capacity in the synthetic solution, for an initial pH 4.50. Final pH represented by dark dots; values of 2.5, 5 and 10 in x-axis represent the S/L in g L^{-1}.

4.3.2.2 Kinetic study

The kinetic study was performed with the same experimental conditions used in G4C-5 and CAC-5 assays with an initial pH of 4.50.

In the kinetic study, the Cr(III) removal efficiency was always higher for G4C-5 than for CAC-5 (**Figure 16**). The final pH of the assays was always below 5.00, meaning that adsorption mechanism mainly ruled Cr(III) removal. G4C-5 and CAC-5 reached the equilibrium at 30 and 20 h, respectively; removal efficiencies of 43.8% and 15.4% were achieved, respectively for G4C-5 and CAC-5.

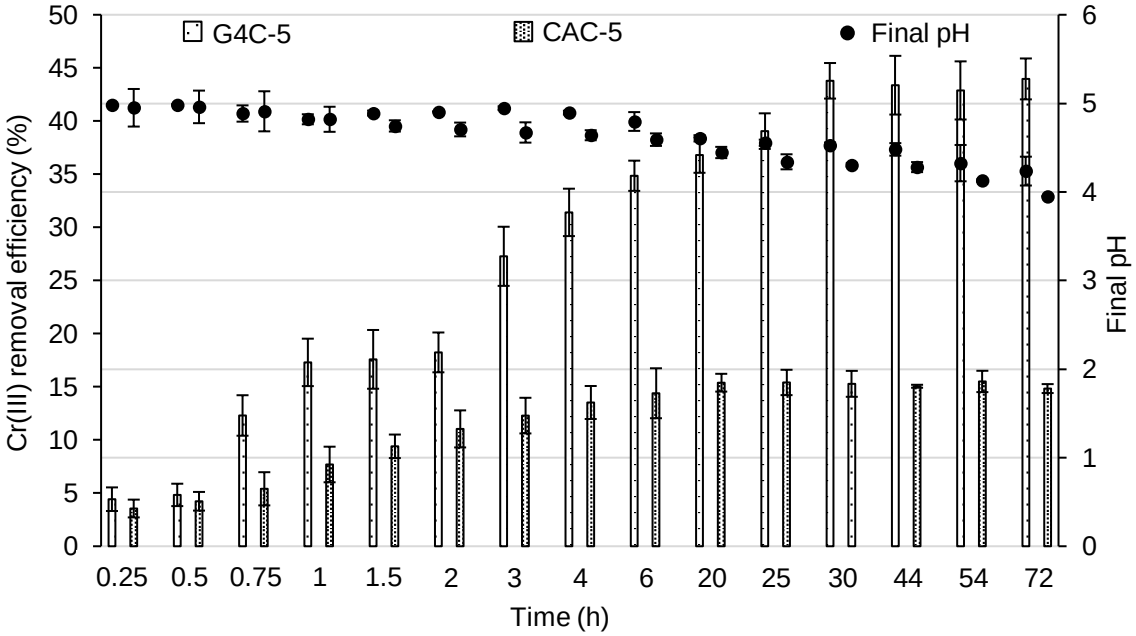

Figure 16. Cr(III) removal efficiency for G4C-5 and CAC-5 along time in the synthetic solution. Final pH represented by dark dots.

The experimental data of Cr(III) uptake capacity for both assays adjusted well to both pseudo-first and pseudo-second order kinetic models (**Figure 17**); however, they adjusted better to the latter kinetic model, reaching uptake capacities of 7.45 mg g^{-1} and 2.70 mg g^{-1} for G4C-5 and CAC-5, respectively (**Table 24**). The results showed that G4C-5 uptake capacity was almost three times higher than for CAC-5, emphasising that Cr(III) removal was mostly driven by ion exchange (G4C) rather than by pore filling (CAC). In this context, the high mineral mobility of G4C (**Table 15**) was more significant in Cr(III) removal than the better textural properties of CAC (**Table 19**).

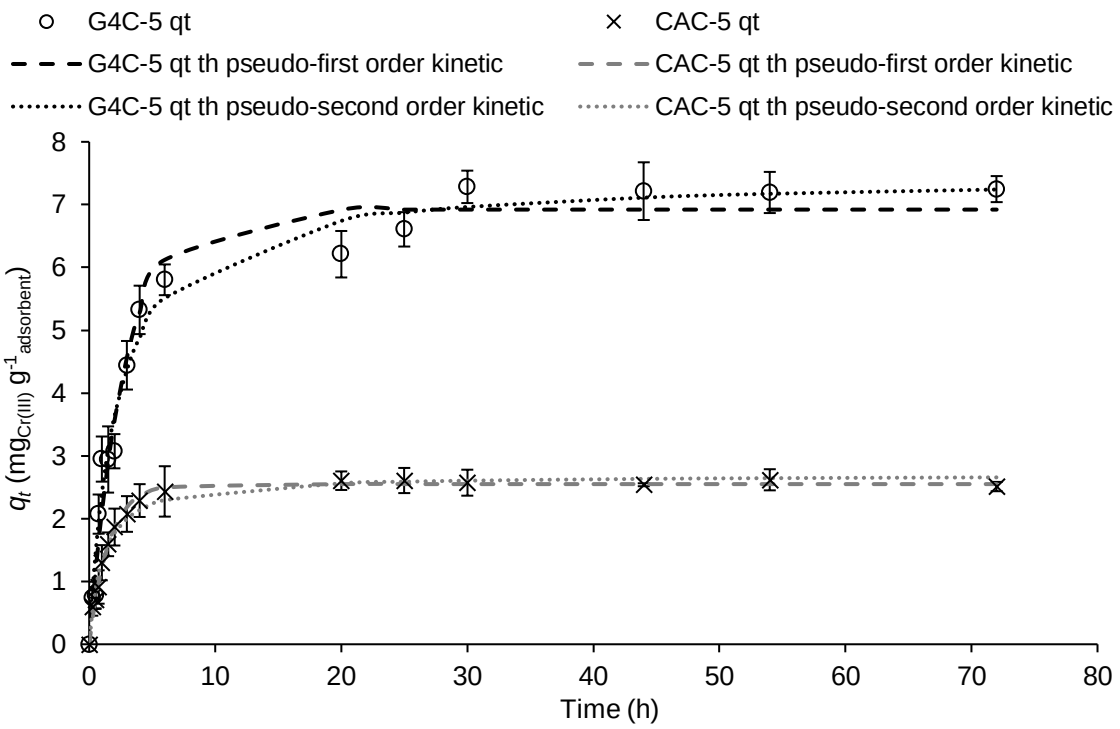

Figure 17. Cr(III) uptake capacity of G4C-5 and CAC-5 in the synthetic solution and adjustment of experimental data to pseudo-first order and pseudo-second order kinetic models (th: theoretical data).

Table 24. Parameters of pseudo-first order and pseudo-second order kinetic models adjusted to the experimental data of G4C-5 and CAC-5 in the synthetic solution.

Kinetic model	Parameter	Adsorbent	
		G4C-5	CAC-5
Pseudo-first order	q_e (mg g^{-1})	6.92	2.55
	k_f (h^{-1})	0.360	0.646
	R^2	0.977	0.993
Pseudo-second order	q_e (mg g^{-1})	7.45	2.70
	k_s (g mg^{-1} h^{-1})	0.063	0.353
	R^2	0.982	0.985

4.3.2.3 Adsorption isotherms

The study on the adsorption isotherms was performed with the same experimental conditions used in the assays with G4C-5 and CAC-5, with an initial pH of 4.50 and a contact time of 30 h.

The data of the adsorption isotherms study (**Figure 18**) showed that in the assays with initial concentrations < 50 $mg_{Cr(III)}$ L^{-1} chromium precipitation occurred, reaching Cr(III) removal percentages closer to 100% (**Figure 18a**). On the other hand, for the assays with initial

concentrations ≥ 50 $mg_{Cr(III)}$ L^{-1} no precipitation was registered. This was due to the dissociation of water molecule by Cr(III), releasing H^+ and promoting the solution acidification. Increases in Cr(III) concentration will favour this phenomenon[24]. At an initial concentration of 30 $mg_{Cr(III)}$ L^{-1}, CAC-5 presented a lower efficiency for Cr(III) removal (74.8%), because the final pH was of 5.06, meaning that only a part of Cr(III) might be precipitated (**Figure 18a**).

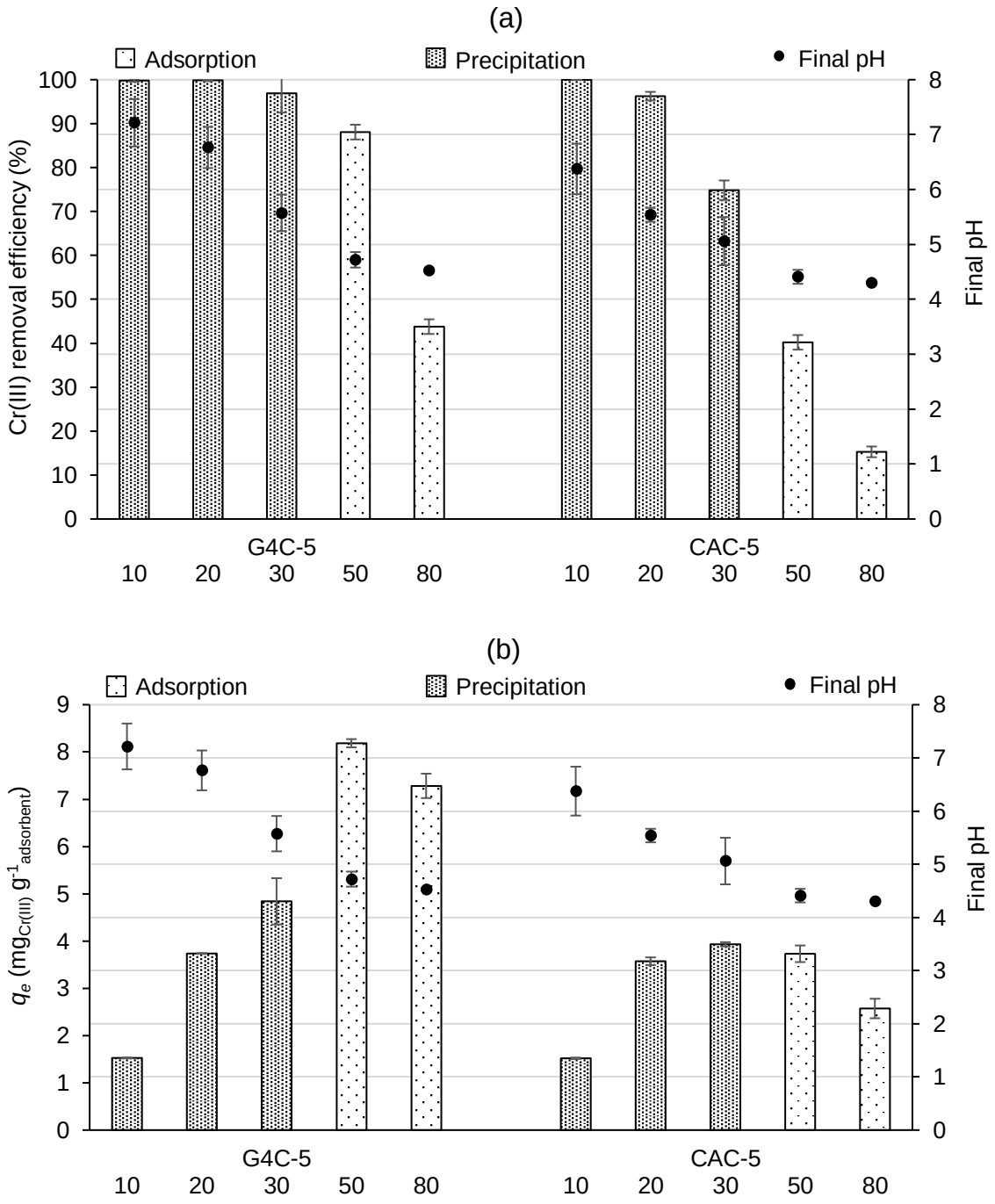

Figure 18. (a) Cr(III) removal efficiency and (b) Cr(III) uptake capacity for G4C-5 and CAC-5 in the synthetic solution for different initial Cr(III) concentrations. Final pH represented by dark dots; values of 10 to 80 in x-axis represent the initial Cr(III) concentrations in mg L^{-1}.

In Cr(III) removal assays with a final pH below 5.00, i.e. ruled by adsorption (assays with initial Cr(III) concentrations of 50 and 80 mg L^{-1}), G4C-5 consistently presented better results than CAC-5. The best result was achieved for an initial concentration of 50 $mg_{Cr(III)}$ L^{-1}, presenting a Cr(III) removal percentage of 88.1% (**Figure 18a**) and an uptake capacity of 8.19 mg g^{-1} (**Figure 18b**).

The experimental data were adjusted to Langmuir's and Freundlich's non-linear adsorption models (**Figure 19**). The results showed that the adjustment to both models was not very good with R^2 values ≤ 0.880 (**Table 25**). Still, the adjustment to Langmuir's model was the best for both adsorbents which suggests that the adsorption occurred through a monolayer process. The maximum uptake capacity for G4C-5 was of 6.95 mg L^{-1}, while for CAC-5 was of 3.45 mg L^{-1}, demonstrating once again the better results obtained by G4C-5.

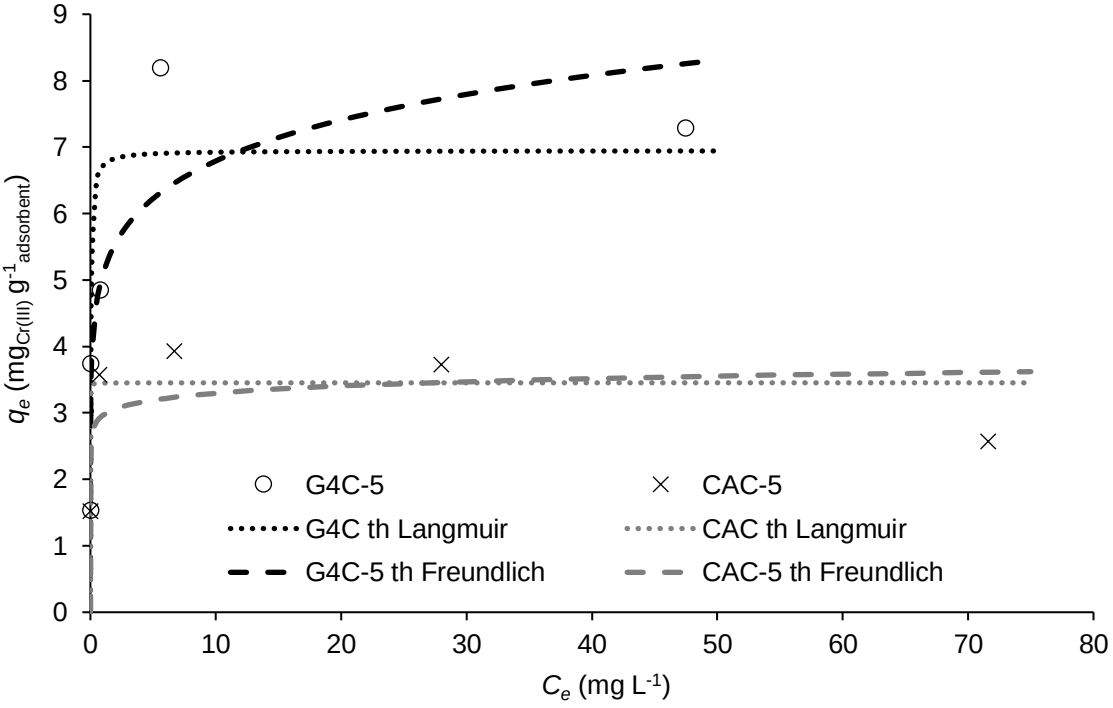

Figure 19. Langmuir's and Freundlich's non-linear adsorption models adjusted to the experimental data of G2C-5 and CAC-5 in the synthetic solution (th: theoretical data).

Pan et al.[22] also studied Cr(III) adsorption by using RS biochars. Similarly to the present work, their experimental data adjusted better to Langmuir's adsorption model (R^2 = 0.99). However, these authors obtained a higher q_{max} (14.0 mg g^{-1}), probably due to the constant pH correction (until stable pH) performed by them during the adsorption assays.

Table 25. Parameters of Langmuir's and Freundlich's non-linear adsorption models adjusted to the experimental data of G4C-5 and CAC-5 in the synthetic solution.

Isotherm model	Parameter	Adsorbent	
		G4C-5	CAC-5
Langmuir's non-linear	q_{max} (mg g^{-1})	6.95	3.45
	b (L mg^{-1})	29.6	787
	R^2	0.880	0.908
Freundlich's non-linear	K_F (mg g^{-1} mg^{-n} L^n)	5.09	2.96
	n (dimensionless)	7.98	21.5
	R^2	0.864	0.793

4.3.3 Cr(III) removal assays from industrial wastewater

Precipitation occurred in the Cr(III) removal assays from the industrial wastewater, with initial concentrations of 50 and 100 $mg_{Cr(III)}$ L^{-1}, once the final pH of all these samples was above 5.00 (**Figure 20**). The assays with an initial concentration of 50 $mg_{Cr(III)}$ L^{-1} presented the highest final pH values (7.22, for G4C-5, and 6.07, for CAC-5) and, consequently, the highest Cr(III) removal efficiencies (94.0%, for G4C-5, and 89.7%, for CAC-5) (**Figure 20a**). However, despite the lower Cr(III) removal efficiencies (69.6%, for G4C-5, and 65.4%, for CAC-5) (**Figure 20a**), the assays with an initial concentration of 100 $mg_{Cr(III)}$ L^{-1} showed the highest uptake capacities (14.9 mg g^{-1}, for G4C-5, and 14.0 mg g^{-1}, for CAC-5) (**Figure 20b**). These results suggest that G4C-5 was more efficient on Cr(III) removal by precipitation than CAC-5.

For an initial concentration of 200 $mg_{Cr(III)}$ L^{-1}, the final pH of all these samples was slightly below 5.00, meaning that a mixture of removal mechanisms (adsorption and precipitation) might be involved in Cr(III) removal. G4C-5 removed 28.8% of Cr(III), obtaining a q_{exp} of 11.5 mg g^{-1}. However, unlike the results in which precipitation occurred, the highest Cr(III) removal efficiency (**Figure 20a**) and uptake capacity (**Figure 20b**) were found for CAC-5, namely 40.4% and 16.1 mg g^{-1}, respectively. This was probably due to other chemical species present in the wastewater that could compete on Cr(III) removal by G4C.

Comparing the removal assays from the synthetic solution with the removal assays from the industrial wastewater, it was concluded that although Cr(III) removal efficiencies were higher in the synthetic solution, the uptake capacities of the adsorbents were much higher in the industrial wastewaters due to the higher concentration of Cr(III).

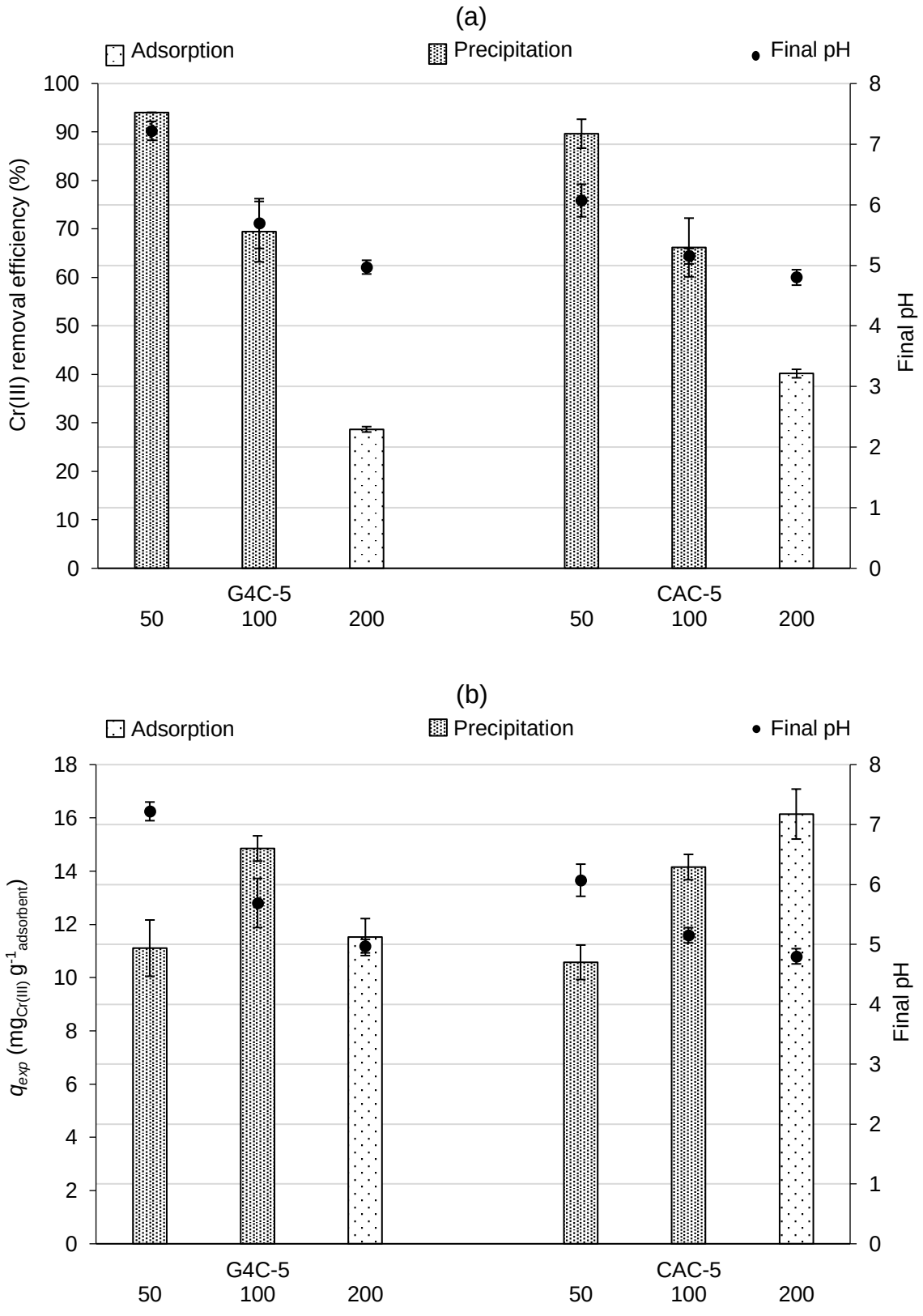

Figure 20. (a) Cr(III) removal efficiency and (b) Cr(III) uptake capacity for G4C-5 and CAC-5 on the removal assays from the industrial wastewater. Final pH represented by dark dots; values of 50, 100 and 200 in x-axis represent the initial Cr(III) concentrations in mg L^{-1}.

4.3.4 Cr(III) removal mechanisms

Due to the weak porous structure of G4C-5 (**Table 14**), ion exchange was probably the most important mechanism in Cr(III) removal by this adsorbent, under the conditions in which the precipitation is limited. The results on the concentration and percentage variation of cations (**Figure 21**) support this conclusion. G4C-5 added 71.9 mg L^{-1} of other chemical elements to the industrial wastewater, mainly Ca (26.8 mg L^{-1}), K (24.6 mg L^{-1}) and Mg (18.8 mg L^{-1}), and removed 61.6 mg L^{-1} of chemical elements from the industrial wastewater, mainly Cr (57.4 mg L^{-1}). These results suggest that Cr(III) removal from the industrial wastewater by G4C-5 was due to ion exchange with Ca, K and Mg. Similar results were obtained in a previous study[24].

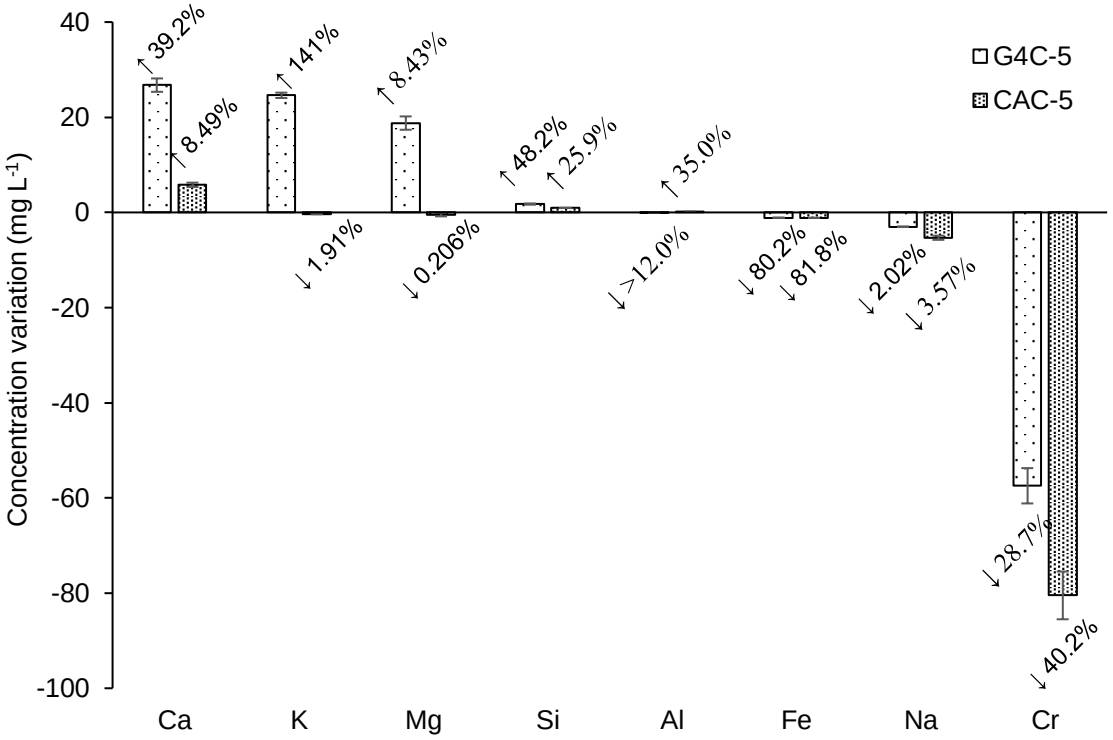

Figure 21. Concentration and percentage variations of cations on the Cr(III) removal assays with G4C-5 and CAC-5 in the industrial wastewater, for an initial concentration of 200 $mg_{Cr(III)}$ L^{-1}.

CAC-5 presented different results, once this adsorbent only added 7.69 mg L^{-1} of other chemical elements to the industrial wastewater, mainly Ca (5.80 mg L^{-1}), and removed 87.74 mg L^{-1} of chemical elements present in the industrial wastewater, mainly Cr (80.5 mg L^{-1}). The results suggest that Cr(III) removal from the industrial wastewater by CAC-5 was mainly due to pore filling.

These results suggest that the lowest Cr(III) removal efficiency and uptake capacity of G4C-5 compared to CAC-5 could be related to the presence of other chemical species in the industrial

wastewater, besides the metals and metalloids studied in this work, which can compete by the adsorption of Cr(III) onto G4C.

4.4 Conclusions

For the removal assays performed in the synthetic solution, both chars presented higher removal efficiencies and uptake capacities than CAC, either by precipitation or adsorption. At a S/L of 5 g L^{-1}, G4C was the char selected to be used in the kinetic studies and adsorption isotherms. This char obtained a highest uptake capacity of 8.19 mg g^{-1} (at an initial concentration of 50 $mg_{Cr(III)}$ L^{-1}) and an uptake capacity in equilibrium (q_e) of 7.45 mg g^{-1}, while CAC-5 only obtained values of 3.93 and 2.70 mg g^{-1}, respectively, emphasizing the best results for the gasification char.

For the removal assays done in the industrial wastewater (performed at a S/L of 5 g L^{-1}), the char G4C presented better results than CAC when precipitation occurred, obtaining uptake capacities of 14.9 mg g^{-1} and 14.0 mg g^{-1}, respectively, at an initial concentration of 100 $mg_{Cr(III)}$ L^{-1}. However, when adsorption ruled (at an initial concentration of 200 $mg_{Cr(III)}$ L^{-1}), CAC obtained better results than G4C (q_{exp} of 11.5 mg g^{-1} and 16.1 mg g^{-1}, respectively).

In general, Cr(III) removal efficiencies were higher in the synthetic solution, but the uptake capacities of the adsorbents were much higher in the industrial wastewaters.

Apart from precipitation, the adsorption mechanisms involved in Cr(III) removal by G4C and CAC were ion exchange and pore filling, respectively. The high mineral content of chars played an important role in Cr(III) removal.

5. CR(III) REMOVAL ASSAYS BY PYROLYSIS ACTIVATED CARBONS UNDER BATCH CONDITIONS

The results presented in this chapter were published, partially or completely, in the following scientific publications:

Papers:

D. Dias, M. Bernardo, N. Lapa, F. Pinto, I. Matos and I. Fonseca, Activated Carbons from the Co-pyrolysis of Rice Wastes for Cr(III) Removal, *Chemical Engineering Transactions*, 65 (2018) 601-606.
(doi: 10.3303/CET1865101)

D. Dias, M. Bernardo, I. Matos, I. Fonseca, F. Pinto, N. Lapa, Activation of co-pyrolysis chars from rice wastes to improve the removal of Cr^{3+} from simulated and real industrial wastewaters, *Journal of Cleaner Production*, 267 (2020) 121993.

Oral Presentations:

D. Dias, M. Miguel, M. Bernardo, N. Lapa, I. Matos, I. Fonseca, F. Pinto. Removal of Cr(III) by using activated carbons produced from rice waste chars, *DCE17 - 2nd Doctoral Congress of Engineering, 8-9 June 2017*, Porto, Portugal

D. Dias, M. Miguel, N. Lapa, M. Bernardo, I. Matos, I. Fonseca and F. Pinto, Efficient activated carbons from chars of the co-pyrolysis of rice wastes, *4th International Conference "WASTES: Solutions, Treatments and Opportunities"*, 25-26 September 2017, Porto, Portugal.

D. Dias, M. Bernardo, N. Lapa, F. Pinto, I. Matos and I. Fonseca, Activated Carbons from the Co-pyrolysis of Rice Wastes for Cr(III) Removal, *International Conference on Biomass (IconBM)*, 17-20 June 2018, Bologna, Italy.

D. Dias, M. Bernardo, N. Lapa, F. Pinto, I. Matos, I. Fonseca, Cr(III) Removal from Aqueous Solution by Activated Carbons obtained through the Co-pyrolysis of Wastes from Rice Production, *13th International Chemical and Biological Engineering Conference (CHEMPOR 2018)*, 2-4 October 2018, Aveiro, Portugal.

5.1 Introduction

In this chapter the pyrolysis-derived activated carbons characterised in Chapter 3 were used in removal assays of Cr(III) from a synthetic solution and from an industrial wastewater. To recall, the activated carbons are P1C+PA (P1C physically activated), P1C+PA+W (P1C physically activated and washed), P1C+PA+CT (P1C physically activated and chemically treated) and P1C+CA (P1C chemically activated).

For comparison purposes, P1C (the pyrolysis char that was in the origin of the pyrolysis-derived activated carbons), CAC and CAC+CT (CAC chemically treated) (section 3.2.1.5) were also used in the Cr(III) removal assays.

5.2 Materials and methods

5.2.1 Cr(III) removal from a synthetic solution

A Cr(III) solution with an initial concentration of 70 ± 5 $mg_{Cr(III)}$ L^{-1} was prepared by diluting a standard $Cr(NO_3)_3$ solution of 1000 $mg_{Cr(III)}$ L^{-1} in HNO_3 0.5 M (Merck) with ultrapure water (Milli-Q Academic). The initial pH of Cr(III) solution was corrected to 4.5, once Cr(III) starts to precipitate at a pH above 5.0 [179]. All Cr(III) removal assays were performed as described in section 4.2.3.

5.2.1.1 Influence of solid/liquid ratio (S/L)

To study the influence of S/L two ratios were tested: 5.0 and 10 g L^{-1}. To simplify the data reading, some codes were created for each assay: the name of the adsorbent was followed by the S/L used (same as described in section 4.2.3.1). The contact time for these assays was 24 h.

Cr(III) removal efficiency, η (%), and experimental adsorbent removal capacity, q_{exp} (mg g^{-1}), were calculated by equations 4.2 and 4.3 (section 4.2.3.1), respectively.

The sample that performed better was selected for the kinetic and adsorption isotherm studies.

5.2.1.2 Kinetic study

Contact times between 0.25 and 96 h were tested. The results were adjusted to pseudo-first order and pseudo-second order kinetic models[171], through the equations 4.4 and 4.5 (section 4.2.3.2), respectively.

5.2.1.3 Adsorption isotherm study

Cr(III) concentrations between 10 and 80 ± 5 mg L^{-1} were tested. The results were adjusted to Langmuir's (equation 4.6 - section 4.2.3.3) and Freundlich's non-linear models (equation 4.7 - section 4.2.3.3)[173].

5.2.1.4. Modelling

The same as described in section 4.2.3.4.

5.2.2 Cr(III) removal from industrial wastewater

The origin and characterisation of the industrial wastewater were already described (sections 4.2.2 and 4.3.1, respectively).

The adsorbent and conditions (S/L and contact time) that performed better on the synthetic solution were selected for the Cr(III) removal assays in the industrial wastewater. By diluting the industrial wastewater with ultrapure water (Milli-Q Academic), two initial concentrations of Cr(III) were tested: 50 and 200 mg L^{-1}. The initial pH of the media was not corrected.

The procedure for the Cr(III) removal assays was the same as described in section 4.2.3.

5.2.3. Cr(III) removal mechanisms

Cr(III) removal from aqueous solutions may occur through different mechanisms, namely pore filling or physical adsorption, chemical adsorption and precipitation. To evaluate if ion exchange mechanism had an important role in Cr(III) removal, Al, Ca, Fe, K, Mg, Na and Si were quantified on the assay that provided the highest Cr(III) removal from the industrial wastewater. These elements were selected because they were present either in the industrial wastewater or in the adsorbent. Concentration variation, CV (mg L^{-1}), and percentage variation, PV (%), were calculated by equations 4.9 and 4.10 (section 4.2.5), respectively.

The procedure for the removal assays was the same as described in section 4.2.3, but instead of just Cr, all elements mentioned above were quantified by ICP-AES.

5.3 Results and discussion

5.3.1 Cr(III) removal from synthetic solution

5.3.1.1 Influence of S/L

P1C, being a non-porous material (**Table 14**), barely removed Cr(III) (≤ 3.66%) from the synthetic solution (**Figure 22a**). However, the optimizations of P1C increased the Cr(III) removal efficiency of the material.

P1C+PA showed the highest Cr(III) removal efficiencies (**Figure 22a**) and uptake capacities (**Figure 22b**) of all pyrolysis-derived ACs. P1C+PA-10 removed almost all Cr(III) from the synthetic solution (99.9%); however the final pH of the assay was 6.65, and above pH 5 Cr(III) precipitates[179], therefore this removal was mainly by precipitation.

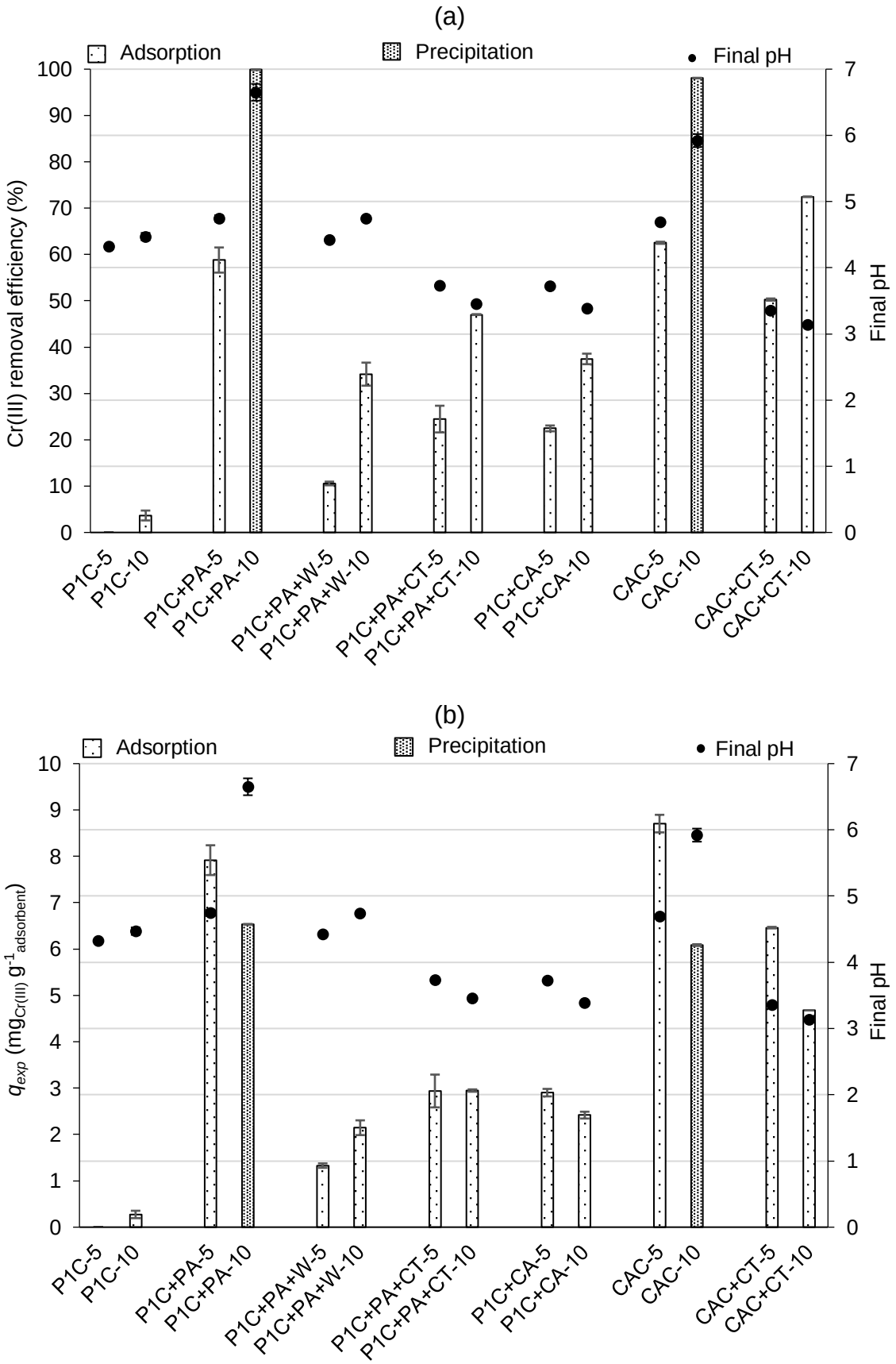

Figure 22. Effect of S/L on the (a) Cr(III) removal efficiency and (b) Cr(III) uptake capacity in the synthetic solution. Final pH is represented by dark dots.

P1C+PA-5 presented a final pH of 4.75, therefore precipitation was limited and Cr(III) removal (58.8%) was likely ruled by adsorption (through ion exchange with the cations provided by the adsorbent - **Table 15**) and pore filling (due to the interesting porous properties of this adsorbent - **Table 19**). P1C+PA-5 presented a higher uptake capacity than P1C+PA-10 (7.92 and 6.53 mg g^{-1}, respectively), so, under these conditions, precipitation was not the most efficient removal mechanism.

The final pH of all the other assays with pyrolysis-derived ACs was below 5, so Cr(III) removal was likely ruled by chemical adsorption and/or pore filling.

P1C+PA+W presented much lower removal efficiencies (10.6% for S/L = 5 and 34.2% for S/L = 10) and uptake capacities (1.33 mg g^{-1} for S/L = 5 and 2.15 mg g^{-1} for S/L = 10) than P1C+PA, despite its better textural properties (**Table 19**). This probably occurred because the washing step removed minerals (**Table 18**) that could have been used for ion exchange, which highlighted the importance of ion exchange in the Cr(III) removal.

P1C+PA+CT also presented lower removal efficiencies (24.5% for S/L = 5 and 47.0% for S/L = 10) and uptake capacities (2.94 mg g^{-1} for S/L = 5 and 2.95 mg g^{-1} for S/L = 10) than P1C+PA. This probably occurred because P1C+PA+CT presented the lowest surface area and pore volume of all ACs tested (**Table 19**), and the acidic treatment and washing removed minerals (**Table 18**) that could have been used for ion exchange. Still, P1C+PA+CT presented slightly higher removal efficiencies and uptake capacities than P1C+PA+W, despite its much lower surface area and pore volume, suggesting that the chemical treatment successfully incorporated some functional groups in the adsorbent's surface.

Finally, P1C+CA presented similar results to P1C+PA+CT, both in the Cr(III) removal efficiencies (22.5% for S/L = 5 and 37.5% for S/L = 10) and uptake capacities (2.90 mg g^{-1} for S/L = 5 and 2.42 mg g^{-1} for S/L = 10), meaning that under these conditions to chemically treat P1C+PA or chemically activate P1C presented no significant differences, even though P1C+CA obtained the highest surface area and pore volume of all adsorbents (**Table 19**). These results suggest that (i) P1C+PA+CT had more functional groups able to form complexes with Cr ions at the surface than P1C+CA, which would compensate the lower surface area and pore volume, and/or (ii) pore filling did not play a significant role and ion exchange seemed to be the main Cr(III) removal mechanism.

Regarding CAC, it presented very similar results to P1C+PA; CAC-10 removed 98.1% of Cr(III) due to precipitation (final pH = 5.92) and CAC-5 removed 62.5% due to pore filling (final pH = 4.69). The highest uptake capacity was also found at the S/L 5 instead of S/L 10 (8.71 and 6.09 mg g^{-1}, respectively), meaning that, again, precipitation was not the most efficient removal mechanism.

CAC+CT presented lower removal efficiencies (50.3% for S/L = 5 and 72.4% for S/L = 10) and uptake capacities (6.46 mg g^{-1} for S/L = 5 and 4.68 mg g^{-1} for S/L = 10) than CAC, indicating that (i) CAC+CT did not had enough functional groups at the surface to compensate the lower surface

area and pore volume (CAC+CT presented a lower surface area and pore volume than CAC - **Table 19**) and/or (ii) pore availability was more important than the presence of functional groups in the adsorbent's surface.

Based on the results of the influence of S/L in Cr(III) removal, P1C+PA-5 and CAC-5 samples were selected to be used in the following studies.

5.3.1.2 Kinetic study

The kinetic study showed that equilibrium was reached at 32h for P1C+PA-5 and 48h for CAC-5, reaching maximum Cr(III) removal efficiencies (**Figure 23**) of 60.4% for P1C+PA and 71.1% for CAC-5. The final pH was always below 5, meaning that precipitation was limited.

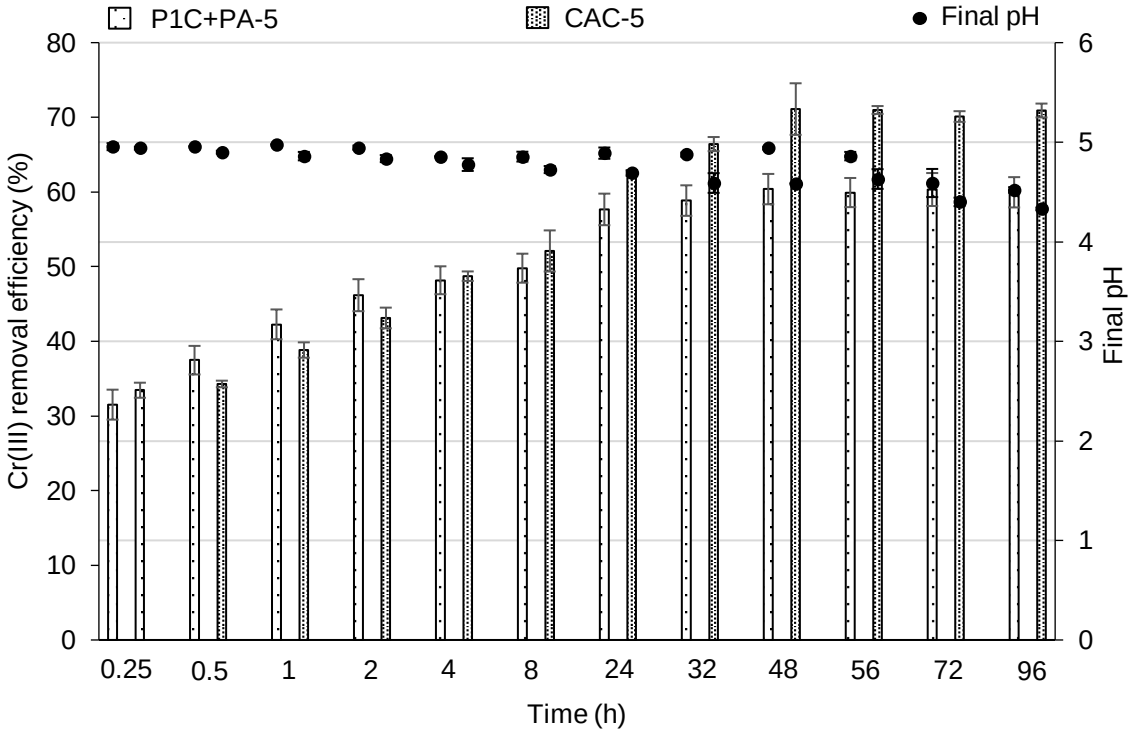

Figure 23. Cr(III) removal efficiency for P1C+PA-5 and CAC-5 along time in the synthetic solution. Final pH represented by dark dots.

Cr(III) uptake capacities of P1C+PA-5 and CAC-5 (**Figure 24)** adjusted better to the pseudo-second order kinetic model (R^2 of 0.957 and 0.903, respectively), obtaining a q_e of 8.05 and 9.25 mg g^{-1}, respectively (**Table 26**).

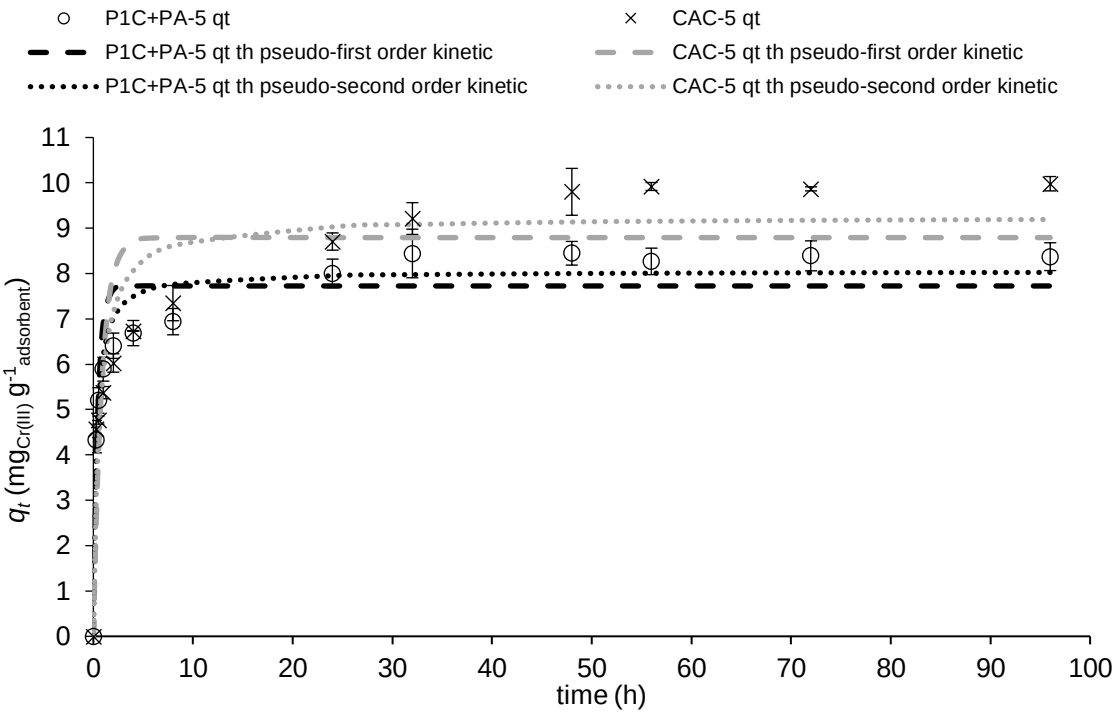

Figure 24. Cr(III) uptake capacity of P1C+PA-5 and CAC-5 in the synthetic solution and adjustment of experimental data to pseudo-first order and pseudo-second order kinetic models (th: theoretical data).

Table 26. Parameters of pseudo-first order and pseudo-second order kinetic models adjusted to the experimental data of P1C+PA-5 and CAC-5 in the synthetic solution.

Kinetic model	Parameter	Adsorbent	
		P1C+PA-5	CAC-5
Pseudo-first order kinetic	q_e (mg g^{-1})	7.73	8.79
	k_f (h^{-1})	2.27	1.19
	R^2	0.893	0.811
Pseudo-second order kinetic	q_e (mg g^{-1})	8.05	9.25
	k_s (g mg^{-1} h^{-1})	0.420	0.184
	R^2	0.957	0.903

5.3.1.3 Adsorption isotherms

For the study on the adsorption isotherms, 48 h assays were performed for both P1C+PA-5 and CAC-5.

The assays with initial concentrations ≤ 30 $mg_{Cr(III)}$ L^{-1} showed Cr(III) removals of almost 100%, for both adsorbents, due to precipitation (**Figure 25a**). For the assays with initial concentrations

≥ 50 $mg_{Cr(III)}$ L^{-1}, Cr(III) removal was limited (pH < 5). Nevertheless, for an initial concentration of 50 $mg_{Cr(III)}$ L^{-1}, almost full removals were obtained (91.8% for P1C+PA-5 and 83.0% for CAC-5). Opposing the previous results (influence of S/L and kinetic studies), P1C+PA-5 obtained a higher Cr(III) removal than CAC-5 for this initial concentration. The assays with initial concentrations > 50 $mg_{Cr(III)}$ L^{-1} obtained lower removal efficiencies for both adsorbents.

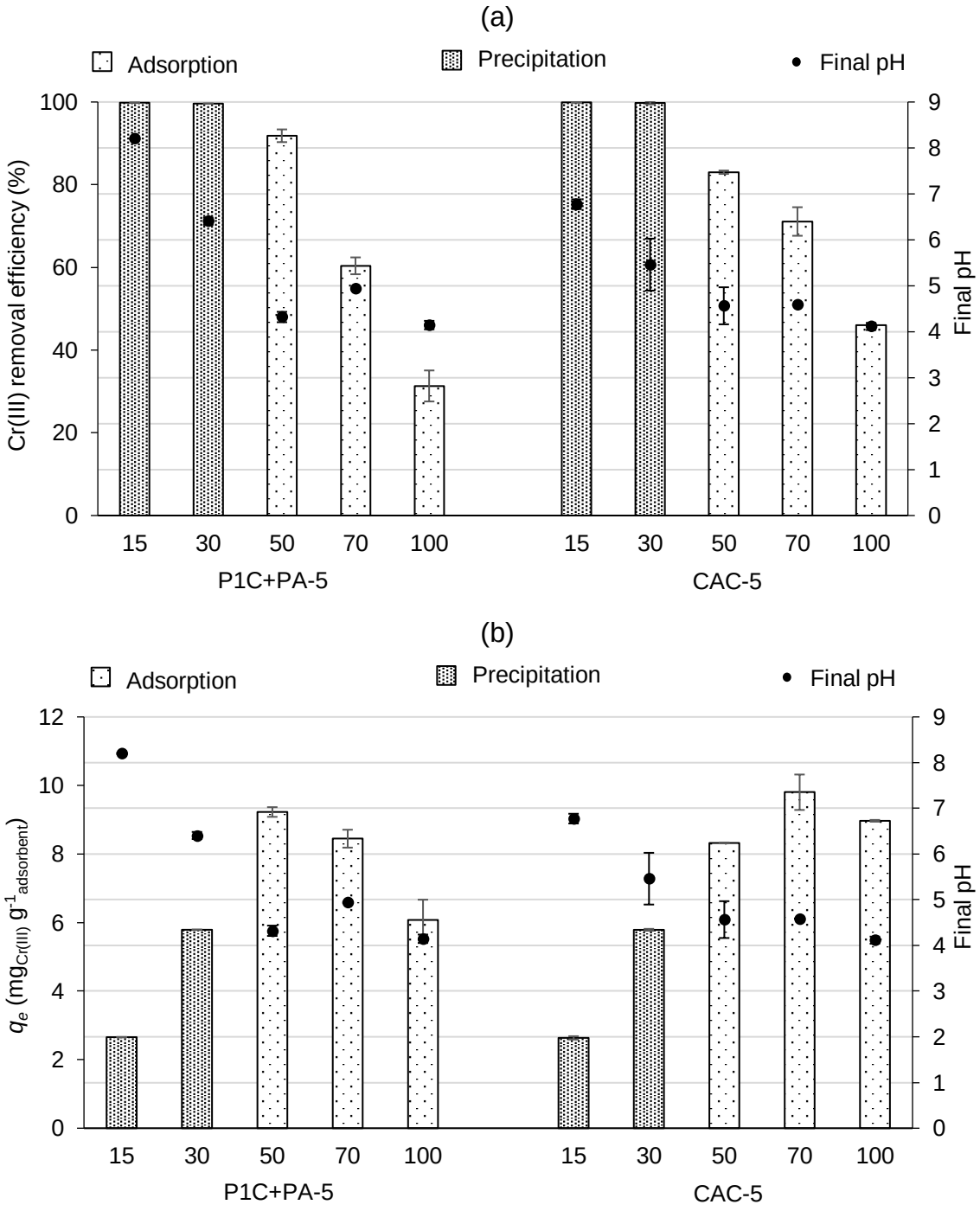

Figure 25. (a) Cr(III) removal efficiency and (b) Cr(III) uptake capacity for P1C+PA-5 and CAC-5 in the synthetic solution for different initial Cr(III) concentrations. Final pH represented by dark dots; values of 15 to 100 in x-axis represent the initial Cr(III) concentrations in mg L^{-1}.

Regarding the Cr(III) uptake capacity (**Figure 25b**), the highest values were found for the initial concentrations of 50 $mg_{Cr(III)}$ L^{-1} for P1C+PA-5 (9.23 mg g^{-1}) and 70 $mg_{Cr(III)}$ L^{-1} for CAC-5 (9.80 mg g^{-1}). As seen in the previous studies, the highest Cr(III) uptake capacities were found for the assays in which the precipitation was limited, emphasizing that the main Cr(III) removal mechanisms were ion exchange and pore filling for P1C+PA-5 and pore filling for CAC-5.

The data adjustment to Langmuir's and Freundlich's isotherms (**Figure 26** and **Table 27**) showed that the experimental data were better adjusted to Langmuir's non-linear adsorption models for both adsorbents, suggesting that the adsorption occurred through a monolayer process. P1C+PA-5 and CAC-5 obtained a q_{max} of 7.94 and 9.03 mg g^{-1}, respectively.

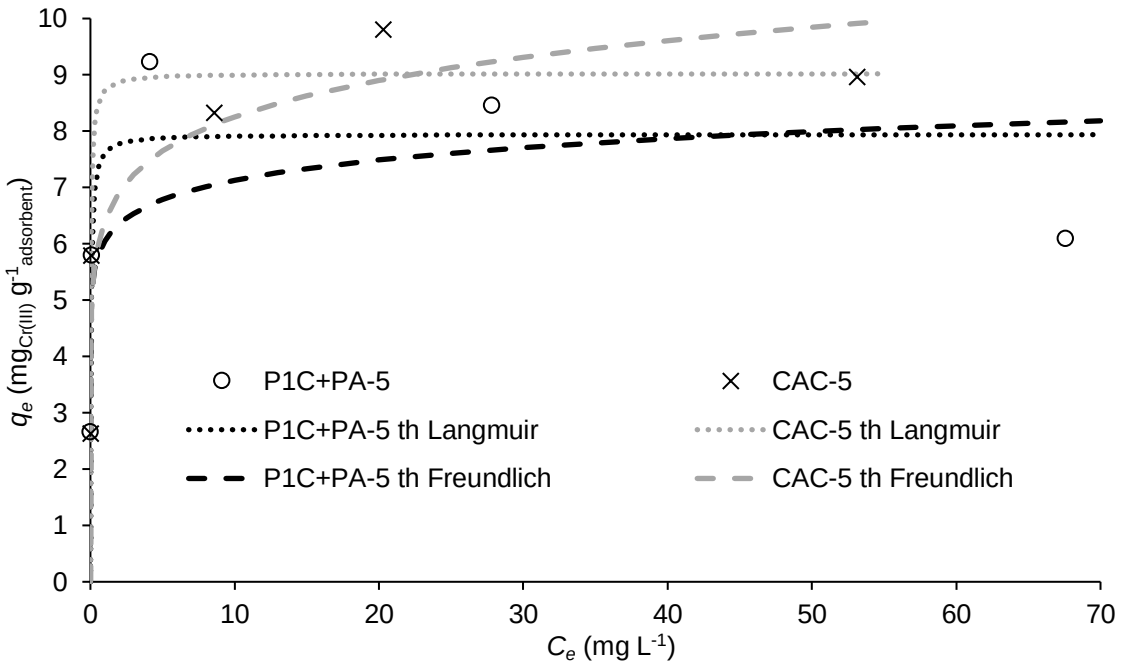

Figure 26. Langmuir's and Freundlich's non-linear adsorption models adjusted to the experimental data of P1C+PA-5 and CAC-5 in the synthetic solution (th: theoretical data).

No bibliography was found on Cr(III) removal by ACs obtained from rice husk pyrolysis, thus the results were compared to rice waste chars and other chars/ACs obtained from pyrolysis of different wastes (**Table 28**). Vassileva et al.[111] used RH chars on Cr(III) removal and obtained similar results to the present work, while Qian et al.[112] used RS chars washed with distilled water and obtained lower uptake capacities that the ones found in this work. Other authors that used different feedstocks to produce chars/ACs obtained slightly higher uptake capacities than the ones reported in this paper[22,107,108]. The different feedstocks and experimental conditions may explain this factor.

Table 27. Parameters of the Langmuir's and Freundlich's non-linear adsorption models adjusted to the experimental data of P1C+PA-5 and CAC-5 in the synthetic solution.

Isotherm model	Parameter	Adsorbent	
		P1C+PA-5	CAC-5
Langmuir's non-linear	q_{max} (mg g^{-1})	7.94	9.03
	b (L mg^{-1})	23.1	29.9
	R^2	0.909	0.985
Freundlich's non-linear	K_F (mg g^{-1} mg^{-n} L^n)	6.05	6.41
	n (dimensionless)	14.1	9.12
	R^2	0.745	0.941

Table 28. Adsorption capacities of chars/ACs from pyrolysis of different wastes for Cr(III) removal from aqueous solutions found in literature.

Temperature (°C)	Feedstocks	Activation/Treatment	Adsorption capacity (mg g^{-1})	Reference
250 – 700	Rice husk	No	4.61 – 10.6	Vassileva et al.[111]
300	Rice husk	No	15.1	Agrafioti et al.[109]
400	Rice straw	No	14.0	Pan et al.[22]
	Peanut straw		25.0	
	Soybean straw		17.2	
	Canola straw		14.6	
100 – 700	Rice straw	Washed with distilled water and sonicated	2.4 – 6.5	Qian et al.[112]
800	*Eucalyptus grandis* wood sawdust	Physically activated with direct CO_2 and oxidized with HNO_3	17.5	Milich et al.[107]
		Physically activated with partial CO_2 and oxidized with HNO_3	25.5	
		Physically activated with partial air and oxidized with HNO_3	29.0	
500	Sugarcane pulp	No	15.9	Yang et al.[108]

5.3.2 Cr(III) removal from industrial wastewater

P1C+PA-5 and CAC-5 presented higher Cr(III) removals on the assays with an initial concentration of 50 $mg_{Cr(III)}$ L^{-1} (86.0% and 89.7%, respectively) than on the assays with an initial concentration of 200 $mg_{Cr(III)}$ L^{-1} (31.9% and 40.2%, respectively) (**Figure 27a**). However, in the first case, precipitation occurred (final pH > 5), while in the second case precipitation was limited (final pH < 5).

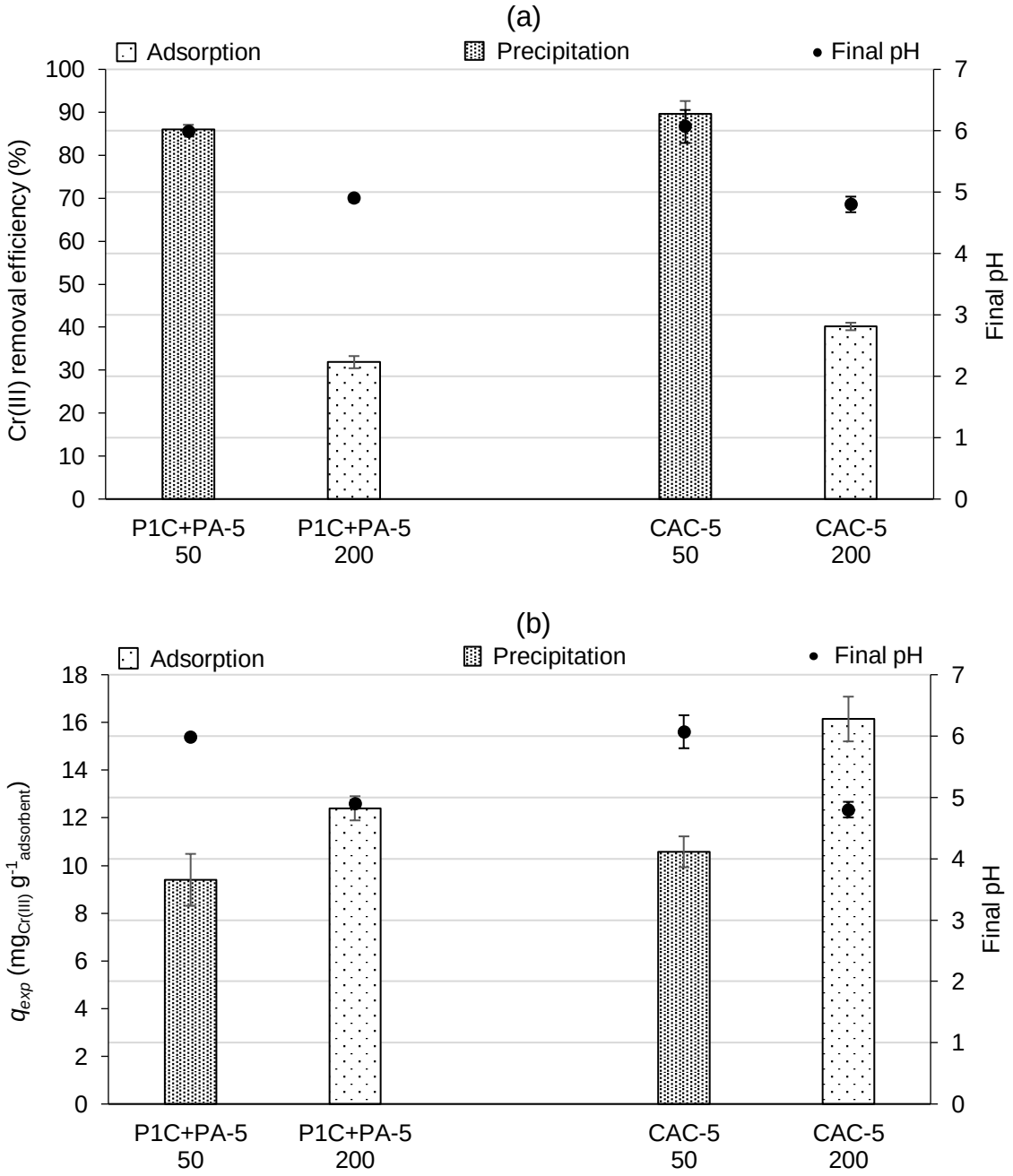

Figure 27. (a) Cr(III) removal efficiency and (b) Cr(III) uptake capacity for P1C+PA-5 and CAC-5 in the industrial wastewater (values of 50 and 200 in x-axis represent the initial Cr(III) concentrations in mg L^{-1}).

The highest Cr(III) uptake capacities (**Figure 27b**) were found for the assays with an initial concentration of 200 $mg_{Cr(III)}$ L^{-1} (12.4 mg g^{-1} for P1C+PA-5 and 16.1 mg g^{-1} for CAC-5). This means that both adsorbents performed better on the industrial wastewater than on the synthetic solution, in which the highest uptake capacity obtained for both adsorbents was much lower (8.05 mg g^{-1} for P1C+PA-5 and 9.25 mg g^{-1} for CAC-5 -**Table 26**). Alike the removal assays on the synthetic solution, the highest Cr(III) uptake capacity was found in the assays in which adsorption ruled the removal mechanisms.

5.3.3 Cr(III) removal mechanisms

Ion exchange was presumably a very important removal mechanism for P1C+PA-5, once 36.1 mg L^{-1} of cations were added to the industrial wastewater by this adsorbent, mainly K (24.7 mg L^{-1}) (**Figure 28**). On the contrary, 72.7 mg L^{-1} of cations were removed from the wastewater, predominantly Cr (63.8 mg L^{-1}). This indicates that half of the removed cations, mainly Cr, may have been removed through ion exchange, mainly through K exchange; in this sense, pore filling also had an important role as a removal mechanism, being probably responsible for the other half removal of Cr(III).

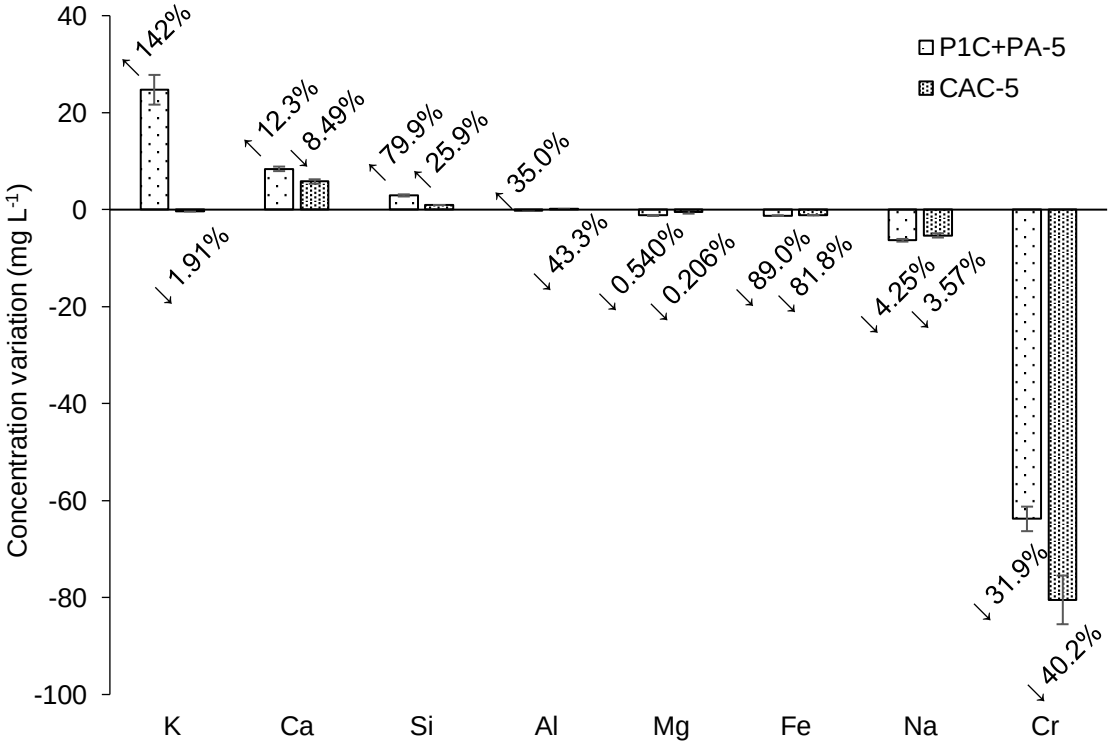

Figure 28. Concentration and percentage variations of cations on the Cr(III) removal assays with P1C+PA-5 and CAC-5 in the industrial wastewater, for an initial concentration of 200 $mg_{Cr(III)}$ L^{-1}.

In contrast, CAC-5 only added 8.86 mg L^{-1} of cations to the wastewater, mainly Ca (5.80 mg L^{-1}), while 87.7 mg L^{-1} of cations were removed from the wastewater, mainly Cr (80.5 mg L^{-1}). These results suggest that ion exchange did not play an important role as removal mechanism by CAC-5 in the industrial wastewater. Instead, as verified for the synthetic solution, pore filling was probably the major removal mechanism.

5.4 Conclusions

The physically activated P1C sample (P1C+PA) presented the best properties of all pyrolysis-derived ACs for Cr(III) removal, due to its high mineral content (allowing removal by ion exchange) and interesting textural properties (allowing removal by pore filling). In the synthetic solution, at a S/L 5 g L^{-1} and an initial Cr(III) of 50 mg L^{-1}, P1C+PA obtained a highest uptake capacity of 9.23, a similar result to the one obtained by CAC (9.80 mg g^{-1}) at a S/L 5 g L^{-1} and an initial Cr(III) of 70 mg L^{-1}. In the equilibrium (q_e) these values decreased to 8.05 and 9.25 mg g^{-1}, respectively.

In the industrial wastewater the uptake capacities of both adsorbents increased, but in this case, CAC (16.1 mg g^{-1}) obtained better results than P1C+PA, (12.4 mg g^{-1}) respectively.

The mechanisms involved on Cr(III) removal by P1C+PA were a mix of ion exchange and pore filling, while Cr(III) removal by CAC was ruled by pore filling.

Although P1C+PA presented slightly lower uptake capacities than CAC in the industrial wastewater, the environmental benefits associated with waste valorisation for the production of adsorbents suggest that P1C+PA may be an alternative to CAC in the removal of Cr(III) from liquid effluents.

6. Cr(III) REMOVAL ASSAYS UNDER CONTINUOUS FLOW

The results presented in this chapter were published, partially or completely, in the following scientific publications:

Papers:

D. Dias, M. Bernardo, F. Pinto, I. Fonseca, N. Lapa, Cr(III) dynamic removal in a fixed-bed column by using a co-gasification char, *Environmental Science and Pollution Research,* submitted.

6.1 Introduction

In order to understand the removal mechanisms under continuous/dynamic conditions, Cr(III) removal assays were carried out in fixed bed columns, with continuous flow, using the char/activated carbon that presented the best performance in the batch assays.

6.2 Materials and methods

6.2.1 Selection of adsorbents

For the column assays, it was decided to select only the adsorbent that performed better in the batch assays. G4C and P1C+PA (at an S/L of 5 g L^{-1}) had similar results in the synthetic effluent (uptake capacities of 7.45 mg g^{-1} (**Table 24**) and 8.05 mg g^{-1} (**Table 26**), respectively) and in the industrial wastewater (uptake capacities of 11.5 mg g^{-1} (**Figure 20**) and 12.4 mg g^{-1} (**Figure 27**), respectively), when adsorption ruled Cr(III) removal. But when precipitation ruled, G4C obtained the highest uptake capacity of all rice-derived adsorbents (14.9 mg g^{-1} in the industrial wastewater - **Figure 20**). To truly simulate the real conditions, the pH of the medium was not altered for the column assays. So, due to the alkaline properties of the adsorbents, precipitation would naturally take place during the column assays (to recall, at pH > 5 Cr(III) precipitation occurs). For that reason, this factor was taken into consideration in the selection of the adsorbent to be used in the column assays; therefore, G4C was the adsorbent selected. Another reason is the fact that G4C did not require an activation process, like P1C+PA did, so, naturally, G4C has more environmental and economic benefits. Before the assay, G4C was sieved to a particle size of 50-100 µm.

For comparison purposes, a commercial activated carbon (Norit GAC 1240) was used also with a particle size of 50-100 µm.

6.2.2 Column assays setup

Figure 29 presents the setup of the column assays.

The initial Cr(III) solution (1), which was previously prepared with known concentrations, was guided to the fixed-bed column (diameter = 0.5 cm; height = 10.0 cm) (4), through a hose (2) by using a Gilson Minipuls 3 peristaltic pump (3) that controlled the flow rate of the Cr(III) solution. The adsorbent (4a) was fixed in the column by placing Whatman® 42 filter papers (4b) on both top and bottom of the column. At the end of the column, a new hose (5) led the solution (post-removal assay) to a collector flask (6).

In order to control the temperature of the assays, a Velp Scientifica open-circulating bath (7) was used. This bath was filled with water (8) and set to a known temperature. The water was recirculated inside the adsorption column, from bottom to top, through circulating hoses (9).

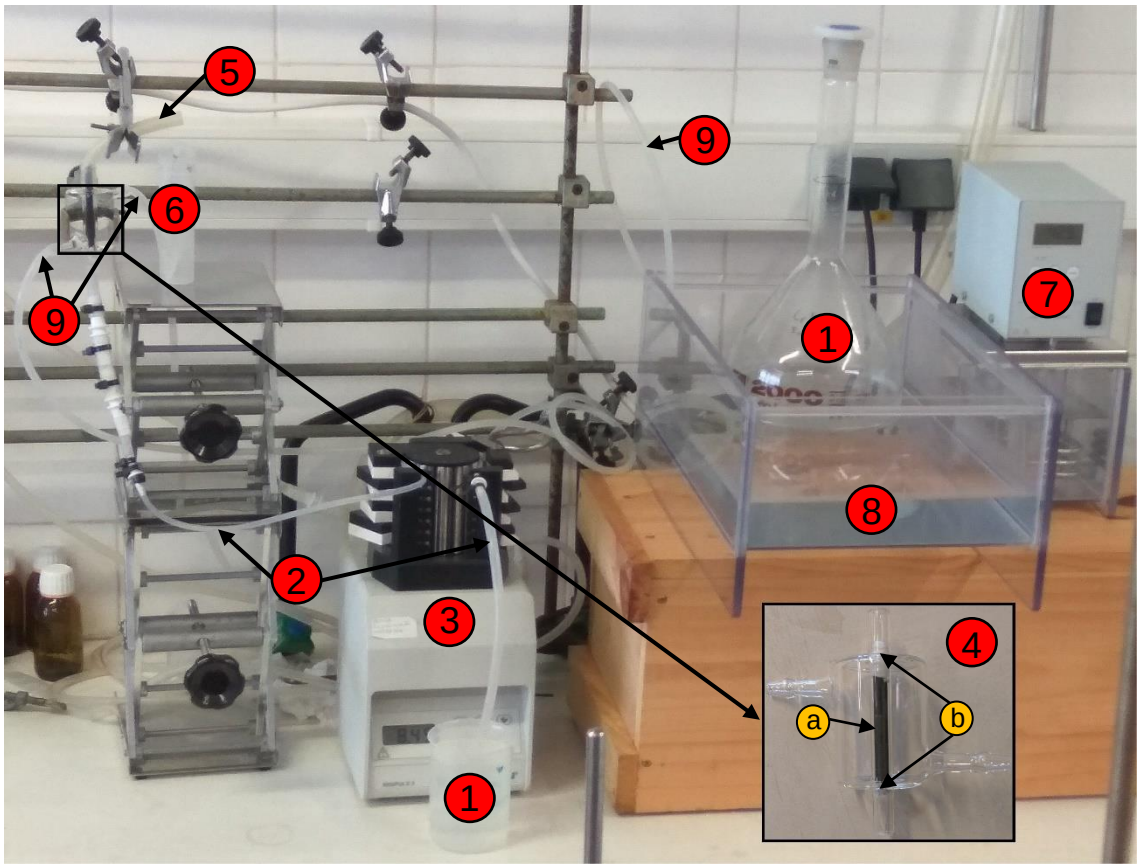

Figure 29. Column assays setup: 1 - initial Cr(III) solution; 2 - column inflow hose; 3 - peristaltic pump; 4 - fixed-bed column (a - adsorbent ; b - filter paper); 5 - column outflow hose; 6 - sample collector flask; 7 - open circulating bath; 8 - water tank; 9 - recirculating hoses.

6.2.3 Cr(III) removal assays from synthetic solution

The synthetic solution was prepared with $CrN_3O_9.9H_2O$ (99% v/v).

All Cr(III) removal assays were performed with a flow rate of 3 mL min^{-1}. Several samples were collected over the testing time, throughout each adsorption test, in order to draw the Cr(III) breakthrough curves for each assay. The pH of each sample was measured by using a Hanna Instruments edge® HI 2002 pH meter. Finally, the samples were acidified with HNO_3 for pH < 2, before Cr quantification by ICP-AES (described in section 2.2.1).

With the objective to maximise the removal potential of the adsorbent, different conditions were tested in the column assays, namely, different inflow concentrations of Cr(III) , different adsorbent masses and different temperatures.

At the end of each assay, several parameters were analysed:

a) Breakthrough time (t_b) – Time at which Cr(III) concentration in the outflow is 5% of the inflow concentration (C_t/C_0 = 0.05) (min).

b) Saturation time (t_s) – Time at which Cr(III) concentration in the outflow is 95% of the inflow concentration (C_t/C_0 = 0.95) (min).

c) pH t_b – pH value at breakthrough time (Sørensen scale).

d) pH t_s – pH value at saturation time (Sørensen scale).

e) Cr(III) mass retained ($m_{Cr(III)\_ads}$) – Total mass of Cr(III) retained until saturation time (mg), which was calculated through the equation 6.1[129]:

$$m_{Cr(III)\_ads} = \frac{Q \times C_0}{1000} \times \int_0^{t_s} \left(1 - \frac{C_t}{C_0}\right) dt \quad (6.1)$$

where, Q is the flow rate of the solution passing through the column (mL min^{-1}), C_0 is the Cr(III) concentration in the inflow (mg L^{-1}) and C_t is the Cr(III) concentration in the outflow on time t (mg L^{-1}).

f) Cr(III) removal efficiency (η) – Ratio between the total mass of Cr(III) retained by the column and total mass of Cr(III) that was passed through the column (%) (equation 6.2)[137]:

$$\eta = \frac{m_{Cr(III)\_ads}}{m_{Cr(III)\_total}} \times 100 \quad (6.2)$$

where, $m_{\mathrm{Cr(III)\_total}}$ is the total mass of Cr(III) that passed through the column (equation 6.3)[137]:

$$m_{Cr(III)\_total} = \frac{Q \times C_0 \times t_s}{1000} \quad (6.3)$$

g) Total uptake capacity (q_{total}) – Removal capacity of the column in the saturation time (t_s) or total uptake capacity of the column (mg$_{Cr(III)}$ g$^{-1}_{adsorbent}$) (equation 6.4)[129]:

$$q_{\mathrm{total}} = \frac{m_{\mathrm{Cr(III)\_ads}}}{m_{ads}} \quad (6.4)$$

where, m_{ads} is the mass of adsorbent in the column (g).

6.2.3.1 Effect of inflow Cr(III) concentration

Five inflow concentrations (C_0) were tested: 2.5, 5, 10, 25 and 50 mg L^{-1}. These assays were performed under the following conditions: m_{ads} = 0.2 g (column height = 1.1 cm); Q = 3 mL min^{-1}; T = 25 °C; t = up to 70 min (until the saturation was reached).

The inflow Cr(III) concentration that originated the assay with the highest uptake capacity was selected for the next assays.

6.2.3.2 Effect of adsorbent mass

To test the influence of the adsorbent mass (m_{ads}) in the removal process, three masses were tested: 0.2, 0.4 and 0.8 g (column height = 1.1, 2.1 and 4.2 cm, respectively). These assays were performed under the following conditions: Q = 3 mL min^{-1}; T = 25 °C; t = up to 150 min (until the saturation was reached); C_0 = concentration that originated the assay with the highest uptake capacity in section 6.2.3.1.

The adsorbent mass that originated the assay with the highest uptake capacity was selected for the next assays.

6.2.3.3 Effect of temperature

To test the influence of the temperature (T) in the removal process, three temperatures were tested: 25, 40 and 50 °C. These assays were performed under the following conditions: Q = 3 mL min^{-1}; t = up to 210 min (until the saturation was reached); C_0 = concentration that originated the assay with the highest uptake capacity in section 6.2.3.1; m_{ads} = mass that originated the assay with the highest uptake capacity in section 6.2.3.2.

The temperature that originated the assay with the highest uptake capacity was selected for the next assays.

6.2.3.4 Comparison with a commercial activated carbon (CAC)

For comparison purposes, CAC (section 3.2.1.5) was used in the column assays. The conditions used in CAC's assays were the following: Q = 3 mL min^{-1}; t = 270 min (until the saturation was reached); C_0 = concentration that originated the assay with the highest uptake capacity in section 6.2.3.1; m_{ads} = mass that originated the assay with the highest uptake capacity in section 6.2.3.2; T = temperature that originated the assay with the highest uptake capacity in section 6.2.3.3.

6.2.3.5 Cr(III) recovery and column regeneration

In order to understand the regeneration capacity of the column, adsorption and desorption cycles were performed. The conditions of these assays were the same as in section 6.2.3.4, and comprised the following steps:

(i) adsorption assay until saturation was reached;

(ii) desorption assay with acetic acid (0.2 M) until Cr(III) concentration in the column outflow < 0.2 mg L^{-1}. The acetic acid was chosen for being a greener solution that the typical acids used in column desorption processes, such as HCl[133,134]. The concentration 0.2M was chosen because at that concentration the acetic acid had a pH of 3 which was the goal.

(iii) desorption assay with ultrapure water (Milli-Q Academic) until Cr(III) concentration in the column outflow < 0.02 mg L^{-1}, in order to remove the excess acid in the column and stabilize the column pH;

(iv) repetition of steps (i) (ii) and (iii) until the maximum regeneration capacity was reached.

For comparison purposes, the same test was performed on CAC.

6.2.4 Cr(III) removal assays from industrial wastewater

In order to replicate real conditions, column assays were also performed with an industrial wastewater rich in Cr. The origin and characterisation of the industrial wastewater were already shown (sections 4.2.2 and 4.3.1, respectively).

As in the removal assays from the synthetic solution, several samples were collected throughout each test in order to draw the breakthrough curves for each assay and the pH of each sample was measured (Hanna Instruments edge® HI 2002 pH meter). The samples collected at the outflow were acidified with HNO_3 for pH < 2, before Cr quantification by ICP-AES (described in section 2.2.1). The parameters characterised in Cr(III) removal assays from synthetic solution (section 6.2.3) were also characterised for the removal assays with the industrial wastewater. The experimental conditions used on the column adsorption assays using industrial wastewater were the same used in section 6.2.3.4.

Once again, CAC was used in these assays for comparison purposes.

6.2.5 Kinetic modelling

The experimental data were adjusted to Thomas's non-linear model (equation 6.5)[180].

$$\frac{C_t}{C_0}(th) = \frac{1}{1 + e^{\left(k_{Th} \cdot q_0 \cdot \frac{m_{ads}}{Q}\right) - (k_{th} \cdot C_0 \cdot t)}} \quad (6.5)$$

where, C_t (mg L^{-1}) is the Cr(III) concentration in the outflow on time t (min), C_0 is the Cr(III) concentration in the inflow (mg L^{-1}), k_{th} is the Thomas rate constant (mL min^{-1} mg^{-1}), q_0 is the maximum adsorption capacity of the column ($mg_{Cr(III)}$ $g^{-1}_{adsorbent}$), m_{ads} is the mass of adsorbent in the column (g) and Q is the flow rate of the solution passing through the column (mL min^{-1}). Thomas model has been the most common model used in column studies. It assumes that in conditions where the external and internal diffusion resistances are very low, the experimental data follow Langmuir adsorption isotherm without axial dispersion, considering that the rate driving force obeys second-order reversible reaction kinetic[128,181].

The model adjustment was done in the same way as described in section 4.2.3.4.

6.3 Results and discussion

6.3.1 Cr(III) removal assays from synthetic solution

6.3.1.1 Effect of the inflow Cr(III) concentration

The results of the column assays for Cr(III) removal from synthetic solution using G4C at different inflow concentrations are shown in **Figure 30** and **Table 29**.

The assays with Cr(III) inflow concentrations (C_0) of 50 and 25 mg L^{-1} presented very similar results, reaching the adsorbent saturation very fast (≤ 2.72 min). Naturally, it was not possible to quantify the breakthrough time (t_b) for these assays. Although the assay with C_0 of 10 mg L^{-1} presented a slightly higher saturation time (t_s) (9.55 min), t_b was still not quantifiable. Only in the assays with C_0 of 5 and 2.5 mg L^{-1} was possible to quantify t_b (0.546 and 3.19 min, respectively). Regarding t_s, the values increased to 25.8 and 47.0 min, respectively. The pH t_s was very close in all the assays, varying between 5.65 and 6.05 indicating that precipitation was ruling Cr(III) removal.

Although the Cr(III) removal efficiency (η) increased by decreasing C_0 from 5.0 to 2.5 mg L^{-1}, the highest uptake capacities for both the experimental data (q_{total}) as the Thomas model (q_0) were found in the assay with a C_0 of 5.0 mg L^{-1} (0.995 and 0.923 mg g^{-1}, respectively).

Taking into consideration these results, the C_0 of 5.0 mg L^{-1} was selected for the next assays.

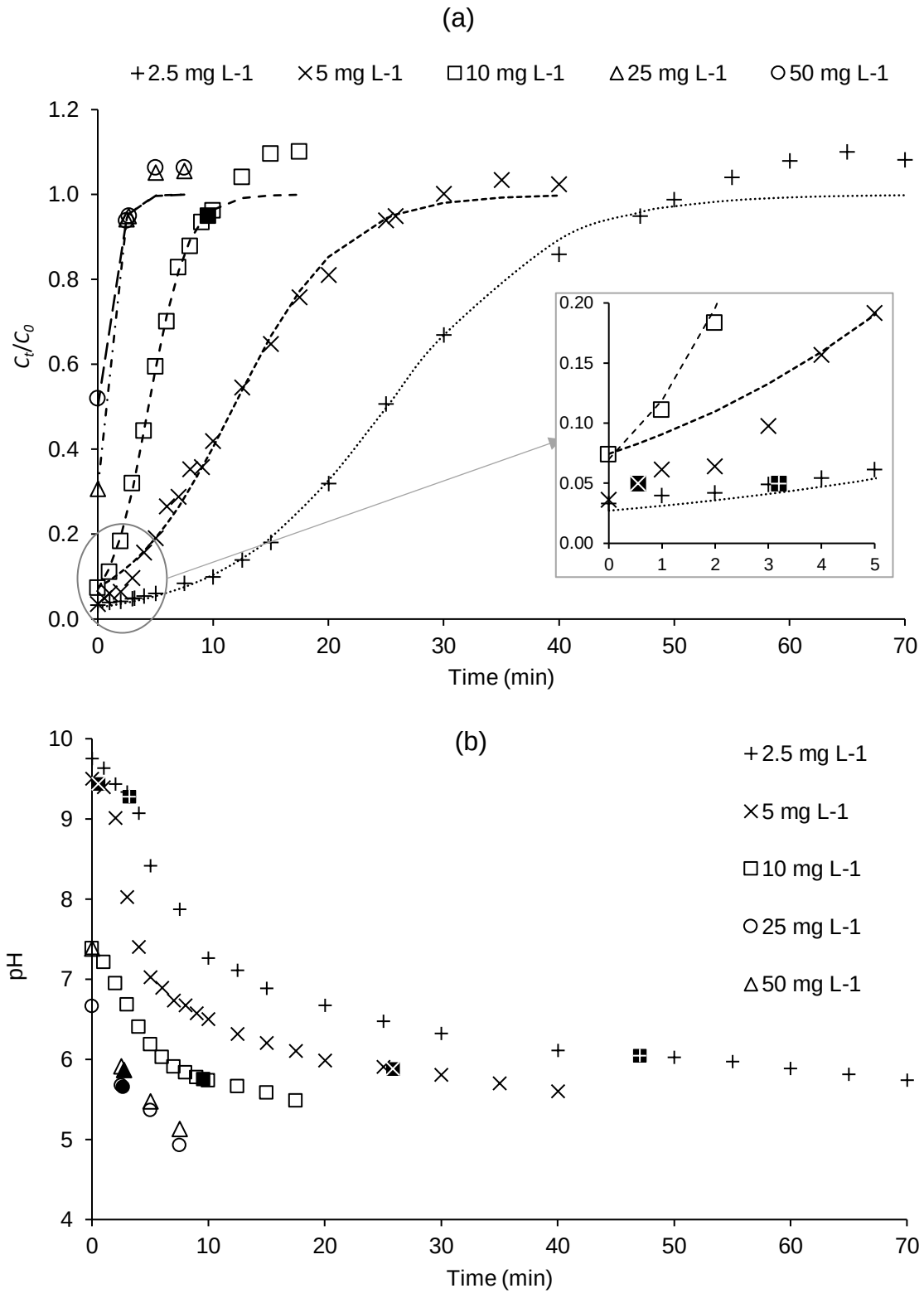

Figure 30. Column assays for Cr(III) removal from synthetic solution using G4C at different inflow concentrations – (a) Breakthrough curves and (b) pH values. The black symbols represent the breakthrough and saturation times, and the lines represent the Thomas's model adjustment.

Table 29. Column assays for Cr(III) removal from synthetic solution using G4C at different inflow concentrations – Experimental data and Thomas's model parameters.

	Experimental data parameters							Thomas model parameters		
C_0 (mg L^{-1})	t_b (min)	pH t_b	t_s (min)	pH t_s	$m_{Cr(III)\_ads}$ (mg)	η (%)	q_{total} (mg g^{-1})	k_{th} (mL min^{-1} mg^{-1})	q_0 (mg g^{-1})	R^2
2.5	3.19	9.28	47.0	6.05	0.182	54.0	0.912	59.7	0.900	0.995
5.0	0.546	9.44	25.8	5.88	0.200	49.2	0.995	40.8	0.923	0.995
10.0	n.q.	n.q.	9.55	5.75	0.137	46.8	0.683	57.6	0.674	0.991
25.0	n.q.	n.q.	2.67	5.65	7.59×10^{-2}	35.5	0.379	55.8	0.226	0.992
50.0	n.q.	n.q.	2.72	5.87	9.91×10^{-2}	25.3	0.495	22.0	n.q.	0.977

n.q. – not quantifiable.

6.3.1.2 Effect of the adsorbent mass

The results of the column assays for Cr(III) removal from synthetic solution using G4C with different mass of adsorbent are shown in **Figure 31** and **Table 30**.

Increasing the mass of adsorbent (m_{ads}) also increased all experimental data parameters (except pH). If, for one side, t_s increased proportionally with the mass, on the other side, t_b increasing was more significant, obtaining values of 6.98 and 33.4 min for m_{ads} of 0.4 and 0.8 g, respectively, in contrast with the t_b of 0.546 min found for a m_{ads} of 0.2 g.

These differences were reflected on the removal efficiency (η), but specially on the uptake capacities (q_{total} and q_0). The assay with a m_{ads} of 0.4 g obtained a η of 56.8%, a q_{total} of 1.02 mg g^{-1} and a q_0 of 1.03 mg g^{-1}, while in the assay with a m_{ads} of 0.8 g those values increased to 58.4%, 1.26 mg g^{-1} and 1.24 mg g^{-1}, respectively. If the differences between the uptake capacities of the assays with masses of 0.2 and 0.4 g were not very significant, in the assay with a m_{ads} of 0.8 those discrepancies were more relevant, with an increase of 26.6% on q_{total} and of 34.4% on q_0, when compared to the initial assay (m_{ads} = 0.2 g). Still, these uptake capacities were, in general, low.

Regarding pH, while the pH t_b decreased with the increase of mass, the pH t_s was again in the same range of the previous assays (between 5.73 and 5.94), meaning that, again, precipitation played a significant role in Cr(III) removal.

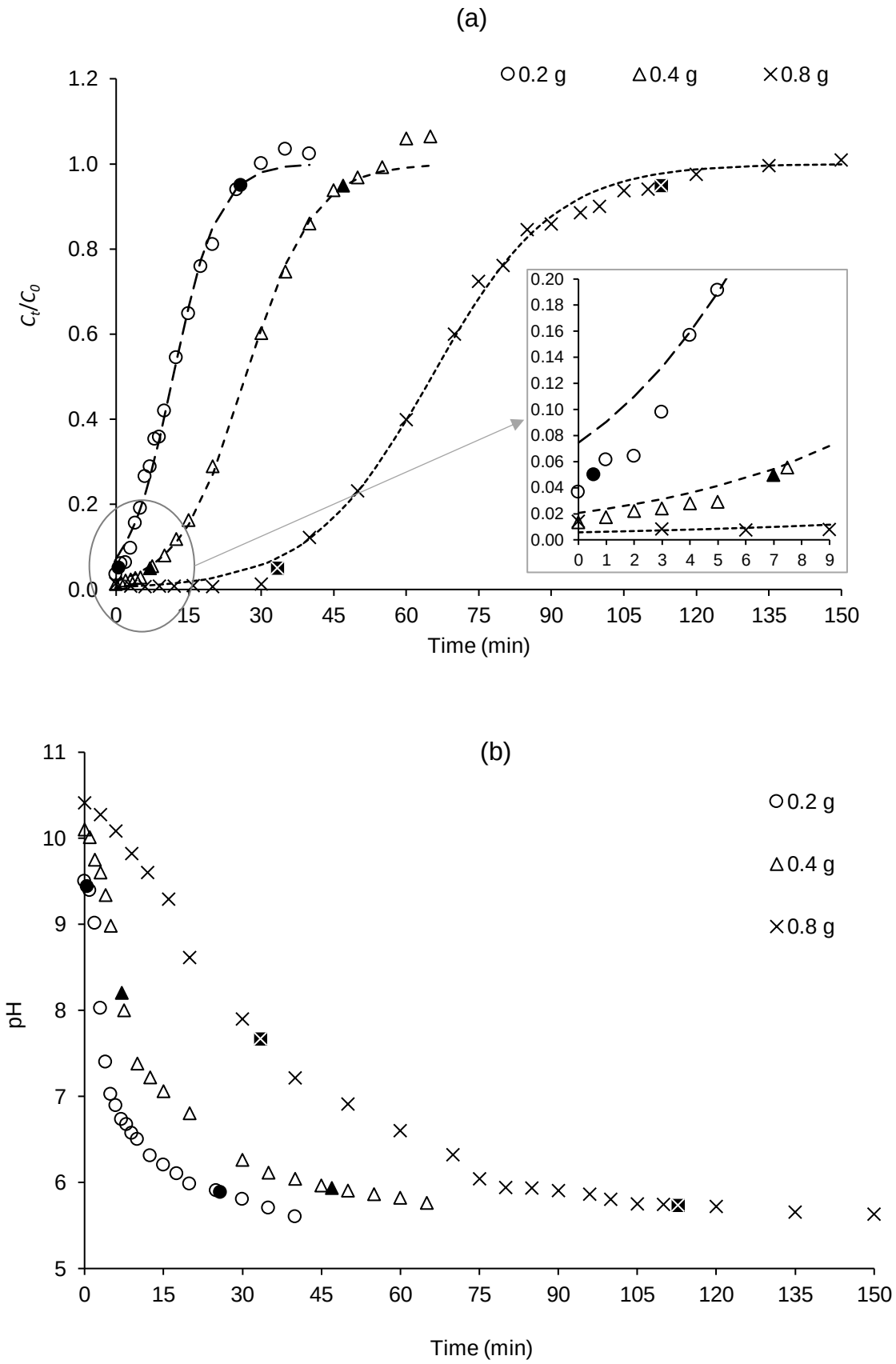

Figure 31. Column assays for Cr(III) removal from synthetic solution using G4C with different mass of adsorbent – (a) Breakthrough curves and (b) pH values. The black symbols represent the breakthrough and saturation times, and the lines represent the Thomas's model adjustment.

Table 30. Column assays for Cr(III) removal from synthetic solution using G4C with different mass of adsorbent – Experimental data and Thomas model parameters.

	Experimental data parameters							Thomas model parameters		
m_{ads} (g)	t_b (min)	pH t_b	t_s (min)	pH t_s	$m_{Cr(III)\_ads}$ (mg)	η (%)	q_{total} (mg g^{-1})	k_{th} (mL min^{-1} mg^{-1})	q_0 (mg g^{-1})	R^2
0.2	0.546	9.44	25.8	5.88	0.200	49.2	0.995	40.8	0.923	0.995
0.4	6.98	8.20	46.9	5.94	0.409	56.8	1.02	28.1	1.03	0.998
0.8	33.4	7.67	113	5.73	1.00	58.4	1.26	15.6	1.24	0.998

In can be concluded that increasing the mass from 0.2 g to 0.4 g wouldn't give a relevant advantage to the process, while increasing the mass to 0.8 g would significantly increase the overall efficiency of the process. For that reason, 0.8 g was the adsorbent mass selected to be used in the next assays.

6.3.1.3 Effect of temperature

The results of the column assays for Cr(III) removal from synthetic solution using G4C at different temperatures are shown in **Figure 32** and **Table 31**.

Differing from the previous results, the breakthrough curves of these assays were similar (**Figure 32**). Although t_b and t_s increased with the temperature, the differences between the assays with temperatures of 25 and 50 °C were not marked. The same happened in the efficiency of Cr(III) removal with values between 54.2% (T = 50 °C) and 58.4% (T = 25 °C). Only in the uptake capacities some differences were found, with values of q_{total} varying between 1.19 (T = 40 °C) and 1.42 mg g^{-1} (T = 50 °C) and values of q_0 varying between 1.15 (T = 40 °C) and 1.38 mg g^{-1} (T = 50 °C).

The pH values followed the tendency of similarity between assays. pH t_b ranged between 7.48 and 7.82 while pH t_s presented similar values as in the previous assays (between 5.49 and 5.73), showing again the importance of precipitation in Cr(III) removal.

The assay with a temperature of 50 °C showed the highest uptake capacities of all assays and, for that reason, this temperature was selected to be used in the following assays.

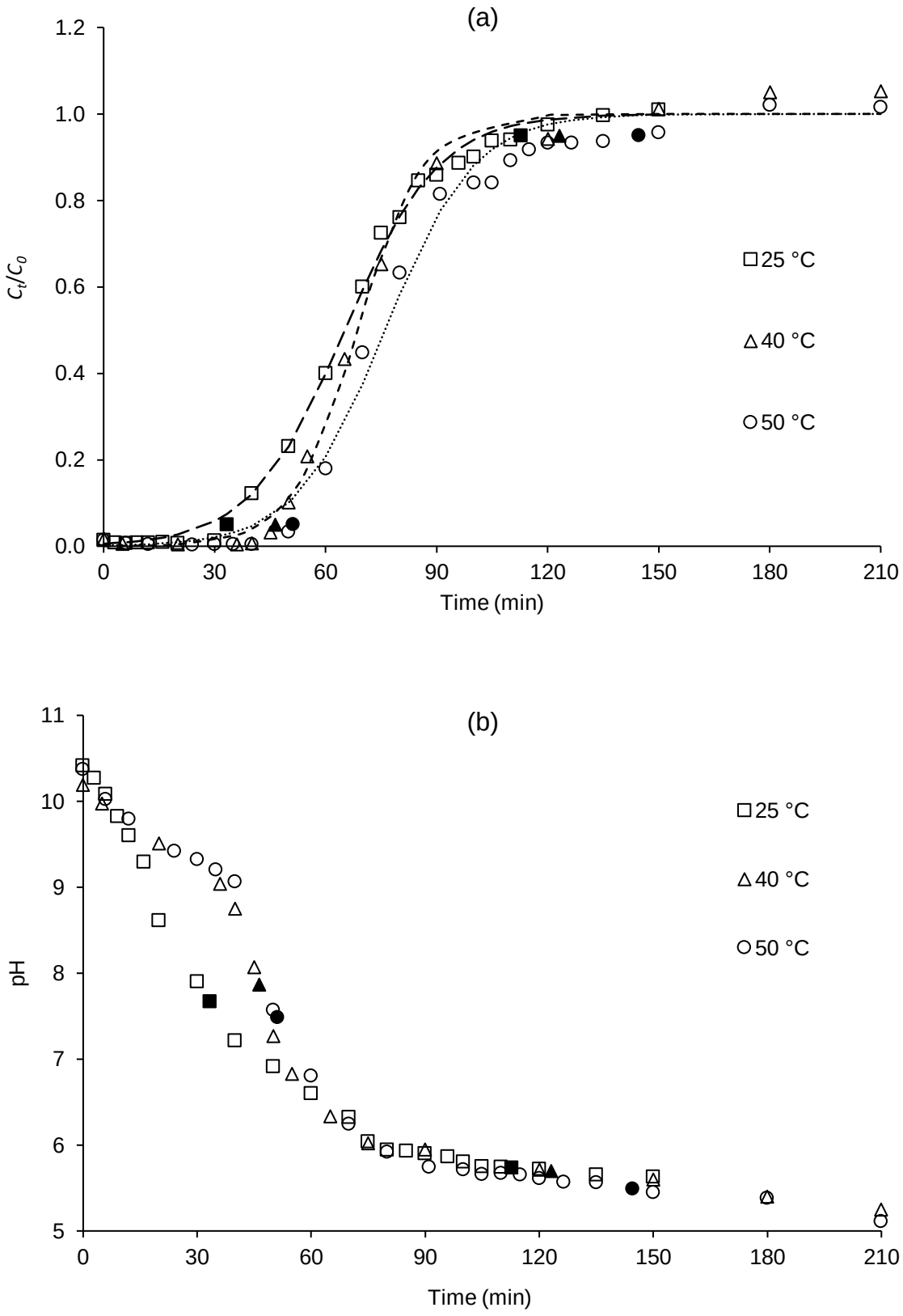

Figure 32. Column assays for Cr(III) removal from synthetic solution using G4C at different temperatures – (a) Breakthrough curves and (b) pH values. The black symbols represent the breakthrough and saturation times, and the lines represent the Thomas's model adjustment.

Table 31. Column assays for Cr(III) removal from synthetic solution using G4C at different temperatures – Experimental data and Thomas model parameters.

	Experimental data parameters							Thomas model parameters		
T (°C)	t_b (min)	pH t_b	t_s (min)	pH t_s	$m_{Cr(III)\_ads}$ (mg)	η (%)	q_{total} (mg g^{-1})	k_{th} (mL min^{-1} mg^{-1})	q_0 (mg g^{-1})	R^2
25	33.4	7.67	113	5.73	1.00	58.4	1.26	15.6	1.24	0.998
40	46.2	7.87	123	5.70	0.954	57.8	1.19	24.7	1.15	0.995
50	51.2	7.48	145	5.49	1.14	54.2	1.42	17.3	1.38	0.992

6.3.1.4 Comparison with a commercial activated carbon (CAC)

As specified before (section 6.2.3.2), G4C presented a column height of 4.2 cm for a mass of 0.8 g. However, once CAC is a different material with a different apparent density, the column height was of 6.0 cm for this same mass of adsorbent.

The results of the column assays for Cr(III) removal from synthetic solution using G4C and CAC are shown in **Figure 33** and **Table 32**.

In general, CAC presented higher parameters than G4C. The t_b of CAC was slightly longer than G4C (59.3 and 51.2 min, respectively) but the difference of t_s was more significant (208 and 145 min, respectively). Although the Cr(III) removal efficiency of CAC was slightly lower than for G4C, the uptake capacities were higher in CAC with values of 2.14 mg g^{-1} for q_{total} and of 2.05 mg g^{-1} for q_0. Due to the slightly lower pH_{pzc} of CAC (9.13 - section 3.3.2.2) when compared to G4C (9.58 - section 2.3.2.4), the pH values of CAC along the assay were, in general, lower than G4C, especially in the beginning of the assay. CAC presented a pH t_s of 5.10, meaning that although there was still some precipitation on the removal of Cr(III), the influence was not as relevant as in G4C.

Very few studies were found in bibliography using chars into Cr(III) removal in column assays and no studies were found on chars produced from rice wastes. For that reason, the results were mainly compared with different biomass/waste-derived adsorbents (**Table 6**). In general, the adsorption capacity of the adsorbents was higher than the adsorption capacity of G4C. The exception occurred for Calero et al.[138], which used olive stone as adsorbent, obtaining adsorption capacities from 0.331 to 0.806 mg g^{-1}.

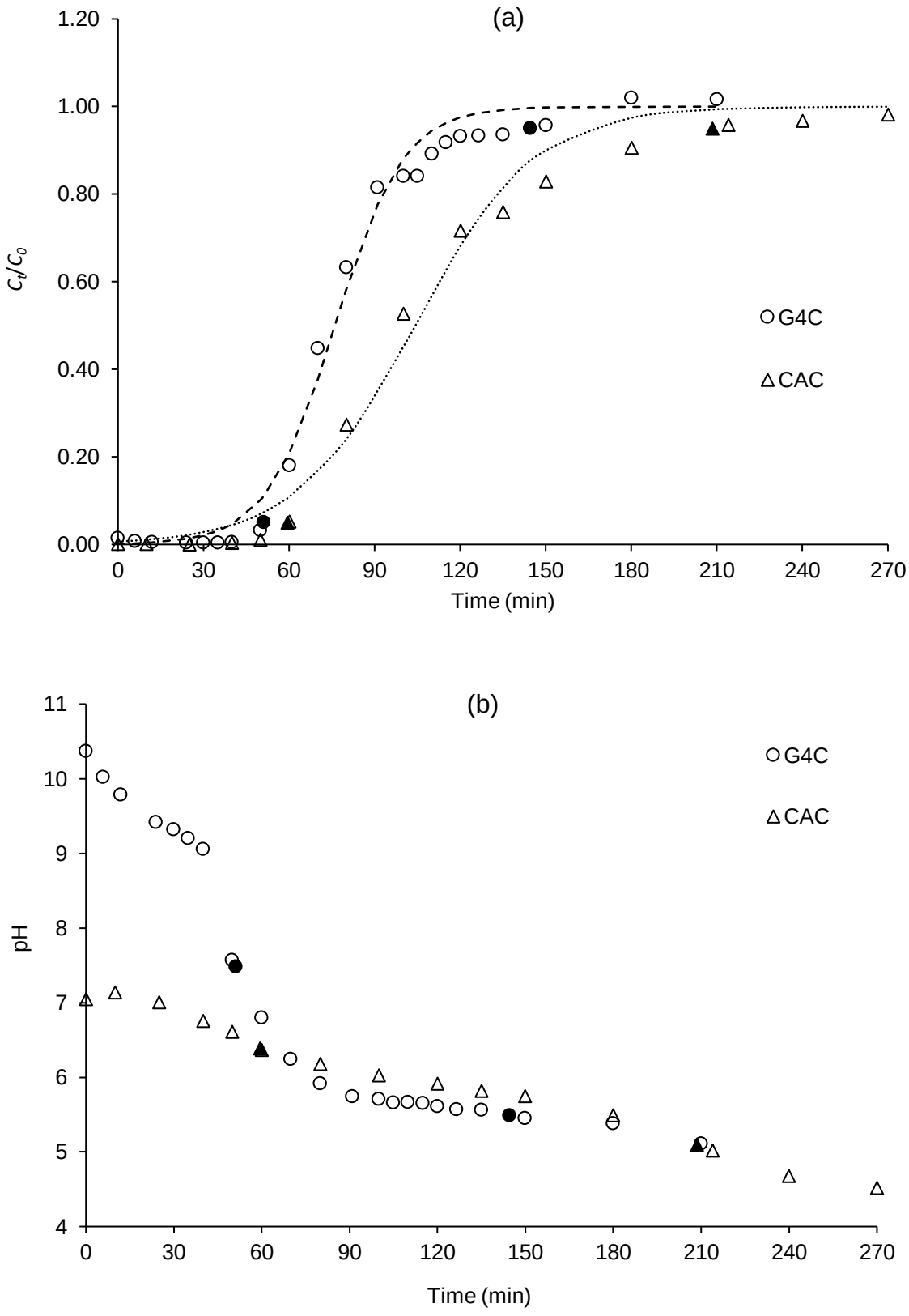

Figure 33. Column assays for Cr(III) removal from synthetic solution using G4C and CAC – (a) Breakthrough curves and (b) pH values. The black symbols represent the breakthrough and saturation times, and the lines represent the Thomas's model adjustment.

Table 32. Column assays for Cr(III) removal from synthetic solution using G4C and CAC – Experimental data and Thomas's model parameters.

	Experimental data parameters							Thomas model parameters		
Adsorbent	t_b (min)	pH t_b	t_s (min)	pH t_s	$m_{Cr(III)\_ads}$ (mg)	η (%)	q_{total} (mg g^{-1})	k_{th} (mL min^{-1} mg^{-1})	q_0 (mg g^{-1})	R^2
G4C	51.2	7.48	145	5.49	1.14	54.2	1.42	17.3	1.38	0.992
CAC	59.3	6.39	208	5.10	1.72	52.2	2.14	9.09	2.05	0.991

6.3.1.5 Cr(III) recovery and column regeneration

Figure 34 presents the four stages of Cr(III) recovery and column regeneration process using G4C and CAC. **Figure 35** presents the pH values of those four stages and **Table 33** presents the experimental data and Thomas model parameters of the adsorption cycles.

As expected, the first adsorption cycle showed similar results to the ones seen in section 6.2.3.4, both for the breakthrough curves (**Figure 34a**) and pH values (**Figure 35a**). However, the differences between G4C and CAC were slightly lower. If in the case of t_b and t_s the results were very similar (except t_s for CAC), in other parameters the differences were slightly higher. For G4C there was a slightly increase in the Cr(III) removal efficiency (56.9%) and uptake capacities (q_{total} = 1.60 mg g^{-1} and q_0 = 1.55 mg g^{-1}). On the other hand, CAC obtained a similar efficiency but slightly lower uptake capacities (q_{total} = 1.86 mg g^{-1} and q_0 = 1.76 mg g^{-1}). In this assay, although CAC still presented slightly better results than G4C, the differences between both adsorbents were much lower.

The differences between the assays in section 6.2.3.4 and the assays on this section may be related to two factors: (i) the assays in section 6.2.3.4 were performed over saturation time (210 min in G4C and 270 min in CAC), while in this section the assay was stopped at saturation time (150 min in G4C and 210 min in CAC); (ii) the heterogeneity of the samples, especially G4C.

The desorption step with acetic acid (**Figure 34b**) showed discrepancies between both adsorbents. For G4C, the desorption was very fast, starting with higher concentrations of Cr(III) desorbed, which quickly decreased. At time 0 (i.e., the first drops of solution after passing the acid through the column), the concentration of Cr(III) (C_t) was 9.78 mg L^{-1}, but only 3 min later C_t was already at 1.67 mg L^{-1}, showing that the highest recovery of Cr(III) was done in the first minutes. At 30 min, C_t was already below 0.2 mg L^{-1} and at 60 min the assay stopped with a C_t around 0.1 mg L^{-1}.

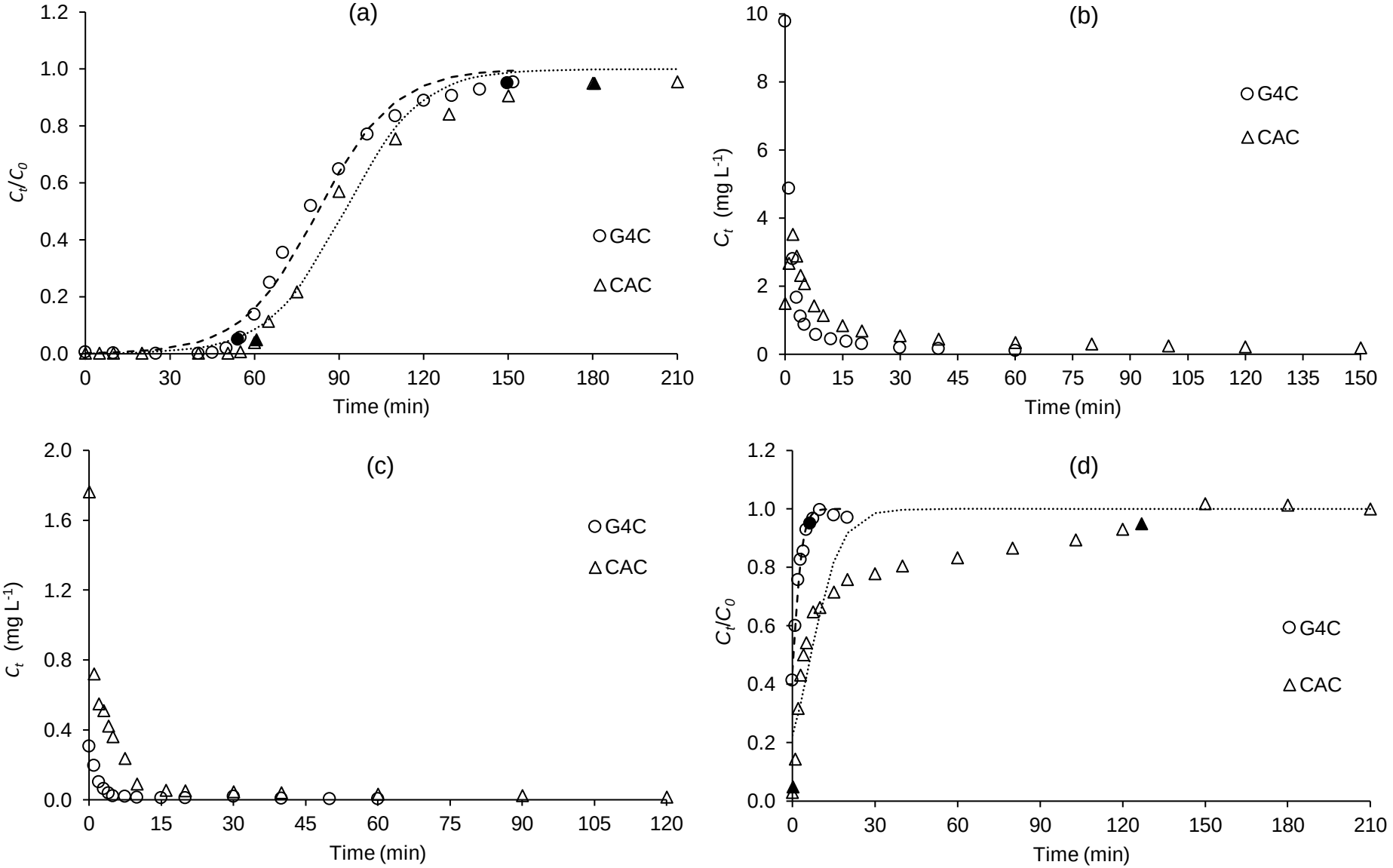

Figure 34. Cr(III) recovery and column regeneration using G4C and CAC – (a) Breakthrough curves of the 1st Cr(III) adsorption cycle from synthetic solution; (b) Desorption of Cr(III) using acetic acid; (c) Desorption of Cr(III) using ultrapure water; (d) Breakthrough curves of the 2nd Cr(III) adsorption cycle from synthetic solution. The black symbols represent the breakthrough and saturation times, and the lines represent the Thomas's model adjustment.

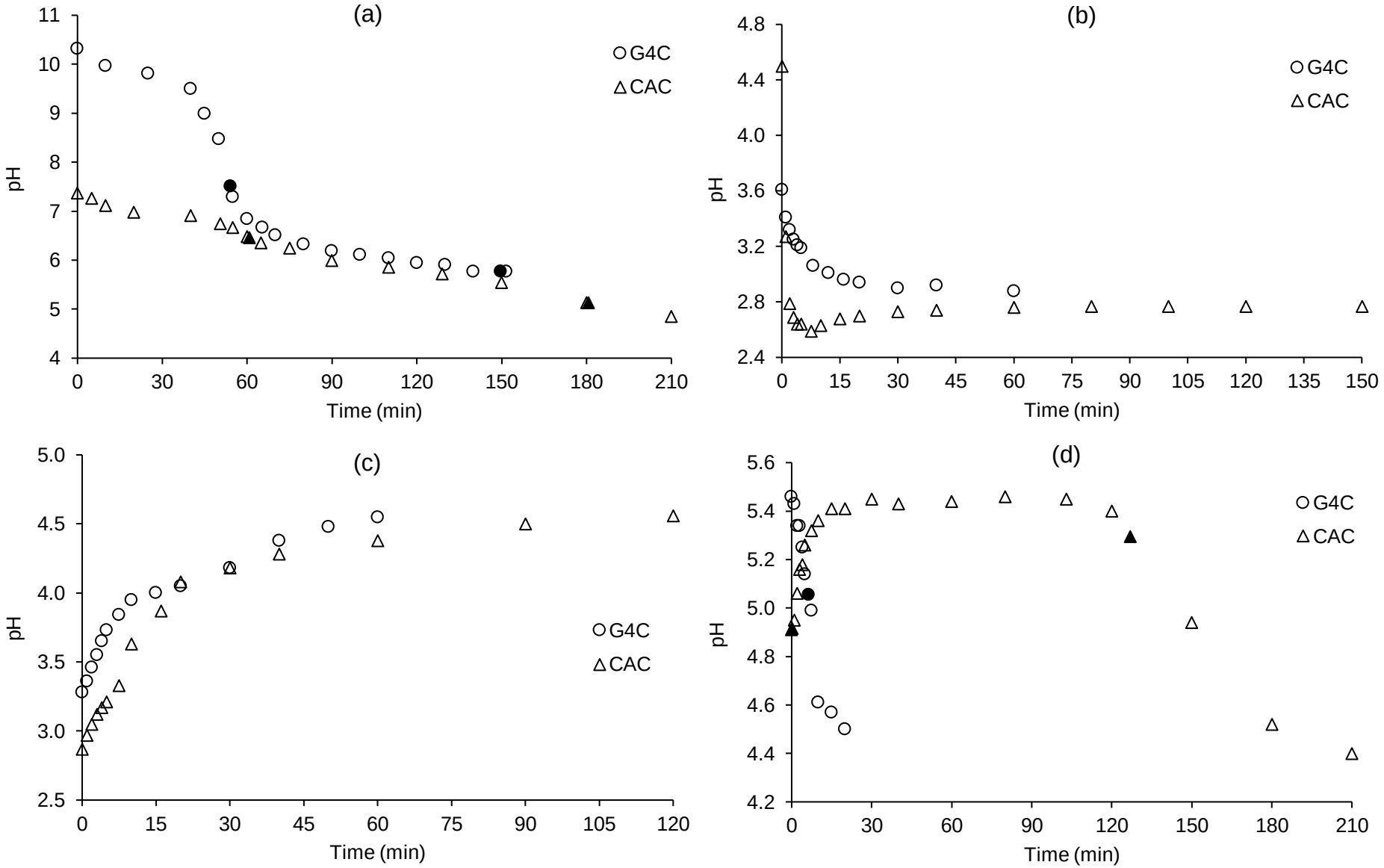

Figure 35. Cr(III) recovery and column regeneration using G4C and CAC – (a) pH values of the 1st Cr(III) adsorption cycle from synthetic solution; (b) pH values of the desorption of Cr(III) using acetic acid; (c) pH values of the desorption of Cr(III) using ultrapure water; (d) pH values of the 2nd Cr(III) adsorption cycle from synthetic solution. The black symbols represent the breakthrough and saturation times.

Table 33. Cr(III) column adsorption cycles from synthetic solution using G4C and CAC – Experimental data and Thomas's model parameters.

		Experimental data parameters							Thomas model parameters		
Adsorbent	Adsorption Cycle	t_b (min)	pH t_b	t_s (min)	pH t_s	$m_{Cr(III)\_ads}$ (mg)	η (%)	q_{total} (mg g^{-1})	k_{th} (mL min^{-1} mg^{-1})	q_0 (mg g^{-1})	R^2
G4C	1st	54.1	7.51	150	5.77	1.28	56.9	1.60	14.8	1.55	0.990
	2nd	n.q.	n.q.	6.42	5.05	2.08×10^{-2}	21.4	2.59×10^{-2}	116	7.50×10^{-3}	0.986
CAC	1st	60.7	6.46	181	5.13	1.49	53.8	1.86	14.6	1.76	0.991
	2nd	0.17	4.92	127	5.30	0.349	18.6	0.436	37.0	0.125	0.878

n.q. – not quantifiable.

On the other hand, in CAC column, in the beginning of the process there was an increase on the concentration of Cr(III) desorbed and only then a slowly decrease of the desorption process. At time 0, C_t was of 1.50 mg L^{-1}, increasing to the highest value of 3.52 mg L^{-1} at 2 min. Then, C_t start to slowly decrease and the assay was stopped at 150 min, when C_t reached a value slightly lower than 0.2 mg L^{-1}.

The 3rd stage of the process (**Figure 34c**) was mainly to wash the column out of the acetic acid. However, in the beginning of the processes there was still some desorption of Cr(III), especially in CAC where C_t was of 1.76 mg L^{-1} at time 0. The washing allowed the pH to increase from 3.28 to 4.55 in G4C and from 2.87 to 4.56 in CAC (**Figure 35c**).

The 4th and last stage of the process – second adsorption cycle (**Figure 34a**), showed that the use of G4C in more than one adsorption cycle was not advantageous, once t_s was reached at 6.42 min and t_b was not even quantifiable. For that reason, the Cr(III) removal efficiency (21.4%) and especially the uptake capacities (q_{total} = 2.59×10^{-2} mg g^{-1} and q_0 = 7.50×10^{-3} mg g^{-1}) were very low.

Regarding CAC, although a second adsorption cycle was performed, the performance was much lower than in the first cycle, so a second cycle is also not viable.

Opposing to all the other assays, the pH of CAC in this assay (**Figure 35d**) increased in the beginning, reached an equilibrium from about 30 min to 103 min and slowly started to decreased has expected until pH 4.4 at 210 min. This may suggest that the releasing of minerals from CAC was much slower and gradual once in G4C the releasing of minerals occurred much faster. Other possibility is that there was still some acid in the column which made the initial pH of the assay be lower than the expected.

No more desorption and adsorption cycles were performed once both adsorbents showed poor properties to be used in more than one adsorption cycle.

6.3.2 Cr(III) removal assays from the industrial wastewater

The results of the column assays for Cr(III) removal from industrial wastewater using G4C and CAC are shown in **Figure 36** and **Table 34**.

In the industrial wastewater both adsorbents performed better than in the synthetic solution, just like it had occurred in the batch assays (Chapter 4). In both cases, t_b was lower (in the case of G4C, 2.25 min), but t_s was much higher (538 and 1100 min for G4C and CAC, respectively), indicating that the removal occurred for a much longer period of time (more 3.7 times for G4C and more 5.27 times for CAC). Although Cr(III) removal efficiencies decreased slightly (31.6% for G4C and 34.8% for CAC), the uptake capacities increased significantly: G4C obtained a q_{total} of 3.25 mg g^{-1} and q_0 of 3.00 mg g^{-1}, while in CAC these values increased to 7.83 ad 6.66 mg g^{-1},

respectively. This means that the uptake capacities increased 2.35 times for G4C and 3.65 times for CAC, which highlights the better results in the industrial wastewater.

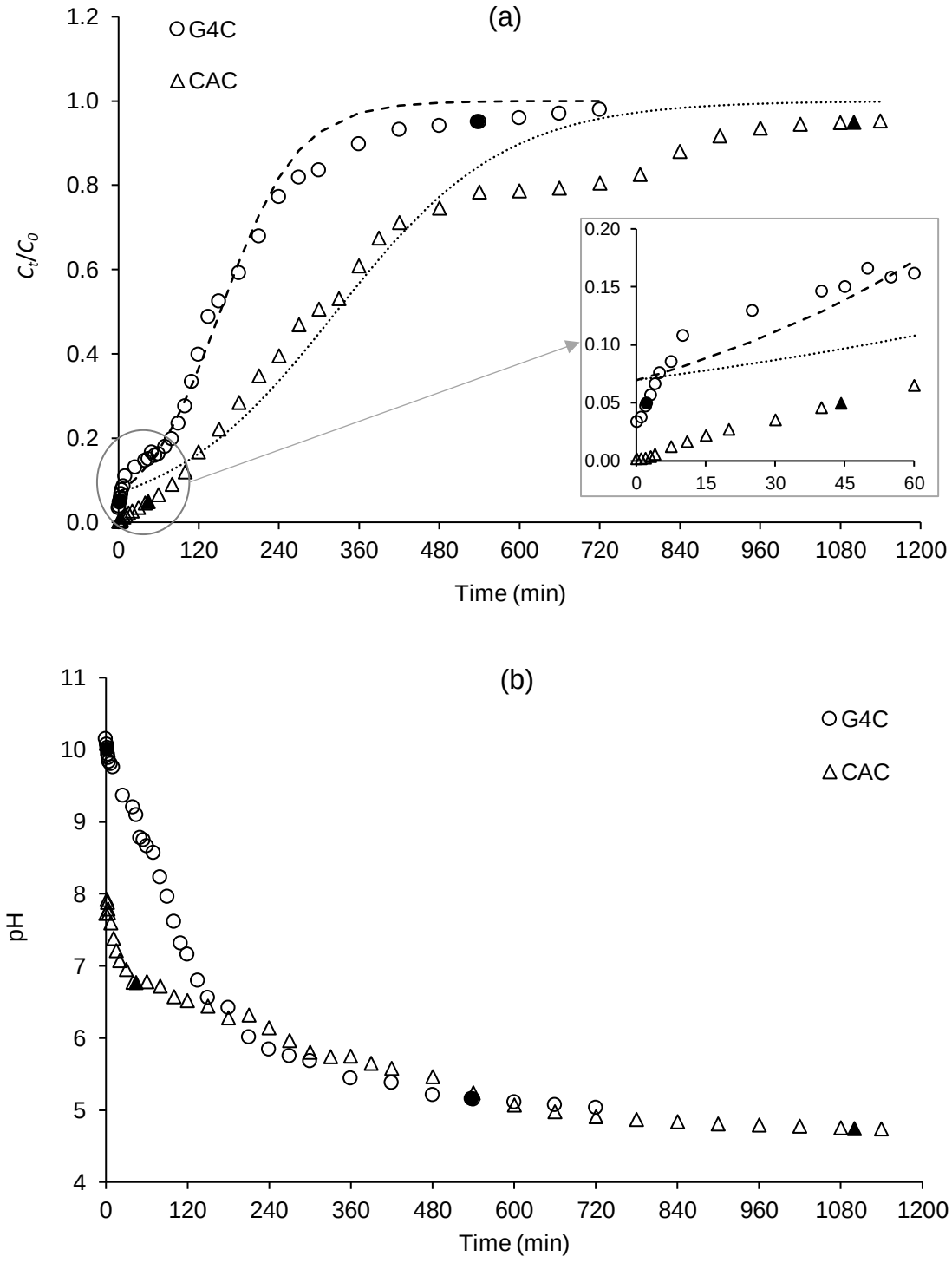

Figure 36. Column assays for Cr(III) removal from industrial wastewater using G4C and CAC – (a) Breakthrough curves and (b) pH values. The black symbols represent the breakthrough and saturation times, and the lines represent the Thomas's model adjustment.

Table 34. Column assays for Cr(III) removal from industrial wastewater using G4C and CAC – Experimental data and Thomas's model parameters.

	Experimental data parameters							Thomas model parameters		
Adsorbent	t_b (min)	pH t_b	t_s (min)	pH t_s	$m_{Cr(III)\_ads}$ (mg)	η (%)	q_{total} (mg g^{-1})	k_{th} (mL min^{-1} mg^{-1})	q_0 (mg g^{-1})	R^2
G4C	2.25	10.0	538	5.15	2.68	31.6	3.35	3.25	3.00	0.980
CAC	44.2	6.77	1 100	4.75	6.26	34.8	7.83	1.46	6.66	0.977

Alike the results in the synthetic solution, CAC performed better than G4C in the Cr(III) removal assays from the industrial wastewater. For GC, at saturation time (538 min) the pH was 5.15, suggesting that the Cr(III) removal by this adsorbent was ruled by precipitation and the ion exchange observed in the batch assays was not a reality in the column assays. At that same time, the pH for CAC was similar (5.24). However, at about 660 min, the pH of CAC was already below 5, indicating that from this point on adsorption started ruling the removal process, and the higher porosity of CAC (section 3.3.2.2) was used for the adsorption of Cr(III) through pore filling. The t_s for CAC was 1100 min with a pH of 4.75, meaning that almost half the assay was ruled by adsorption. So, for Cr(III) removal, opposing the results verified in the batch assays, in the fixed-bed column assays the higher porosity of CAC was more determinant than the highest mineral content of G4C. Still, the uptake capacities obtained in the batch assays were much higher than the ones verified in the column assays.

6.4 Conclusion

The experimental conditions that promoted the best Cr(III) removal results from the synthetic solution were the following: Q = 3 mL min^{-1}; t = 210 min for G4C and 270 min for CAC; C_0 = 5 mg L^{-1}; m_{ads} = 0.8 g; T = 50 °C. Under these conditions, the highest uptake capacities were found at a t_s of 150 min for G4C and 208 min for CAC, with a q_{total} of 1.60 and 2.14 mg g^{-1}, respectively.

Both G4C and CAC showed no capacity to be used in more than one adsorption cycle.

Both adsorbents performed better in the industrial wastewater with a t_s of 538 min for G4C and 1100 min for CAC, obtaining a q_{total} of 3.25 and 7.83 mg g^{-1}, respectively.

While in the batch assays G4C presented better results than CAC, in the column assays CAC presented better results than G4C for both the synthetic solution and industrial wastewater. This

was probably because Cr(III) removal by G4C only occurred due to precipitation, while CAC removed Cr(III) by precipitation and pore filling increasing the amount of Cr(III) removed.

For both adsorbents, Cr(III) removal was much more effective in the batch assays than in the column assays.

7. ORIGIN AND PROPERTIES OF ACTIVATED CARBONS USED IN TUNGSTATE (WO_4^{2-}) ADSORPTION ASSAYS

The results presented in this chapter were published, partially or completely, in the following scientific publications:

Papers:

D. Dias, D. Don, J. Jandosov, M. Bernardo, F. Pinto, I. Fonseca, A. Sanches, P. S. Caeteno, S. Lyubchyk, N. Lapa, Highly efficient porous carbons for the removal of W(VI) oxyanion from wastewaters, *Journal of Hazardous Materials*, under revision - major revisions.

Oral Presentations:

D. Dias, D. Don, J. Jandosov, M. Bernardo, I. Fonseca, F. Pinto, N. Lapa, Tungstate adsorption onto porous carbons obtained from rice wastes, *5th International Conference "WASTES: Solutions, Treatments and Opportunities"*, 4-6 September 2019, Caparica, Portugal.

7.1 Introduction

Tungstate (WO_4^{2-}) is an anion, so ion exchange with the cations present in the gasification and pyrolysis chars (**Table 13**) is not a possibility. Furthermore, both gasification and pyrolysis chars presented low surface areas and pore volumes (**Table 14**). Therefore, no chars were tested for WO_4^{2-} removal. On the other hand, the activations performed to P1C for the Cr(III) removal assays (Chapter 3) may not be the most adequate for WO_4^{2-} removal, once the removal mechanisms applied on these elements may be quiet different, once Cr(III) is a cation and WO_4^{2-} an anion that frequently assumes polyoxometalates speciation. For that reason, new activated carbons (ACs) were produced. ACs' production followed the criteria of maximising (i) the textural properties of ACs and (ii) the number of functional groups present on the ACs' surface.

This chapter describes how the ACs used in the tungstate (WO_4^{2-}) adsorption assays were prepared and characterised.

This chapter was performed in collaboration with the team of Dr. Jakpar Jandosov from the Institute of Combustion Problems, Kazakhstan.

7.2 Materials and methods

7.2.1 Origin of activated carbons used in the WO_4^{2-} adsorption assays

In order to maximise the surface area and pore volume of the ACs and the presence of functional groups on the ACs' surface, only chemical activations were performed. Six ACs were used: three originated from P1C (section 2.2.2), 2 originated from a new pyrolysis-derived char only composed by rice husk (P4C) and one originated from a direct activation of rice husk with H_3PO_4 (RH+H_3PO_4). The preparation of P4C-derived activated carbons and RH+H_3PO_4 were performed by the team of Dr. Jakpar Jandosov from the Institute of Combustion Problems, Kazakhstan and the details were previously published[182–184].

For comparison purposes, the commercial activated carbon (CAC) used in the Cr(III) removal assays was also used in the WO_4^{2-} adsorption assays. The characterisation of CAC was performed in Chapter 3.

7.2.1.1 Preparation of P1C-derived activated carbons

P1C activations were performed in a quartz reactor placed in a custom-made electric vertical tube furnace (**Figure 11**) already described in section 3.2.1.

Pyrolysis-derived char P1C (please, see pyrolysis conditions in section 2.2.2 and char's properties in section 2.3.2) was chemically activated with three different chemical agents: (i) KOH, (ii) K_2CO_3 and (iii) H_3PO_4. In the end of the activation processes all activated carbons were milled and sieved to <100 μm.

(i) Chemical activation of P1C with KOH – P1C was impregnated with KOH (wet impregnation) under a mass ratio of 1:3. The mixture was placed in a 250 mL beaker and filled with ultrapure water (Milli-Q Academic). The solution was heated-up to 50 °C, kept for 5 h under constant agitation, and dried at 130 °C. The char was then activated at 800 °C, for 2 h, under a N_2 flow of 150 cm^3 min^{-1}. The heating process was carried out under 5 °C min^{-1}. After cooling, the sample was then washed with hot deionized water until a stable pH close to 5.5 (deionized water) was reached. The sample was dried at 100 °C overnight. The code P1C+KOH was attributed to the activated carbon (AC) resulting from the chemical activation of P1C with KOH.

(ii) Chemical activation of P1C with K_2CO_3 – P1C was mixed with K_2CO_3 (dry impregnation) under a mass ratio of 1:4. The mixture was placed in the quartz reactor and activated at 800 °C, for 1 h, under a N_2 flow of 150 cm^3 min^{-1}. The heating process was carried out under 5 °C min^{-1}. After cooling, the sample was then washed and dried as described in item (i). The code P1C+K_2CO_3 was attributed to the AC resulting from the chemical activation of P1C with K_2CO_3.

(iii) Chemical activation of P1C with H_3PO_4 – P1C was impregnated with H_3PO_4 (wet impregnation) under a mass ratio of 1:3. The mixture was placed in a 100 mL volumetric flask with ultrapure water (Milli-Q Academic). The solution was agitated for 5 h, at 50 °C, and dried at 150 °C. The char was then activated at 500 °C, for 2 h, under a N_2 flow of 150 cm^3 min^{-1}. The heating process was carried out under 5 °C min^{-1}. After the activation stage, the sample was submitted to a post-treatment which consisted in boiling the sample with a solution of NaOH (1M), for 30 min, to promote the removal of silicates and other impurities. Finally, the sample was washed and dried as described in item (i). The code P1C+H_3PO_4 was attributed to the AC resulting from the chemical activation of P1C with H_3PO_4.

7.2.1.2 Preparation of P4C-derived activated carbons

P4C was a pyrolysis-derived char produced with only rice husk (RH) as feedstock. The pyrolysis was performed at 475 °C, for 30 min, in a spherical rotary steel reactor (**Figure 37**). In order to remove some minerals from the char, a demineralization was performed: P4C was boiled with a HCl (1.5 M), for 15 minutes. Finally, the char was washed three times with boiling deionized water and dried at 105 °C, for 12 hours.

P4C was chemically activated with two different solutions: (i) KOH and (ii) K_2CO_3. Both activations were performed in a cylindrical steel reactor placed inside a vertical electric furnace (**Figure 38**). In the end, all activated carbons were milled and sieved to <100 µm.

The activation of P4C was performed as follows:

(i) Chemical activation of P4C with KOH – P4C was impregnated with KOH (dry impregnation) under a mass ratio of 1:4 and activated at 850 °C, for 2 h, in self-generated atmosphere. The sample was then washed with hot deionized water, until a pH 7-8 and dried until constant weight. The code P4C+KOH was attributed to the AC resulting from the chemical activation of P4C with KOH.

(ii) Chemical activation of P4C with K_2CO_3 – P4C was mixed with K_2CO_3 (dry impregnation) under a mass ratio of 1:4 for 24 h and activated at 950 °C, for 1 h, in inert atmosphere (Argon). The sample was then washed with KOH (12%) to remove the residual silica, followed by hot deionized water washing to remove potassium silicate until pH 7-8 and dried until constant weight. The code P4C+K_2CO_3 was attributed to the AC resulting from the chemical activation of P4C with K_2CO_3.

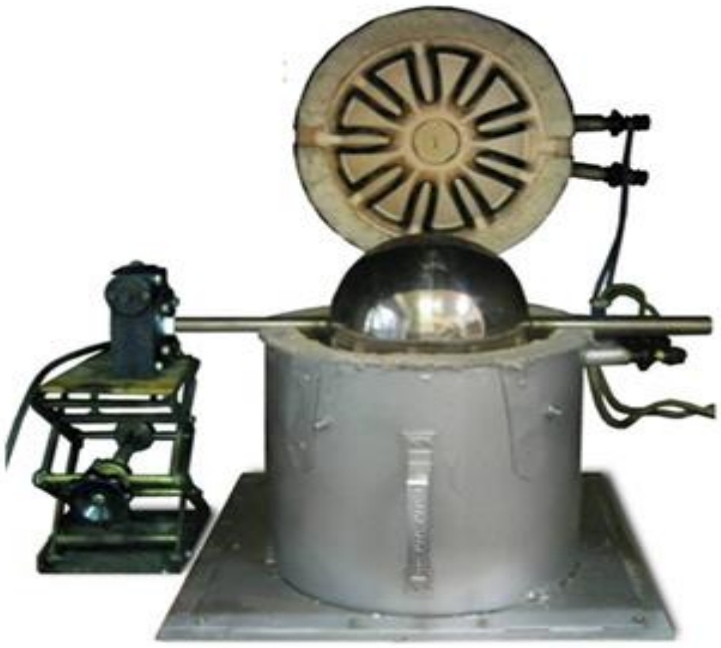

Figure 37. Spherical rotary steel reactor that originated P4C.

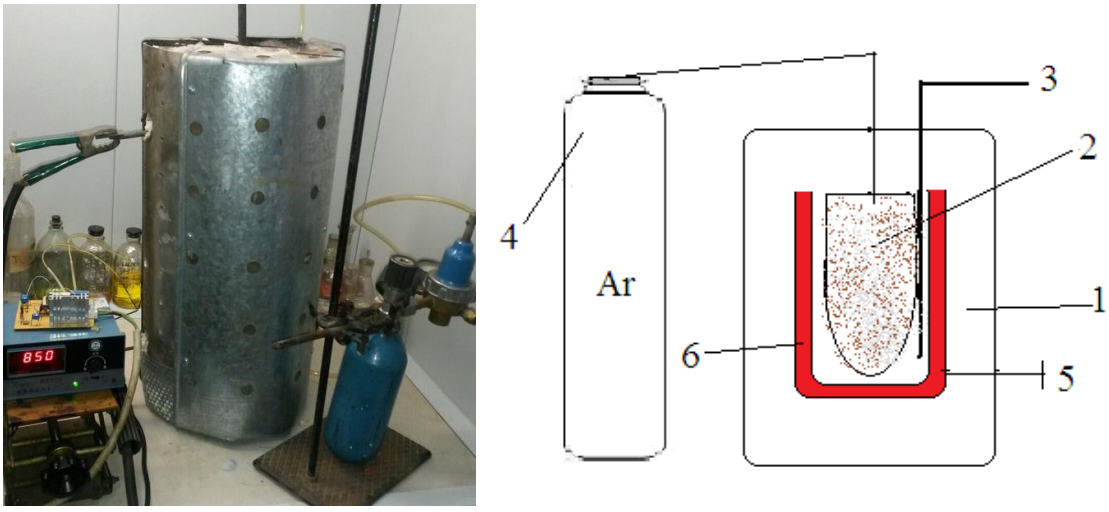

Figure 38. P4C activation setup: 1 - cylindrical electric furnace; 2 - reactor; 3 - thermocouple; 4 - argon (Ar) gas bottle; 5 - insulator; 6 - electric resistance heating.

7.2.1.3 Preparation of RH+H_3PO_4 activated carbon

Rice husk (RH) was impregnated with H_3PO_4 under a mass ratio of 1:2. The mixture was placed in cylindrical quartz reactor, heated at 200 ºC overnight and activated (in the same reactor as described in section 7.2.1.1) at 500 °C, for 1 h, in self-generated atmosphere. After the activation stage, the sample was washed with hot deionized water to remove most H_3PO_4 and submitted to a post-treatment with NaOH 1M (described in 7.2.1.1, item (iii)). Finally, the sample was washed with boiling deionized water until pH 7-8. Finally, it was dried at 105 °C, for 12 hours. In the end, the activated carbon was milled and sieved to <100 µm. The code RH+H_3PO_4 was attributed to the AC resulting from the direct chemical activation of RH with H_3PO_4.

7.2.2 Characterisation of activated carbons used in the WO_4^{2-} adsorption assays

All activated carbons were characterised for the following assays:

a) Proximate analysis – The same as described in section 2.2.3;

b) Elemental analysis – The same as described in section 2.2.1;

c) Mineral content – The same as described in section 2.2.1;

d) Textural analysis – The same as described in section 2.2.3;

e) pH_{pzc} – The same as described in section 2.2.4.

CAC was characterised in Chapter 3.

7.3. Results and discussion

7.3.1 Proximate and elemental analyses

The proximate and elemental analyses of the activated carbons used in WO_4^{2-} adsorption assays are shown in **Table 35**.

All ACs were mainly composed by fixed-C followed by volatile matter. The low ash content revealed that the removal of minerals was successful. The higher moisture content of P1C+H_3PO_4 and RH+H_3PO_4 indicated that H_3PO_4 as activating agent produced quite hydrophilic carbons.

7.3.2 Mineral content

The mineral content of the activated carbons used in WO_4^{2-} adsorption assays are shown in **Table 36**.

Table 35. Proximate and elemental analyses of the activated carbons used in the WO_4^{2-} adsorption assays.

Parameter	Activated carbons					
	P1C+KOH	P1C+K_2CO_3	P1C+H_3PO_4	P4C+KOH	P4C+K_2CO_3	RH+H_3PO_4
Proximate analysis (% w/w ar)						
Moisture content	4.50	5.68	12.06	8.27	5.63	10.83
Volatile matter	29.83	37.16	25.03	40.56	35.84	23.71
Ashes	1.56	4.54	9.30	2.14	6.58	3.35
Fixed carbon	64.11	52.62	53.61	49.03	51.95	62.11
Elemental analysis (% w/w ar)						
C	83.53	78.60	67.90	83.84	83.97	79.73
H	0.33	0.48	2.12	0.06	0.04	0.55
N	0.85	0.80	0.77	0.57	< 0.2	0.43
S	< 0.03	< 0.03	< 0.03	< 0.03	< 0.03	< 0.03

ar: as-received basis

Table 36. Mineral content (mg kg^{-1} db; $\overline{X} \pm \sigma$) of the activated carbons used in the WO_4^{2-} adsorption assays.

Chemical element	Activated carbons					
	P1C+KOH	P1C+K_2CO_3	P1C+H_3PO_4	P4C+KOH	P4C+K_2CO_3	RH+H_3PO_4
Si	10 030 ± 822	23 076 ± 1425	3 890 ± 273	920 ± 91	6 470 ± 127	431 ± 36
Ca	1 833 ± 117	3 605 ± 311	3 877 ± 373	2 310 ± 92	4 577 ± 416	154 ± 10
Na	736 ± 65	413 ± 33	2 013 ± 99	< 4.36×10^{-2}	< 4.36×10^{-2}	200 ± 5
Mg	390 ± 27	1 147 ± 112	856 ± 62	848 ± 14	2 230 ± 53	101 ± 1
Fe	682 ± 6	511 ± 45	212 ± 18	6 873 ± 171	7 810 ± 627	150 ± 5
Al	578 ± 26	638 ± 45	91.5 ± 6.8	17.3 ± 1.0	138 ± 1	< 1.12
K	188 ± 12	390 ± 20	232 ± 7	2 499 ± 35	24 960 ± 967	58.0 ± 4.3
Zn	292 ± 17	97.8 ± 2.6	124 ± 10	20.3 ± 0.7	16.6 ± 0.2	16.9 ± 0.3
Ti	79.6 ± 4.9	80.8 ± 15.1	52.4 ± 1.1	< 1.12	< 1.12	< 1.12
Ba	24.0 ± 1.5	35.8 ± 3.5	69.6 ± 5.6	11.9 ± 1.0	16.9 ± 1.4	4.32 ± 0.39
Cr	51.7 ± 4.4	40.4 ± 3.9	20.3 ± 1.4	293 ± 14	217 ± 5	< 0.381
Ni	42.6 ± 1.8	25.0 ± 1.2	< 3.03	82.8 ± 2.5	< 7.58	< 0.897
Cu	15.2 ± 0.1	20.5 ± 1.0	15.3 ± 1.1	12.8 ± 0.1	46.5 ± 3.4	< 0.852
W	< 7.58	< 7.58	< 7.58	< 7.58	< 7.58	< 7.58
Se	< 3.79	< 3.79	< 3.79	< 3.79	< 3.79	< 3.79
Mo	< 0.455	< 0.455	< 0.455	< 0.455	< 0.455	< 0.455
Pb	< 0.379	< 0.379	< 0.379	< 0.379	< 0.379	< 0.379
Sb	< 0.379	< 0.379	< 0.379	< 0.379	< 0.379	< 0.379
As	< 0.379	< 0.379	< 0.379	< 0.379	< 0.379	< 0.379
Cd	< 0.303	< 0.303	< 0.303	< 0.303	< 0.303	< 0.303
Hg	< 2.27×10^{-2}	< 2.27×10^{-2}	< 2.27×10^{-2}	< 2.27×10^{-2}	< 2.27×10^{-2}	< 2.27×10^{-2}

db: dry basis; $\overline{X} \pm \sigma$: average ± standard deviation.

Si was the major element in all P1C-derived ACs, due to the mineral composition of RH (**Table 10**).

P4C+K_2CO_3 was the AC with the highest mineral content of all ACs, mainly due to the high concentration of K in the AC. This occurred due to the presence of this element both in the raw material (RH), activation agent (K_2CO_3) and washing solution (KOH).

RH+H_3PO_4 presented the lower mineral content of all ACs, which can be explained by the fact that the activation was performed directly to a feedstock instead of a char. Also, both ACs activated with H_3PO_4 presented the lower mineral content meaning that the activation with H_3PO_4 and the post-treatment with NaOH (1M) properly removed most minerals present in the ACs. Overall, all ACs were rich in alkaline and alkaline-earth elements such as Ca, Na, Mg, K, but also Fe and Al were present in high concentrations.

7.3.3 Textural analysis and pH_{pzc}

According to the IUPAC classification[73], the N_2 adsorption-desorption isotherms of P1C-derived ACs (**Figure 39a**), of P4C-derived ACs and of RH+H_3PO_4 (**Figure 39b**) were a mix of type I (in the beginning of the isotherm) and type IV (at the end of the isotherm) isotherms with H4 hysteresis, indicating the presence of narrow slit-shaped micropores and the presence of mesopores.

Table 37 presents the textural properties and pH_{pzc} of the ACs used in the WO_4^{2-} adsorption assays.

Overall, the ACs derived from only RH (P4C-derived ACs and RH+H_3PO_4) presented higher surface areas and total pore volumes than the ACs derived from RH+PE (P1C-derived ACs). On the other hand, the ACs derived from only RH presented more mesopores than micropores, while the ACs derived from RH+PE presented more micropores than mesopores. P4C+KOH presented the highest surface area and pore volume of all ACs, while P1C+KOH presented the highest values of all P1C-derived ACs, meaning that KOH was the activating agent that promoted the ACs with the highest surface areas and pore volumes.

Regarding pH_{pzc}, P1C-derived ACs presented acidic pH_{pzc} values, P4C+KOH and RH+H_3PO_4 presented neutral to slightly acidic values and P4C+K_2CO_3 obtained alkaline values, probably due to the high K concentration in the AC (**Table 36).**

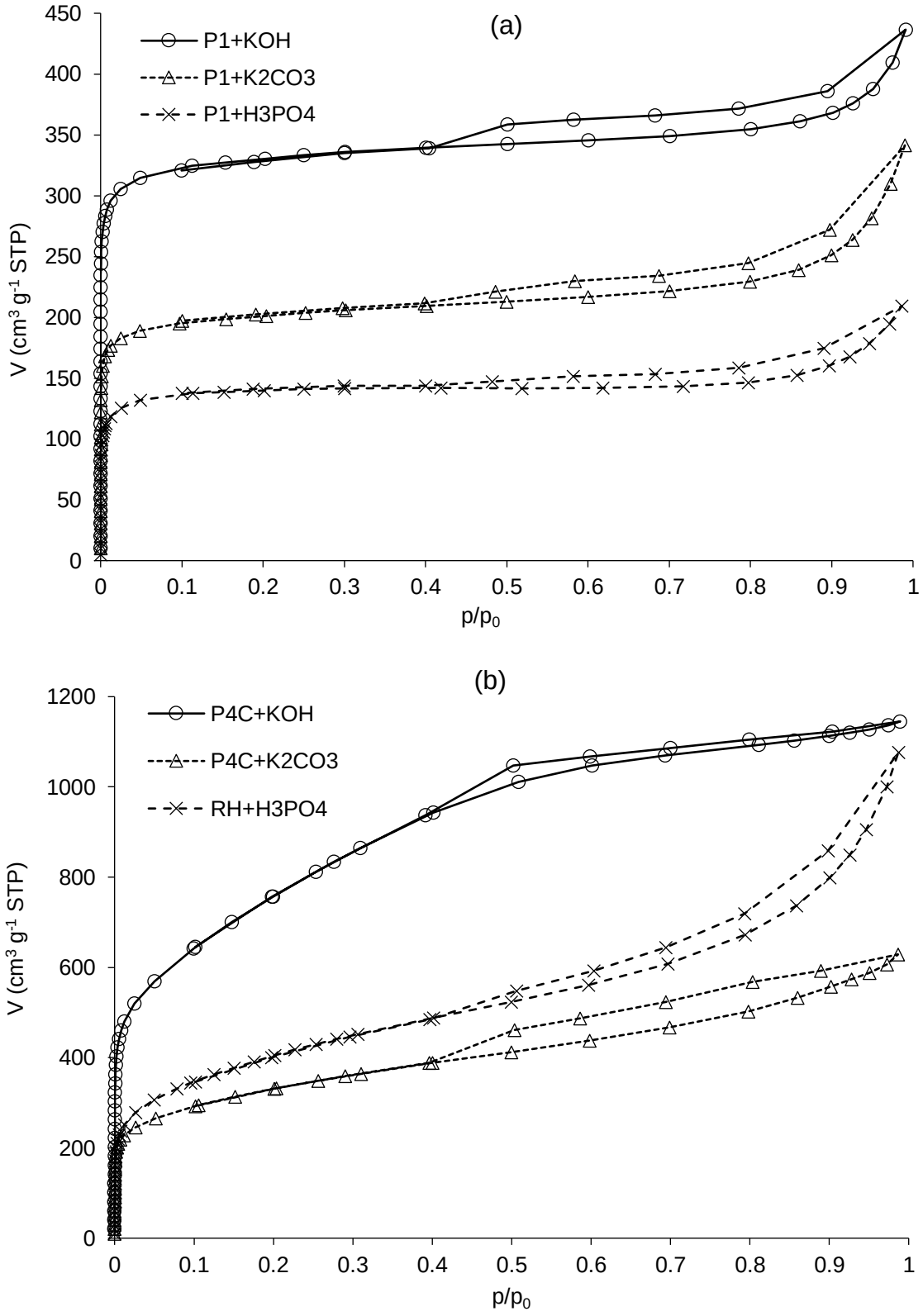

Figure 39. N_2 adsorption-desorption isotherms and textural properties of (a) P1C-derived activated carbons and (b) P4C-derived activated carbons and RH+H_3PO_4.

Table 37. Textural properties and pH_{pzc} of the activated carbons used in the WO_4^{2-} adsorption assays.

Parameter	Activated carbons					
	P1C+KOH	P1C+K_2CO_3	P1C+H_3PO_4	P4C+KOH	P4C+K_2CO_3	RH+H_3PO_4
S_{BET} (m^2 g^{-1})	1 315	790	554	2 610	1 151	1 402
V_{total} (cm^3 g^{-1})	0.60	0.44	0.28	1.74	0.91	1.40
V_{micro} (cm^3 g^{-1})	0.47	0.26	0.19	0.60	0.28	0.29
V_{meso} (cm^3 g^{-1})	0.13	0.18	0.09	1.14	0.63	1.11
pH_{pzc}	3.94	4.00	2.38	6.92	9.56	6.14

7.4 Conclusions

All the ACs were mainly composed by fixed-C followed by volatile matter.

P4C+K_2CO_3 was the AC with the highest mineral content of all ACs, mainly due to K, while RH+H_3PO_4 presented the lower mineral content of all ACs. Overall, all ACs were rich in Si and alkaline and alkaline-earth metals.

P4C+KOH presented the highest surface area and pore volume of all ACs once KOH was the activating agent that promoted the ACs with the highest surface areas and pore volumes.

P1C-derived ACs presented acidic pH_{pzc} values, while P4C+K_2CO_3 obtained an alkaline value.

8. TUNGSTATE ADSORPTION ASSAYS UNDER BATCH CONDITIONS

The results presented in this chapter were published, partially or completely, in the following scientific publications:

Papers:

D. Dias, D. Don, J. Jandosov, M. Bernardo, F. Pinto, I. Fonseca, A. Sanches, P. S. Caeteno, S. Lyubchyk, N. Lapa, Highly efficient porous carbons for the removal of W(VI) oxyanion from wastewaters, *Journal of Hazardous Materials*, under revision - major revisions.

Oral Presentations:

D. Dias, D. Don, J. Jandosov, M. Bernardo, I. Fonseca, F. Pinto, N. Lapa, Tungstate adsorption onto porous carbons obtained from rice wastes, *5th International Conference "WASTES: Solutions, Treatments and Opportunities"*, 4-6 September 2019, Caparica, Portugal.

8.1. Introduction

In this chapter, the activated carbons characterised in Chapter 7 (P1C+KOH, P1C+K_2CO_3, P1C+H_3PO_4, P4C+KOH, P4C+K_2CO_3 and RH+H_3PO_4) were used in adsorption assays of tungstate (WO_4^{2-}) from a synthetic solution and from a mining wastewater.

For comparison purposes, CAC (section 3.2.1.5) was also used in the WO_4^{2-} adsorption assays.

8.2 Materials and methods

8.2.1 WO_4^{2-} synthetic solution

A WO_4^{2-} synthetic solution with an initial WO_4^{2-} concentration of 50 ± 5 mg L^{-1} was prepared by diluting a standard Ammonium Tungstate $(NH_4)_2WO_4$ solution of 1000 mg L^{-1} (Scharlau) with ultrapure water (Milli-Q Academic).

8.2.2 Mining wastewater – origin and characterisation

The mining wastewater was collected in a Wolframite mine. Due to confidentiality request, additional information about the origin of the mining wastewater is unknown.

The mining wastewater was characterised for:

(a) pH and conductivity – The same as described in section 4.2.2;

(b) Total solids (TS), fixed solids (FS), total suspended solids (TSS) and volatile solids (VS) – The same as described in section 4.2.2;

(d) Mineral content in filtered mining wastewater – The same as described in section 4.2.2, but the selected metals and metalloids were the following: Al, Ca, Cu, Fe, K, Mg, Na, Ni, Si, V, W and Zn;

(e) Mineral content after acidic digestion – The same as described in section 4.2.2, but the selected metals and metalloids were the ones mentioned in item (d).

(f) Solubility of the species in the wastewater by equation 4.1 (section 4.2.2).

8.2.3 WO_4^{2-} adsorption assays from synthetic solution

All WO_4^{2-} adsorption assays were performed as described in section 4.2.3.

For comparison reasons, the commercial activated carbon (CAC) used in the Cr(III) removal assays (Norit GAC 1240) was also used in the WO_4^{2-} adsorption assays.

8.2.3.1 Effect of initial pH and solid/liquid ratio (S/L)

All adsorbents were submitted to a preliminary study, in which the effect of two parameters on the WO_4^{2-} adsorption assays was tested: (i) the initial pH value of the solution and (ii) the adsorbent loading, defined as the solid/liquid ratio (S/L). All these assays were performed for 24 h. First, the S/L was fixed at 1 g L^{-1} and five initial pH were tested (2, 4, 6, 8 and 10). Then, the initial pH that originated the assay with the highest uptake capacities was fixed and three S/L ratios were tested (0.1, 0.25 and 1 g L^{-1}).

The adsorbent and conditions (S/L and initial pH) that originated the assay with the highest uptake capacities were selected to be used in the kinetic and adsorption isotherm studies.

WO_4^{2-} removal efficiency, η (%), and experimental adsorbent removal capacity, q_{exp} (mg g^{-1}), were calculated through the equations 4.2 and 4.3 (section 4.2.3.1), respectively.

8.2.3.2 Kinetic study

Contact times between 5 min and 48 h were tested. The results were adjusted to pseudo-first order and pseudo-second order kinetic models, through the equations 4.4 and 4.5[171] (section 4.2.3.2), respectively.

8.2.3.3 Adsorption isotherm study

WO_4^{2-} concentrations between 10 and 200 ± 5 mg L^{-1} were tested. The contact time of the assays was selected according to the results of the kinetic study.

The results were adjusted to 5 isotherm models:

(i) Langmuir's non-linear model - equation 4.6[173] (section 4.2.3.3).

(ii) Freundlich's non-linear model - equation 4.7[173] (section 4.2.3.3).

(iii) Sips model - equation 8.1[185]:

$$q_e = \frac{q_{max} \times b \times C_e^{\frac{1}{n}}}{1 + b \times C_e^{\frac{1}{n}}} \quad (8.1)$$

where q_e is the WO_4^{2-} removal capacity in the equilibrium (mg g^{-1}), q_{max} is the maximum uptake capacity (mg g^{-1}), b is the Langmuir's constant (L mg^{-1}), C_e is the concentration of WO_4^{2-} in the equilibrium (mg L^{-1}) and n is a measure of the heterogeneity of the binding surface (dimensionless). Sips model is a combination of Langmuir and Freundlich models, whose origin is related to the heterogeneous adsorption systems and circumventing the limitation of the rising

adsorbate concentration associated with Freundlich isotherm model. At low adsorbate concentrations, the model tends to Freundlich isotherm, while at high concentrations, it tends to Langmuir isotherm[136,173].

(iv) Redlich-Peterson model - equation 8.2[185]:

$$q_e = \frac{K_R \times C_e}{1 + a_R \times {C_e}^{\beta}} \qquad \text{where } \beta \leq 1 \tag{8.2}$$

Where, C_e is the concentration of WO_4^{2-} in the equilibrium (mg L^{-1}), K_R (L g^{-1}) and a_R (L mg^{-1}) are the Redlich-Peterson's constants, and β (dimensionless) is also an intensity parameter. Redlich-Peterson model also includes Langmuir and Freundlich isotherms. But in this case, the model has a linear dependence on concentration in the numerator and an exponential function in the denominator to represent adsorption equilibria over a wide concentration range. Due to its versatility it can be applied to both homogeneous and heterogeneous systems. At high concentration, when β is closer to 0, the model tends to Freundlich isotherm, while at low concentrations, when β is closer to 1, it tends to Langmuir isotherm[173].

(v) Multi-step isotherm model - equation 8.3[186]:

$$q_e = \sum_{i=1}^{s} \left\{ \frac{q_{Ti} \times K_i \times (c - b_i + |c - b_i|)^{n_i}}{2^{n_i} + K_i \times (c - b_i + |c - b_i|)^{n_i}} \right\} \tag{8.3}$$

where, s is the total number of steps, q_{Ti} is the adsorption capacity (mg g^{-1}) of the layer n_i, K_i is the equilibrium constant [(L $mg^{-1})^n$], c is the concentration of WO_4^{2-} in the equilibrium (mg L^{-1}), b_i describes the critical concentration limit (mg L^{-1}) and n_i indicates the solute's average degree of association. The multi-step isotherm model was obtained from geometric series of modified Langmuir equation with the assumption that the surface sites can be covered by more than one molecule in the form of associated complexes. Layers of associated complexes of different composition are formed characterized by the solute's average degree of association (n), starting with a single layer of the solute, continued with the layer of dimers (n=2), trimers (n=3), and so on[186,187].

8.2.3.4. Model adjustment

The same as described in section 4.2.3.4.

8.2.4 WO_4^{2-} adsorption assays from mining wastewater

The adsorbent and conditions (S/L and contact time) that performed better on the synthetic solution were selected for the WO_4^{2-} adsorption assays from the mining wastewater. The adsorption assays were performed with the filtered wastewater and because the concentration of soluble tungsten in the wastewater was below the detection limit (please, see section 8.3.3), the medium was spiked with Ammonium Tungstate solution used in the synthetic solution (section 8.2.1). The wastewater was spiked with the same concentration of the assay that presented the highest uptake capacity in the adsorption isotherm study. Two initial pH values were tested: (i) pH of the wastewater as-received; and (ii) optimum pH for tungstate removal, selected according to the assays performed in the synthetic solution (section 8.2.3.1).

Again, for comparison reasons, CAC was used in WO_4^{2-} adsorption assays from the mining wastewater.

8.2.5 Mineral interactions in the mining wastewater during WO_4^{2-} adsorption assays

In order to understand the importance of minerals in WO_4^{2-} adsorption assays, several minerals were quantified before and after the WO_4^{2-} adsorption assays in mining wastewater. This set of assays enabled to study (i) the possible competition mechanism with other ions, (ii) the salting-out effect due to the presence of cationic species reducing the available solvent due to ionic hydration, and (iii) the release of other minerals to the wastewater by the adsorbent.

The elements quantified in this study were Al, Ca, Fe, K, Mg and Si. These elements were selected because they were present either in the industrial wastewater or in the adsorbent.

Concentration variation, CV (mg L^{-1}), and percentage variation, PV (%), were calculated by equations 4.9 and 4.10 (section 4.2.5), respectively.

The procedure for the removal assays was the same as described in section 4.2.3, but instead of Cr, the elements quantified by ICP-AES were the ones mentioned two paragraphs above.

8.2.6 Ecotoxicity in the WO_4^{2-} adsorption assays from mining wastewater

An ecotoxicological evaluation was performed before and after the WO_4^{2-} adsorption assays from mining wastewater by using Microtox® assay. Before the adsorption assays both wastewaters (original pH and optimal pH) were submitted to an ecotoxicological analysis. After the adsorption assays, the samples were filtered through Whatman® ME 25/21 ST membrane filters (0.45 µm), the pH was measured (Hanna Instruments edge® HI 2002 pH meter) and the filtered samples were also sent for the ecotoxicological analysis. The procedure was the same as described in section 2.2.1.

8.3 Results and discussion

8.3.1 WO_4^{2-} adsorption assays in synthetic solution

8.3.1.1 Effect of initial pH and solid/liquid ratio (S/L)

Figure 40 shows the results of WO_4^{2-} adsorption assays by the ACs from synthetic solution, for different initial pH values.

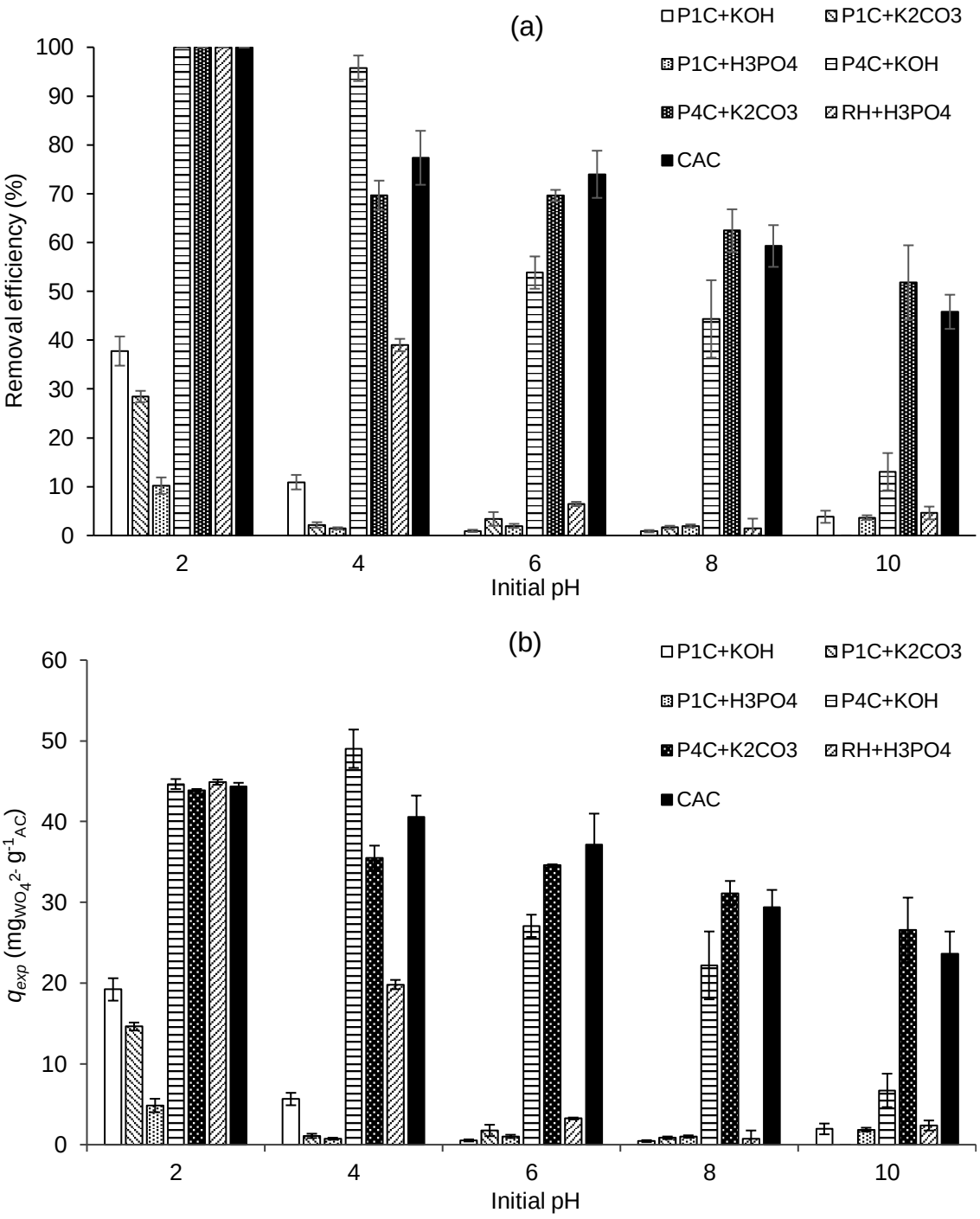

Figure 40. Effect of the initial pH on the WO_4^{2-} (a) removal efficiency and (b) uptake capacity in the synthetic solution.

In general, the lower was the initial pH, the higher were the WO_4^{2-} removal efficiency and uptake capacity. In fact, for the initial pH 2, four activated carbons (P4C+KOH, P4C+K_2CO_3, RH+H_3PO_4 and CAC) presented removal efficiencies of around 100%. This can be explained by the difference between the pH_{pzc} of ACs and the pH of the solution. When the pH of a medium is lower than the pH_{pzc} of the AC, the AC's surface will be positively charged due to the release of hydroxyl groups and/or acquisition of protons[188,189]. The highest this difference is, the more positively charged the AC surface will be.

Being an oxyanion, positively charged surfaces increase tungstate adsorption, particularly because tungsten creates poly-oxometallates (POMs), which are very large ions formed by three or more oxyanions linked together by sharing oxygen atoms. POMs create wide and complex 3D structures and can have negative valences (up to -10)[190] (**Figure 41**). Therefore, strong electrostatic interaction can be formed between the negatively charged tungstate species and the positively charged carbon surface.

These results allowed understanding that, in addition to the chemical surface properties of the ACs, the textural properties also had a major role in the adsorption process, since the ACs with higher surface areas and pore volumes (P2C-KOH, P2C-K_2CO_3, RH-H_3PO_4 - **Table 37**) presented the highest WO_4^{2-} removal efficiencies and uptake capacities. However, at pH 2, POMs are formed (**Figure 41**). Considering that POMS are nanosized cluster anions with sizes ranging from 1-6 nm[191], it can be assumed that, along with the surface area and pH_{pzc} of the AC, the mesopore volume also played an important role on the adsorption process.

Although CAC presented slightly poorer textural properties (surface area and mesopore volume - **Table 19**) when compared to the other ACs, its high alkaline character allowed it to still achieve some interesting results.

Once P1-derived AC presented acidic pH_{pzc} values, besides lower surface areas (**Table 37**), their removals were lower than for the other ACs. Between P1C-derived ACs, P1C presented the best results due to the highest surface area and pore volume (**Table 37**).

Once P4C+KOH, P4C+K_2CO_3, RH+H_3PO_4 and CAC presented removal efficiencies of around 100% at pH 2, lower S/L values were tested in order to maximize the uptake capacity of each AC (**Figure 42**).

P4C+KOH was the AC that presented the best relation between the chemical surface properties (pH_{pzc}) and textural properties (surface area/pore volume). It obtained removals of around 100% at S/L 0.25 and 1 g L^{-1}, and 73.8% at S/L 0.1 g L^{-1}, achieving the highest q_e of 330 mg g^{-1} at that same S/L. On the other hand, CAC obtained a highest q_e of 88.6 mg g^{-1} at S/L 0.25 g L^{-1}. This means that P4C+KOH achieved a substantial higher uptake capacity than CAC. For that reason, P4C+KOH was the AC selected to be used in the following assays, along with CAC (for comparison purposes).

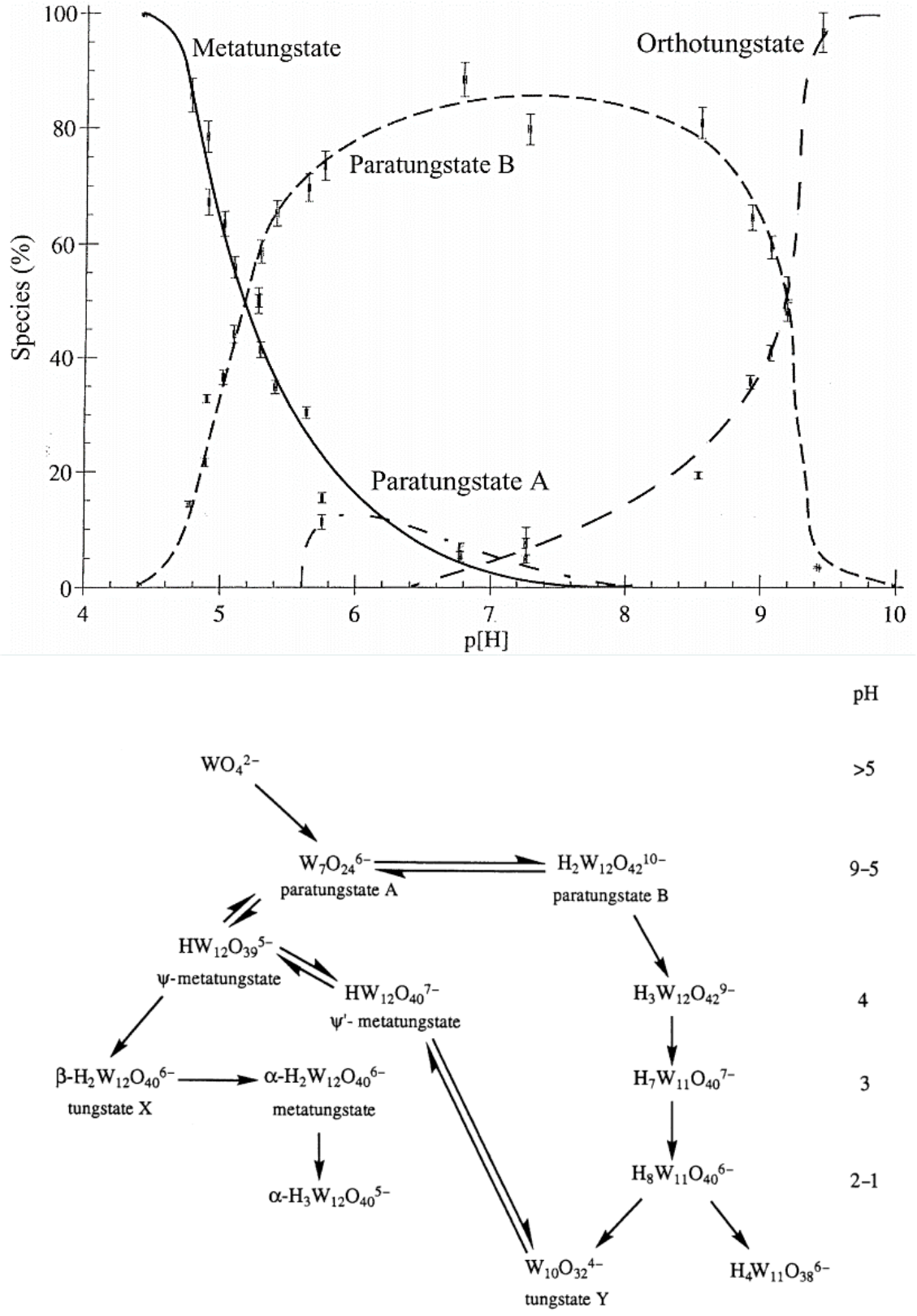

Figure 41. Influence of pH on tungsten speciation[190] (reproduced under the kind permission of CSIRO Publishing).

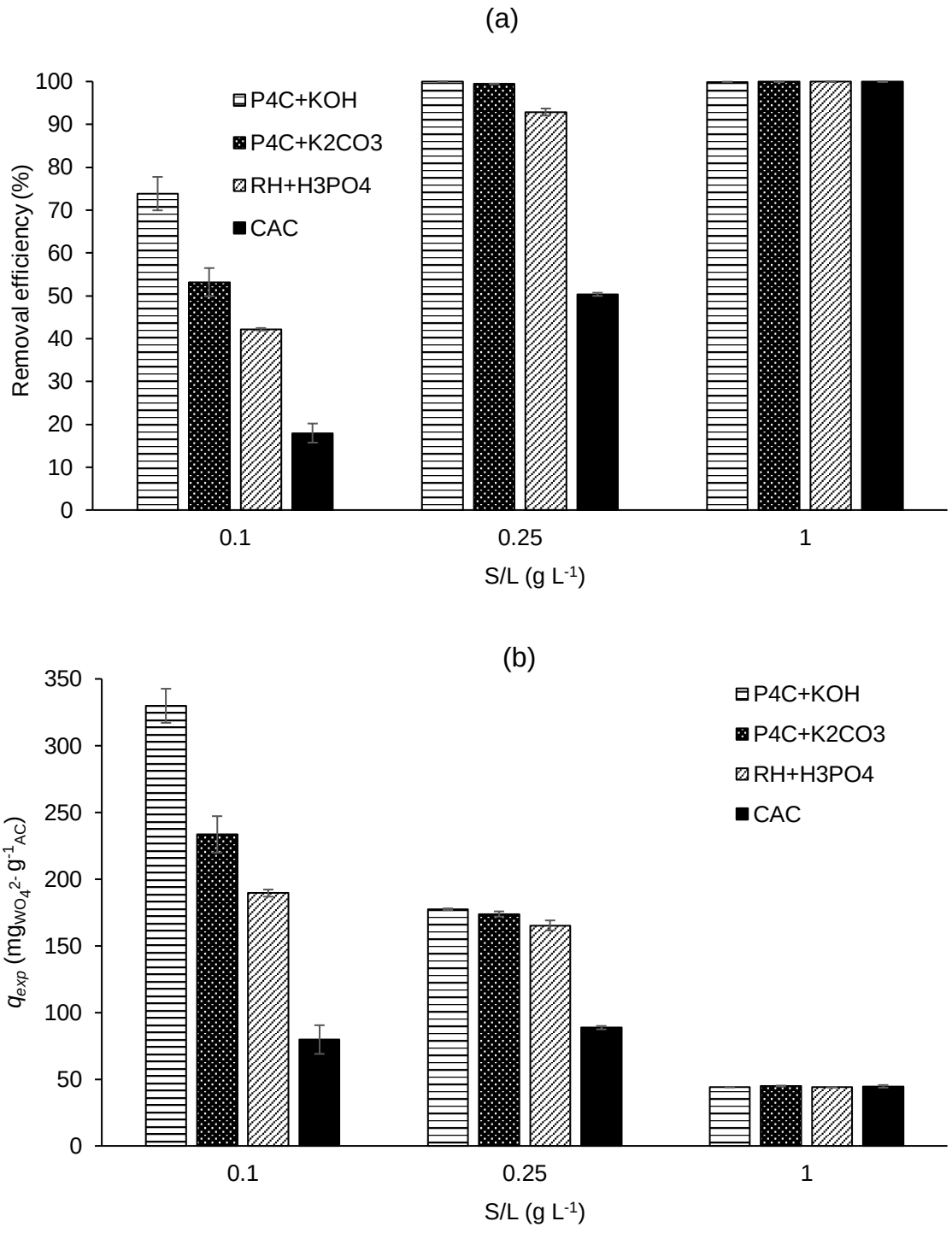

Figure 42. Effect of S/L on the WO_4^{2-} (a) removal efficiency and (b) uptake capacity in the synthetic solution at pH 2.

8.3.1.2 Kinetic study

The kinetic study assays were performed with P4C+KOH and CAC, at an initial pH 2 and a S/L 0.1 g L^{-1}. The experimental data were then adjusted to pseudo-first order and pseudo-second order kinetic models. All the results of this study are shown in **Figure 43** and **Table 38**.

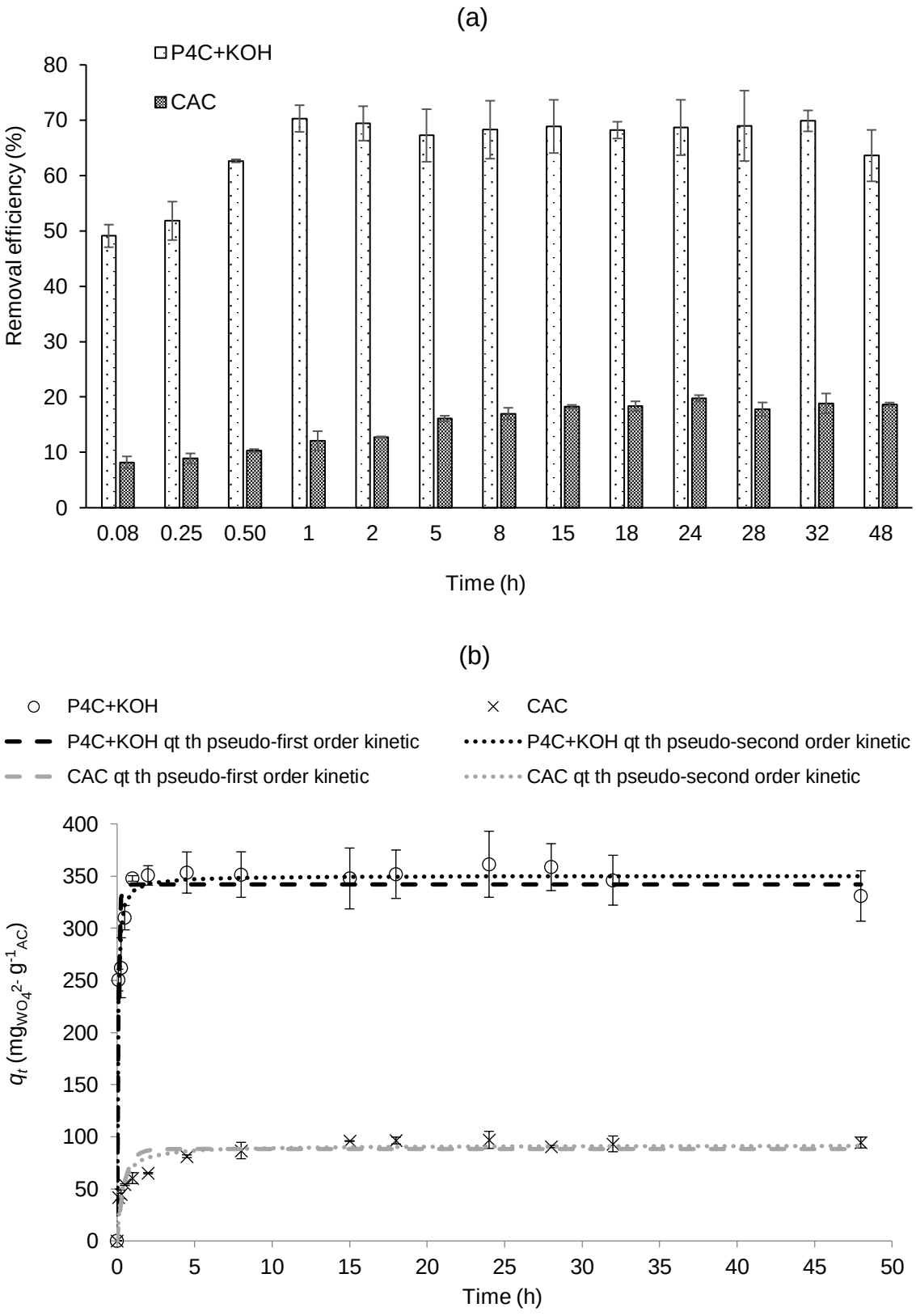

Figure 43. Kinetic study of P4C+KOH and CAC along time in the synthetic solution at an initial pH 2 and a S/L 0.1 g L^{-1}: (a) WO_4^{2-} removal efficiency and (b) WO_4^{2-} uptake capacity and adjustment of experimental data to pseudo-first order and pseudo-second order kinetic models (th: theoretical data).

Table 38. Parameters of pseudo-first order and pseudo-second order kinetic models adjusted to the experimental data of P4C+KOH and CAC in the synthetic solution at an initial pH 2 and a S/L 0.1 g L^{-1}.

Kinetic model	Parameter	Adsorbent	
		P4C+KOH	CAC
Pseudo-first order	q_e (mg g^{-1})	341	88.2
	k_f (h^{-1})	13.0	2.08
	R^2	0.560	0.846
Pseudo-second order	q_e (mg g^{-1})	350	91.7
	k_s (g mg^{-1} h^{-1})	6.51×10^{-2}	3.72×10^{-2}
	R^2	0.830	0.916

The results showed that P4C+KOH obtained significantly better results than CAC, achieving equilibrium after 1 h with removal efficiencies of around 70% and uptake capacities of around 350 mg g^{-1}. The highest uptake capacity was found at 24 h with a q_t of 361 mg g^{-1}. In contrast, CAC reached equilibrium only after 15 h with removal efficiencies of less than 20% and uptake capacities of around 90 mg g^{-1}.

The experimental data were better adjusted to the pseudo-second order kinetic model for both carbons, obtaining a q_e of 350 mg g^{-1} for P4+KOH and 91.7 mg g^{-1} for CAC, meaning that, at equilibrium, the uptake capacity of the pyrolysis-derived carbon was almost 4 times higher than the commercial activated carbon.

8.3.1.3 Adsorption isotherm study

The adsorption isotherm study assays were performed with P4C+KOH and CAC, at an initial pH 2 and a S/L 0.1 g L^{-1} for 24 h.

The results showed that, for all assays, P4C+KOH presented higher removal efficiencies (**Figure 44a**) and uptake capacities (**Figure 44b**) than CAC. For initial WO_4^{2-} concentrations ≤ 30 mg L^{-1}, P4C+KOH achieved removal percentages of around 100%. However, the highest uptake capacity was found for an initial WO_4^{2-} concentration of 150 mg L^{-1} with a q_t of 854 mg g^{-1}. In contrast, the highest q_t of CAC was of 113 mg g^{-1} at an initial WO_4^{2-} concentration of 100 mg L^{-1}. P4C+KOH obtained a q_t almost 8 times higher than CAC. These results clearly highlight the better properties of P4C+KOH on WO_4^{2-} removal from synthetic solution when compared to CAC.

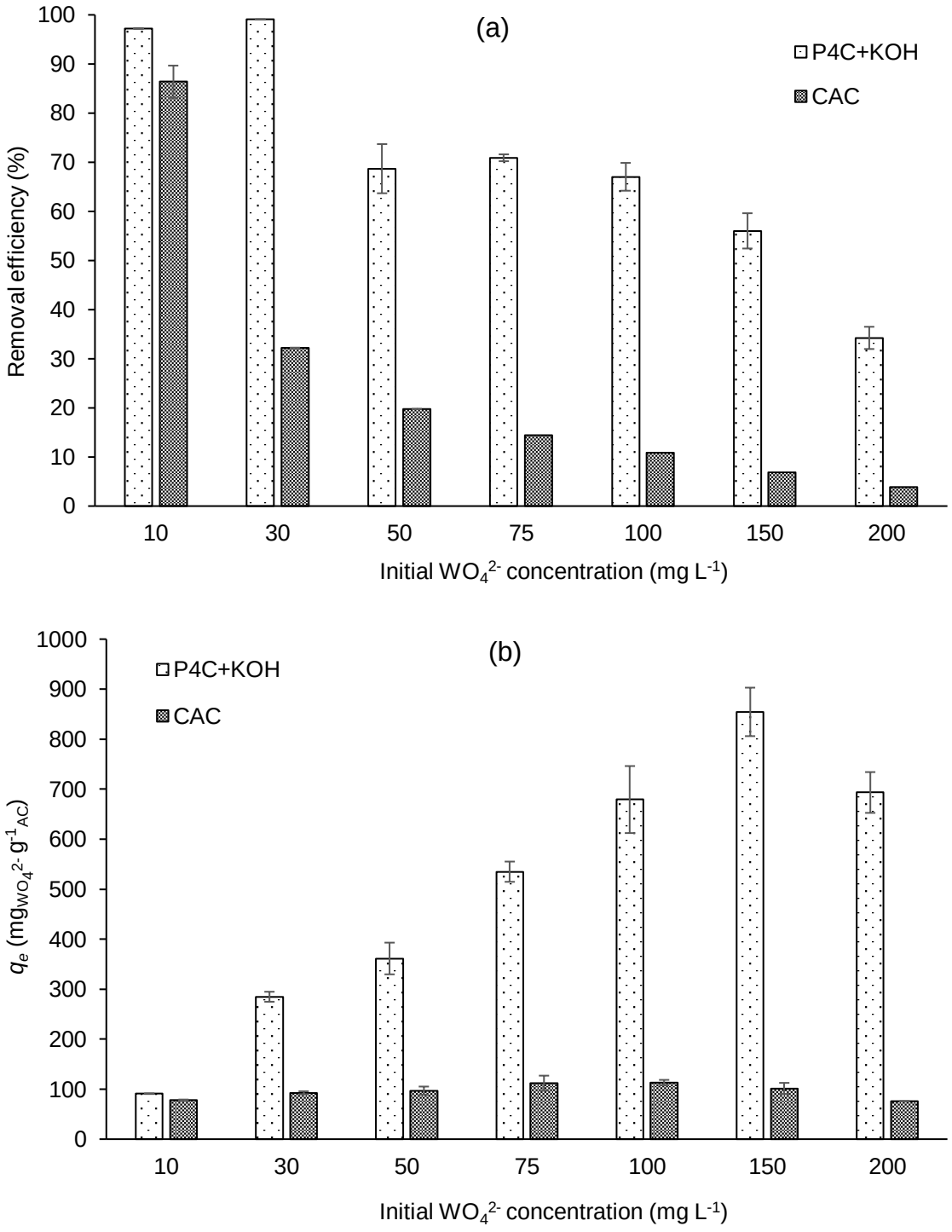

Figure 44. (a) WO_4^{2-} removal efficiency and (b) WO_4^{2-} uptake capacity for P4C+KOH and CAC in the synthetic solution for different initial WO_4^{2-} concentrations.

The experimental data were adjusted to several isotherm models (**Figure 45** and **Table 39**). The modelling showed that WO_4^{2-} adsorption was performed in a two-step process, which was supported by the best fitting to the Multi-step isotherm model, both for P4C+KOH (R^2 = 0.949) and CAC (R^2 = 0.901). Fitting for all other models was poorer (R^2 < 0.9), specially concerning P4C+KOH, confirming that the adsorption could be composed of different mechanisms occurring

in different moments. This consideration is strongly supported by the chemistry of the metal element. As mentioned above, tungsten can form POMs, so its adsorption is most likely composed by a first monolayer adsorption and a consequent solute-solute interaction, generating the second step in the experimental distribution.

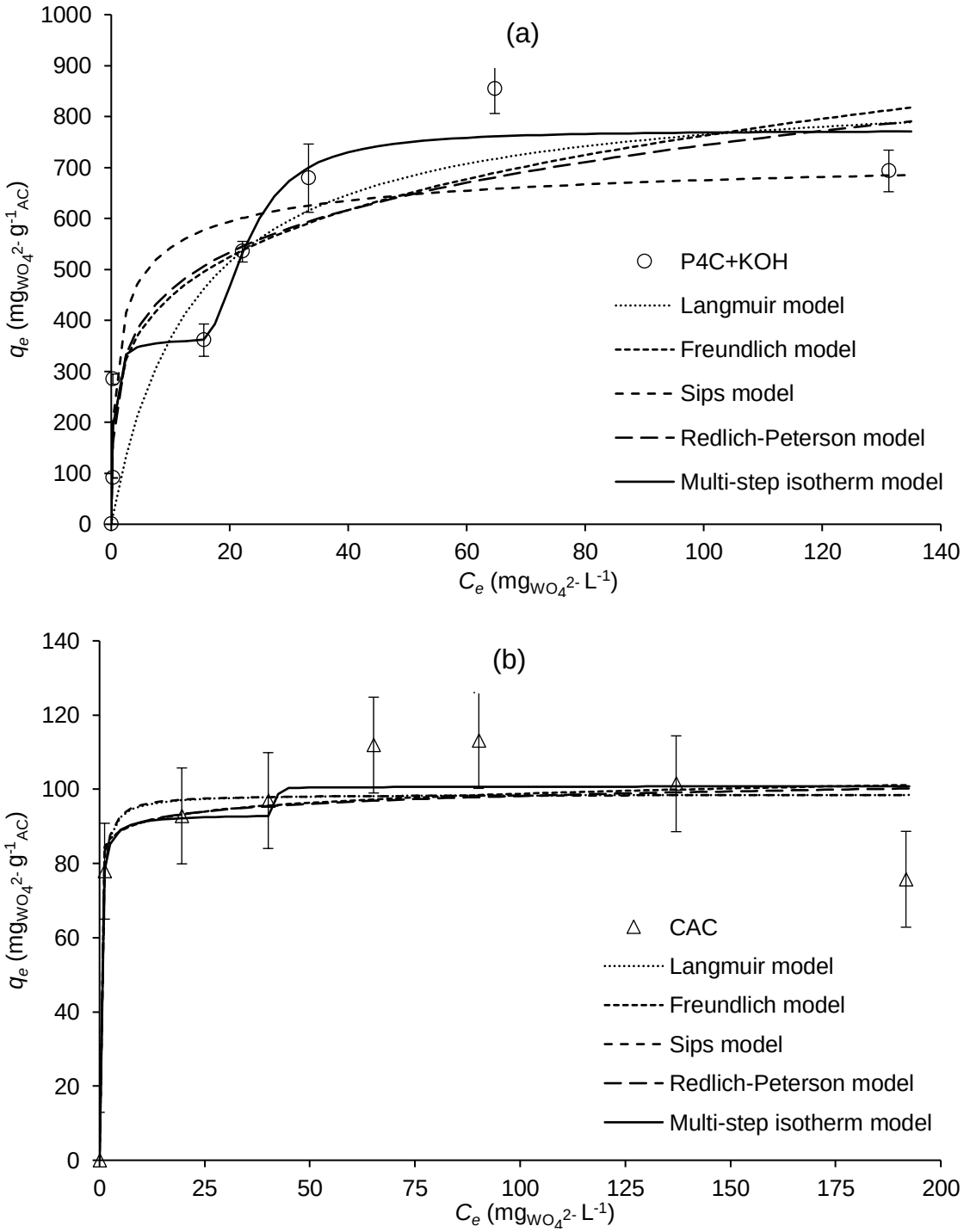

Figure 45. Isotherm models adjusted to the experimental data of (a) P4C+KOH and (b) CAC in the synthetic solution (th: theoretical data).

Table 39. Parameters of the isotherm models adjusted to the experimental data of P4C+KOH and CAC in the synthetic solution.

Isotherm model	Parameter	Adsorbent	
		P4C+KOH	CAC
Langmuir's non-linear model	q_{max} (mg g^{-1})	870	98.6
	b (L mg^{-1})	7.26×10^{-2}	3.04
	R^2	0.865	0.898
Freundlich's non-linear model	K_F (mg g^{-1} mg^{-n} L^n)	262	83.8
	n (dimensionless)	4.31	28.1
	R^2	0.868	0.880
Sips model	q_{max} (mg g^{-1})	947	105
	b (L mg^{-1})	0.600	2.82
	n (dimensionless)	1.85	0.940
	R^2	0.831	0.898
Redlich-Peterson model	K_R (L g^{-1})	2 071	2 262
	a_R (L mg^{-1})	6.99	26.5
	β (dimensionless)	0.799	0.970
	R^2	0.867	0.883
Multi-step isotherm model	q_{T1} (mg g^{-1})	366	93.3
	q_{T2} (mg g^{-1})	407	7.58
	K_1 [(L mg^{-1})^n]	4.07	4.24
	K_2 [(L mg^{-1})^n]	1.44×10^{-2}	16.7
	b (mg L^{-1})	15.1	42.0
	R^2	0.949	0.901

No studies on tungstate adsorption performed by chars or ACs were found in literature. However, other adsorbents were already used in tungstate removal as already mentioned in **Table 5**. The highest uptake capacity found in the literature was from Afkhami et al.[113]. These authors used a carbon cloth obtained by pyrolyzing a phenolic C-film polymer between 800 and 900 °C in N_2. Two different treatments were made to the adsorbent: i) a distilled water washing to avoid leaching from the adsorbent, and ii) an acidic treatment with H_2SO_4 for the modification of surface functional groups and porous structures. The highest uptake capacity was found for the acidic treatment, with a value of 208 mg g^{-1}. To recall, the highest uptake capacity obtained for the carbon P4C+KOH was 854 mg g^{-1}, a value more than 4 times higher than the one found by Afkhami et al., a result that emphasizes the extremely encouraging results achieved by the PCs developed in this work.

8.3.2 Characterisation of mining wastewater

Table 40 presents the mining wastewater characterisation.

Table 40. Mining wastewater characterisation ($\overline{X}$ ± σ; n=2; pH in Sørensen scale; conductivity in μS cm^{-1}; TS, FS, VS, TSS, and chemical elements in mg L^{-1}; Solubility in %).

Parameters	Mining wastewater	Chemical element	Mining wastewater		
			Acidic eluate	Filtrate	Solubility
pH	8.11 ± 0.03	Fe	23 772 ± 1 484	(4.56 ± 0.22)×10^{-2}	1.92×10^{-4}
Conductivity	2 512 ± 16	Al	9 782 ± 840	0.473 ± 0.034	4.84×10^{-3}
TS	250 438 ± 19 906	Zn	5 414 ± 519	(4.10 ± 0.39)×10^{-2}	7.57×10^{-4}
FS	247 904 ± 19 725	K	4 096 ± 347	70.7 ± 1.8	1.73
VS	2 560 ± 173	Mg	3 472 ± 317	69.4 ± 0.5	2.00
TSS	44 753 ± 898	Ca	2 947 ± 279	572 ± 3	19.4
		Cu	1 080 ± 99	< 3.80 x10^{-3}	< 3.52×10^{-4}
		Si	801 ± 78	3.02 ± 0.01	0.377
		W	299 ± 27	0.244 ± 0.006	8.16×10^{-2}
		V	18.4 ± 1.7	< 2.00×10^{-4}	< 1.09×10^{-3}
		Ni	15.2 ± 1.0	< 4.00×10^{-3}	< 2.63×10^{-2}
		Na	6.46 ± 0.03	1.88 ± 0.01	29.0

TS: Total Solids; FS: Fixed Solids; VS: Volatile Solids; TSS: Total Suspended Solids.

The mining wastewater was characterised as alkaline and with a high conductivity due to the high content of inorganic material, namely Fe but also Al, Zn, K, Mg and Ca. However, a very low solubility was found for almost all elements. Only Ca presented a significant concentration in the filtrate (572 mg L^{-1}) with a solubility of 19.4%; Na presented the highest solubility of all the elements analysed (29.0%), but the filtrate concentration was still low (1.88 mg L^{-1}). In summary, most elements were present in the solid fraction of the wastewater and presented low mobility. W was quantified with a low concentration both in the acidic eluate and filtrate, since it is the main resource recovered in the mining extraction process. No ecotoxicity was found for the bacterium *V. fischeri* as the EC_{50}–30 min was >99% v/v.

8.3.3 WO_4^{2-} adsorption assays from mining wastewater

The tungstate adsorption assays from mining wastewater were performed with the adsorbents and conditions that performed better on the synthetic solution (adsorbents: P4C+KOH and CAC; S/L: 0.1 g L^{-1}; time: 24 h; initial WO_4^{2-} concentration: 150 ± 30 mg L^{-1}; initial pH: 8.11 – as-received and 2.00 ± 0.04 – optimum pH).

Figure 46 shows the results of tungstate adsorption assays from mining wastewater.

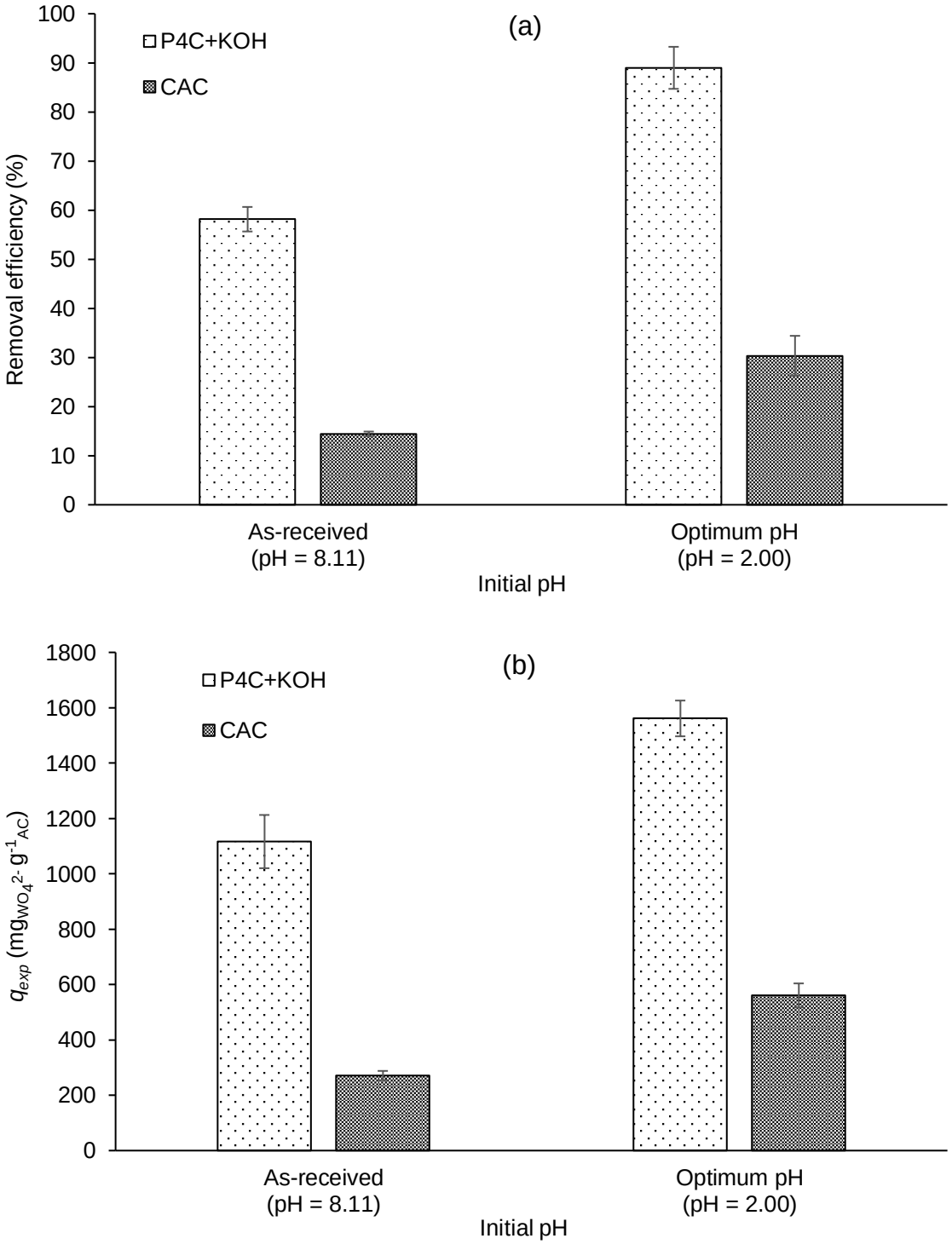

Figure 46. (a) WO_4^{2-} removal efficiency and (b) WO_4^{2-} uptake capacity for P4C+KOH and CAC in the mining wastewater spiked with 150 mg_{WO4}^{2-} L^{-1} for an initial pH of 8.11 (as-received) and an initial pH of 2.00 (optimum pH).

For all assays, P4C+KOH performed significantly better than CAC in WO_4^{2-} adsorption and, as seen in the synthetic solution, the assays with an initial pH of 2.00 originated better results. For pH 8.11, 58.2% of tungstate was removed by P4C+KOH obtaining a q_e of 1116 mg g^{-1}, while for pH 2.00 those values increased to 89.0% and 1561 mg g^{-1}, respectively. CAC only removed 14.4% of tungstate on the assay with an initial pH of 8.11 and 30.3% on the assay with an initial pH of 2.00, obtaining uptake capacities of 271 and 561 mg g^{-1}, respectively. In summary, P4C+KOH uptake capacity was more than 4 times higher than CAC's in the assays with pH 8.11 and almost 3 times higher in the assays with pH 2.

When comparing the uptake capacities of both ACs in the synthetic solution and in the mining wastewater, the results of the latter were higher than the former of about 2 times for P4C+KOH and 5 times for CAC. This can be explained by the presence of other ions in the mining wastewater that promoted the salting-out effect. When there is a high concentration of dissolved salts in a medium (especially cations), their hydration due to the weak bonding between salt ions and water ions, effectively reduces the volume of available solvent for the other species diffusion[192,193]. As seen in **Table 40**, K, Mg and Ca were the main elements involved in this phenomenon. These cations present the highest hydration radius among single element ions – Mg^{2+} (0.395 nm) > Ca^{2+} (0.348 nm) > K^+ (0.315 nm)[194], meaning that adding the reduced available medium to the strongly positive surface of the ACs due to the low pH system, forced a higher quantity of tungstate anions onto the carbon.

8.3.4 Mineral interactions in the WO_4^{2-} adsorption assays from mining wastewater

Figure 47 shows the concentration and percentage variations of cations in the WO_4^{2-} adsorption assays performed in the mining wastewater.

For the assays with an initial pH of 8.11 (**Figure 47a**), the concentration variation of minerals was very low; only 9.58 and 3.06 mg L^{-1} of minerals were added to the medium by P4C+KOH and CAC, respectively, especially Ca (8.08 and 2.93 mg L^{-1}, respectively). On the other hand, apart from W, only 6.70 and 4.02 mg L^{-1} of minerals were removed from the medium by P4C+KOH and CAC, respectively, especially K (6.70 and 4.02 mg L^{-1}, respectively). This means that, for an initial pH of 8.11, the influence of the minerals added/removed by the ACs was very low.

For the assays with the optimum initial pH (2.00) (**Figure 47b**), the concentration variation of minerals was more significant once 37.2 and 23.6 mg L^{-1} of minerals were added to the medium by P4C+KOH and CAC, respectively; again, mainly Ca was added by P4C+KOH and CAC (30.3 and 19.9 mg L^{-1}, respectively). In contrast, excluding W, only 0.862 and 7.31 mg L^{-1} of minerals were removed from the solution by P4C+KOH and CAC, respectively, especially K (0.600 and 6.81 mg L^{-1}, respectively). Thus, in this case the elements present in the wastewater did not compete with W in the adsorption process, but instead a significant amount of Ca was released for the solution in both assays, due to the extreme acidic conditions of the medium that helped

the solubilisation. This led probably to an increase of available pores on the ACs' surfaces, and to the increase of cations in the solution that promoted the salting out effect and, consequently, a higher removal of tungstate.

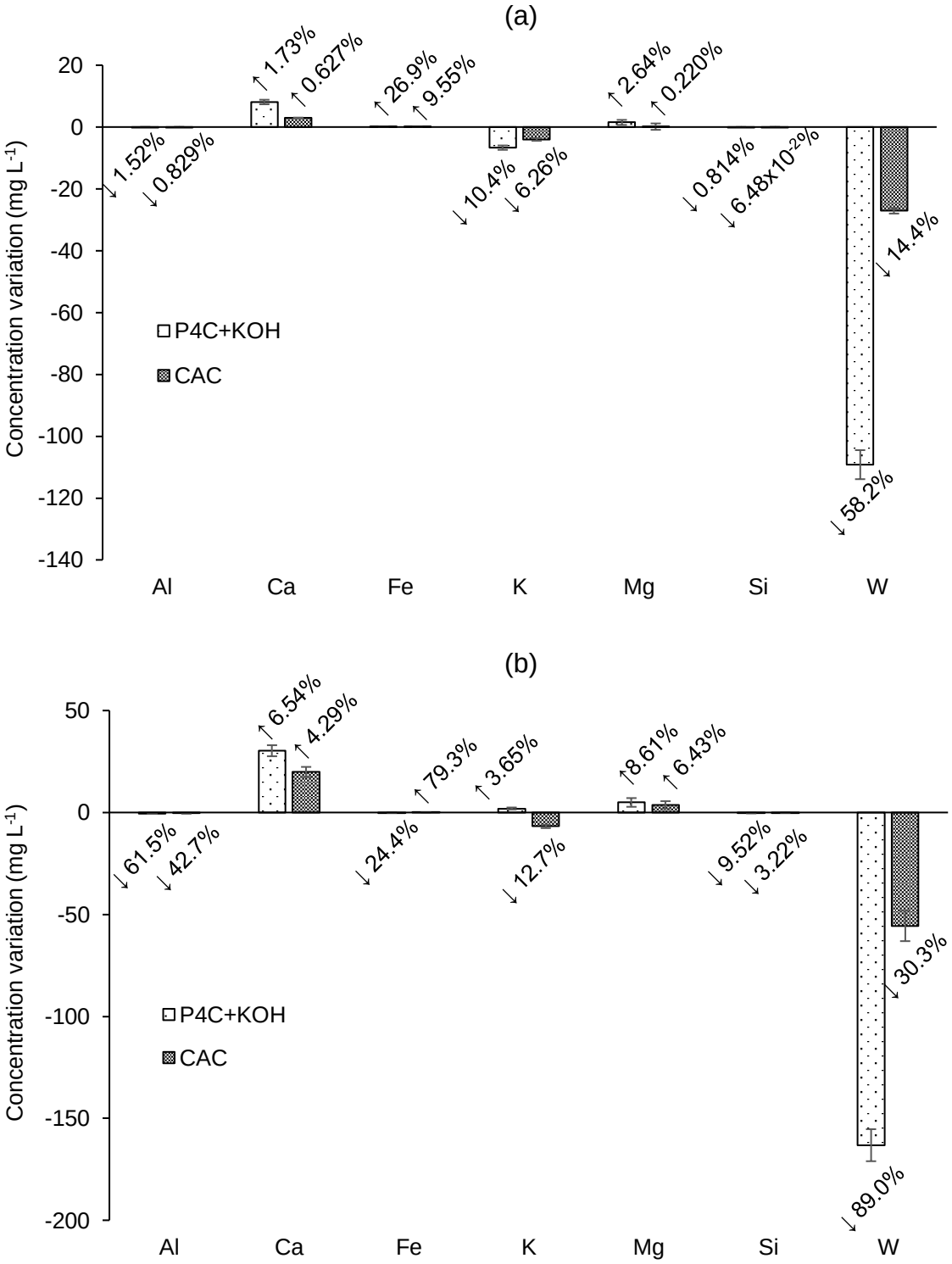

Figure 47. Concentration and percentage variations of cations on the WO_4^{2-} adsorption assays for P4C+KOH and CAC in the mining wastewater spiked with 150 mg_{WO4}^{2-} L^{-1} for (a) an initial pH of 8.11 (as-received) or (b) an initial pH of 2.00 (optimum pH).

8.3.5 Ecotoxicity in the WO_4^{2-} adsorption assays from mining wastewater

The ecotoxicological evaluation of mining wastewater before and after the WO_4^{2-} adsorption assays (**Table 41**) showed that at its original pH (8.11) (which is in the range of the optimal pH for *V. fischeri*) no ecotoxicity was found, neither before nor after the adsorption assays. For an initial pH of 2.00, high ecotoxicity was found once this bacterium is very sensitive to pH variations with an optimal range of 6.0 to 8.5[165]. However, after pH correction, no ecotoxicity was found.

Table 41. Ecotoxicity assessment of the mining wastewater before and after WO_4^{2-} adsorption assays.

Initial pH	EC_{50}–30 min (% v/v)					
	Before adsorption assays		After adsorption assays			
			P4C+KOH		CAC	
	Before pH correction	After pH correction	Before pH correction	After pH correction	Before pH correction	After pH correction
8.11	>99	n. a.	>99	n. a.	>99	n. a.
2.00	1.61	>99	1.54	>99	1.48	>99

n.a. not applicable

8.4 Conclusions

The properties that most influenced the adsorption process were the pH of the solution, and the pH_{pzc}, surface area and mesopore volume of the ACs. Solutions with lower pH and ACs with higher pH_{pzc}, surface areas and mesopore volumes benefit WO_4^{2-} adsorption.

For the adsorption assays from the synthetic solution, P4C+KOH was the AC that presented the best properties for WO_4^{2-} adsorption obtaining a q_e of 330 mg g^{-1} at S/L of 0.1 g L^{-1}, while CAC only obtained a q_e of 88.6 mg g^{-1} at S/L 0.25 g L^{-1}.

P4C+KOH reached the equilibrium after 1 h with removal efficiencies of around 70% and uptake capacities of around 350 mg g^{-1}, while CAC reached equilibrium only after 15 h with removal efficiencies of less than 20% and uptake capacities of around 90 mg g^{-1}.

The highest uptake capacity of P4C+KOH was found for an initial WO_4^{2-} concentration of 150 mg L^{-1} with a q_t of 854 mg g^{-1}, while the highest q_t of CAC was of 113 mg g^{-1} at an initial WO_4^{2-} concentration of 100 mg L^{-1}.

The mining wastewater presented a pH of 8.11 with a high concentration of minerals, especially Fe. Most elements were present in the solid fraction of the wastewater and presented low mobility,

except for Ca which presented a solubility of 19.4% and a concentration of 572 mg L^{-1} in the filtrates.

For the adsorption assays from the mining wastewater, the best results were found at pH 2.00, with P4C+KOH obtaining a η of 89.0% and a q_e of 1561 mg g^{-1}, and CAC obtaining values of 14.4% and 561 mg g^{-1}, respectively. In the assays at pH 2.00, there was a significant release of Ca from the ACs to the solution that promoted tungstate removal, due to an increase of the available pores on the ACs' surfaces and the increase of cations on the solution that promoted the salting out effect.

P4C+KOH clearly showed better properties than CAC on WO_4^{2-} adsorption, obtaining uptake capacities almost 8 times higher in the synthetic solution and almost 3 times higher in the mining wastewater. These results suggest that P4C+KOH seems to be a more efficient and alternative to CAC in the adsorption of WO_4^{2-} from liquid effluents.

9. GENERAL CONCLUSIONS

The main objective of this work was to characterise chars resulting from the co-gasification and co-pyrolysis of rice waste streams and use them in the removal of Cr and W from aqueous solutions. Activations were necessary in order to improve the chars' properties for the adsorption/removal processes.

Due to the different characteristics of the Cr and W ions used in this work, once one is a cation (Cr(III)) and the other an anion (WO_4^{2}), different chars were prepared and used for the adsorption/removal of these ions.

Regarding the chars used in Cr(III) removal, the gasification chars were mainly constituted by carbonized ashes composed of Si and AAEMs. In contrast, pyrolysis chars were mainly composed by carbon, but still with a significant amount of volatile matter. Although in lower amounts than in the gasification chars, high concentrations of Si were found in the pyrolysis chars followed by AAEMs and Ti due to the use of PE as feedstock.

Globally, all chars presented low surface areas (up to 62.9 $m^2\ g^{-1}$ in the gasification chars and up to 5.63 $m^2\ g^{-1}$ in the pyrolysis chars). However, the high mineral content of the gasification chars (important for ion exchange mechanism) allowed their use in Cr(III) removal assays without any kind of activation process. On the other hand, the pyrolysis chars required further physical and/or chemical activations before such valorisation, aiming to remove the volatile matter that was blocking the char's pores and concentrate the ash content. Some of the activations tested increased the porosity of the char and promoted the adsorption by ion exchange due to ash concentration.

Two gasification chars (G4C and G5C) were selected to be used in Cr(III) removal assays under batch conditions. One pyrolysis char (P1C) was selected to be optimized through physical and chemical activations/treatments; then, the resulting activated carbons (ACs) were also used in the Cr(III) removal assays under batch conditions.

Four physical activations were performed to P1C. The most favourable experimental conditions were 800 ºC for 4 h. These activations removed most volatile matter present in P1C, leading to higher surface areas and pore volumes. The chemical activation generated the pyrolysis-derived AC (P1C+CA) with the highest surface area (415 $m^2\ g^{-1}$) and pore volume (0.22 $cm^3\ g^{-1}$) as some ashes were also removed. Still, these areas and volumes were significantly lower than the ones of the commercial activated carbons (with and without treatment).

In the Cr(III) removal assays from the synthetic solution by gasification chars, both chars (G4C and G5C) presented higher removal efficiencies and uptake capacities than CAC, due to their high ion exchange capacity. G4C at a S/L of 5 g L^{-1} obtained the highest uptake capacity of all chars with a value of 8.19 mg g^{-1}, a value significantly higher than for CAC (3.93 mg g^{-1}). For the removal assays from the industrial wastewater, G4C presented better results than CAC when precipitation occurred, but when adsorption ruled the removal process CAC obtained slightly better results than G4C. The highest uptake capacity found for G4C was 14.9 mg g^{-1}, while this value increased slightly for CAC (16.1 mg g^{-1}).

Regarding the pyrolysis activated carbons (PAC), P1C+PA presented the best properties of all PACs for Cr(III) removal, due to its high mineral content (allowing removal by ion exchange) and interesting textural properties (allowing removal by pore filling). At a solid/liquid ratio (S/L) of 5 g L^{-1}, P1C+PA and CAC obtained the highest uptake capacities of 9.23 and 9.80 mg g^{-1}, respectively, in the synthetic solution, and 12.4 and 16.1 mg g^{-1}, respectively, in the industrial wastewater.

In the conditions where precipitation did not occur, the mechanisms involved on Cr(III) removal by the gasification chars were ion exchange, while in the pyrolysis activated carbons a mix of ion exchange and pore filling was registered. Cr(III) removal by CAC was ruled by pore filling.

G4C was selected to be used in the column assays. The performance of both G4C and CAC was lower than in the batch assays, obtaining uptake capacities of 1.60 and 2.14 mg g^{-1}, respectively, in the synthetic solution and 3.25 and 7.83 mg g^{-1}, respectively, in the industrial wastewater. Both G4C and CAC showed no capacity to be used in more than one adsorption cycle.

These results suggest that, under batch conditions, G4C and P1C+PA showed good properties to be alternative adsorbents in the removal of Cr(III) from liquid effluents, especially G4C that, even without any activation process, obtained similar or even better results than CAC. However, under continuous flow, G4C did not performed has expected, probably because diffusion constraints were more significant for G4C than for CAC due to the lower porosity in the former compared to the latter.

For WO_4^2 adsorption assays, only pyrolysis-derived activated carbons were produced, once the high mineral content of the gasification chars was not an advantage in this case. WO_4^{2-} is an anion and the minerals present in the gasification chars are mainly cations, thus ion exchange could not be a possibility for WO_4^2 removal. Six activated carbons were produced, three derived from P1C, two from P4C and one from a direct carbonization/activation of rice husk.

The properties that most influenced the adsorption process were pH of the solution (lower values benefit WO_4^{2-} adsorption) and pH_{pzc}, surface area and mesopore volume of ACs (higher values benefit WO_4^{2-} adsorption). Of all ACs tested, P4C+KOH presented the highest surface area (2 610 m^2 g^{-1}) and mesopore volume (1.14 cm^3 g^{-1}) and the second highest pH_{pzc} (6.92). For that reason, it led to the best results on WO_4^2 adsorption. The highest uptake capacities found for P4C+KOH were 854 mg g^{-1} in the synthetic solution and 1561 mg g^{-1} in the mining wastewater, while CAC's values were significantly lower (113 and 572 mg L^{-1}, respectively). P4C+KOH clearly showed better properties than CAC on WO_4^{2-} adsorption, obtaining uptake capacities almost 8 times higher in the synthetic solution and almost 3 times higher in the mining wastewater. These results suggest that P4C+KOH seems to be a more efficient alternative to CAC in the adsorption of WO_4^{2-} from liquid effluents.

The main objective of the work was achieved as for both Cr and W removal it was possible to produce alternative adsorbents to the typical commercial activated carbon. Concerning Cr, the adsorbents produced obtained similar results to CAC, while for W the expectations were widely exceeded, as the produced adsorbents largely overcame CAC's results.

VISIONS FOR FUTURE

This work allowed to study the use of different chars and activated carbons in the removal of Cr(III) and WO_4^{2-} from aqueous solutions. However, being a long and diverse work, several questions came out during the PhD period that, due to the time limitation, were not possible to be answered. For that reason, and in order to fill the gaps that have emerged along the work, the following future visions are suggested for future:

- At the end of Cr(III) removal assays it was concluded that the ion exchange was the main mechanism for Cr(III) removal. For that reason, it would be interesting to selected, from the immense set of chars produced in "Ricevalor" project, the ones that had the highest mineral content, namely AAEMs, to study their performance in Cr(III) removal.

- The pyrolysis-derived activated carbons used in Cr(III) removal assays fell short of expectations. However, the pyrolysis-derived activated carbons used in the WO_4^{2-} adsorption assays presented really good surface properties. For that reason, it would be interesting to test these set of ACs in Cr(III) removal, both in batch and column assays.

- Due to the physical limitation of the columns, it was not possible to use higher masses of char in the column assays. For that reason, adsorption assays in bigger columns should be performed in order to overcome mass adsorbent limitations.

- Test lower flow rates in the column assays to increase the contact time and consequently the uptake capacity.

- The WO_4^{2-} adsorption assays obtained really good results in the batch assays. Unfortunately, there was no time left to perform the column assays. In order to complete this study, it would be very important to perform column assays with the ACs used in the batch assays, especially P4C+KOH.

- Unfortunately, the mining wastewater used on the WO_4^{2-} adsorption assays had no tungsten in solution. For that reason, tungstate was added to the wastewater. It would be interesting to use a real wastewater that had already tungsten in solution, in order to compare the results with the ones obtained for the mining wastewater.

- To test the different carbonaceous materials produced in this work in the removal of other critical elements from wastewaters.

- After having all previous questions answered, adsorption and desorption studies at a pilot scale should be performed.

SCIENTIFIC OUTPUTS

Papers:

D. Dias, N. Lapa, M. Bernardo, D. Godinho, I. Fonseca, M. Miranda, F. Pinto, F. Lemos, Properties of chars from the gasification and pyrolysis of rice waste streams towards their valorisation as adsorbent materials, *Waste Management*, 65 (2017) 186–194.
(doi: 10.1016/j.wasman.2017.04.011)

D. Dias, N. Lapa, M. Bernardo, W. Ribeiro, I. Matos, I. Fonseca, F. Pinto, Cr(III) removal from synthetic and industrial wastewaters by using co-gasification chars of rice waste streams, *Bioresource Technology*, 266 (2018) 139-150.
(doi: 10.1016/j.biortech.2018.06.054)

D. Dias, M. Bernardo, N. Lapa, F. Pinto, I. Matos and I. Fonseca, Activated Carbons from the Co-pyrolysis of Rice Wastes for Cr(III) Removal, *Chemical Engineering Transactions*, 65 (2018) 601-606.
(doi: 10.3303/CET1865101)

D. Dias, M. Bernardo, I. Matos, I. Fonseca, F. Pinto, N. Lapa, Activation of co-pyrolysis chars from rice wastes to improve the removal of Cr^{3+} from simulated and real industrial wastewaters, *Journal of Cleaner Production*, 267 (2020) 121993.

D. Dias, M. Bernardo, F. Pinto, I. Fonseca, N. Lapa, Cr(III) dynamic removal in a fixed-bed column by using a co-gasification char, *Environmental Science and Pollution Research,* submitted.

D. Dias, D. Don, J. Jandosov, M. Bernardo, F. Pinto, I. Fonseca, A. Sanches, P. S. Caeteno, S. Lyubchyk, N. Lapa, Highly efficient porous carbons for the removal of W(VI) oxyanion from wastewaters, *Journal of Hazardous Materials*, under revision - major revisions.

Oral Presentations:

D. Dias, N. Lapa, M. Bernardo, D. Godinho, I. Fonseca, H. Lopes, M. Miranda, F. Pinto, F. Lemos, Bed chars from the co-gasification of rice wastes: chemical and ecotoxic properties, *The Energy & Materials Research Conference (EMR2015)*, 25-27 February 2015, Madrid, Spain.

D. Dias, M. Miguel, M. Bernardo, N. Lapa, I. Matos, I. Fonseca, F. Pinto. Removal of Cr(III) by using activated carbons produced from rice waste chars, *DCE17 - 2nd Doctoral Congress of Engineering, 8-9 June 2017*, Porto, Portugal.

D. Dias, W. Ribeiro, N. Lapa, M. Bernardo, I. Matos, I. Fonseca, F. Pinto, Chars from co-gasification of rice wastes as Cr(III) removal agents, *4th International Conference "WASTES: Solutions, Treatments and Opportunities"*, 25-26 September 2017, Porto, Portugal.

D. Dias, M. Miguel, N. Lapa, M. Bernardo, I. Matos, I. Fonseca and F. Pinto, Efficient activated carbons from chars of the co-pyrolysis of rice wastes, *4th International Conference "WASTES: Solutions, Treatments and Opportunities"*, 25-26 September 2017, Porto, Portugal.

D. Dias, M. Bernardo, N. Lapa, F. Pinto, I. Matos and I. Fonseca, Activated Carbons from the Co-pyrolysis of Rice Wastes for Cr(III) Removal, *International Conference on Biomass (IconBM)*, 17-20 June 2018, Bologna, Italy.

D. Dias, M. Bernardo, N. Lapa, F. Pinto, I. Matos, I. Fonseca, Cr(III) Removal from Aqueous Solution by Activated Carbons obtained through the Co-pyrolysis of Wastes from Rice Production, *13th International Chemical and Biological Engineering Conference (CHEMPOR 2018)*, 2-4 October 2018, Aveiro, Portugal.

D. Dias, D. Don, J. Jandosov, M. Bernardo, I. Fonseca, F. Pinto, N. Lapa, Tungstate adsorption onto porous carbons obtained from rice wastes, *5th International Conference "WASTES: Solutions, Treatments and Opportunities"*, 4-6 September 2019, Caparica, Portugal.

Poster:

D. Dias, M. Bernardo, F. Pinto, N. Lapa, Recovery of high-value metals through adsorption onto chars produced from waste streams of rice production: the case-study of Cr^{3+}, *1st Scientific Meeting of the Doctoral Programme in Sustainable Chemistry (PDQS)*, 26 September 2016, Aveiro, Portugal.

REFERENCES

1. Fu, F. & Wang, Q. Removal of heavy metal ions from wastewaters: A review. *J. Environ. Manage.* **92**, 407–418 (2011).

2. Burakov, A. E. *et al.* Adsorption of heavy metals on conventional and nanostructured materials for wastewater treatment purposes: A review. *Ecotoxicol. Environ. Saf.* **148**, 702–712 (2018).

3. Song, Q. & Li, J. A review on human health consequences of metals exposure to e-waste in China. *Environ. Pollut.* **196**, 450–461 (2015).

4. European Commission. *Study on the review of the list of critical raw materials*. *European Comission* (2017).

5. Godlewska, P., Schmidt, H. P. & Oleszczuk, P. Biochar for composting improvement and contaminants reduction. A review. *Bioresour. Technol.* **246**, 193–202 (2017).

6. Ahmad, M. *et al.* Biochar as a sorbent for contaminant management in soil and water: A review. *Chemosphere* **99**, 19–33 (2014).

7. Qambrani, N. A., Rahman, M. M., Won, S., Shim, S. & Ra, C. Biochar properties and eco-friendly applications for climate change mitigation, waste management, and wastewater treatment: A review. *Renewable and Sustainable Energy Reviews* **79**, (2017).

8. Moreira, M. T., Noya, I. & Feijoo, G. The prospective use of biochar as adsorption matrix – A review from a lifecycle perspective. *Bioresour. Technol.* **246**, 135–141 (2017).

9. Faria, P. C. ., Órfão, J. J. . & Pereira, M. F. . Adsorption of anionic and cationic dyes on activated carbons with different surface chemistries. *Water Res.* **38**, 2043–2052 (2004).

10. Danish, M. & Ahmad, T. A review on utilization of wood biomass as a sustainable precursor for activated carbon production and application. *Renew. Sustain. Energy Rev.* **87**, 1–21 (2018).

11. Kirubakaran, V. *et al.* A review on gasification of biomass. *Renew. Sustain. Energy Rev.* **13**, 179–186 (2009).

12. Ramos, A., Monteiro, E., Silva, V. & Rouboa, A. Co-gasification and recent developments on waste-to-energy conversion: A review. *Renew. Sustain. Energy Rev.* **81**, 380–398 (2018).

13. Czajczyńska, D. *et al.* Potential of pyrolysis processes in the waste management sector. *Therm. Sci. Eng. Prog.* **3**, 171–197 (2017).

14. Bridgwater, A. V. Review of fast pyrolysis of biomass and product upgrading. *Biomass and Bioenergy* **38**, 68–94 (2012).

15. Lim, J. S., Abdul Manan, Z., Wan Alwi, S. R. & Hashim, H. A review on utilisation of biomass from rice industry as a source of renewable energy. *Renew. Sustain. Energy Rev.* **16**, 3084–3094 (2012).

16. André, R. N., Pinto, F., Miranda, M., Carolino, C. & Costa, P. Co-Gasification of Rice Production Wastes. *Chem. Eng. Trans.* **39**, 1633–1638 (2014).

17. Pinto, F., Miranda, M. & Costa, P. Co-pyrolysis of Wastes Mixtures Obtained from Rice Production. Upgrading of Produced Liquids. *Chem. Eng. Trans.* **43**, 2053–2058 (2015).

18. Akgün, O. & Luukkanen, J. Extension of rice husk gasification technology for electricity generation in Cambodia. *Energy Procedia* **14**, 1244–1249 (2012).

19. Quispe, I., Navia, R. & Kahhat, R. Energy potential from rice husk through direct combustion and fast pyrolysis: A review. *Waste Manag.* **59**, 200–210 (2017).

20. Liu, W.-J., Zeng, F.-X., Jiang, H. & Zhang, X.-S. Preparation of high adsorption capacity bio-chars from waste biomass. *Bioresour. Technol.* **102**, 8247–52 (2011).

21. Tong, X. & Xu, R. Removal of Cu(II) from acidic electroplating effluent by biochars generated from crop straws. *J. Environ. Sci.* **25**, 652–658 (2013).

22. Pan, J., Jiang, J. & Xu, R. Adsorption of Cr(III) from acidic solutions by crop straw derived biochars. *J. Environ. Sci. (China)* **25**, 1957–1965 (2013).

23. Pellera, F.-M. *et al.* Adsorption of Cu(II) ions from aqueous solutions on biochars prepared from agricultural by-products. *J. Environ. Manage.* **96**, 35–42 (2012).

24. Godinho, D. *et al.* Adding value to gasification and co-pyrolysis chars as removal agents of Cr3+. *J. Hazard. Mater.* **321**, 173–182 (2017).

25. FAO. *Rice Market Monitor*. *Food And Agriculture Organization of the United Nations* **XXI**, (2018).

26. FAO. FAOSTAT. Available at: http://www.fao.org/faostat/en/#data/QC. (Accessed: 29th November 2019)

27. Prasara-A, J. & Gheewala, S. H. Sustainable utilization of rice husk ash from power plants: A review. *J. Clean. Prod.* **167**, 1020–1028 (2017).

28. Sangon, S. *et al.* Valorisation of waste rice straw for the production of highly effective carbon based adsorbents for dyes removal. *J. Clean. Prod.* **172**, 1128–1139 (2018).

29. Zhou, C. *et al.* A new strategy for co-composting dairy manure with rice straw: Addition of different inocula at three stages of composting. *Waste Manag.* **40**, 38–43 (2015).

30. Iyagba, E. T., Mangibo, I. a & Mohammad, Y. S. The study of cow dung as co-substrate with rice husk in biogas production. *Sci. Res. Essays* **4**, 861–866 (2009).

31. Jabeen, M., Yousaf, S., Haider, M. R. & Malik, R. N. High-solids anaerobic co-digestion of food waste and rice husk at different organic loading rates. *Int. Biodeterior. Biodegradation* **102**, 149–153 (2015).

32. Binod, P. *et al.* Bioethanol production from rice straw: An overview. *Bioresour. Technol.* **101**, 4767–74 (2010).

33. Fang, X., Shen, Y., Zhao, J., Bao, X. & Qu, Y. Status and prospect of lignocellulosic bioethanol production in China. *Bioresour. Technol.* **101**, 4814–9 (2010).

34. Lo, Y.-C., Saratale, G. D., Chen, W.-M., Bai, M.-D. & Chang, J.-S. Isolation of cellulose-hydrolytic bacteria and applications of the cellulolytic enzymes for cellulosic biohydrogen production. *Enzyme Microb. Technol.* **44**, 417–425 (2009).

35. Cheng, J., Su, H., Zhou, J., Song, W. & Cen, K. Microwave-assisted alkali pretreatment of rice straw to promote enzymatic hydrolysis and hydrogen production in dark- and photo-fermentation. *Int. J. Hydrogen Energy* **36**, 2093–2101 (2011).

36. Delivand, M. K., Barz, M. & Gheewala, S. H. Logistics cost analysis of rice straw for biomass power generation in Thailand. *Energy* **36**, 1435–1441 (2011).

37. Ahmed, I. I., Nipattummakul, N. & Gupta, A. K. Characteristics of syngas from co-gasification of polyethylene and woodchips. *Appl. Energy* **88**, 165–174 (2011).

38. Sathitruangsak, P., Madhiyanon, T. & Soponronnarit, S. Rice husk co-firing with coal in a short-combustion-chamber fluidized-bed combustor (SFBC). *Fuel* **88**, 1394–1402 (2009).

39. Vitali, F., Parmigiani, S., Vaccari, M. & Collivignarelli, C. Agricultural waste as household fuel: Techno-economic assessment of a new rice-husk cookstove for developing countries. *Waste Manag.* **33**, 2762–2770 (2013).

40. Said, N., Bishara, T., Garc??a-Maraver, A. & Zamorano, M. Effect of water washing on the thermal behavior of rice straw. *Waste Manag.* **33**, 2250–2256 (2013).

41. Liu, Y. *et al.* Thermochemical liquefaction of rice husk for bio-oil production in mixed solvent (ethanol–water). *Fuel Process. Technol.* **112**, 93–99 (2013).

42. Chen, K. *et al.* Separation of phenolic compounds with modified adsorption resin from aqueous phase products of hydrothermal liquefaction of rice straw. *Bioresour. Technol.* **182**, 160–8 (2015).

43. Mastellone, M. L. & Zaccariello, L. Gasification of polyethylene in a bubbling fluidized bed operated with the air staging. *Fuel* **106**, 226–233 (2013).

44. Pinto, F., Costa, P., Gulyurtlu, I. & Cabrita, I. Pyrolysis of plastic wastes. 1. Effect of plastic waste composition on product yield. *J. Anal. Appl. Pyrolysis* **51**, 39–55 (1999).

45. Huang, Y.-F. *et al.* Microwave pyrolysis of rice straw to produce biochar as an adsorbent for CO2 capture. *Energy* **84**, 75–82 (2015).

46. Pinto, F., Miranda, M. & Costa, P. Production of liquid hydrocarbons from rice crop wastes mixtures by co-pyrolysis and co-hydropyrolysis. *Fuel* **174**, 153–163 (2016).

47. European Parliament and Council. *Directive 2008/98/EC of the European Parliament and of the Council of 19 November 2008 on waste and repealing certain directives (Waste framework*. *EU* (2008).

48. Qian, K., Kumar, A., Zhang, H., Bellmer, D. & Huhnke, R. Recent advances in utilization of biochar. *Renew. Sustain. Energy Rev.* **42**, 1055–1064 (2015).

49. Kumar, A., Jones, D. D. & Hanna, M. A. Thermochemical biomass gasification: A review of the current status of the technology. *Energies* **2**, 556–581 (2009).

50. Guo, D. *et al.* Direct reduction of oxidized iron ore pellets using biomass syngas as the reducer. *Fuel Process. Technol.* **148**, 276–281 (2016).

51. Genieva, S., Turmanova, S., Dimitrov, A., Petkov, P. & Vlaev, L. Thermal degradation of rice husks on a pilot plant: Utilization of the products as adsorbents for oil spill cleanup. *J. Therm. Anal. Calorim.* **110**, 111–118 (2012).

52. Asadullah, M. Barriers of commercial power generation using biomass gasification gas: A review. *Renew. Sustain. Energy Rev.* **29**, 201–215 (2014).

53. Paradela, F., Pinto, F., Gulyurtlu, I., Cabrita, I. & Lapa, N. Study of the co-pyrolysis of biomass and plastic wastes. *Clean Technol. Environ. Policy* **11**, 115–122 (2009).

54. Pütün, A. E., Apaydın, E. & Pütün, E. Rice straw as a bio-oil source via pyrolysis and steam pyrolysis. *Energy* **29**, 2171–2180 (2004).

55. Paradela, F. M. R. Estudo da pirólise de misturas de resíduos de plásticos, pneus e biomassa. (Universidade Nova de Lisboa - Faculdade Nova de Lisboa, 2007).

56. Heo, H. S. *et al.* Fast pyrolysis of rice husk under different reaction conditions. *J. Ind. Eng. Chem.* **16**, 27–31 (2010).

57. Anca-Couce, A. Reaction mechanisms and multi-scale modelling of lignocellulosic biomass pyrolysis. *Prog. Energy Combust. Sci.* **53**, 41–79 (2016).

58. Brennan Pecha, M., Arbelaez, J. I. M., Garcia-Perez, M., Chejne, F. & Ciesielski, P. N. *Progress in understanding the four dominant intra-particle phenomena of lignocellulose pyrolysis: Chemical reactions, heat transfer, mass transfer, and phase change*. *Green Chemistry* **21**, (Royal Society of Chemistry, 2019).

59. Collard, F.-X. & Blin, J. A review on pyrolysis of biomass constituents: Mechanisms and composition of the products obtained from the conversion of cellulose, hemicelluloses and lignin. *Renew. Sustain. Energy Rev.* **38**, 594–608 (2014).

60. Ma, L. *et al.* A review of thermal-chemical conversion of lignocellulosic biomass in China. *Biotechnol. Adv.* **30**, 859–73 (2012).

61. Costa, P. A. *et al.* Kinetic Evaluation of the Pyrolysis of Polyethylene Waste. *Energy & Fuels* **21**, 2489–2498 (2007).

62. Arena, U. & Di Gregorio, F. Energy generation by air gasification of two industrial plastic wastes in a pilot scale fluidized bed reactor. *Energy* **68**, 735–743 (2014).

63. Galhetas, M. *et al.* Characterization, leachability and valorization through combustion of

residual chars from gasification of coals with pine. *Waste Manag.* **32**, 769–79 (2012).

64. Griessacher, T., Antrekowitsch, J. & Steinlechner, S. Charcoal from agricultural residues as alternative reducing agent in metal recycling. *Biomass and Bioenergy* **39**, 139–146 (2012).

65. Suopajärvi, H., Pongrácz, E. & Fabritius, T. The potential of using biomass-based reducing agents in the blast furnace: A review of thermochemical conversion technologies and assessments related to sustainability. *Renew. Sustain. Energy Rev.* **25**, 511–528 (2013).

66. Kastner, J. R., Miller, J., Kolar, P. & Das, K. C. Catalytic ozonation of ammonia using biomass char and wood fly ash. *Chemosphere* **75**, 739–44 (2009).

67. Lehmann, J. *et al.* Biochar effects on soil biota – A review. *Soil Biol. Biochem.* **43**, 1812–1836 (2011).

68. Runtti, H. *et al.* Chemically activated carbon residue from biomass gasification as a sorbent for iron(II), copper(II) and nickel(II) ions. *J. Water Process Eng.* **4**, 12–24 (2014).

69. Rojas-Mayorga, C. K., Silvestre-Albero, J., Aguayo-Villarreal, I. A., Mendoza-Castillo, D. I. & Bonilla-Petriciolet, A. A new synthesis route for bone chars using CO2 atmosphere and their application as fluoride adsorbents. *Microporous Mesoporous Mater.* **209**, 38–44 (2015).

70. Tan, X. *et al.* Application of biochar for the removal of pollutants from aqueous solutions. *Chemosphere* **125**, 70–85 (2015).

71. Mohan, D., Sarswat, A., Ok, Y. S. & Pittman, C. U. Organic and inorganic contaminants removal from water with biochar, a renewable, low cost and sustainable adsorbent – A critical review. *Bioresour. Technol.* **160**, 191–202 (2014).

72. Inyang, M. I. *et al.* A review of biochar as a low-cost adsorbent for aqueous heavy metal removal. *Critical Reviews in Environmental Science and Technology* **46**, (2016).

73. Thommes, M. *et al.* Physisorption of gases, with special reference to the evaluation of surface area and pore size distribution (IUPAC Technical Report). *Pure Appl. Chem.* **87**, 1051–1069 (2015).

74. Ahmad, M. *et al.* Effects of pyrolysis temperature on soybean stover- and peanut shell-derived biochar properties and TCE adsorption in water. *Bioresour. Technol.* **118**, 536–544 (2012).

75. Qiu, Y., Zheng, Z., Zhou, Z. & Sheng, G. D. *Effectiveness and mechanisms of dye adsorption on a straw-based biochar*. *Bioresource Technology* **100**, (2009).

76. Mohan, D. & Pittman, C. U. Activated carbons and low cost adsorbents for remediation of tri- and hexavalent chromium from water. *J. Hazard. Mater.* **137**, 762–811 (2006).

77. Mohan, D., Singh, K. P. & Singh, V. K. Trivalent chromium removal from wastewater using low cost activated carbon derived from agricultural waste material and activated carbon

fabric cloth. *J. Hazard. Mater.* **135**, 280–95 (2006).

78. Maneerung, T. *et al.* Activated carbon derived from carbon residue from biomass gasification and its application for dye adsorption: Kinetics, isotherms and thermodynamic studies. *Bioresour. Technol.* **200**, (2016).

79. Li, H. *et al.* Mechanisms of metal sorption by biochars: Biochar characteristics and modifications. *Chemosphere* **178**, 466–478 (2017).

80. Xu, X. *et al.* Indispensable role of biochar-inherent mineral constituents in its environmental applications: A review. *Bioresour. Technol.* **241**, 887–899 (2017).

81. Mohan, D. *et al.* Sorption of arsenic, cadmium, and lead by chars produced from fast pyrolysis of wood and bark during bio-oil production. *J. Colloid Interface Sci.* **310**, 57–73 (2007).

82. Liu, Z., Zhang, F.-S. & Wu, J. Characterization and application of chars produced from pinewood pyrolysis and hydrothermal treatment. *Fuel* **89**, 510–514 (2010).

83. Chen, X. *et al.* Adsorption of copper and zinc by biochars produced from pyrolysis of hardwood and corn straw in aqueous solution. *Bioresour. Technol.* **102**, 8877–8884 (2011).

84. Tong, X., Li, J., Yuan, J. & Xu, R. Adsorption of Cu(II) by biochars generated from three crop straws. *Chem. Eng. J.* **172**, 828–834 (2011).

85. Bernardo, M. *et al.* Removal of lead (Pb2+) from aqueous medium by using chars from co-pyrolysis. *J. Colloid Interface Sci.* **409**, 158–65 (2013).

86. Kılıç, M., Kırbıyık, Ç., Çepelioğullar, Ö. & Pütün, A. E. Adsorption of heavy metal ions from aqueous solutions by bio-char, a by-product of pyrolysis. *Appl. Surf. Sci.* **283**, 856–862 (2013).

87. Qian, L. & Chen, B. Interactions of aluminum with biochars and oxidized biochars: Implications for the biochar aging process. *J. Agric. Food Chem.* **62**, 373–380 (2014).

88. Jing, D. A. I. & Yangsheng, L. I. U. Adsorption of Pb2+ and Cd2+ onto biochars derived from pyrolysis of four kinds of biomasses. *J. Peking Univ. Heal. Sci.* **49**, 1–8 (2013).

89. Xu, X., Cao, X. & Zhao, L. Comparison of rice husk- and dairy manure-derived biochars for simultaneously removing heavy metals from aqueous solutions: role of mineral components in biochars. *Chemosphere* **92**, 955–61 (2013).

90. Rostamian, R., Heidarpour, M., Mousavi, S. F. & Afyuni, M. Preparation, characterization and sodium sorption capability of rice husk carbonaceous adsorbents. *Fresenius Environ. Bull.* **24**, 1649–1658 (2015).

91. Shen, Z., Zhang, Y., McMillan, O., Jin, F. & Al-Tabbaa, A. Characteristics and mechanisms of nickel adsorption on biochars produced from wheat straw pellets and rice husk. *Environ. Sci. Pollut. Res.* **24**, 12809–12819 (2017).

92. Yakout, S. M. & Elsherif, E. Biosorption behavior of Sr2+using straw-derived biochar: equilibrium and isotherm study. *Desalin. Water Treat.* **57**, 7262–7269 (2016).

93. Dai, Z., Brookes, P. C., He, Y. & Xu, J. Increased agronomic and environmental value provided by biochars with varied physiochemical properties derived from swine manure blended with rice straw. *J. Agric. Food Chem.* **62**, 10623–10631 (2014).

94. Tan, X. *et al.* Biochar as potential sustainable precursors for activated carbon production: Multiple applications in environmental protection and energy storage. *Bioresour. Technol.* **227**, 359–372 (2017).

95. Menya, E., Olupot, P. W., Storz, H., Lubwama, M. & Kiros, Y. Production and performance of activated carbon from rice husks for removal of natural organic matter from water: A review. *Chem. Eng. Res. Des.* **129**, 271–296 (2018).

96. Yahya, M. A., Al-Qodah, Z. & Ngah, C. W. Z. Agricultural bio-waste materials as potential sustainable precursors used for activated carbon production: A review. *Renew. Sustain. Energy Rev.* **46**, 218–235 (2015).

97. Ternero-Hidalgo, J. J. *et al.* Functionalization of activated carbons by HNO3 treatment: Influence of phosphorus surface groups. *Carbon N. Y.* **101**, 409–419 (2016).

98. Shim, J.-W., Park, S.-J. & Ryu, S.-K. Effect of modification with HNO3 and NaOH on metal adsorption by pitch-based activated carbon fibers. *Carbon N. Y.* **39**, 1635–1642 (2001).

99. Moreno-Castilla, C., López-Ramón, M. . & Carrasco-Marín, F. Changes in surface chemistry of activated carbons by wet oxidation. *Carbon N. Y.* **38**, 1995–2001 (2000).

100. Castro, J. B., Bonelli, P. R., Cerrella, E. G. & Cukierman, A. L. Phosphoric acid activation of agricultural residues and bagasse from sugar cane: Influence of the experimental conditions on adsorption characteristics of activated carbons. *Ind. Eng. Chem. Res.* **39**, 4166–4172 (2000).

101. Sizmur, T., Fresno, T., Akgül, G., Frost, H. & Moreno-Jiménez, E. Biochar modification to enhance sorption of inorganics from water. *Bioresour. Technol.* **246**, 34–47 (2017).

102. Abioye, A. M. & Ani, F. N. Recent development in the production of activated carbon electrodes from agricultural waste biomass for supercapacitors: A review. *Renew. Sustain. Energy Rev.* **52**, (2015).

103. EC. *On the review of the list of critical raw materials for the EU and the implementation of the Raw Materials Initiative*. *European Commission* **1**, (2014).

104. Shanker, A. K. & Venkateswarlu, B. Chromium: Environmental Pollution, Health Effects and Mode of Action. in *Encyclopedia of Environmental Health* 650–659 (2011).

105. Aoyama, M., Tsuda, M., Cho, N.-S. & Doi, S. Adsorption of trivalent chromium from dilute solution by conifer leaves. *Wood Sci. Technol.* **34**, 55–63 (2000).

106. Li, B. *et al.* The effects of alumina reinforcement and nickel activated sintering on

nanosized tungsten matrix. *J. Alloys Compd.* **692**, 420–426 (2017).

107. Milich, P., Möller, F., Píriz, J., Vivó, G. & Tancredi, N. The influence of preparation methods and surface properties of activated carbons on Cr(III) adsorption from aqueous solutions. *Sep. Sci. Technol.* **37**, 1453–1467 (2002).

108. Yang, Z. H., Xiong, S., Wang, B., Li, Q. & Yang, W. C. Cr(III) adsorption by sugarcane pulp residue and biochar. *J. Cent. South Univ.* **20**, 1319–1325 (2013).

109. Agrafioti, E., Kalderis, D. & Diamadopoulos, E. Arsenic and chromium removal from water using biochars derived from rice husk, organic solid wastes and sewage sludge. *J. Environ. Manage.* **133**, 309–314 (2014).

110. Chen, T., Zhou, Z., Xu, S., Wang, H. & Lu, W. Adsorption behavior comparison of trivalent and hexavalent chromium on biochar derived from municipal sludge. *Bioresour. Technol.* **190**, 388–394 (2015).

111. Vassileva, P., Detcheva, A., Uzunov, I. & Uzunova, S. Removal of Metal Ions from Aqueous Solutions Using Pyrolyzed Rice Husks: Adsorption Kinetics and Equilibria. *Chem. Eng. Commun.* **200**, 1578–1599 (2013).

112. Qian, L. *et al.* Effective removal of heavy metal by biochar colloids under different pyrolysis temperatures. *Bioresour. Technol.* **206**, 217–224 (2016).

113. Afkhami, A., Madrakian, T. & Amini, A. Mo(VI) and W(VI) removal from water samples by acid-treated high area carbon cloth. *Desalination* **243**, 258–264 (2009).

114. Ogata, F., Iwata, Y. & Kawasaki, N. Adsorption of Tungsten onto Zeolite Fly Ash Produced by Hydrothermally Treating Fly Ash in Alkaline Solution. *Chem. Pharm. Bull.* **62**, 892–897 (2014).

115. Ogata, F., Iwata, Y. & Kawasaki, N. Properties of novel adsorbent produced by hydrothermal treatment of waste fly ash in alkaline solution and its capability for adsorption of tungsten from aqueous solution. *J. Environ. Chem. Eng.* **3**, 333–338 (2015).

116. Ogata, F., Iwata, Y. & Kawasaki, N. Kinetic and Equilibrium Investigations of Cobalt (II), Nickel (II), and Tungsten (VI) Adsorption on Fly Ash Processed by Hydrothermal Treatment in an Alkaline Solution. *J. Water Environ. Technol.* **13**, 359–370 (2015).

117. Ogata, F. *et al.* Adsorption of tungsten ion with a novel Fe-Mg type hydrotalcite prepared at different Mg2+/Fe3+ ratios. *J. Environ. Chem. Eng.* **5**, 3083–3090 (2017).

118. Ruiping, L., Chunye, L. & Xitao, L. Adsorption of tungstate on kaolinite: adsorption models and kinetics. *RSC Adv.* **6**, 19872–19877 (2016).

119. Wang, Y., Chen, K., Mo, L., Li, J. & Xu, J. Removal of tungsten from electroplating wastewater by acid- and heat-treated sepiolite. *Desalin. Water Treat.* **56**, 232–238 (2015).

120. Gecol, H., Miakatsindila, P., Ergican, E. & Hiibel, S. R. Biopolymer coated clay particles for the adsorption of tungsten from water. *Desalination* **197**, 165–178 (2006).

121. Gecol, H., Ergican, E. & Miakatsindila, P. Biosorbent for tungsten species removal from water: Effects of co-occurring inorganic species. *J. Colloid Interface Sci.* **292**, 344–353 (2005).

122. Cui, M. & Johannesson, K. H. Comparison of tungstate and tetrathiotungstate adsorption onto pyrite. *Chem. Geol.* **464**, 57–68 (2017).

123. Muir, B., Andrunik, D., Hyla, J. & Bajda, T. The removal of molybdates and tungstates from aqueous solution by organo-smectites. *Appl. Clay Sci.* **136**, 8–17 (2017).

124. Sun, J. & Bostick, B. C. Effects of tungstate polymerization on tungsten(VI) adsorption on ferrihydrite. *Chem. Geol.* **417**, 21–31 (2015).

125. Dinker, M. K., Patil, N. V. & Kulkarni, P. S. A diamino based resin modified silica composite for the selective recovery of tungsten from wastewater. *Polym. Int.* **65**, 1387–1394 (2016).

126. Kailasam, V. & Rosenberg, E. Oxyanion removal and recovery using silica polyamine composites. *Hydrometallurgy* **129**–**130**, 97–104 (2012).

127. Wojnicki, M. *et al.* Batch reactor vs. flow column – Mechanistic investigation and modeling of Au(III) ions adsorption from aqueous solutions containing Ni2+, Na+, Cl− and ClO4− as impurities. *Sustain. Mater. Technol.* **23**, e00142 (2020).

128. Patel, H. Fixed-bed column adsorption study: a comprehensive review. *Appl. Water Sci.* **9**, 1–17 (2019).

129. de Franco, M. A. E., de Carvalho, C. B., Bonetto, M. M., de Pelegrini Soares, R. & Féris, L. A. Diclofenac removal from water by adsorption using activated carbon in batch mode and fixed-bed column: Isotherms, thermodynamic study and breakthrough curves modeling. *J. Clean. Prod.* **181**, 145–154 (2018).

130. Pérez Marín, A. B. *et al.* Biosorption of chromium (III) by orange (Citrus cinensis) waste: Batch and continuous studies. *Chem. Eng. J.* **155**, 199–206 (2009).

131. Farooq, U., Athar, M., Khan, M. A. & Kozinski, J. A. Biosorption of Pb(II) and Cr(III) from aqueous solutions: Breakthrough curves and modeling studies. *Environ. Monit. Assess.* **185**, 845–854 (2013).

132. Cossich, E. S., Da Silva, E. A., Tavares, C. R. G., Filho, L. C. & Ravagnani, T. M. K. Biosorption of chromium(III) by biomass of seaweed Sargassum sp. in a fixed-bed column. *Adsorption* **10**, 129–138 (2004).

133. Abdolali, A. *et al.* Application of a breakthrough biosorbent for removing heavy metals from synthetic and real wastewaters in a lab-scale continuous fixed-bed column. *Bioresour. Technol.* **229**, 78–87 (2017).

134. Baharlouei, A., Jalilnejad, E. & Sirousazar, M. Fixed-bed column performance of methylene blue biosorption by Luffa cylindrica: statistical and mathematical modeling. *Chem. Eng. Commun.* **205**, 1537–1554 (2018).

135. Arim, A. L., Neves, K., Quina, M. J. & Gando-Ferreira, L. M. Experimental and mathematical modelling of Cr(III) sorption in fixed-bed column using modified pine bark. *J. Clean. Prod.* **183**, 272–281 (2018).

136. Kegl, T. *et al.* Adsorption of rare earth metals from wastewater by nanomaterials: A review. *J. Hazard. Mater.* **386**, (2020).

137. Aksu, Z. & Gönen, F. Biosorption of phenol by immobilized activated sludge in a continuous packed bed: Prediction of breakthrough curves. *Process Biochem.* **39**, 599–613 (2004).

138. Calero, M., Hernáinz, F., Blázquez, G., Tenorio, G. & Martín-Lara, M. A. Study of Cr (III) biosorption in a fixed-bed column. *J. Hazard. Mater.* **171**, 886–893 (2009).

139. Zhang, Y. P., Adi, V. S. K., Huang, H. L., Lin, H. P. & Huang, Z. H. Adsorption of metal ions with biochars derived from biomass wastes in a fixed column: Adsorption isotherm and process simulation. *J. Ind. Eng. Chem.* **76**, 240–244 (2019).

140. Ferraz, A. I., Amorim, C., Tavares, T. & Teixeira, J. A. Chromium(III) biosorption onto spent grains residual from brewing industry: equilibrium, kinetics and column studies. *Int. J. Environ. Sci. Technol.* **12**, 1591–1602 (2015).

141. Tofan, L., Paduraru, C., Teodosiu, C. & Toma, O. Fixed bed column study on the removal of chromium (III) ions from aqueous solutions by using hemp fibers with improved sorption performance. *Cellul. Chem. Technol.* **49**, 219–229 (2015).

142. Elangovan, R., Philip, L. & Chandraraj, K. Biosorption of hexavalent and trivalent chromium by palm flower (Borassus aethiopum). *Chem. Eng. J.* **141**, 99–111 (2008).

143. Pinto, F. *et al.* Co-gasification study of biomass mixed with plastic wastes. *Fuel* **81**, 291–297 (2002).

144. Pinto, F. *et al.* Comparison of Co-gasification of Wastes Mixtures Obtained from Rice Production Wastes Using Air or Oxygen. *Chem. Eng. Trans.* **43**, 2227–2232 (2015).

145. Chakma, S., Ranjan, A., Choudhury, H. A., Dikshit, P. K. & Moholkar, V. S. Bioenergy from rice crop residues: Role in developing economies. *Clean Technol. Environ. Policy* **18**, 373–394 (2016).

146. Yang, H., Yan, R., Chen, H., Lee, D. H. & Zheng, C. Characteristics of hemicellulose, cellulose and lignin pyrolysis. *Fuel* **86**, 1781–1788 (2007).

147. Worasuwannarak, N., Sonobe, T. & Tanthapanichakoon, W. Pyrolysis behaviors of rice straw, rice husk, and corncob by TG-MS technique. *J. Anal. Appl. Pyrolysis* **78**, 265–271 (2007).

148. Raveendran, K., Ganesh, A. & Khilar, K. C. Pyrolysis characteristics of biomass and biomass components. *Fuel* **75**, 987–998 (1996).

149. Zweifel, H., Maier, R. & Schiller, M. *Plastics Additives Handbook*. (Hanser, 2009).

150. Tavlieva, M. P., Genieva, S. D., Georgieva, V. G. & Vlaev, L. T. Thermodynamics and kinetics of the removal of manganese(II) ions from aqueous solutions by white rice husk ash. *J. Mol. Liq.* **211**, 938–947 (2015).

151. Tarley, C. R. T. & Arruda, M. A. Z. Biosorption of heavy metals using rice milling by-products. Characterisation and application for removal of metals from aqueous effluents. *Chemosphere* **54**, 987–995 (2004).

152. Liu, H., Zhang, L., Han, Z., Xie, B. & Wu, S. The effects of leaching methods on the combustion characteristics of rice straw. *Biomass and Bioenergy* **49**, 22–27 (2013).

153. Karnowo, Zahara, Z. F., Kudo, S., Norinaga, K. & Hayashi, J. Leaching of Alkali and Alkaline Earth Metallic Species from Rice Husk with Bio-oil from Its Pyrolysis. *Energy Fuels* **28**, 6459–6466 (2014).

154. Pode, R. Potential applications of rice husk ash waste from rice husk biomass power plant. *Renew. Sustain. Energy Rev.* **53**, 1468–1485 (2016).

155. Shen, Y., Zhao, P., Shao, Q., Takahashi, F. & Yoshikawa, K. In situ catalytic conversion of tar using rice husk char/ash supported nickel–iron catalysts for biomass pyrolytic gasification combined with the mixing-simulation in fluidized-bed gasifier. *Appl. Energy* **160**, 808–819 (2014).

156. Wang, Y., Hu, Y., Zhao, X., Wang, S. & Xing, G. Comparisons of biochar properties from wood material and crop residues at different temperatures and residence times. *Energy and Fuels* **27**, 5890–5899 (2013).

157. Prakongkep, N., Gilkes, R. J., Wiriyakitnateekul, W. & Duangchan, A. The Effects of Pyrolysis Conditions on the Chemical and Physical Properties of Rice Husk Biochar. *Int. J. Mater. Sci.* **3**, 97–103 (2013).

158. Bian, R. *et al.* Pyrolysis of crop residues in a mobile bench-scale pyrolyser: Product characterization and environmental performance. *J. Anal. Appl. Pyrolysis* **119**, 52–59 (2016).

159. Jeong, C. Y., Dodla, S. K. & Wang, J. J. Fundamental and molecular composition characteristics of biochars produced from sugarcane and rice crop residues and by-products. *Chemosphere* **142**, 4–13 (2016).

160. Sing, K. S. W. *et al.* Reporting physisorption data for gas/solid systems with special reference to the determination of surface area and porosity (Recommendations 1984). *Pure Appl. Chem.* **57**, 603–619 (1985).

161. Hu, S. *et al.* Characterization of char from rapid pyrolysis of rice husk. *Fuel Process. Technol.* **89**, 1096–1105 (2008).

162. Fu, P. *et al.* Evaluation of the porous structure development of chars from pyrolysis of rice straw: Effects of pyrolysis temperature and heating rate. *J. Anal. Appl. Pyrolysis* **98**, 177–

183 (2012).

163. Fu, P. *et al.* Evolution of char structure during steam gasification of the chars produced from rapid pyrolysis of rice husk. *Bioresour. Technol.* **114**, 691–7 (2012).

164. Yi, S. *et al.* Removal of levofloxacin from aqueous solution using rice-husk and wood-chip biochars. *Chemosphere* **150**, 694–701 (2016).

165. International Organization for Standardization. *ISO 11348-3:1998 - Water quality — Determination of the inhibitory effect of water samples on the light emission of Vibrio fischeri*. (1998).

166. Kumagai, S., Shimizu, Y., Toida, Y. & Enda, Y. Removal of dibenzothiophenes in kerosene by adsorption on rice husk activated carbon. *Fuel* **88**, 1975–1982 (2009).

167. Li, M., Wu, S. C., Peng, Y.-H. & Shih, Y. Adsorption of volatile organic vapors by activated carbon derived from rice husk under various humidity conditions and its statistical evaluation by linear solvation energy relationships. *Sep. Purif. Technol.* **170**, 102–108 (2016).

168. Liou, T.-H. & Wu, S.-J. Characteristics of microporous/mesoporous carbons prepared from rice husk under base- and acid-treated conditions. *J. Hazard. Mater.* **171**, 693–703 (2009).

169. Li, Z. *et al.* Leaf char: An alternative adsorbent for Cr(III). *Desalination* **264**, 70–77 (2010).

170. APHA/AWWA/WEF. *Standard Methods for the Examination of Water and Wastewater*. *Standard Methods* (2012).

171. Ho, Y.-S. Review of second-order models for adsorption systems. *J. Hazard. Mater.* **136**, 681–689 (2006).

172. Simonin, J.-P. On the comparison of pseudo-first order and pseudo-second order rate laws in the modeling of adsorption kinetics. *Chem. Eng. J.* **300**, 254–263 (2016).

173. Foo, K. Y. & Hameed, B. H. Insights into the modeling of adsorption isotherm systems. *Chem. Eng. J.* **156**, 2–10 (2010).

174. Russo, V., Trifuoggi, M., Di Serio, M. & Tesser, R. Fluid-Solid Adsorption in Batch and Continuous Processing: A Review and Insights into Modeling. *Chem. Eng. Technol.* **40**, 799–820 (2017).

175. Mella, B., Glanert, A. C. & Gutterres, M. Removal of chromium from tanning wastewater and its reuse. *Process Saf. Environ. Prot.* **95**, 195–201 (2015).

176. Ramírez-Estrada, A. *et al.* Cr(III) removal from synthetic and real tanning effluents using an electro-precipitation method. *J. Environ. Chem. Eng.* **6**, 1219–1225 (2018).

177. George, J. S., Ramos, A. & Shipley, H. J. Tanning facility wastewater treatment: Analysis of physical–chemical and reverse osmosis methods. *J. Environ. Chem. Eng.* **3**, 969–976 (2015).

178. Guo, Z.-R., Zhang, G., Fang, J. & Dou, X. Enhanced chromium recovery from tanning wastewater. *J. Clean. Prod.* **14**, 75–79 (2006).

179. Dias, D. *et al.* Cr(III) removal from synthetic and industrial wastewaters by using co-gasification chars of rice waste streams. *Bioresour. Technol.* **266**, 139–150 (2018).

180. Thomas, H. C. Chromatography; a problem in kinetics. *Ann. N. Y. Acad. Sci.* **49**, 161–182 (1948).

181. Rosales, E., Meijide, J., Pazos, M. & Sanromán, M. A. Challenges and recent advances in biochar as low-cost biosorbent: From batch assays to continuous-flow systems. *Bioresour. Technol.* **246**, 176–192 (2017).

182. Jandosov, J. M. *et al.* Synthesis , Morphostructure , Surface Chemistry and Preclinical Studies of Nanoporous Rice Husk-Derived Biochars for Gastrointestinal Detoxification. *Eurasian Chem. J.* **19**, 303–313 (2017).

183. Jandosov, J., Mansurov, Z. A., Tulepov, M. I. & Ismagilov, Z. Synthesis of Microporous-Mesoporous Carbons from Rice Husk via H3PO4- Activation. *Adv. Mater. Res.* **602–604**, 85–89 (2013).

184. Satayeva, A. R. *et al.* Investigation of rice husk derived activated carbon for removal of nitrate contamination from water. *Sci. Total Environ.* **630**, 1237–1245 (2018).

185. Pérez-Marín, A. B. *et al.* Removal of cadmium from aqueous solutions by adsorption onto orange waste. *J. Hazard. Mater.* **139**, 122–131 (2007).

186. Czinkota, I., Földényi, R., Lengyel, Z. & Marton, A. Adsorption of propisochlor on soils and soil components equation for multi-step isotherms. *Chemosphere* **48**, 725–731 (2002).

187. Tolner, L. The determination of parameters of multi-step adsorption isotherm by sequential simplex optimization. *Appl. Ecol. Environ. Res.* **6**, 109–117 (2008).

188. Babić, B. M., Milonjić, S. K., Polovina, M. J. & Kaludierović, B. V. Point of zero charge and intrinsic equilibrium constants of activated carbon cloth. *Carbon N. Y.* **37**, 477–481 (1999).

189. Kosmulski, M. pH-dependent surface charging and points of zero charge. IV. Update and new approach. *J. Colloid Interface Sci.* **337**, 439–448 (2009).

190. Smith, B. J. & Patrick, V. A. Quantitative Determination of Sodium Metatungstate Speciation by 183W N.M.R. Spectroscopy. *Aust. J. Chem.* **53**, 965–970 (2000).

191. Surman, A. J. *et al.* Sizing and Discovery of Nanosized Polyoxometalate Clusters by Mass Spectrometry. *J. Am. Chem. Soc.* **138**, 3824–3830 (2016).

192. Furter, W. F. Salt effect in distillation: A literature review II. *Can. J. Chem. Eng.* **55**, 229–239 (1977).

193. Fang, J., Zhao, R., Wang, H., Li, C. & Liu, J. Salting-out effect of ionic liquids on isobaric vapor-liquid equilibrium of acetonitrile-water system. *Chinese J. Chem. Eng.* **23**, 1369–

1373 (2015).

194. Tanganov B. B. About sizes of the hydrated salt ions - the components of sea water. *Eur. J. Nat. Hist.* **1**, 36–37 (2013).